Modified Oligonucleotides for the Functionalisation of Nanoscale Materials

by

Jennifer Anne Dougan

2009

University of Strathclyde

Department of Pure and Applied Chemistry

Modified Oligonucleotides for the Functionalisation

of Nanoscale Materials

by

Jennifer Anne Dougan

A thesis presented to the Department of Pure and Applied Chemistry, University of Strathclyde, in fulfilment of the requirements for the degree of Doctor of Philosophy.

2009

I   *Acknowledgements*

I would like to thank my supervisors Prof. Duncan Graham and Prof. W. Ewen Smith for discussions and suggestions throughout my PhD.

For their tireless assistance, discussion and (where necessary) criticism I thank Dr. Robert J. Stokes and Fiona McKenzie whose enthusiasm helped push through the troughs. I thank Dr. David Robson for getting me started, Dr. Andrew Ingram for synthetic discussions and Dr. Aaron Hernandez-Santana for definitely NOT looking like a spectrometer. I also thank Andrew Reid for his advice regarding H-phosphonate chemistry.

For general support, chat, and friendship along the journey, I thank Fiona, Sarah, Victoria, Charlotte, Colette, Jane and the other girls of R5.34. It has been, at times, challenging, sometimes rewarding and always thought-provoking. To all my co-workers past and present I would say thank you for listening to, and indulging, my rants either chemistry related or otherwise - "and I'll tell you why!"

Finally, I would like to thank my loved ones for their endless support throughout this seemingly never-ending-saga. Samar for believing in me, helping me maintain perspective and pushing me forward. My parents for teaching me to not be afraid to question anything (or everything as the case may be) and who supported me throughout, for that I am forever thankful. Thanks, individually, to my dad who accepted without question my unwillingness to discuss the progress of the "unmentionable" and my mum for putting up with some terrible moods. My sister, Jo (with the Big Toe™) I thank, for friendship and understanding (mostly) my absence – Tao Tao. My weekend babies I thank for the laughter and the love. Nan and Gran I thank for being the best grandmothers a girl could hope for, teaching me to enjoy the nice things in life and to value the right things in life. My good friends Ann and Katy, I thank for just being there.

II   *Abstract*

The overall aim of this research was to develop a novel ligand for biomolecular functionalisation with a view to enhancing the stability of oligonucleotide-nanoparticle conjugates and assessing the suitability of a nanostructured surface for the detection of hybridisation events by surface enhanced resonance Raman scattering (SERRS).

Thioctic acid was considered a suitable linker group with which to tether oligonucleotides to nanoparticle substrates. As such, routes to the modification of oligonucleotides by thioctic acid are reported herein. Although the phosphoramidite method was found to be unsuccessful, the H-phosphonate method has been shown to be effective for direct modification. In addition, a key intermediate - the *N*-hydroxysuccinimidyl ester of thioctic acid - has been isolated and employed in the modification of oligonucleotides. Pre- and post-synthetic modification of oligonucleotides by thioctic acid is shown. As a result of this research thioctic acid modified oligonucleotides are now commercially available as is the *N*-hydroxysuccinimidyl ester intermediate.

Thioctic acid modified oligonucleotides have been conjugated to both gold and silver nanoparticles. The successful preparation of these materials was confirmed and the ability of both gold and silver nanoparticle conjugates to function as hybridisation sensors has been shown. This has extended the methodology of hybridisation induced aggregations from gold to silver nanoparticles. The stability of the thioctic acid oligonucleotide nanoparticle conjugates was investigated and found to be greatly enhanced with respect to monothiol linked analogues.

A commercially available nanostructured surface was used to confirm the suitability of dye labelled thioctic acid modified oligonucleotides for SERRS detection. The ability to detect a hybridisation event was also investigated. The NHS-ester of thioctic acid was employed as a surface activation group. Dip pen nanolithography was used to immobilise thioctic acid modified oligonucleotides for the detection of an unmodified, biologically relevant, target sequence by SERRS.

III   Abbreviations

A	Adenine
Ac	Acetyl
AFM	Atomic Force Microscopy
AU	Absorbance Units
BODIPY-650	6-(((4,4-difluoro-5-(2-pyrrolyl)-4-bora-3a,4a-diaza-*s*-indacene-3-yl)styryloxy)acetyl)aminohexanoic acid
bp	Base pairs
BTT	5-Benzylthio-1*H*-tetrazole
C	Cytosine
CCD	Charge Coupled Device
CDI	1,1-Carbonyldiimidazole
Conc.	Concentration
CPG	Controlled Pore Glass
d	Doublet (NMR)
d	Deoxy (DNA)
D	Dextrorotatory
dd	Doublet of doublets
Δ	Heat
DCM	Dichloromethane
DEAE	Diethylaminoethyl
DIPEA	Di-*iso*-propylethylamine
DLS	Dynamic Light Scattering
DMF	*N,N*-Dimethylformamide
DMSO	Dimethylsulfoxide
DMTr	Dimethoxytrityl
4-DMAP	4-*N,N*-Dimethylaminopyridine
DNA	2'-Deoxyribose Nucleic Acid

DPN	Dip-pen nanolithography
Ds	Disulfide
DTT	Dithiothreitol
E	Electronic excited state
EDC	*N*-(3-Dimethylaminopropyl)-*N*'-ethylcarbodiimide
EDITH	3-Ethoxy-1,2,4-dithiazoline-5-one
EI	Electron Impact
EPSRC	Engineering and Physical Sciences Research Council
eq	Equivalents
Et	Ethyl
ETT	5-Ethylthio-1*H*-tetrazole
FAM	Carboxyl Fluorescein
Fmoc	9-Fluorenylmethoxycarbonyl
FRET	Förster Resonance Energy Transfer
G	Guanine
h	Hour(s)
HATU	2-(7-Aza-1H-benzotriazole-1-yl)-1,1,3,3-tetramethyluronium hexafluorophosphate
HH	Head-to-head
HIV	Human Immunodeficiency Virus
HOBT	Hydroxybenzotriazole
HPA	Hydroxypiccolinic acid
HPLC	High Performance Liquid Chromatography
IE	Ion-exchange
IPA	*iso*-propyl alcohol
IR	Infrared
L	Litre
LCAA	Long Chain Alkyl Amine
LFM	Lateral Force Microscopy
LNA	Locked Nucleic Acid
LWD	Long Working Distance

M	Molar
MALDI-TOF	Matrix-Assisted Laser Desportion Ionisation – Time of Flight
Mass spec.	Mass Spectrometry
Max.	Maximum
MBA	Mercaptobenzoic acid
Me	Methyl
MHA	Mercaptohexadecanoic acid
min	Minute(s)
MMTr	Monomethoxy trityl
mod	modified
MQ	Milli-Q®
MRSA	methicillin-resistant *Staphylococcus aureus*
MS	Mass Spectrometry
m/z	Mass/charge ratio
NA	Numerical Aperture
NHS	*N*-Hydroxysuccinimide
NMR	Nuclear Magnetic Resonance
Nᵒ	Number
NP	Nanoparticle
NWST	North Western Spot Test
ODT	1-Octadecanethiol
Oligo	Oligonucleotide
PAGE	Polyacrylamide gel electrophoresis
PBS	Phosphate buffered saline
PCR	Polymerase Chain Reaction
p.p.m.	Parts per million
QCM	Quartz crystal microbalance
RNA	Ribonucleic acid
RP	Reversed phase
r.p.m.	Revolutions per minute
RSD	Relative Standard Deviation

s	Singlet
SAM	Self Assembled Monolayer
SDS	Sodium dodecyl sulfate
SEC	Size Exclusion Chromatography
SEM	Scanning Electron Microscopy
SERS	Surface Enhanced Raman Scattering
SERRS	Surface Enhanced Resonance Raman Scattering
SNP	Single Nucleotide Polymorphism
SPR	Surface Plasmon Resonance
t	Triplet
T	Thymine
TA	Thioctic acid
TEAA	Triethylammonium acetate
TEAB	Triethylammonium bicarbonate
TEM	Transmission Electron Microscopy
THF	Tetrahydrofuran
TLC	Thin Layer Chromatography
T_m	Melting Temperature
TMAMC	Tetramethylammonium chloride
Tris	Tris(hydroxymethyl)aminomethane
Trt	Trityl
TT	Tail-to-tail
U	Uracil
UV	Ultra Violet
vis	Visible
vs	Versus

IV   *Contents*

1 Introduction

Deoxyribonucleic acid, DNA, is the central substance of all life on earth. For the post-"double helix" generation the beauty and simplicity of its arrangement is accepted almost without question. The precision of the Watson-Crick base pairing, the seemingly random ordering of bases, and the elegant coiling of the helices all impart the features of DNA crucial to its biological function. [1] [2] [3] It is surely the fundamental nature of DNA to life itself that ensnares researchers from all scientific disciplines, [4] with inspiration from the physicist Erwin Schrödinger's classic text "What is Life" [5] to the advent of the molecular biology revolution. [6]

1.1   DNA: Structure, Synthesis and Modification

In their seminal paper Watson and Crick proposed the double helix as the secondary structure of deoxyribose nucleic acid, DNA. [1] Their work was based on previously published experimental results, X-ray diffraction patterns and stereochemical arguments. [1] [7] [8] [9] It was their paper that confirmed the complementarity of DNA binding, providing a basis for the copying mechanism of genetic material. [1] [2] [3] A consideration of the primary structure of DNA leads directly to the secondary structure and subsequently to the biochemical implications. [6] [10] [11]
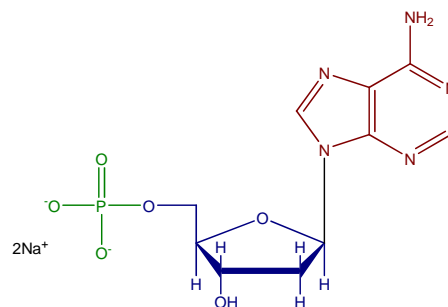
Figure 1.1: Adenosine monophosphate; the nitrogenous base is shown in red, the 2-deoxyribose sugar in blue and the phosphate in green.

Adenine   Guanine
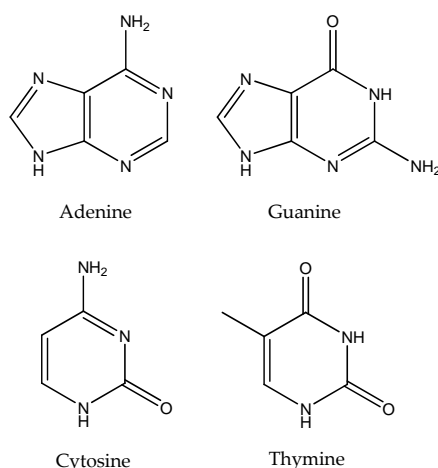
Cytosine   Thymine

Figure 1.2: The DNA bases. Purines: adenine and guanine; pyrimidines: cytosine and thymine.

1.1.1 DNA: Primary structure

DNA is a polymeric species comprised of a series of monomeric units which are known as nucleotides. Each nucleotide is comprised of three sub units – sugar, phosphate and base (Figure 1.1). There are four possible bases from which the genetic diversity of DNA, and indeed life, is derived – adenine (A), cytosine (C), guanine (G) and thymine (T). The four bases can be separated into two groups: the bicyclic purines, adenine and guanine; and the monocyclic pyrimidines, cytosine and thymine (Figure 1.2). [In RNA (where the sugar is the oxygenated β-D-ribose) the thymine is replaced by uracil (U) which is distinguished by the absence of the 5'-methyl group.] The sugar of DNA is 2-deoxy-β-D-ribose (Figure 1.3).

When only the base and sugar are attached *i.e.* omission of the phosphate unit, the structure is termed a nucleo*side* (Figure 1.4). The base is attached to the sugar *via* an *N*-glycosidic bond from C-1' of the 2'-deoxyribose sugar through N-9 of the purines and N-1 of the pyrimidines as shown in red in Figure 1.4. This locks the
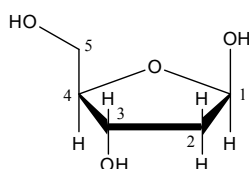
Figure 1.3: 2-Deoxy-β-D-ribose; the sugar of DNA.

2
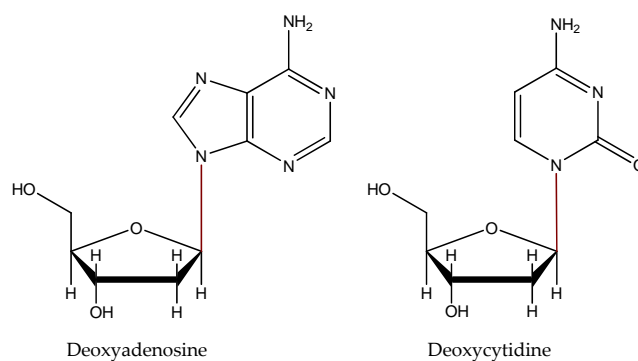
Figure 1.2: Examples of nucleosidic units; deoxyadenosine and deoxycytidine. Note, the N-glycosidic bond shown in red from C-1' to N-9 of adenine and N-1 of cytosine.

sugar into its β configuration. It is worthy to note that the bases exist almost exclusively (> 99.99 %) in their keto- and amino- tautomeric forms (rather than the enol- and imino- forms assumed prior to the 1950's). [1]

A sequence of DNA is a polynucleotide; comprised of nucleoside units tethered by phosphodiester groups which bridge between the 3'-hydroxyl of one and the 5'-hydroxyl of the other, as shown in the dimer of Figure 1.5.
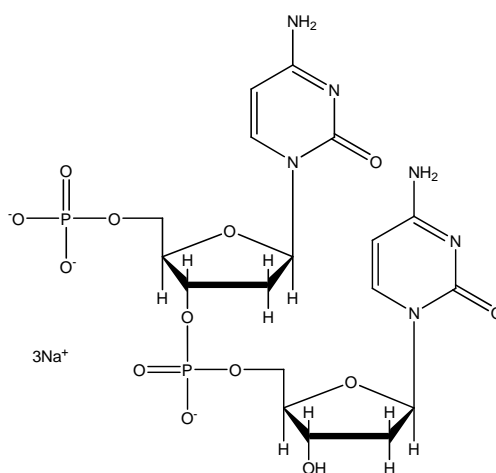
Figure 1.5: A DNA dimer. The 5'-3' phosphate bridging of two sugar units is shown above.
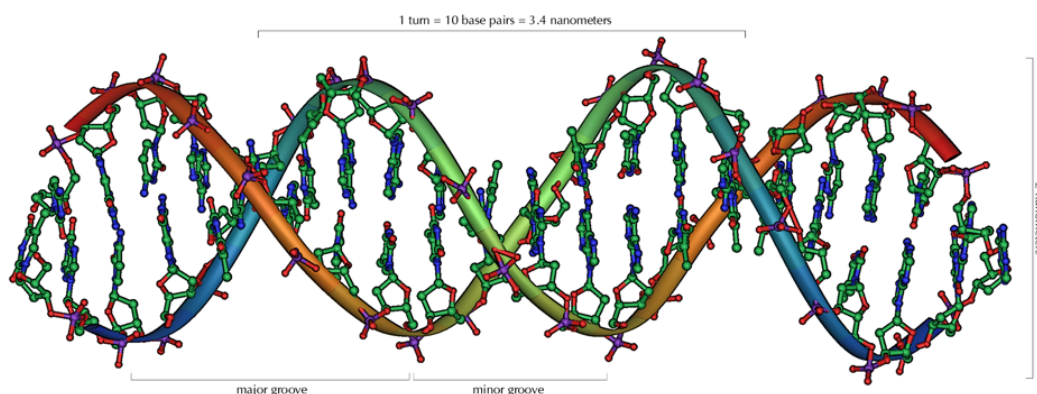
Figure 1.6: A representation of the double helix structure of DNA with the interweaving strands emphasised by the coloured ribbon. [12]

1.1.2 DNA: Secondary structure

In their 1953 paper James Watson and Francis Crick announced the secondary structure for deoxyribose nucleic acid. [1] They stated that the secondary structure of DNA consists of two right-handed helical chains coiled around a common axis, running anti-parallel to one another (Figure 1.6). Each chain is comprised of phosphate diester groups linking 2-deoxyribose units *via* 3'- and 5'-hydroxyl sites with a base attached to each sugar. Hydrogen bonding between nitrogenous bases of opposing chains dominates the intermolecular attractions, giving rise to complementarity.

The bases in a DNA sequence occur in seemingly random order, although every A of one chain is hydrogen bonded to a T on the opposing chain and each G is paired with a C. This was first observed by Chargaff who had shown that whilst the base composition of DNA was irregular from species to species it consistently had a 1:1 ratio of A to T and G to C. [13] This was shown by Watson and Crick to be stereo-chemically compatible with their double helix structure as the A·T and G·C pairs gave the best hydrogen-bonding agreement (Figure 1.7). [1] [2] [3] There are two H-bonds for each A·T pair and three for each G·C pair. The H-bonds have an average (individual) strength of 6 - 10 kJ mol^{-1}. [11] Although this constitutes a relatively weak bonding situation, the contribution from each hydrogen bond is additive.
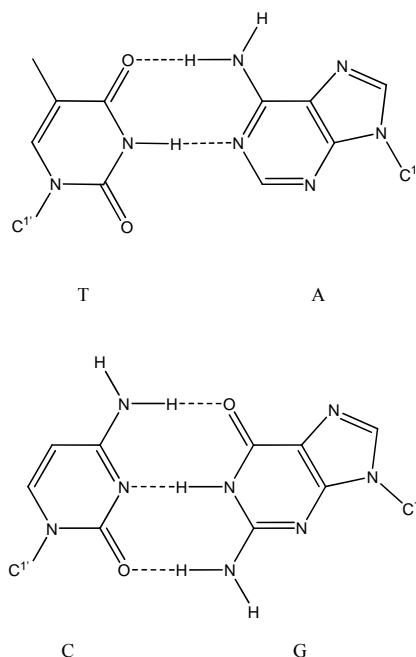
Figure 1.7: "Watson-Crick" base-pairing of A·T and G·C maximizes hydrogen bonding interactions (shown as dashed lines).

It is easy to appreciate, therefore, how the double helix of long chain polynucleotides is relatively stable. Indeed, G·C rich regions/sequences are more stable than A·T due to the contribution of the extra H-bond *per* base pair and π-stacking contributions. [14] It is the hydrogen bonding between bases of the chains that hold the two helices together. H-Bonding is also key to the regularity of the DNA duplex since the Watson-Crick base pairs of A·T and G·C pairs exhibit isomorphous geometry. Other base pairs are known but are only significant in certain situations: in the compact structure of RNAs (which maximize H-bonding and base-stacking characteristics); in triplex formation; and between mis-matched bases. [11] Overwhelmingly, though, the chemistry of DNA base-pairing is dominated by Watson-Crick pairing.

The bases exist at the core of the double helix H-bonded to their complement while the phosphodiester-sugar units create a rigid, polyanionic backbone. Watson and Crick reported this in agreement with the observations of Wilkins (with whom they shared the 1962 Nobel Prize in Physiology or Medicine), [9] Franklin [8] and Gulland. [7] Maurice Wilkins realized the necessity of keeping the DNA fibres moist

whilst conducting X-ray diffraction experiments. He showed that the X-ray patterns obtained from isolated moist DNA were consistent with those obtained from intact biological material. [9] His co-worker, Rosalind Franklin, reported two forms of DNA - the A-form found at low humidity and the B-form at high humidity - she argued that for the presence, or absence, of water to change the form of DNA the polyanionic phosphates would be required to form the outside of the structure with the bases, concomitantly, inside. [8] Meanwhile, Gulland had shown that in aqueous solution the carbonyl and amino groups of the bases could not be titrated, whereas the phosphate groups were readily accessible. [7] As the secondary structure of DNA was established, its biological significance was investigated.

1.1.3 DNA: Biological Implications

DNA is responsible for the genetic propagation of our inheritable traits. Within the cell DNA is organized into chromosomes which are a long continuous piece of DNA with distinct regions comprised of genes, regulatory sequences, and so-called "junk DNA"; the entire sequence is known as the genome. Genes are the regions of DNA which code for inheritable traits. DNA is not a "functional" biomolecule; it stores genetic information which is then translated into functional biomolecules *i.e.* RNA and proteins. It is these "functional products" that are expressed as the physical characteristics, development, and to an extent behaviour (although it is
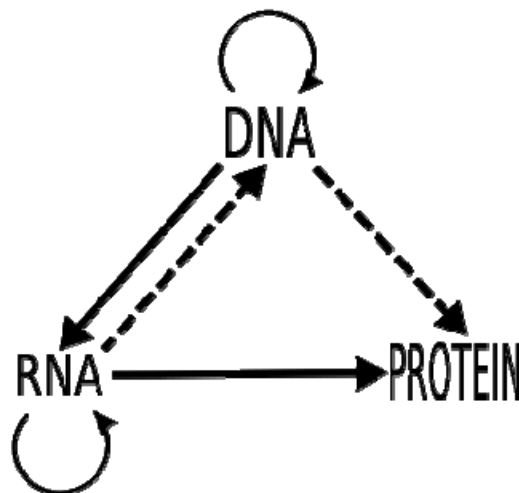
Figure 1.8: Depiction of the "Central Dogma", as proposed by Francis Crick. [13] [14] *Solid arrows represent those processes known to occur, hashed arrows are thought to occur and absent arrows, i.e. those originating at protein are not considered valid.*

beyond the scope of this thesis to discuss the nature/nurture argument of behavioural attributes) of an organism.

According to the "Central Dogma" the flow of genetic information is one-directional, most generally from DNA to RNA to proteins (Figure 1.8). [13] This was put forth by Francis Crick in the 1950's and it holds true today (a few abnormal circumstances notwithstanding). [14] DNA provides the template for protein synthesis. [15] However, protein synthesis occurs in the cytoplasm of a cell and DNA is, in eukaryotic cells, held in the nucleus. Within the nucleus, DNA is "read" and transcribed into the corresponding RNA sequence, known as pre-mRNA. Pre-mRNA then undergoes a series of steps before being rendered suitable for transport out of the nucleus, into the cytoplasm as mRNA (messenger RNA). Once in the cytoplasm it is the mRNA that is used as a template to code for protein synthesis. The sequence of the mRNA is read by triplets of tRNA (transfer RNA) that are linked to specific amino acids which are the building blocks of proteins. The triplets of mRNA that are recognized by the tRNA are known as codons and their matched tRNA partners are known as anti-codons. This process relies on the fidelity of nucleotide base pairing as only the amino acid corresponding to the correct triplet of nucleotides is added to the growing polypeptide chain. The sequence of amino acids incorporated, which is directly related to the original nucleic acid sequence, is known as the primary structure of the resulting protein. The behaviour and role of proteins are complex and cannot be easily predicted from their primary structure. Secondary, tertiary and, indeed, quaternary structures can and do dominate protein chemistry. Nevertheless, the sequence of coding DNA is crucial to cellular and organism function. The sequence of DNA dictates the sequence of RNA and thus the sequence of protein, which in turn affects the protein's function (by influencing secondary, tertiary and quaternary structure). Determining the sequence of DNA, in a highly selective manner for the rapid detection of genetic mutations and disease states is of ever growing interest and central to a number of new approaches to disease management. In order to achieve this, synthesis of oligonucleotide sequences of interest is an important first step. Subsequently, robust analytical techniques are required for development.

1.1.4 DNA: Chemical Synthesis

There have been significant advances in the field of DNA chemistry since the elucidation of the structure of DNA by Watson and Crick in 1953. [1] One such development is the chemical synthesis of oligonucleotides. The chemical synthesis of DNA produces oligonucleotide probes and primers; which are pre-requisites for DNA sequencing, [16] and the Polymerase Chain Reaction (PCR) [17] - vital to genome research and the biotechnology industry. Chemical synthesis of DNA allows for the development of non-natural sequences and modifications, greatly increasing the library of information available to researchers. Although the initial procedures for the synthesis of oligonucleotides were limited to use by experienced synthetic chemists, [18] oligonucleotide synthesis is now an accessible process carried out on automated synthesizers and is available for use by analysts, biologists and chemists alike. Since the early 1980's, and the development of the phosphoramidite approach, [19] [20] [21] in which monomeric "nucleotide" derivatives are supplied as phosphoramidites to a growing chain on a solid support, the synthetic cycle of DNA has remained essentially unchanged. Automated synthesizers routinely prepare any sequence of DNA required by researchers.

1.1.4 (a) Protection

A protection strategy for the exocyclic amino groups, the 5' alcohol and the P-OH of the phosphate chain was established by H. Gobind Khorana in the 1960's. [22] [23] [24] These remain the standard protecting groups employed today; isobutyryl for guanosine, benzoyl for adenosine and acetyl for cytidine as shown in Figure 1.9.

N-benzoyl adenine   *N*-acetyl cytosine   *N*-isobutyryl guanine
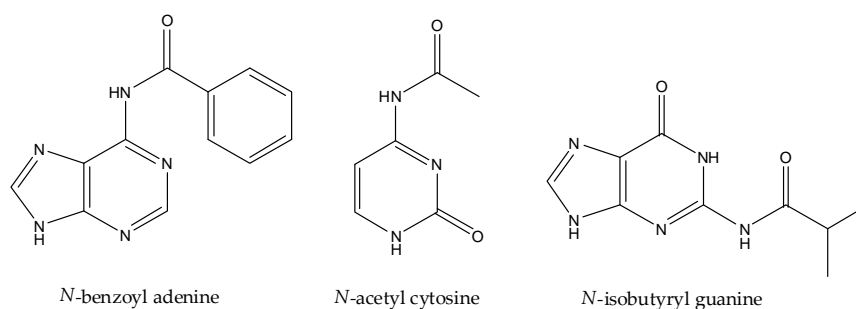
Figure 1.9: The exocyclic amines of the bases are protected as shown during the DNA synthesis cycle.

Other protecting groups are now available for exocyclic amine protection. For example, phenoxyacetyl dA [25] and dimethylformamidine dG [26] allow for quick and mild deprotection conditions. [27] The 5' alcohol is protected as the dimethoxytrityl ether which is readily cleaved under acidic conditions. The would-be free alcohol of the phosphate backbone is protected as a cyanoethyl ester, [28] [29] this functionality is readily cleaved under basic conditions *via* β elimination.

The protection strategy remains essentially unchanged from that introduced by Khorana during the 1960's with orthogonal base-labile exocyclic amine protection and acid-labile alcohol protection.

1.1.4 (b) Solid-support

Oligonucleotide synthesis is usually carried out on automated synthesisers using controlled pore glass (CPG) [30] solid supports which, as standard, are already base-functionalised. All 4 bases immobilised on solid support are available commercially. They are attached to the CPG *via* a 3'-ester linkage. The 5'- hydroxyl is protected with the dimethoxytrityl moiety and the nitrogenous base is suitably protected (Figure 1.10). CPG which is not base-functionalised, called "universal" support, is also available. Regardless of whether standard or universal CPG is used, the functionalised supports, which contain a dimethoxytrityl protected alcohol, are held in columns which are fitted in-line on the synthesiser. The reagents are all supplied as solutions which are passed through the column and washed away after each step of the cycle.
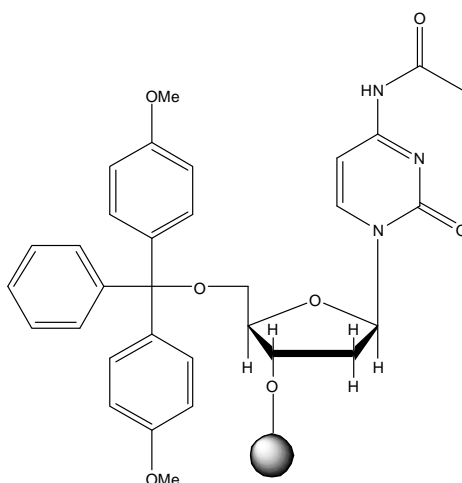
Figure 1.10: A typical "standard" support as used for oligonucleotide synthesis.

1.1.4 (c) The Synthetic Cycle

In contrast to enzymatic DNA synthesis, [17] [31] DNA synthesis by chemical means progresses in the 3' to 5' direction. [32] The synthesis cycle involves 4 key steps (Scheme 1.1):

	i	Deprotection.
	ii	Coupling.
	iii	Capping.
	iv	Oxidation.
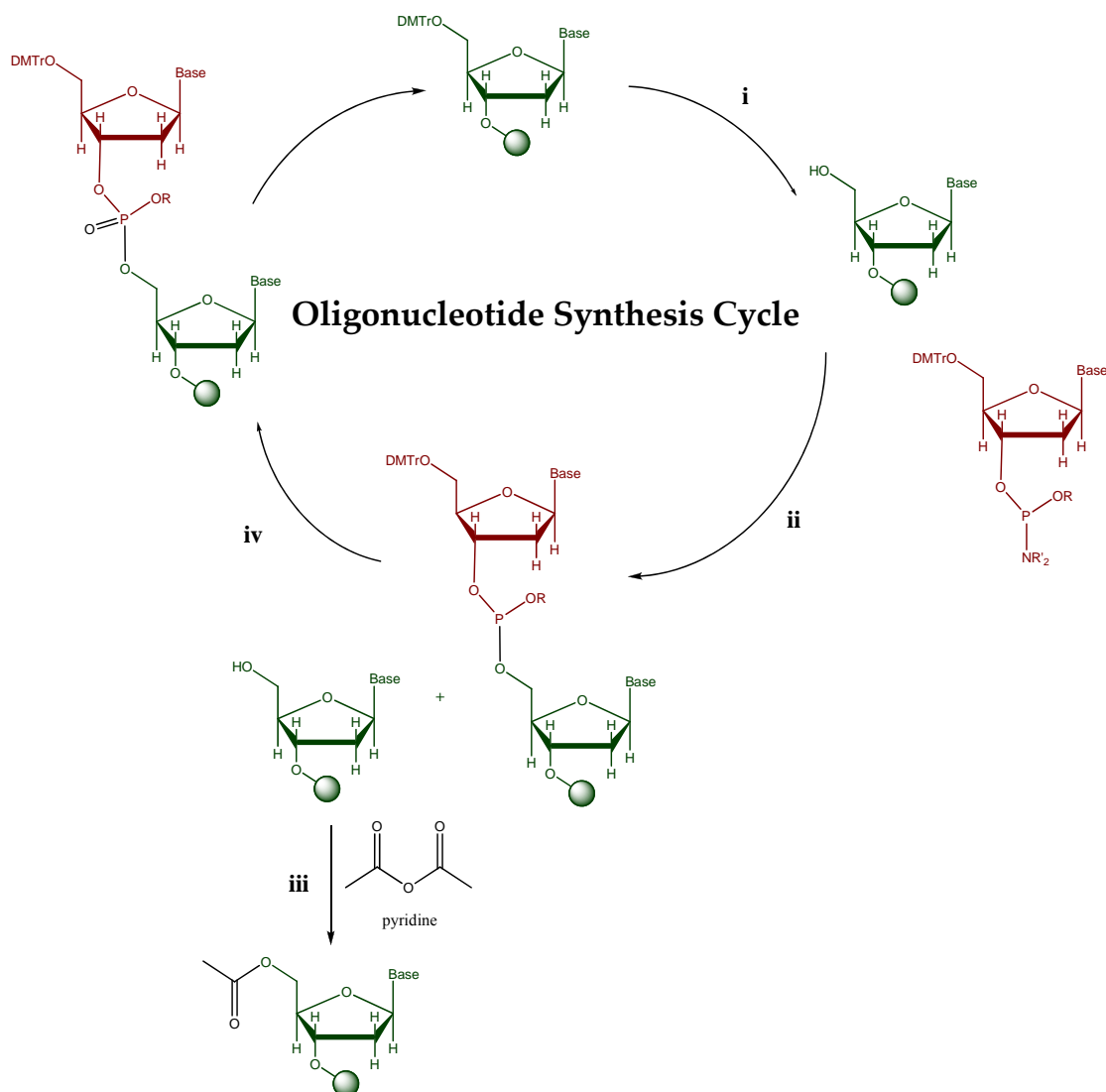
Scheme 1.1: An overview of oligonucleotide synthesis which is comprised of four main steps: i, Deprotection; ii, Coupling; iii, Capping; iv, Oxidation. Where R is a cyanoethyl group.
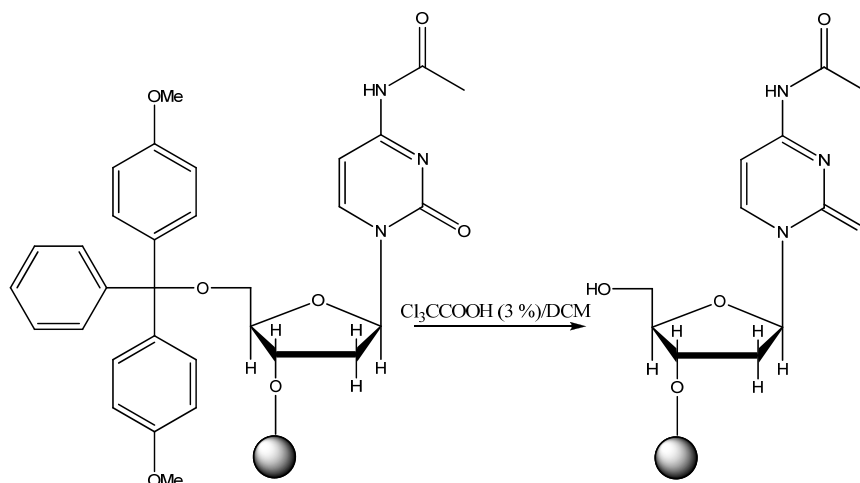
Scheme 1.2: Deprotection of dimethoxytrityl cation, liberating free 5'-hydroxyl for coupling to second base of sequence.

i. Deprotection

The solid supports, whether standard or universal, are functionalised with a dimethoxytrityl protected alcohol. The dimethoxytrityl group is readily hydrolysed under acidic conditions [23] [33] and indeed is quantitatively removed using 3 % trichloroacetic acid in DCM (Scheme 1.2). [34] The resulting dimethoxytrityl cation is bright orange with a high molar extinction coefficient allowing in-line monitoring of reaction progress as it gives an indication of the preceding coupling efficiency. The free 5'-hydroxyl is then available to react with the second base of the sequence.

ii. Coupling

The second base, with the 5'-alcohol protected as a dimethoxytrityl ether, is supplied as an anhydrous solution of phosphoramidite (Figure 1.11) and is activated by a weak acid, traditionally tetrazole. [19] [35] Recently, it has become more
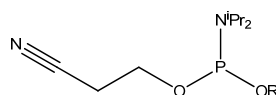
Figure 1.11: Alkyl phosphoramidite routinely employed as monomer in oligonucleotide synthesis, where "R" is a protected nucleoside. Note, in the case of 5'-modified oligonucleotides R can be from any alcohol and terminates the cycle.

commonplace for a tetrazole derivative (*5*-benzylthiotetrazole, BTT or 5-ethylthiotetrazole, ETT) to be used as the transport of tetrazole is problematic and it suffers solubility problems. The phosphoramidite and tetrazole derivative are introduced to the column sequentially, the activated phosphoramidite then couples with the free 5'- hydroxyl of the preceding nucleotide. The product of this reaction is a dinucleotide with the 5'-OH of the immobilised nucleotide linked to the 3'- OH of the second by a phosphite link (Figure 1.12). The coupling step proceeds with > 98 % efficiency. [36] The only major side-reaction, phosphitylation of the O^6 position of guanosine is fortuitously reversed during the capping step of synthesis. [37]

iii. Capping

The coupling step proceeds with > 98 % efficiency [36] leaving the remaining 1 - 2 % of molecules with a free 5'-hydroxyl group. These unreacted groups are capped to prevent further reaction, minimizing the complexity of failure sequences. The 5'-OH is acetylated by acetic anhydride in THF/pyridine solution, catalysed by *N*-methylimidazole (Figure 1.13). As noted in the previous section, the capping step also reverses any phosphitylation of the O^6 position of guanosine providing *N*-methylimidazole is used as the base. [37]
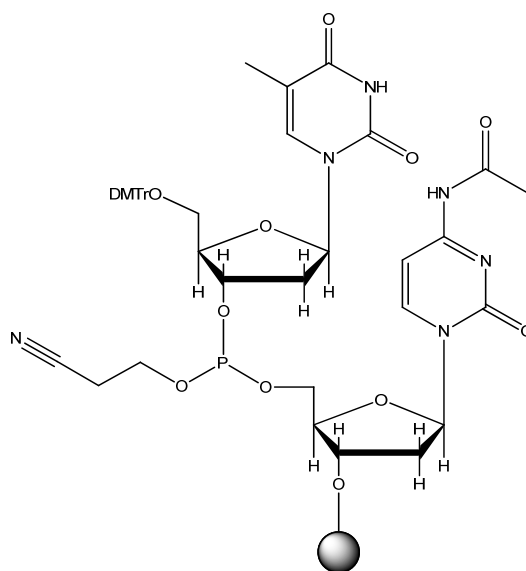
Figure 1.12: Typical phosphite triester linked dinucleotide after coupling step of synthesis cycle.
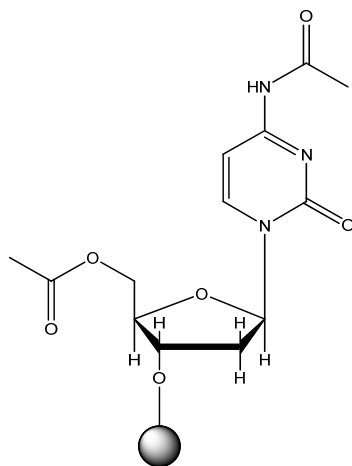
Figure 1.13: The uncoupled nucleotide is acetylated to prevent reaction during the next synthesis cycle.

iv. Oxidation

The final stage of the cycle is the oxidation from the reactive P^{III} phosphite triester intermediate to a pentavalent phosphotriester (Figure 1.14). The oxidation is achieved by an I_2/THF/water solution with pyridine added to neutralize liberated HI. [38] [39]
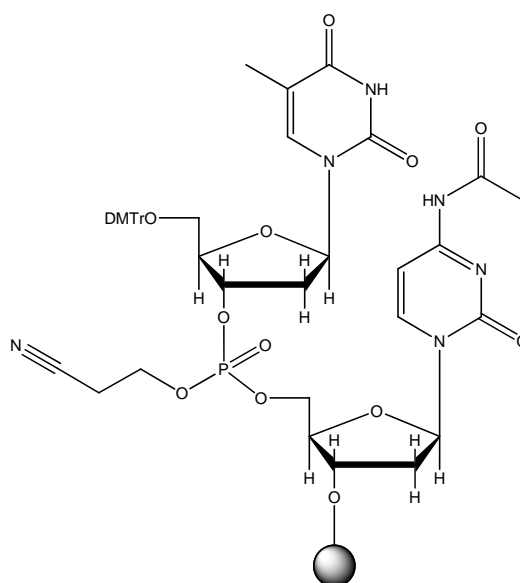
Figure 1.14: Oligonucleotide dimer as produced by an automated DNA synthesizer with DMTr protected 5'-hydroxyl ready for the next cycle.

After oxidation the next cycle is undertaken and is repeated until the sequence of desired length is prepared. Whether the final DMTr is left on the 5'-end of the oligonucleotide is at the discretion of the operator and usually depends upon the purification method (as covered in section 1.1.6).

Chemical synthesis by the phosphoramidite method traditionally occurs in the 3'- to 5'- direction. In some cases it may be desirable to synthesise chemically from the 5'- to the 3'- in which case the same cycle is undertaken using reverse monomers. That is, a series of DMTr protected 3'- and phosphitylated 5'-phosphoramidites. [40] Reverse monomers and subsequently reverse synthesis is more expensive than standard and is used only in special circumstances.

1.1.4 (d) Cleavage and Deprotection

Once the desired sequence has been generated the columns are removed from the synthesiser. The sequences are cleaved from the solid support by treatment with conc. ammonium hydroxide at room temperature for 1 h. However, to deprotect the phosphorus *via* β-elimination of the cyanoethyl group and to remove the protecting groups from the exocyclic amines of the nitrogenous bases treatment with ammonium hydroxide is required, typically at 55 °C for 16 h. When employing mild protection strategies for the nitrogenous bases lower treatment times and temperatures are possible along with alternative deprotection agents. [41], [42]

1.1.5 DNA Modification

It is often desirable to modify synthetic DNA with surface attachment groups, fluorescent tags *etc*. for use in molecular beacons, [43] DNA microarrays, [44] PCR [17] amongst other applications. Synthetic DNA can be readily modified at the 5'-, 3'- or mid-sequence sites as well as at the sugar and backbone. Sugar and backbone modifications are usually employed to confer extra stability, either thermal or nuclease, to the oligonucleotide sequence.
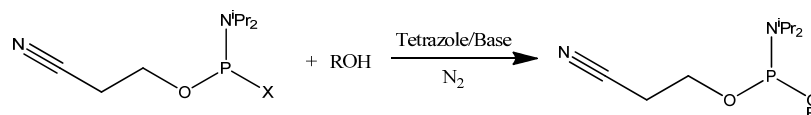
Scheme 1.3: Phosphitylation of an alcohol for incorporation as the last "monomer" of a synthetic cycle, where R could be a fluorescent label, or other functional group for derivatisation. X is either another diisopropylamino group (in which case the activator tetrazole is used) or a chloride (in which case the reaction is carried out in the presence of a hindered base).

1.1.5 (a) 5'-Modification

5'-Modification is, perhaps, the most common method of modifying a DNA sequence. It involves the preparation of a modified phosphoramidite which is then incorporated as the terminal "base" of the sequence. As an extension of Caruthers' original phosphoramidite approach, [19] most alcohols can be incorporated into an oligonucleotide sequence by phosphitylation. Some common modifications (amino, thiol, dye labels *etc.*) are commercially available as phosphoramidites and are easy to use. Alternatively, a wider variety of modified phosphoramidites can be prepared in the laboratory.

1.1.5 (b) 3'-Modification

With synthetic DNA the 3'-end is attached to the controlled pore glass (CPG) beads within the reaction column. It follows, therefore, that functionalisation of the groups on the CPG will allow modification at the 3'- end of the oligomer, providing a DMTr-protected alcohol is present which allows subsequent oligonucleotide synthesis. [45] Solid phase synthesis of 3'-modified oligonucleotides can be readily achieved. Simple, easily derivatised columns are also commercially available. An example of this is CPG beads with both DMTr protected hydroxyl and Fmoc protected amino groups on the same carbon chain (Figure 1.15). Other examples include columns pre-functionalized with fluorescent probes, or protected thiols. This type of support is called a universal support and the first base of the DNA must be added by the synthesizer to generate the desired sequence.
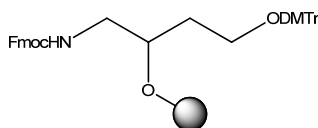
Figure 1.15: An example of a CPG functionalized for 3'-modification.

1.1.5 (c) Mid-Sequence/Base Modification

As well as at the termini of the sequence, DNA can also be modified at mid-sequence sites. There are a variety of methods by which a base can be functionalized for mid-sequence modification. Of these, perhaps, the most popular is utilizing 5'-iodouridine, a derivatised nucleoside capable of undergoing a Sonogashira reaction [46] with a suitable alkyne yielding a modified base ready for phosphitylation (Figure 1.16). [47] The 3'-OH is phosphitylated ready for coupling to the previous base after which the 5'-DMTr is deprotected in the standard fashion for subsequent base addition. [48]

1.1.5 (d) Sugar Modification

Modification of the sugar in an oligonucleotide sequence has been studied as a means of improving thermal stability and resistance to nucleases. One of the most famous examples of this are locked nucleic acid (LNA) oligonucleotides which show
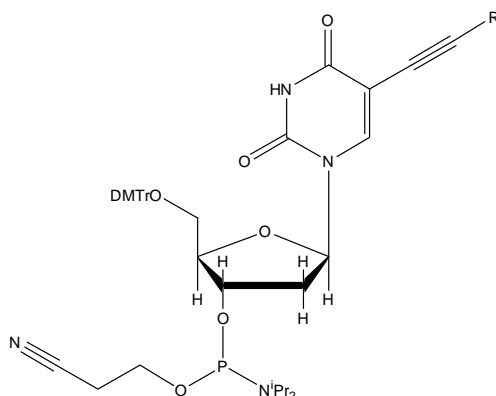
Figure 1.16: Generic mid-sequence modified phosphoramidite. R could be a fluorescent tag, surface binding group or simply a protected amino group.
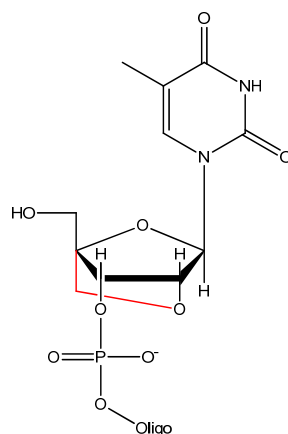
Figure 1.17: Locked nucleic acid (LNA) where the 2'-hydroxyl of the ribose sugar is bridged to C-4 by a methylene group (shown in red).

very high binding affinities to complementary nucleic acids sequences. [49] LNA differs from DNA in that the 2'-OH is bridged, through a methylene unit, to the C-4 of the ribose sugar (Figure 1.17). The synthesis of LNA sequences occur in the same manner to DNA synthesis, replacing DNA phosphoramidites with LNA analogues. However, LNA phosphoramidite chemistry is heavily licensed and, as such, their synthesis is expensive.

1.1.5(e) Backbone Modification

One method of backbone modification investigated has been the replacement of the charged oxygen of the backbone with a sulfur atom, producing phosphorothioates (Figure 1.18). [50] These can readily be prepared by swapping the oxidising reagent on a DNA synthesiser with a sulfurising agent, 3-ethoxy-1,2,4-dithiazoline-5-one, (EDITH). The phosphorothioate linkage of the modified oligonucleotide prevents the backbone of the probe from entering the active site of nucleases, producing a probe of enhanced stability.
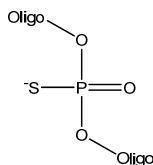
Figure 1.18: A phosphorothioate linkage, in which the O⁻ is substituted by sulfur.

1.1.6 DNA: Purification

Having synthesized a sequence of oligonucleotide it is important to purify the sequence; removing, predominantly shorter, failure sequences. The main separation and analytical techniques used for oligonucleotides are polyacrylamide gel electrophoresis (PAGE) and high performance liquid chromatography (HPLC): ion-exchange, reversed phase and size exclusion.

1.1.6 (a) Polyacrylamide Gel Electrophoresis (PAGE)

Polyacrylamide Gel Electrophoresis (PAGE) is a technique for the purification of oligonucleotide sequences of varying length. [51] The most common format has the polyacrylamide gel held between two glass plates with a buffered electrolyte solution on the top and bottom through which an electric field is applied. It is important that the electrolytic solution is denaturing so that the DNA does not form secondary structures which can affect its mobility. PAGE works on the principle that charged molecules migrate through the gel matrix under the influence of the applied electric field. In the case of oligonucleotides, since the mass-to-charge ratio is relatively constant (each increase in mass as the result of an additional base is balanced by an increase in charge due to the phosphate that accompanies it) it is their relative size which dictates the rate at which they will progress through the medium. As such there is a separation with larger oligonucleotides retarded greatest by the gel medium and moving slowest, and lower order oligonucleotides moving fastest. The sequence does affect the mobility of the oligonucleotide but the critical factor is length. The oligonucleotides can be visualized by dye-staining, UV-shadowing and autoradiography, of which UV-staining is the easiest, most common and a photograph can be taken under UV light and kept as a record.

1.1.6 (b) High Performance Liquid Chromatography (HPLC)

Chromatography is a separation technique where an analyte, contained in a mobile phase is pumped through a stationary phase for which the components of the mobile phase have differing affinities. In the case of biomolecule separations, high performance liquid chromatography (HPLC) is used. [52] An HPLC separation method consists of passing the biological sample, in a liquid (and usually aqueous) mobile phase through a column with a stationary phase of either hydrophilic silica

particles or, for reversed phase, hydrophobic hydrocarbons. The choice of which separation method to use, is dependent up on features of the mixtures to be separated.

i. Ion Exchange HPLC

Ion exchange high performance liquid chromatography (IE-HPLC) separates analytes on the basis of charge differences. Oligonucleotides (and other biomolecules) of varying lengths, and therefore varying charges, are separated on the basis of this charge difference. The stationary phase of an ion-exchange column usually consists of agarose or cellulose beads with covalently attached charged groups. To separate biomolecules with positive charges a cation exchanger, like carboxy methyl is used. Whereas, for negatively charged biomolecules, such as oligonucleotides, an anion exchanger like diethyl aminoethyl (DEAE) is commonly used. The mobile phase will include a buffer, maintaining the pH within a suitable range for the biomolecule and the column (since high pHs will deprotonate the surface groups, rendering the column useless). A salt solution will be selected that competes with adsorbed analytes for the charged functional groups of the stationary phase. This is often introduced with a gradient, where the concentration of the salt is increased incrementally allowing the bound oligonucleotides to be desorbed consecutively according to their net charge. IE-HPLC is usually followed by a size exclusion chromatography to remove the added salts.

ii. Reversed phase HPLC

Reversed phase high performance liquid chromatography (RP-HPLC) is used to separate oligonucleotides (and other classes of biomolecules) on the basis of differences in hydrophobicity. The stationary phase usually consists of silica particles, surface modified with long alkyl chains from C_2-C_{18} (ethyl silane – n-octadecyl silane), of which, octyl silane, C_8, and n-octadecyl silane, C_{18}, are the most common. The mobile phase employs a polar solvent system with an organic solvent, such as acetonitrile or methanol mixed with an aqueous buffer system, which is selected to maintain pH. Oligonucleotides are negatively charged analytes and as such it is favourable to use an ion-pairing buffer, such as triethylammonium acetate (TEAA) (or other suitable tri-alkyl ammonium salts) to bind to the negatively charged analytes increasing their retardation by the column. TEAA is also an

attractive choice of buffer as the counter ions on the eluted oligonucleotide are volatile and can be removed in a subsequent freeze-drying step.

RP-HPLC separates analytes on the basis of their hydrophobicity, with the more hydrophobic species having a greater affinity for the column and being retarded longest. The organic component of the buffer system, *e.g.*, acetonitrile, is usually incrementally raised in concentration – a gradient elution – which when balanced correctly allows for resolved elution in minimum run time.

A particularly useful method of separating oligonucleotides is to leave the final dimethoxytrityl group "on" the last base at the last stage of the synthesis as this large hydrophobic group allows for easy separation of the full length oligonucleotide from the non-DMTr-labelled failures. The sample requires an extra deprotection step after the HPLC purification. Nevertheless, this remains an attractive option as the resolution gained vastly improves the chromatographic step. In addition, use of volatile counter ions negates a requirement for size exclusion chromatography.

iii. Size Exclusion Chromatography

Size exclusion chromatography separates molecules on the basis of size
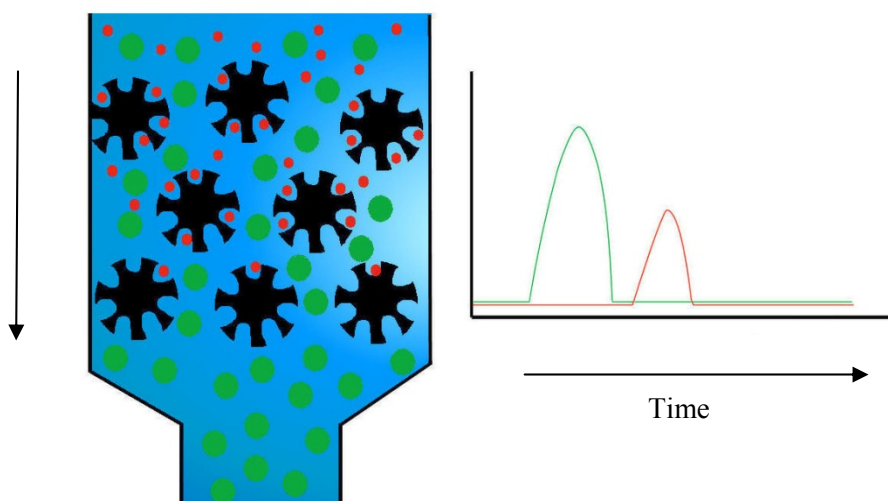
Figure 1.19: A pictorial representation of size exclusion chromatography. Large molecules are represented by green and the salt, or other small molecules, represented by red.

differences. The stationary phase is comprised of a porous material, a polymeric gel. The pore size is selected such that large molecules cannot enter. When a mixture of large and small molecules, for example, oligonucleotide and salt ions are passed through the size exclusion column, the salt ions enter the pores whilst the oligonucleotide cannot. The oligonucleotide, therefore, passes unretarded through the column and is thus separated from the salt molecules (Figure 1.19). This process, commonly employed after ion-exchange chromatography where copious salt is introduced to the sample, is often referred to as "desalting". The mobile phase, in this case, is used purely as solvent and is not involved in the separation process. Various size exclusion media can be used with molecules of varying molecular weight (related to size) and is not limited to removing salt, other small-molecule modifying groups or indeed small biomolecules can be removed in this way providing size exclusion media of the appropriate pore size is selected.

1.1.7 DNA: Duplex Stability

The UV-vis absorption characteristics of DNA provide a useful means of indicating the stability of a double stranded sequence, or duplex. Oligonucleotides absorb strongly in the UV with a sequence variable absorption maximum from 260-280 nm. The absorbance is the result of electronic transitions in the purine and pyrimidine bases. DNA in its duplex form absorbs less UV light than in the single stranded form; base-base stacking transitions result in a lowering of the absorptivity; an effect known as hypochromicity. This effect can be exploited to assess the effect of a modification on an oligonucleotide sequence, for example.
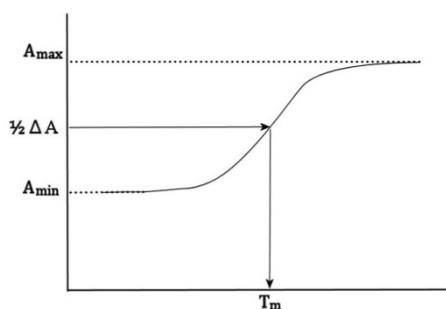
Figure 1.20: Representation of DNA melting experiment, with absorbance as a function of temperature.

Essentially, the absorption maxima is monitored as a function of temperature and the resulting curve is known as a "melting curve" (Figure 1.20). The temperature at the mid-point of the absorption transition is known as the melting temperature, T_m. The factors that affect the degree of hybridization (and thus T_m) of two strands of DNA include:

i.   **Base composition**

G·C Base pairs have three hydrogen bonds, compared with only two hydrogen bonds for A·T pairs. This results in duplexes with a high G·C content having higher melting temperatures.

ii. **Temperature**

The association of two strands of DNA into a duplex is a function of temperature. At low temperatures the re-association rate is determined by the difference in free energy between the unassociated and transition state. At high temperatures, the stability of the duplex is reduced to the point of being unstable and the hybrid melts *i.e.* re-association is reduced to the point of being non-existent at high temperatures.

iii. **Cation concentration**

Cations help to stabilize the duplex form of DNA, as such, lower salt concentrations result in lower melting temperatures. Although divalent cations offer a pronounced stabilization of the duplex they are less commonly used in hybridization studies with sodium chloride the most prevalent choice.

iv. **Sequence length**

For DNA hybrids shorter than a few hundred base pairs the melting temperature is length dependent. Use of tetramethylammonium chloride (3 M TMAMC) renders the T_m independent of base composition and therefore directly proportional to its length.

v.   **Modification**

Modification of one (or both) of the sequences involved in the hybrid can cause either an enhancement or reduction in duplex stability. The result in either case is a change of melting temperature. Modified duplexes can be melted and compared with unmodified sequences in order to ascertain the effect of the modification on duplex stability.

1.1.8 Biotechnology

Since the fundamental role of DNA to life itself has been established there has obviously been a remarkable level of research undertaken. The areas of molecular biology and genetics were realized and their impact on the understanding of life, the role of hereditary and the cause of disease has been pivotal to the development of medical care and diagnosis. The study of the chemical synthesis of DNA has spawned the biotechnology industry and leads continued research towards improved health and the application of genetically modified species. To comment on all these developments is beyond the scope of this thesis. Instead, a particularly interesting facet of the developing technology has been the merge of DNA chemistries with nanotechnology.

1.2 Bio-Nanotechnology

In his visionary, "Plenty of Room at the Bottom", speech of 1959 the physicist Richard P. Feynman outlined the, then unnamed, field of nanotechnology. [53] In it, he made the key differentiation between the "top down" approach and the "bottom up"; arguing that the "bottom up" was far more favourable. He asked "Why cannot we write the entire 24 volumes of the *Encyclopaedia Britannica* on the head of a pin?"; postulating this would be possible in a future of manipulating objects on the atomic scale. He made the connection between the "marvelous biological system" and organization on the nanoscale, suggesting that manipulating objects on the atomic scale and improving the electron microscope sufficiently would allow us to probe the key problems of biology. The link between biology and nanotechnology was thus introduced prior, even, to the technology that would facilitate their interaction. It is certainly true that technology took some time to catch up with Feynman's vision. Indeed, it wasn't until 1974 that the term "nanotechnology" was coined by Norio Taniguchi. The term is now generally accepted to describe the manipulation of objects with at least one facet on the scale $1 - 100$ nm.

Over the same time-frame organic synthesis matured into a sophisticated discipline capable of preparing macromolecules as well as modifying and

synthesizing bio-macromolecules. In fact, these two disciplines, bio- and nano-, technology now met on the nano-scale.

Attractive materials of the "bottom-up" approach should fulfil some specific criteria; they should contain intrinsic functionality for exploitation such as steric, optical or electronic properties, they should be programmable in a reproducible manner and/or they should bridge the gap from "small-molecule" organic synthesis to that of photolithography *i.e.* 10-100 nm. Biomolecular species such as proteins and nucleic acids were found to intersect at the desired dimensions with colloidal, metallic nanoparticles and semi-conductor quantum whilst fulfilling the desired criteria. The focus of this report will be on the convergence of Au and Ag metallic nanoparticles (NP) with biomolecules.

1.2.1 Gold Nanoparticles - History

Gold nanoparticles have distinctive colorimetric properties that were used in antiquity to colour glass and ceramics. A famous, and informative, example of this is the Lycurgus cup (Figure 1.21), made in the 5th-4th century B.C.E. [54] The Lycurgus cup appears red in transmitted light and green in reflected light, a
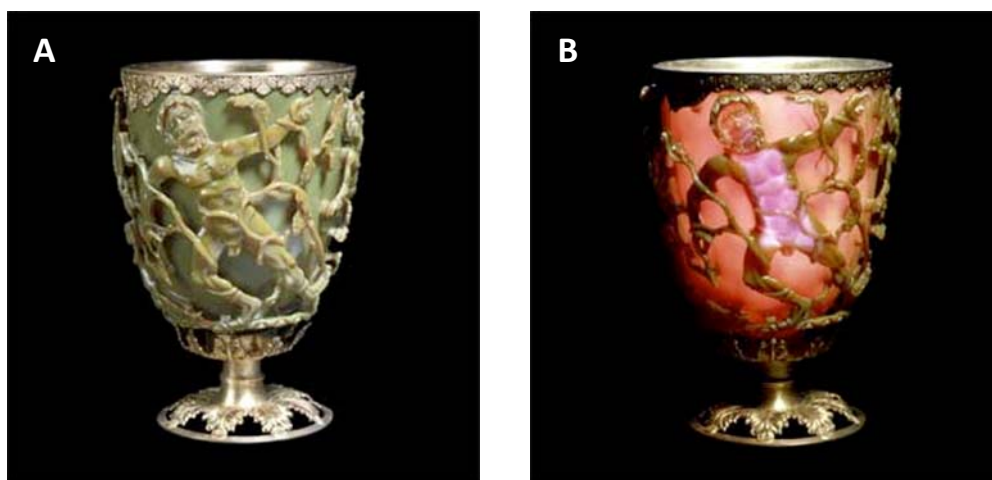
Figure 1.21: The Lycurgus cup, held in the British Museum. It is coloured by colloidal gold, which appears green, in reflected (A), and red, in transmitted light (B).© Trustees of the British Museum. [54]

colorimetric property of the nanoparticles, dispersed within the glass. This property is exploited by scientists in the modern day. However, the Lycurgus cup was not made "scientifically". A brief historical perspective of gold colloids was provided by Daniel and Astruc in their 2004 Chemical Review. [55] In which they reported that gold colloids were used throughout the middle ages for their curative powers that are detailed in a book dedicated to colloidal gold in 1618. Further reported examples of the use of colloidal gold occur during the 16th and 17th century with the colorimetric properties being described as a consequence of the degree of "subdivision" of the gold in solution. Nevertheless, it is Michael Faraday who, reporting in 1857 the formation of the characteristic deep-red solution of gold colloid by aqueous reduction of chloroaurate, is widely attributed with publishing the first paper on gold colloid synthesis. [56] In this first paper he observed the reversible nature of the colorimetric change in films of the colloid upon mechanical compression.

1.2.2 Gold Nanoparticles - Synthesis

In 1951 Turkevitch reported a method of gold nanoparticle synthesis involving the aqueous reduction of $HAuCl_4$ by sodium citrate (Scheme 1.4). [57] Frens, in 1973, reported an alteration of the original Turkevitch citrate method whereby altering the trisodium citrate to gold ratio led to monodisperse nanoparticles of desired size in the range 16 – 147 nm. [58] This method is still used to prepare gold nanoparticles of predictable size with a loose ligand shell. [59] [60] Although thiol-gold adsorption was a well-studied phenomenon, [61] [62] the use of gold-thiol chemistry to stabilize gold nanoparticles was not reported until 1993. [63] Mulvaney was also the first to show two-dimensional ordering of gold colloid. This was achieved by electrophoretic
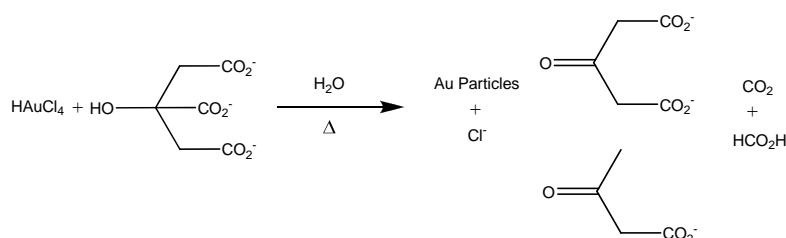
Scheme 1.4: Gold nanoparticle synthesis by citrate reduction.

immobilization of the alkanethiol coated colloid. Following shortly thereafter, in 1994, was a two-phase sodium borohydride reduction, the Brust-Schiffrin method, that also exploited the established gold-thiol surface chemistry in preparing direct thiol-derivatised gold nanoparticles. [64] [65]

Nanoparticles of predictable size, suitable monodispersity and relative stability can thus be prepared in the size range of 1-100 nm. This size range falls between the realms of individual atoms and aggregates that are large enough to be considered "bulk" material. The physical properties of these nanomaterials are not like those displayed by the bulk or of molecular compounds. Their properties are influenced by their composition, particle size, shape, inter-particle distance and the nature of surface adsorbate.

1.2.3 Gold Nanoparticles - Structure

Challenges facing the elucidation of the structure of gold nanoparticles include: the difficulty in obtaining a suitably homogenous sample that will allow representative structure determination by X-ray crystallography; and the nature of the gold-sulfur bond which, although not yet fully understood, is considered to be mobile, which hinders structural analysis. Nevertheless, Jadzinsky *et al.* [66] were able to prepare, and determine the structure of, *p*-mercaptobenzoic acid (*p*-MBA) capped gold nanoparticle crystals (15 crystals were screened with the same gold-thiol values). The structure was found to be comprised of 102 Au atoms surrounded by 44 *p*-MBA molecules. It is proposed that this particular arrangement is promoted by electronic shell closing, such that each gold atom contributes one valence electron (with 44 of them involved in bonding to sulfur) thus leaving 58 electrons, which is a well-known filled shell.

1.2.4 Gold Nanoparticles - Optical Properties

When light interacts with nanoparticles a surface plasmon oscillation is induced. That is, the conduction electrons of the particle move under the influence of the incoming electromagnetic field (Figure 1.22). The result of this is a net displacement of the negative charge from the positive (heavier) core causing a charge difference
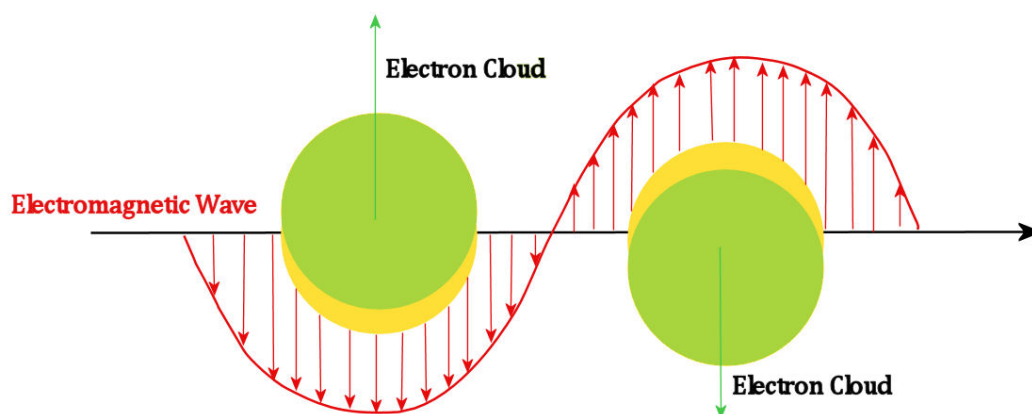
F igure 1.22: Depiction of nanoparticle plasmon resonance as induced by electromagnetic irradiation.

across the nanoparticle. A restorative force is invoked and a dipolar oscillation is created. This is known as the surface plasmon oscillation and, for gold nanoparticles (15 nm diameter), is induced by the interaction with light of a wavelength centred at 520 nm. The characteristic plasmon resonance band of gold nanoparticles is thus centred at 520 nm.

The nature of the surface plasmon band was rationalized by Mie in 1908 when he solved Maxwell's equations for spherical particles with a diameter smaller than the wavelength of interrogating light. [67] Mie attributes the plasmon band of spherical particles to the dipole oscillations of the free electrons in the conduction band occupying energy states immediately above the Fermi energy level. Independent experimental analyses have found particles of the appropriate size range (5-100 nm) and shape (spherical) to be in agreement with Mie's solutions. [68] [69]

The surface plasmon band is affected by the size and shape of the particles as well as the dielectric constant of the surrounding medium and the temperature. [70] The surface plasmon oscillation is dramatically altered in situations where discrete nanoparticles are brought into close proximity with one another. This is significant where the cluster-cluster distance is less than, or equal to, five times the radius of the

A'B'
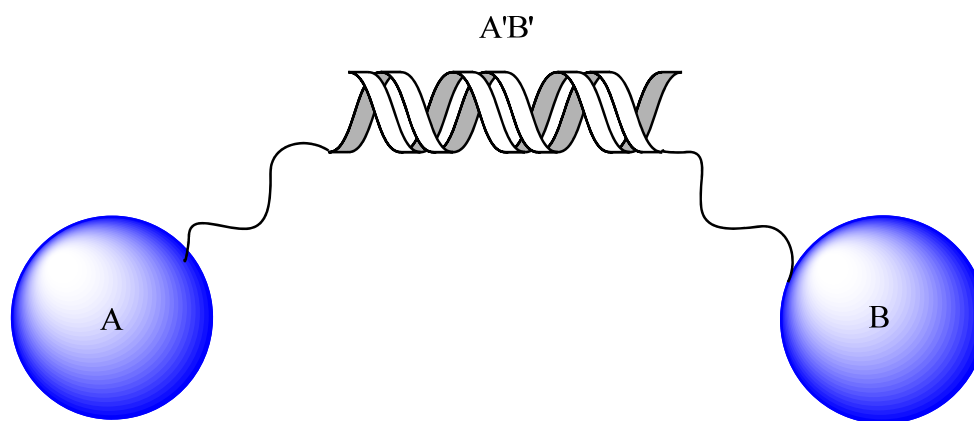
Figure 1.23: Representation of a head-to-tail oligonucleotide nanoparticle conjugate hybridization induced aggregation. Where "A" and "B" denote nanoparticles with different non-complementary sequences and "A'B'" denotes the target sequence with regions complementary to both nanoparticle probes with which a duplex is formed. Note the colour blue is used to emphasise the blue colour of the nanoparticles in the aggregate state.

particles. The result of aggregation is the coupling of individual nanoparticle plasmons which results in a broadening and red-shifting of the longitudinal plasmon by up to 250 nm. [70] [71] The resulting nanoparticle suspension (Au, 15 nm) appears blue to the eye and absorbs, broadly, in the region 600 to 750 nm.

1.2.5 Gold nanoparticles and DNA

It was in 1996 that two groups independently reported the exploitation of thiol-Au NP surface chemistry by immobilising thiol-modified oligonucleotide sequences on gold nanoparticles. [72] [73] These reports of oligonucleotide-nanoparticle conjugate preparation represented a significant step forward in "nano-bio" methodology. A biomolecular recognition event, oligonucleotide hybridization, was manipulated to induce controlled aggregation of a AuNP-DNA system, forming discrete nanoparticle assemblies (Figure 1.23). [72] Moreover, the assembly process was reversible simply by heating above the melting temperature of the duplex and was accompanied by a significant colorimetric signalling change, creating a new avenue for bioanalytical detection. [73]

1.2.6 Gold Nanoparticle-DNA Conjugates – Materials Science

Alivisatos' group controlled the stoichiometry of oligonucleotide to gold nanoparticle in a 1:1 ratio. Both 3'- and 5'- thiol modified oligonucleotide probes were prepared and immobilized on nanoparticle substrates with sequences chosen that had no complementarity for each other. A target sequence was devised that had regions complementary to both probe systems. When introduced under hybridization conditions, controlled aggregation occurred, as a result of DNA duplex formation. Different probe/target systems were prepared to produce both "head to head" and "head to tail" dimeric and a trimeric arrangement of the nanoparticles. These conjugates were purified by gel electrophoresis and the predicted, "simple" structures were shown by transmission electron microscopy (TEM). [72] This result confirmed the applicability of DNA's inherent programmability to Nanoscale, "bottom up" materials synthesis strategies.

From a materials science perspective, DNA is an attractive scaffold due to the control that its complementarity affords the conjugate materials. Early publications from Alivisatos *et al.*, showed the controlled formation of nanoparticle dimers and trimers as supported by oligonucleotide scaffolds. [72] [74] DNA as a template for materials synthesis was reviewed in 1999 by Chad Mirkin. [75] Since that time when the field was in its infancy, headway has been made by various groups. Oligonucleotides were used by Niemeyer's group to assemble nanoparticles in a rational, tiered manner. [76] Control of the distance between nanoparticles by varying oligonucleotide sequence length has been used, by Alivisatos *et al.*, to establish a molecular ruler based on the plasmon coupling of nanoparticles. [77] DNA, immobilized on a silicon wafer was used to electrostatically guide gold nanoparticles in a controlled manner allowing the formation of a nanowire. [78] Recently, as shown independently by two groups, oligonucleotide sequences have been used to guide nanoparticle "crystallisation" as desired in 3-dimensions. [79] [80] Additionally, selective manipulation of DNA-nanoparticle conjugates by DNA processing enzymes has been shown to be effective, thereby providing tools with which to control materials science assemblies. [81]
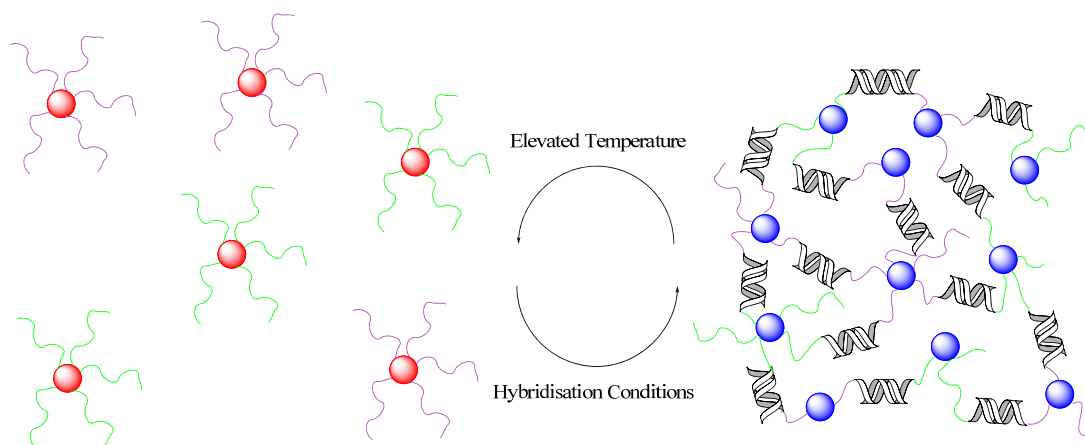
Figure 1.24: Schematic representation of hybridization-induced aggregation of gold nanoparticles.

1.2.7 *Gold Nanoparticle-DNA Conjugates – An Analytical Tool*

Mirkin's group, on the other hand, added an excess of thiol-modified oligonucleotide probe to the AuNPs during conjugate preparation. [73] This resulted in each nanoparticle bearing multiple oligonucleotides. Two probes, non-complementary to one another, were separately conjugated with nanoparticles generating two distinct batches of probe conjugate. These non-complementary conjugates were added together and a "target" sequence was introduced which was composed of regions complementary to each of the probe systems. Under hybridization conditions, aggregation of the nanoparticles was observed, as a result of duplex formation (Figure 1.24). A colorimetric change of the conjugates was observed from red to blue as the nanoparticles move from discrete particles to an aggregated network. The proximity of particles induces a coupling of the surface plasmons and a distinctive red-shifting of the spectra. As such, the hybridization process was monitored by UV-vis spectroscopy at 700 nm (aggregate plasmon maxima) and plotted against temperature as *per* a standard UV-melting experiment (see Section 1.1.7). The aggregation process was shown to be reversible as heating above the melting temperature caused denaturing of the duplex and re-separation of the probe conjugates. [73] In addition the melting transition process occurred over a greatly reduced temperature range giving a particularly sharp melting temperature profile. [82]

The advantage of having such a sharp melting transition compared with unconjugated duplex melting experiments is that single nucleotide polymorphisms (SNPs) can easily be detected by UV-vis spectroscopy. Upon further investigation, it was observed that the melting temperature of the conjugate system resulting in the colorimetric change, T_C was close to, but not equal to, the melting temperature of the duplex, T_m. [82] [83] A thorough investigation revealed a number of factors that contribute to DNA-NP conjugate melts: [84] [85]

i. **Oligonucleotide density on Au NP surface**

   T_m decreases with decreasing surface density

ii. **Au nanoparticle size**

   T_m decreases with increasing particle size

iii. **Salt concentration**

   T_m decreases with decreasing salt concentration

iv. **Inter-particle distance**

   T_m decreases with decreasing inter-particle distance

In an analytical sense the conjugation of DNA with gold nanoparticles proved particularly effective. Published in Science in 1997, [82] Mirkin *et al.* showed the efficacy of the DNA-nanoparticle conjugate system for detecting single nucleotide polymorphisms. Whereas nucleic acid diagnostics is a field dominated by fluorescence-based assays using expensive enzyme-based amplification procedures (PCR), Mirkin's group showed that spotting 1-3 μl of the oligonucleotide-nanoparticle conjugate on a C_{18} silica plate in the presence of a target sequence makes the identification of hybridisation (or lack thereof) much simpler and a record can be kept (Figure 1.25). Upon spotting, the sample appears red when hybridization has either not occurred or when the sample is spotted at a temperature above the melting temperature of the system. Alternatively, the spot appears blue only if the complement is present and the sample is below the melting temperature at the time of sampling. This "Northwestern Spot Test" (NWST) has proven so efficacious that the difference in hybridization can be observed over a 1 °C temperature range and can detect single base mismatches. However, the NWST is unable to compete with PCR-based techniques due to its relatively high, 10 fmol limit of detection.
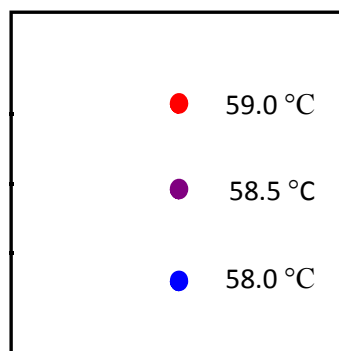
Figure 1.25: Representation of the "Northwestern spot test" in which oligonucleotide-DNA conjugates are spotted on a C_{18} silica plate at various temperatures leaving a record of the hybridization event.

Mirkin extended this methodology to a "real" target for detection. Two probes were generated that would bind to an interior region of a 141-mer Anthrax PCR product. Targeting duplex DNA requires denaturing at elevated temperatures (as would occur in T_m melting experiments) in the presence of nanoparticle immobilized probes for the interior region. Since the probe strands were shorter they were kinetically more favourable to hybridise (as opposed to *re*-hybridisation of the full length complementary strand). This was observed and the Anthrax target was detected with a blue spot observed by the "Northwestern Spot Test", a red spot was observed for the control experiment (no Anthrax present). [86]

Nevertheless, the main hurdle to enhancing sensitivity using the NP-DNA detection technique is the inability to detect NPs at lower concentrations. This, coupled with the necessity to form large aggregates to achieve a detectable colorimetric shift, limits the sensitivity of the technique. A large number of 15 nm gold particles are required to provide a measurable shift in the plasmon band. This requires, in practical terms, a molar excess of target over NPs to promote the formation of large aggregates.

A related approach reported by Storhoff *et al.* [87] afforded a limit of detection four orders of magnitude greater than the "Northwestern Spot Test". Storhoff *et al.* used 40 – 50 nm nanoparticles instead of 15 nm and utilised the efficiency of the nanoparticles to scatter light rather than absorb. Instead of spotting onto a C_{18} silica

plate and observing the reflected light from the sample, Storhoff *et al.*, spotted their oligonucleotide-nanoparticle conjugates onto a glass microscope slide. The samples were excited, by planar illumination, with white light and observed the scattering. The negative control sample showed green scatter, typical of unaggregated gold nanoparticles, whereas the conjugate in the presence of synthetic complementary target showed intense orange scattering. Assessing varying target concentrations, no more than 333 zmol of target was required to induce a colour change (to yellow) required for detection. Indeed, when the samples were spotted onto a C_{18} plate for comparison the probes could not be detected by eye as the probe concentration was only 8 pM. Even more impressive was the use of this technique to detect the *mecA* gene in unamplified clinical samples of MRSA (methicillin-resistant *Staphylococcus aureus*) with only 15 minutes of hybridisation. This set-up used 4 Au NP probes for detection and resulted in a colour change with only 33 zmol target, which equates to 20,000 copies of target in the presence of total bacterial DNA in the spotted aliquot. There was no need for amplification.

DNA-Gold nanoparticle probes have been applied to a large number of targets such as the ebola virus, HIV, anthrax, cystic fibrosis and (as mentioned above) MRSA. [87] [88] [89] All of these methods involve DNA-NP conjugates targeting a gene sequence, which has been rendered single stranded, coding for a specific disease. DNA occurs naturally in double stranded form, and recently a double stranded target was detected *via* triplex formation using LNA functionalized Au NP probes. [90] Two NP probes were designed to form a triplex with an established duplex through Hoogsteen base pairing, causing aggregation and detection in the normal fashion. In addition oligonucleotide aptamers have been raised against a variety of targets, including the protein thrombin. The aptamer sequence, immobilised on gold nanoparticles, interacts with the thrombin *via* two binding sites causing target-induced aggregation resulting in the familiar change in surface plasmon band. [91] As well as proteins, nanoparticle bound aptamers have also been exploited to detect small molecules, such as adenosine [92] and cocaine.

The ultimate aim of any research in this area is for effective clinical applications to be developed. In a letter published in *Clinical Chemistry* an argument was made

for the adoption of DNA-AuNP detection of *Mycobacterium tuberculosis* in a clinical setting. [93] A round of PCR was required first, but the experiments were fast, simple and inexpensive to run with detection achieved visually or *via* UV-vis analysis. The overall cost was given as less than $0.35 per sample (including PCR) which was reported as less than existing methods with a possible increase in clinical sensitivity.

In addition to these simple detection strategies based on the absorption or scattering of light many other methods have been used for detection using DNA-Au NPs including electrochemical sensing, [94] surface plasmon resonance (SPR), [95] and monitoring gravimetric changes *via* quartz crystal microbalance (QCM). [96] Moreover, protein targets have been detected using AuNP-DNA conjugates linked to streptavidin and bound to a biotinylated antibody. The antibody coated NPs were then used for protein detection *via* AuNP promoted silver deposition. [97] Alternative nucleic acids have been used with dye-labelled RNA-NP conjugates prepared and hybridized to DNA, the action of an enzyme chosen to digest only the RNA portion of the duplex allowed detection of the DNA sequence by separating the dye from the nanoparticle and giving a gain in fluorescence signal. [98]

1.2.8 Gold nanoparticle-DNA Conjugates: Limitations

Although there had been considerable advances in the methodology of gold nanoparticle-DNA conjugate detection systems there remained a requirement to improve the stability of the conjugates. Whilst the stability of 15 nm Au particles employed *in vitro* in idealized conditions (0.3 M PBS, pH7, moderate temperature) was reasonable, the situation worsened when moving to more strenuous conditions. It was found that larger nanoparticles, > 30 nm, for example, were less stable at elevated temperatures and under high salt conditions (0.3 – 1 M NaCl). [99] By far the greatest instability of thiol-oligonucleotide gold nanoparticle conjugates occurs in the presence of common biological buffer additives such as dithiothreitol (DTT) or mercaptoethanol. [100] These biological additives strip the thiolated oligonucleotides from the nanoparticle surface. Upon thiol desorption, irreversible aggregation occurs and the probe system is rendered inactive.
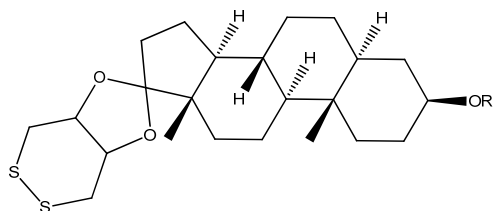
Figure 1.26: Cyclic dithiane-epiandrosterone linker for gold nanoparticle functionalisation, where R is an oligonucleotide sequence.

In order to increase the stability of the oligonucleotide-nanoparticle probes a new group for surface attachment was developed. In place of the linear alkyl monothiol linker unit, the cyclic dithiane-epiandrosterone anchor group was used (Figure 1.26). [101] Testing the stability of the new linking system was carried out by treating the oligonucleotide nanoparticle conjugates with DTT (10 mM). As the DNA was stripped from the nanoparticle surface and replaced with DTT, the nanoparticles aggregated irreversibly. This process was monitored by spotting samples of the conjugates on reversed phase TLC plates and observing the colour change. By this method it was reported that monothiol-oligonucleotide nanoparticle conjugates were fully aggregated in 5 minutes with significant aggregation occurring in the first 20 s of treatment. The steroidal disulfide linkage afforded stability that was not lost until 40-100 min after treatment. When monitoring the stability of the conjugates by UV-vis absorption, the steroidal disulfide was found to offer stability for 2 h and was completely aggregated by 6 h upon treatment with DTT (10 mM).[101]

A trithiol linker group (Figure 1.27) was also prepared and assessed for stability in the same way. The conjugates linked by the trithiol group were stable for 10 h with complete aggregation over the following 10 h.[100]
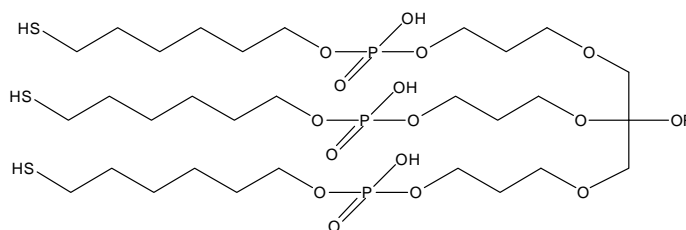
Figure 1.27: Trithiol linker group for attachment for gold nanoparticle functionalisation; where R is an oligonucleotide sequence.

Although both of these modifications result in a marked increase in conjugate stability, neither was applied to silver nanoparticles to assess for their applicability in these detection systems. In addition, they are structurally cumbersome, synthetically demanding and are not commercially available.

1.3 Surface Enhanced Resonance Raman Scattering (SERRS)

Underpinning all of the platforms for bioanalysis are the techniques with which to detect a recognition event. Techniques utilizing the strong plasmon-derived absorption of nanoparticles conjugated to oligonucleotides were discussed in section 1.2. While significant progress has been made with varied targets and increasing sensitivity, multiplexing (the detection of multiple analytes in a single pot) is not achievable due to the single colour change invoked. Multiplex analysis of DNA has been achieved by fluorescence techniques. [102] Unfortunately, fluorescence suffers from broad, overlapping spectra of molecular fluorophores, photobleaching and the requirement for multiple excitation sources. Advances have been made in the field of fluorescence detection by the development of quantum dots which are specially designed nanocrystals generated to produce a relatively narrow fluorescence emission profile coupled with a broad excitation profile. [103] However, a technique perhaps even more suited to multiplexing is surface enhanced resonance Raman scattering (SERRS) spectroscopy. [104]

1.3.1 Optical Processes

Absorption, fluorescence, Raman and other optical techniques for analysis result from the interaction of light with a sample and the ability to translate that into an informative signal. When a photon of light interacts with a molecule it may undergo one of three processes:

i. **Absorption followed by non-radiative energy loss**
ii. **Absorption followed by emission**
iii. **Scattering**
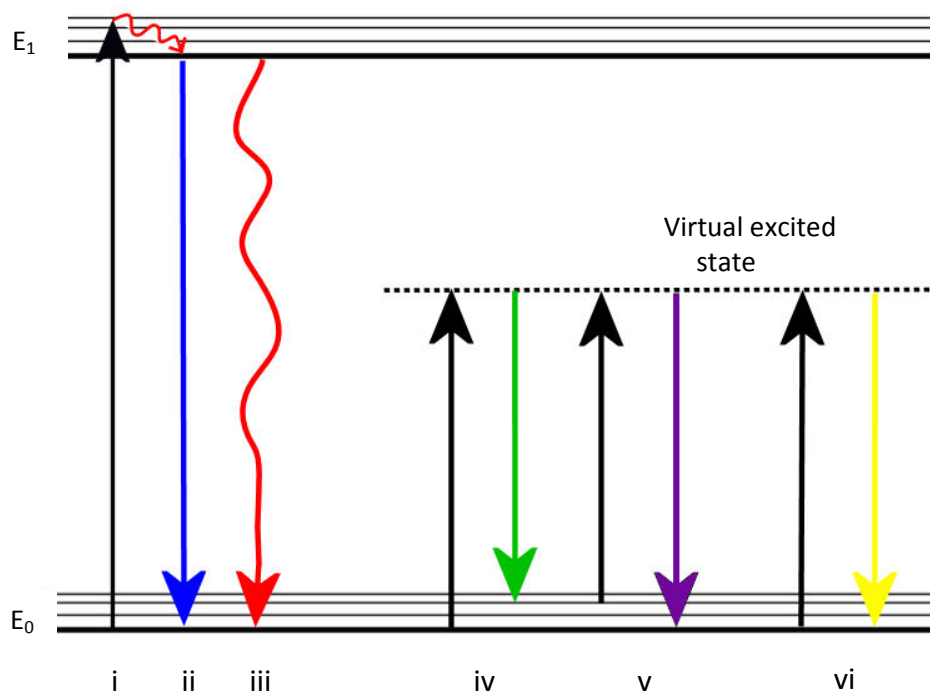
Figure 1.28: Jablonski diagram depicting the processes involved in fluorescence and Raman optical spectroscopy, where i = absorption; ii = fluorescence; iii = non-radiative decay; iv = Stokes Raman scattering; v = anti-Stokes Raman scattering; vi = Rayleigh scattering.

The absorption process can occur if the energy of the incident photon is the same as the energy difference between an occupied energy level and a vacant energy level of the molecule. Thus information can be gleaned from absorptive processes, IR spectroscopy or UV-vis spectroscopy, for example. When the absorption process is followed by emission, it may be termed fluorescence or phosphorescence (depending upon the mode of decay) (Figure 1.28).

However, when a beam of light, of given energy, interacts with a molecule most of the photons of light interact with the molecule in such a way as to distort the electron cloud surrounding the nuclei thereby causing the light to scatter. Two different scattering processes are possible. If the wavelength of scattered light is equal to the wavelength of incident light, as in most instances, the scattering is said to be elastic and is termed Rayleigh scattering. However, if the wavelength of

scattered light is different to that of the incident light, the energy will correspond to the energy difference between two vibrational levels of the molecules. This scattering is inelastic and is termed Raman scattering, first observed in 1928 by the eponymous Nobel Laureate C. V. Raman and K. S. Krishnan. [105] Only one photon in every millions is involved in Raman scattering. Two types of Raman scattering are observed, of which, Stokes is the most abundant (that is, scattered light is of lower energy than the incident). Unlike IR, Raman spectroscopy can be conducted in water (poor scatterer) although requires an analyte concentration of 10^{-3} M.

1.3.2 Resonance Raman

When the wavelength of light lies close to the absorption maxima of the molecule being interrogated, significant enhancements of the Raman signal may be observed. This is known as the Resonance Raman effect and can lead to enhancements of up to 10^4 in the intensity of the Raman signal. [106] A disadvantage of Resonance Raman is the competing fluorescence process which can swamp the Raman signal.

1.3.3 Surface Enhanced Raman Scattering (SERS)

Pronounced enhancement of the Raman process occurs when the analyte is adsorbed on a roughened metal surface. This was first observed in 1974 and is known as Surface Enhanced Raman Scattering. [107] Many metal surfaces have been investigated, of which the coinage metals – silver, gold and copper are the most effective. [108]

1.3.4 Surface Enhanced Resonance Raman Scattering (SERRS)

A combination of SERS and Resonance Raman, SERRS is an extremely sensitive analytical technique. Indeed, single molecule detection has been reported. [109] [110] SERRS was first reported in 1983 by Stacy and Van Duyne. [111] SERRS requires use of a chromophore adsorbed onto a suitably roughened metal surface. The wavelength of light is chosen to be close to the absorption maxima of the chromophore. SERRS offers an enhancement of 3 to 4 orders of magnitude over SERS, and indeed, 10^{10} enhancement over normal Raman. Of particular note is that

problems of background signal can be overcome by the presence of the metal and its ability to quench fluorescence. [112]

1.3.4 (a) Suitable Surfaces

A wide range of metallic substrates have been studied. The coinage metals Au, Ag, Cu are of the greatest practical use due to the position of their plasmon band in the visible/near IR region of the electromagnetic spectrum, suitable surface roughness and their relative stability under typical experimental conditions. [108] The roughened metal surface required for SERS/SERRS have been prepared in a variety of manners. The most commonly used substrates are colloidal suspensions of the desired metal. [58] [113] [114] [115] Colloids are attractive as they are readily prepared, relatively stable and reproducible. Colloids are inexpensive and a fresh batch can be used each time.

1.3.4 (b) SERRS for DNA Detection

Nanoparticles have found use as suitable surface enhancement substrates for SER(R)S detection strategies. SERRS has been investigated for the detection of many species such as oligonucleotides, [88] [116] [117] [115] proteins, enzymes [118] and small molecules. [119] [120] Nanoparticles have also been exploited, due to strong proximity-dependent plasmon resonance absorption profiles, in the detection of biological events, such as DNA hybridization, [72] [73] protein-aptamer recognition, [91] and antibody-antibody interactions. [97] A natural progression, therefore, was the combination of these methodologies to create a nanoparticle-based SERRS platform for biological analysis.

To achieve meaningful SERRS spectra of dye labelled oligonucleotides not only must a dye be selected and matched with an appropriate excitation source, but a suitable surface must be used which complements not only the dye but the wavelength of excitation. [115] Lastly, to achieve sensitive SERRS detection aggregation of the colloid must be achieved. This process is necessary to generate "hot spots" at the interstices of the aggregated particles from which the SERRS response is greatest. [121] [122] This introduces an added variable to the assay system;

that of dynamic aggregation which must be controlled in order to achieve linearly concentration dependent results *i.e.* quantitation. [117]

SERRS has been shown to have huge potential for the detection of dye labelled oligonucleotides. In a comprehensive "proof of principle" investigation Faulds *et al.* showed that direct quantitative detection of dye labelled oligonucleotides was possible and was, in some circumstances, more sensitive than fluorescence. [117] This involved detection of various concentrations of dye labelled oligonucleotides. By doing this, the SERRS conditions for dye-labelled oligonucleotide detection were fully optimized and the systems rendered quantitative. Of course, in a practical situation the oligonucleotide target of an assay would not be dye labelled. The target would, instead, be completely unmodified and a hybridization event to probes designed to seek a specific sequence and that simultaneously bear a uniquely identifiable label would be used.

Mirkin has used SERRS to detect various disease coding sequences, including (amongst others): hepatitis A virus, human immunodeficiency virus (HIV), ebola virus and variola virus (smallpox). [88] A "capture" probe was immobilized on a glass slide and was hybridized, in a sandwich assay *via* the unmodified target, with a "reporter" probe which contained a SERRS active dye and a gold nanoparticle at the terminus. Colloid aggregation could not be achieved in order to induce the "hot spots" necessary for SERRS enhancement; therefore, silver deposition was carried out across the surface which provided signal enhancement. In the absence of target the dye-labelled nanoparticle tethered probe would not be adhered to the slide and no SERRS was observed. Eight disease coding sequences were evaluated, each with a unique SERRS reporter dye. It was possible, due to the information-rich SERRS spectra obtained, to identify which particular disease target sequence (or combination thereof) was present.

Vo-Dinh reported the use of SERRS to detect the *BRCA1* breast cancer gene using a silver metal film as the enhancing surface. [116]

Investigations by Stokes *et al.* greatly increased the understanding of SERRS as applied to DNA detection by systematically investigating the detection of numerous

dye labelled oligonucleotides, on both gold and silver colloids, at three different wavelengths. [115] This extended the methodology of SERRS for DNA detection, which had largely been applied to silver colloids, to gold colloids. This is advantageous since gold nanoparticles are more attractive substrates for biological analysis. In addition, the grounds for easily multiplexed detection systems by SERRS were established.

Whilst the publication of Mirkin and co-workers [88] was certainly an impressive foray into the field of SERRS for multiplexed bio-detection it required a complex experimental setup. The work of Faulds et al. [117] certainly showed the powerful nature of SERRS when applied to DNA detection but required the control of a dynamic aggregation event to be quantitative. In addition, the work of Faulds et al. was concerned with the direct detection of dye-labelled DNA which is not representative of the end point of an assay.

Neither work harnessed the organizing ability of DNA to aggregate nanoparticles, thereby generating the "hotspots" that allows SERRS detection of a DNA target. In a letter published in *Nature Nanotechnology*, [123] work conducted by D. Thompson at the University of Strathclyde did just that. Two batches of silver nanoparticles were dye-coded and then functionalized with non-complementary probe sequences of thiol-modified DNA. In a fashion analogous to the oligonucleotide-gold nanoparticle hybridisation systems discussed in Section 1.2.7., hybridisation-induced aggregation with a target complementary to both probes allowed detection by SERRS. This was made possible by the inclusion of a dye on the nanoparticle surface. In the absence of target, and therefore hybridization-induced aggregation, the SERRS response from the dye was minimal. However, in the presence of target DNA, the SERRS signal was greatly enhanced due to the aggregation development of "hot spots". [123]

1.4   Introductory Conclusions

The development of oligonucleotide-nanoparticle conjugates and their application to the field of bio-diagnostics has been significant for bioanalytical

chemistry. As discussed, they have been applied in a variety of detection systems to good effect. Increasingly, though, there is a need to develop oligonucleotides probes for increasingly demanding environments – PCR, complex assays and within cellular environments. This leaves a gap in which to develop more stable oligonucleotide-nanoparticle conjugates.

1.5 Chapter 1: References

1.   Watson, J. D. and Crick, F. H. C., **1953**, *Nature*, 171, 737-738.

2.   Watson, J. D. and Crick, F. H. C., **1953**, *Nature*, 171, 964-965.

3.   Watson, J.D. and Crick, F. H. C., **1954**, *Proc. R. Soc. A*, 223, 80-96.

4.   Watson, J. D., *DNA - The Secret of Life.* London: Random House, **2003**.

5.   Schrödinger, E., *What is Life?* Cambridge: Cambridge Unversity Press, **1944**.

6.   Morange, M., *A History of Molecular Biology.* Cambridge, MA: Harvard University Press, **1998**.

7.   Gulland, J. M., Jordan, D. O., Taylor, H. F. W., **1947**, *J. Chem. Soc.*, 1131-1141.

8.   Franklin, R. E., Gosling, R. G., **1953**, *Nature*, 171, 740-741.

9.   Wilkins, M. H. F., Stokes, A. R., Wilson, H. R., **1953**, *Nature*, 171, 738-740.

10.   Bloomfield, V. A., Crothers, D. M., Tinoco Jr., I., *Nucleic Acids: Structures, Properties and Functions.* Sausalito, CA: University Science Books, **2000**.

11.   Blackburn, G. M., Gait, M. J., Loakes, D., Williams, D. M., *Nucleic Acids in Chemistry and Biology.* 3rd Ed., Cambridge: The Royal Society of Chemistry, **2006**.

12.   Strock, Michael., Image: DNA Overview. *Wikipedia.* [Online] [Cited: 11 09 2009.] http://en.wikipedia.org/wiki/Image:DNA_Overview.png.

13.   Crick, F. H. C., **1958**, *Symp. Soc. Exp. Biol. XII*, 139-163.

14.   Crick, F. H. C., **1970**, *Nature*, 227, 561-563.

15.   Glitz, D., *Textbook of Biochemistry With Clinical Correlations*. [ed.] Devlin, T. M., 5th Ed., **2002**, 233-273.

16.   Manz, A., Pamme, N., Lossifidis, D., *Bioanalytical Chemistry*. London: Imperial College Press, **2004**, 156-167.

17.   Saiki, R. S., Bugawan, T. L., Horn, G. T., Mullis, K. B., Erlich, H. A., **1986**, *Nature*, 324, 163-166.

18.   Michelson, A. M., Todd, A. R., **1955**, *J. Chem. Soc.*, 2632-2638.

19.   Beaucage, S. L., Caruthers, M. H., **1981**, *Tetrahedron Lett.*, 22, 1859-1862.

20.   McBride, L. J., Caruthers, M. H., **1983**, *Tetrahedron Lett.*, 24, 245-248.

21.   Matteucci, M. D., Caruthers, M. H., **1981**, *J. Am. Chem. Soc.*, 24, 3185-3191.

22.   Weimann, G., Khorana, H. G., **1962**, *J. Am. Chem. Soc.*, 84, 419-430.

23.   Smith, M., Rammler, D. H., Goldberg, I. H., Khorana, H. G., **1961**, *J. Am. Chem. Soc.*, 84, 430-440.

24.   Schaller, H., Weimann, G., Lerch, B., Khorana, H. G., **1963**, *J. Am. Chem. Soc.*, 85, 3821-3827.

25.   Schulhof, J. C., Molko, D., Teoule, R., **1987**, *Nucleic Acids Res.*, 15, 397-416.

26.   Vu, H., McCollum, C., Jacobson, K., Theisen, P., **1990**, *Tetrahedron Lett.*, 31, 7269-7272.

27.   Gillet, L. C. J., Alzeer, J., Scharer, O.D., **2005**, *Nucleic Acids Res.*, 33, 1961-1969.

28.   Tener, G. M., **1961**, *J. Am. Chem. Soc.*, 83, 159-168.

29.   Letsinger, R. L., Ogilvie, K. K., **1969**, *J. Am. Chem. Soc.*, 91, 3350-3355.

30.   Gough, G. R., Brunden, M. J., Gilham, P. T., **1981**, *Tetrahedron Lett.*, 22, 4177-4180.

31.   Edenberg, H. J. *Textbook of Biochemistry with Clinical Correlations.* [ed.] Devlin, T. M., 5th Ed., New York: Wiley-Liss, **2002**.

32.   Reese, C. B., **2005**, *Org. Biomol. Chem.*, 3, 3851-3868.

33.   Russell, M. A., Laws, A. P., Atherton, J. H., Page, M. I., **2009**, *Org. Biomol. Chem.*, 7, 52-57.

34.   Tanaka, T., Oishi, T., **1985**, *Chem. Pharm. Bull.*, 33, 5178-5183.

35.   Berner, S., Muhlegger, K., Seliger, H., **1989**, *Nucleic Acids Res.*, 17, 853-864.

36.   Nielson, J., Taagaard, M., Marugg, J. E., van Boom, J. H., Dahl, O., **1986**, *Nucleic Acids Res.*, 14, 7391-7403.

37.   Eadie, J. S., Davidson, D. S., **1987**, *Nucleic Acids Res.*, 15, 8333-8349.

38.   Letsinger, R. L., Finnan, J. L., Heavner, G. A., Lunsford, W. B., **1975**, *J. Am. Chem. Soc.*, 97, 3278-3279.

39.   Letsinger, R. L., Lunsford, W. B., **1976**, *J. Am. Chem. Soc.*, 98, 3655-3661.

40.   Wagner, T., Pfleiderer, W., **2000**, *Helv. Chim. Acta*, 83, 2023-2035.

41.   Reddy, M. P., Hanna, N. B., Faroqui, F., **1994**, *Tetrahedron Lett.*, 35, 4311-4314.

42.   Surzhikov, S. A., Timofeev, E. N., Chernov, B. K., Golova, J. B., Mirzabekov, A. D., **2000**, *Nucleic Acids Res.*, 28, e29.

43.   Tyagi, S., Kramer, F. R., **1996**, *Nat. Biotechnol.*, 14, 303-308.

44.   Sassolas, A., Leca-Bouvier, B. D. and Blum, L. J., **2008**, *Chem. Rev.*, 108, 109-139.

45. Stetsenko, D. A., Gait, M. J., **2001**, *Bioconjug. Chem.*, 12, 576-586.

46. Sonogashira, K., Tohda, Y., Hagihara, N., **1975**, *Tetrahedron Lett.*, 4467-4470.

47. Robins, M. J., Barr, P. J., **1981**, *Tetrahedron Lett.*, 22, 421-424.

48. Cruickshank, K. A., Stockwell, D. L., **1988**, *Tetrahedron Lett.*, 29, 5221-5224.

49. Kaur, H., Babu, B. R., Maiti, S., **2007**, *Chem. Rev.*, 107, 4672-4697.

50. D.-Mesmaekder, A., Haner, R., Martin, P., Moser, H. E., **1995**, *Acc. Chem. Res.*, 28, 366-374.

51. Rickwood, D., Hames, B. D., [ed.]. *Gel Electrophoresis of Nucleic Acids - A Practical Approach.* 2nd Ed. New York: Oxford University Press, **1990**.

52. Oliver, R. W. A., [ed.]. *HPLC of Macromolecules - A Practical Approach.* Oxford: Oxford University Press, **1989**.

53. Feynman, Richard P. Feynman Online: Nanotechnology. [Online] [Cited: 10 March 2008.] http://www.feynman.com/.

54. British Museum - The Lycurgus Cup. [Online] [Cited: 11 09 2009.] http://www.britishmuseum.org/explore/highlights/highlight_image.aspx?imag i=k737.jpg&retpage=20945 http://www.britishmuseum.org/explore/highlights/highlight_image.aspx?imag e=k741.jpg&retpage=20945

55. Daniel, M.-C., Astruc, D. L., **2004**, *Chem. Rev.*, 104, 293-346.

56. Faraday, M., **1857**, *Philos. Trans. R. Soc. Lond.*, 147, 145-181.

57. Turkevitch, J., Stevenson, P. C., Hillier, J., **1951**, *Discuss. Faraday Soc.*, 11, 55-75.

58. Frens, G., **1973**, *Nature Phys. Sci.*, 241, 20-22.

59. Grabar, K. C., Freeman, R. G., Hommer, M. B., Natan, M. J., **1995**, *Anal. Chem.*, 67, 735-743.

60. Grabar, K. C., Brown, K. R., Keating, C. D., Stranick, S. J., Tang, S.-J., Natan, M. J., **1997**, *Anal. Chem.*, 69, 471-477.

61. Nuzzo, R. G., Allara, D. L., **1983**, *J. Am. Chem. Soc.*, 105, 4481-4483.

62. Bain, C. D., Whitesides, G. M., **1989**, *Angew. Chem. Int. Ed. Engl.*, 28, 506-512.

63. Giersig, M., Mulvaney, P., **1993**, *Langmuir*, 9, 4408-3413.

64. Brust, M., Walker, M., Bethell, D., Schiffrin, D., Whyman, R., **1994**, *J. Chem. Soc., Chem. Commun.*, 801-802.

65. Brust, M., Fink, J., Bethell, D., Schiffrin, D. J., Kiely C., **1995**, *J. Chem. Soc. Chem. Commun.*, 1655-1666.

66. Jadzinsky, P.D., Calero, G., Ackerson, C. J., Bushnell, D. A., Kornberg, R. D., **2007**, *Science*, 318, 430-433.

67. Mie, G., **1908**, *Annals of Physics*, 25, 377-445.

68. Yguerabide, J., Yguerabide, E. E., **1998**, *Anal. Biochem.*, 262, 137-156.

69. Yguerabide, J., Yguerabide, E. E., **1998**, *Anal. Biochem.*, 262, 157-176.

70. Ghosh, S. K., Pal, T., **2007**, *Chem. Rev.*, 107, 4797-4862.

71. Turkevich, J., **1985**, *Gold Bull.*, 18, 125-131.

72. Alivisatos, A. P., Johnsson, K. P., Peng, X., Wilson, T. E., Loweth, C. J., Bruchez Jr, M. P., Schultz, P. G., **1996**, *Nature*, 382, 609-611.

73. Mirkin, C. A., Letsinger, R. L., Mucic, R. C., Storhoff, J. J., **1996**, *Nature*, 382, 607-609.

74.   Loweth, C. J., Caldwell, W. B., Peng, X., Alivisatos, A. P., Schultz, P. G., **1999**, *Angew. Chem. Int. Ed. Engl.*, 38, 1808-1812.

75.   Storhoff, J. J., Mirkin, C. A., **1999**, *Chem. Rev.*, 99, 1849-1862.

76.   Niemeyer, C. M., Ceyhan, B., Hazarika, P., **2003**, *Angew. Chem. Int. Ed. Engl.*, 42, 5766-5770.

77.   Reinhard, B. M., Siu, M., Agarwal, H., Alivisatos, A. P., Liphardt, J., **2005**, *Nano Lett.*, 5, 2246-2252.

78.   Kim, H. J., Roh, Y., Hong, B., **2006**, *J. Vac. Sci. Technol. A*, 24, 1327-1331.

79.   Nykypanchuk, D., Maye, M. M., van der Lelie, D., Gang, O., **2008**, *Nature*, 451, 549-552.

80.   Park, S. Y., Lytton-Jean, A. K. R., Lee, B., Weigand, S., Schatz, G. C., Mirkin, C. A., **2008**, *Nature*, 451, 553-556.

81.   Kanaras, A. G., Wang, Z., Brust, M., Cosstick, R., Bates, A. D., **2007**, *Small*, 3, 590-594.

82.   Elghanian, R., Storhoff, J. J., Mucic, R. C., Letsinger, R. L., Mirkin, C. A., **1997**, *Science*, 277, 1078-1081.

83.   Storhoff, J. J., Elghanian, R., Mucic, R. C., Mirkin, C. A., Letsinger, R. L., **1998**, *J. Am. Chem. Soc.*, 1998, 1959-1964.

84.   Jin, R., Wu, G., Li, Z., Mirkin, C. A., Schatz, G. C., **2003**, *J. Am. Chem. Soc.*, 125, 1643-1654.

85.   Storhoff, J. J., Lazarides, A. A., Mucic, R. C., Mirkin, C. A., Letsinger, R. L., Schatz, G. C., **2000**, *J. Am. Chem. Soc.*, 122, 4640-4650.

86.   Mirkin, C.A., **2000**, *Inorg. Chem.*, 39, 2258-2272.

87.   Storhoff, J. J., Lucas, A. D., Garimella, V., Bao, Y. P., Muller, U. R., **2004**, *Nat. Biotechnol.*, 22, 883-887.

88.   Cao, Y. C., Jin, R., Mirkin, C. A., **2002**, *Science*, 297, 1536-1540.

89.   Murphy, D., O'Brien, P., Redmond, G., **2004**, *Analyst*, 129, 970-974.

90.   McKenzie, F., Faulds, K., Graham, D. **2008**, *Chem. Commun.*, 2367-2369.

91.   Pavlov, V., Xiao, Y., Shlyahovsky, B, Willner, I., **2004**, *J. Am. Chem. Soc.*, 126, 11768-11769.

92.   Liu, J., Lu, Y., **2004**, *Anal. Chem.*, 76, 1627-1632.

93.   Baptista, P.V., Koziol-Montewka, M., Paluch-Oles, J., Doria, G., Franco, R., **2006**, *Clin. Chem.*, 52, 1433-1434.

94.   Castaneda, M. T., Alegret, S., Merkoci, A., **2007**, *Electroanalysis*, 19, 743-753.

95.   Lyon, L. A., Musick, M., Natan, M. J., **1998**, *Anal. Chem.*, 70, 5177-5183.

96.   Mo, Z., Wang, H., Liang, Y., Liu, F., Xue, Y., **2005**, *Analyst*, 130, 1589-1594.

97.   Niemeyer, C. M., Ceyhan, B., **2001**, *Angew. Chem. Int. Ed. Engl.*, 40, 3685-3688.

98.   Kim, J. H., Estabrook, R. A., Braun, G., Lee, B. R., Reich, N. O., **2007**, *Chem. Commun.*, 4342-4344.

99.   Herdt, A. R., Drawz, S. M., Kang, Y., Taton, T. A., **2006**, *Colloids Surf. B Biointerfaces*, 51, 130-139.

100.   Li, Z., Jin, R., Mirkin, C. A., Letsinger, R. L., **2002**, *Nucleic Acids Res.*, 30, 1558-1562.

101.   Letsinger, R. L., Elghanian, R., Viswanadham, G., Mirkin, C. A., **2000**, *Bioconjug. Chem.,* 11, 289-291.

102. Kim, J. H., Chaudhary, S., Ozkan, M., **2007**, *Nanotechnology*, 18, 195105 (7 pages).

103. Nirmal, M., Brus, L., **1999**, *Acc. Chem. Res.*, 32, 407-414.

104. Faulds, K., McKenzie, F., Smith, W. E., Graham, D., **2007**, *Angew. Chem., Int. Ed. Engl.*, 46, 1829-1831.

105. Raman, C. V., Krishnan, K. S., **1928**, *Nature*, 121, 501-502.

106. Smith, W. E., *Resonance Raman Scattering*. [ed.] 1st Edition. *Modern Raman Spectroscopy.* s.l. : John Wiley and Sons Ltd., **2005**, 93-112.

107. Fleischmann, M., Hendra, P. J., McQuillan, A. J., **1974**, *Chem. Phys. Lett.*, 26, 163-166.

108. Smith, W. E., **2008**, *Chem. Soc. Rev.*, 37, 955-964.

109. Nie, S., Emory, S. R., **1997**, *Science*, 275, 1102-1106.

110. Kneipp, K., Wang, Y., Kneipp, H., Perelman, L. T., Itzkan, I., Dasari, R. R., Feld, M. S., **1997**, *Phys. Rev. Lett.*, 78, 1667-1670.

111. Stacy, A. M., Van Duyne, R. P., **1983**, *Chem. Phys. Lett.*, 102, 365-370.

112. Pineda, A. C., Ronis, D., **1985**, *J. Chem. Phys.*, 83, 5330-5337.

113. Munro, C. H., Smith, W. E., Garner, M., Clarkson, J., White, P. C., **1995**, *Langmuir*, 11, 3712-3720.

114. Heard, S. M., Grieser, F., Barraclough, C. G., **1983**, *J. Colloid Interface Sci.*, 93, 545-555.

115. Stokes, R. J., MacAskill, A., Lundahl, P. J., Smith, W. E., Faulds, K., Graham, D., **2007**, *Small*, 9, 1593-1601.

116. Allain, L. R., Vo-Dinh, T., **2002**, *Anal. Chim. Acta*, 149-154.

117.   Faulds, K., Barbagallo, R. P., Keer, J. T., Smith, W. E., Graham, D., **2004**, *Analyst*, 129, 567-568.

118.   Moore, B. D, Stevenson, L., Watt, A., Flitsch, S., Turnet, N. J., Casidy, C., Graham, D., **2004**, *Nat. Biotechnol.*, 22, 1133-1138.

119.   Hildebrandt, P., Stockburger, M., **1984**, *J. Phys. Chem. B*, 88, 5935-5944.

120.   Vo-Dinh, T., Hiromoto, M. Y. K., Begun, B. M., Moody, R. L., **1984**, *Anal. Chem.*, 56, 1667-1670.

121.   Khan, I., Cunningham, D., Graham, D., McComb, D. W., Smith, W. E., **2005**, *J. Phys. Chem. B*, 109, 3454-3459.

122.   Khan, I., Cunningham, D., Littleford, R. E., Graham, D., Smith, W. E, McComb, D. W., **2006**, *Anal. Chem.*, 78, 224-230.

123.   Graham, D., Thompson, D. G., Smith, W. E., Faulds, K., **2008**, *Nat. Nanotechnol.*, 3, 548-551.

2 Aims

➢ To synthesise thioctic acid modified oligonucleotides.

- o Synthesis of thioctic acid derivatives as precursors for oligonucleotide modification.

- o 5'-Modification of oligonucleotides to be investigated by phosphoramidite approach.

- o 3'-Modification of oligonucleotides to be investigated by use of a commercially available modified CPG support.

➢ To prepare thioctic acid modified oligonucleotide nanoparticle conjugates (gold and silver) and investigate their stability.

- o To confirm the retention of biological activity through hybridisation induced nanoparticle aggregation of the conjugates.

- o To extend the oligonucleotide-gold nanoparticle hybridisation detection methodology to silver nanoparticle analogues.

- o To assess the stability of the thioctic acid oligonucleotide nanoparticle conjugates.

➢ To use thioctic acid modified oligonucleotides to modify a commercially available nanostructured surface and examine its suitability as a SERRS detection substrate.

- o To investigate the compatibility of the Klarite™ surface with SERRS detection of dye labelled oligonucleotides.

- o To apply the modification of the Klarite™ surface to the detection of a target sequence of DNA by SERRS.

- o To investigate the synergy of Dip-Pen-Nanolithography as an immobilisation tool for thioctic acid modified oligonucleotides with SERRS as the oligonucleotide detection technique.

3 Modification of DNA with Thioctic Acid

D isulfide-modified oligonucleotides were desired with a view to developing oligonucleotide-nanoparticle conjugates of enhanced stability. The most widely used linking methodology for DNA-nanoparticle conjugates employs the use of monothiol-modified oligonucleotides to tether to gold nanoparticles *via* the thiol moiety. Steroidal disulfides and trithiol-linkers group have also been investigated by Mirkin *et al.* [1] [2] Whilst they did confer extra stability to the conjugates, the linkers were structurally cumbersome and/or synthetically challenging. As an alternative, it was decided to investigate thioctic acid as a disulfide linker molecule for DNA-nanoparticle conjugates. Thioctic acid was considered an attractive candidate since it is comprised of a disulfide group, short alkyl chain and readily modifiable carboxylic acid group. Thioctic acid, also known as α-lipoic acid, is employed in the body as an important co-factor involved in a variety of oxidation-reduction enzymatic reactions. [3] The work described herein is not concerned with harnessing the biological activity of thioctic acid, rather it is investigating its applicability as a gold substrate binding linker. Thioctic acid, and derivatives thereof, are known to bind to gold nanoparticles – spherical [4] [5] [6] [7] [8] and rod-shaped, [9] gold electrodes [10] and chips. [7] It has been used in investigations ranging from the immobilization of tetrathiofulvalenes as cation sensors on gold electrodes [10] and metal ion chelation, [4] to the probing of nanoparticle surface adsorption by nitroxide-modified thioctic acid spin labelled probes. [5] [6] Indeed, thioctic acid has also been used to immobilize molecules for bioanalytical applications; carbohydrates to investigate non- specific protein interactions, [7] antibodies, [9] and transition metal complexes for protein
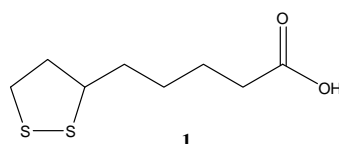
Figure 3.1: Thioctic Acid.

capture. [8] In addition, the reduced, dithiol, form of thioctic acid has been used for quantum dot surface coverage, [11] [12] which have been used in cellular imaging studies. [12] It should be noted that a thioctic acid modified oligonucleotide had been prepared *via* multistep post-synthetic modification. [13] Until this body of work, however, a simple route to isolate thioctic acid modified oligonucleotides had not been reported, nor had their subsequent employment with gold and silver nanoparticles been investigated. Some routes to thioctic acid modification of oligonucleotides are discussed in the following sections, *via* the phosphoramidite approach (Section 3.1), the H-phosphonate approach (Section 3.2) and the active ester approach (Section 3.3). The applications of these oligonucleotides are discussed in Chapters 4 and 5.

3.1 The Phosphoramidite Approach

Modification of the 5'- end of a synthetic oligonucleotide with thioctic acid (TA), **1**, was attempted according to standard phosphoramidite protocols. [14] The most obvious synthetic method for 5'- modification uses the phosphoramidite chemistry developed by Caruthers *et al.* in the early 1980's. [15] [16] [17] The phosphoramidite method requires phosphitylation of a primary alcohol. Therefore, in order to phosphitylate thioctic acid and, thus, incorporate it at the 5'- terminus, an alcohol derivative was required. An amide formation was attempted, between aminohexanol, **2**, and thioctic acid, **1**. This was to allow the phosphoramidite approach to be investigated by introducing a suitable alcohol moiety. In addition, amide bonds are stable to both the phosphitylation reaction chemistry and the subsequent DNA synthesis and deprotection chemistries.

3.1.1 Preparation of N-(6-hydroxyhexyl)-5-(1,2-dithiolan-3-yl)pentamide, 3

There are a great many methods for the preparation of the ubiquitous amide bond. [18] Carbonyldiimidazole (CDI) was used as a coupling reagent since it is an efficient mediator of amide formation with side products that are easily removed (imidazole and carbon dioxide). The acid starting material, in this case thioctic acid,
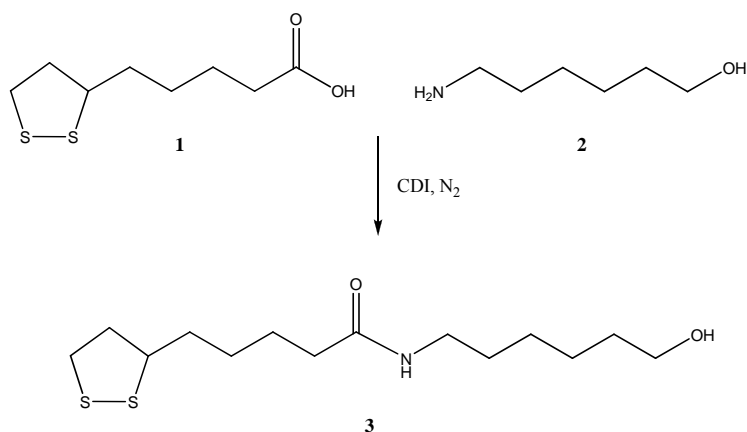
Scheme 3.1, Experimental 7.2.1: Amide formation between thioctic acid and aminohexanol, yielding the required product, 3, with disulfide and alcohol moieties

and CDI were pre-mixed in order to produce an activated acid; the reaction occurring with the release of CO_2 as a driving force. Introduction of the amine, in this case aminohexanol, to the activated acid allowed amide formation to occur, facilitated by the loss of the second mole of imidazole. CDI itself is reactive with water and as such anhydrous solvents were used and the reaction carried out in a N_2 environment. The preparation of amide **3** was achieved with typical isolated yields ranging from 54 % to 69 % (Scheme 3.1, Experimental 7.2.1). However, the reaction was carried out a number of times, with the outcome initially found to be somewhat unpredictable. The desired product is a pale yellow powder but initial experiments often yielded an undesirable yellow resinous mass. This "jelly"-like material was insoluble in all the solvent systems attempted, including: MeOH, MeCN, DCM, Et$_2$O, EtOAc, acetone, DMSO, hexane, DMF and combinations thereof. As such, when formed, the resinous material rendered continuation of the reaction work-up unfeasible due to difficulty achieving dissolution. It was suspected that temperature played a critical role in the generation of this resinous species; the literature showed this had previously been reported by Reed and Wagner. [19] [20] [21] The argument put forward was that the unwanted resin was a linear, inter-molecularly linked, disulfide polymer. In order to avoid the formation of this polymeric species, the amide formations were not carried out at elevated temperature. Additionally, DMF, the solvent of choice was not easily removed *in vacuo* and was instead washed out with an Et$_2$O:water system. Optimising the reaction scheme to account for the

temperature instability of the starting material and product resulted in the substitution of DMF with DCM which could be easily removed at room temperature. Incidentally, the amides were initially purified by flash column chromatography, however, precipitation of the product (dissolved in the minimum amount of DCM) from hexane proved a simpler and equally effective means of purification.

Temperature did not appear to be the only factor contributing to resin formation, it is believed that exposure to UV light may also induce it. [22] For that reason, all reactions using thioctic acid were conducted in covered glassware as well as the avoidance of elevated temperatures. Taking these precautionary measures greatly improved the syntheses of thioctic acid derivatives by successfully avoiding resin formation.

3.1.2 The Phosphoramidite Modifier

With the suitable alcohol derivative of thioctic acid in hand, phosphitylation was assessed as a method of modifying oligonucleotides with the TA moiety (Scheme 3.2, Experimental 7.2.2). The starting material and, indeed, product of phosphitylation reactions are P^{III} species that are extremely oxophilic and will react
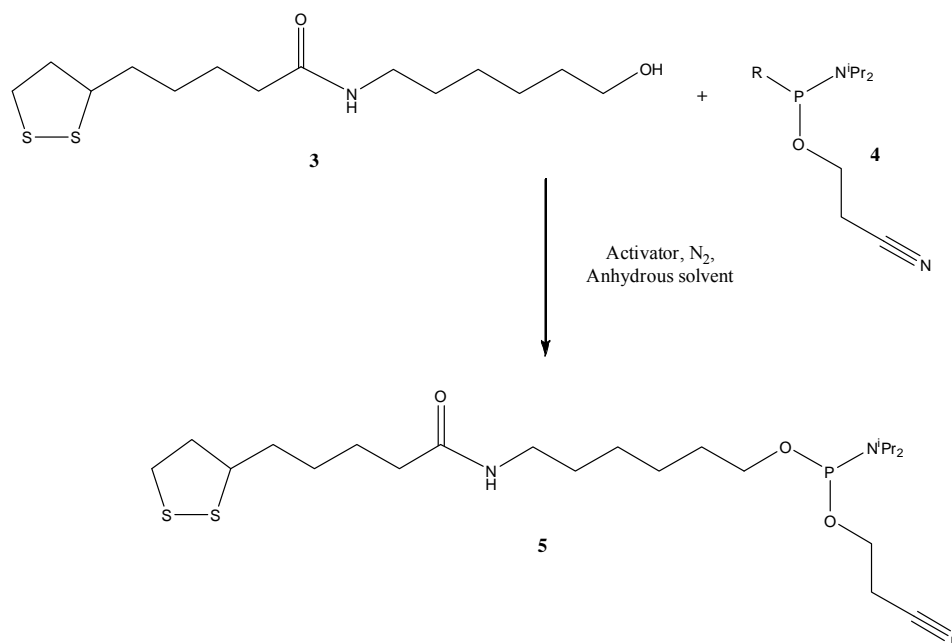
Scheme 3.2: Experimental 7.2.2, attempted phosphitylation of amide 3 to yield the phosphoramidite for oligonucleotide modification, Where "R" may be a di-iso-propylamino- (4a) or chloro- (4b) group.

readily with trace amounts of moisture or dissolved oxygen to give unwanted pentavalent phosphorous side-products. As such, phosphitylation reactions are somewhat capricious. In order to minimize the occurrence of oxidation, the reactions were carried out with oven-dried, N_2 purged glassware, needles and syringes. Rigorously dried solvents: DCM, THF and acetonitrile were used.

Initial attempts were carried out using the 2-cyanoethoxy-bis(*N,N*-diisopropylamino)phosphine phosphitylating reagent (**4a**) with BTT (a tetrazole derivative) in anhydrous acetonitrile as the activator. The tetrazole derivative serves to protonate the diisopropylamino moiety, thereby activating the group for displacement by an incoming nucleophile. Attempts to purify the crude products were carried out by flash column chromatography on pre-basified silica under N_2 pressure. It is important to basify the silica as even trace amounts of acid will activate the phosphoramidite product (which still retains a di-*iso*-propylamino group) causing it to degrade during the purification process. Thereafter, it is crucial that all traces of triethylamine are removed prior to addition on the DNA synthesizer, otherwise coupling would be inhibited as the tetrazole-derived activator used in the coupling step of oligonucleotide synthesis would protonate any residual triethylamine, rather than activating the remaining di-*iso*-propylamino group of the phosphoramidite. Rigorous removal of Et_3N was carried out and confirmed by ^{1}H NMR. This involved co-evaporation in dry solvent followed by drying the sample overnight over P_2O_5 in a vacuum desiccator or drying pistol.

Attempts were subsequently made using the more reactive (and therefore less stable) chloro-analogue, 2-cyanoethoxy-*N,N*-diisopropylaminochlorophosphine. No "activator" is required with the highly reactive chloro-analogue; however, a hindered base such as DIPEA is added to quench hydrochloric acid liberated during the reaction. The chloro- analogue is a less popular reagent due to its inherent instability, which can lead to rapid oxidation. However, failure to prepare the desired product using the di-isopropylamino analogue resulted in attempts to use the more reactive chloro- in the hope that the required product would be obtained.

^{31}P NMR from the attempted phosphitylations generally showed a mixture of phosphorus species that suggested a mixture had been formed. However, it can be

fairly common for ^{31}P NMR to give spurious results (where the dryness of the deuterated solvent was called into question, rendering the sample used for NMR inactive but the stock sample still viable). As such, it was common to attempt DNA modification with the monomer, given that successful HPLC and MALDI data of the synthesized oligonucleotide would suggest (by inference) that the desired phosphoramidite intermediate had been prepared, albeit not fully characterised.

After the flash column chromatography, the sample was dissolved in the required amount of MeCN/THF (anhydrous) to a concentration of 0.1 M and placed on a line of the DNA synthesizer. Multiple couplings with extended coupling times were automatically programmed. Each synthesis was run on a standard column (where the column has the first base of the sequence immobilized). The attempted phosphoramidite, **5**, was added as the final monomer after the synthesis of a 12- or 22-mer sequence. Typically, deprotection is achieved by treatment with conc. ammonium hydroxide for 1 h to cleave the sequence from the column and then heated at 40 °C overnight to deprotect the exocyclic amines of the oligonucleotide chain and the cyanoethyl group of the phosphate. However, the temperature instability of the thioctic acid group required room temperature deprotection to be adopted instead. After deprotection, the ammonium hydroxide was removed *in vacuo* and the oligonucleotide sequences were stored in distilled water at 4 °C prior to HPLC analysis and purification.

The oligonucleotides were purified by ion exchange chromatography since the introduction of an additional phosphate at the 5'-terminus would increase the ionic charge by one (Experimental 7.4.1). A typical trace is shown in Figure 3.2. The last peak using this method should correspond to the TA-modified oligonucleotide if the phosphitylation and coupling steps were successful. To ascertain if this was the case the samples were thoroughly desalted using size exclusion chromatography (Experimental 7.4.2) and sent to the EPSRC Mass Spectrometry service in Swansea for MALDI-TOF analysis. However, results from Swansea failed to show any thioctic acid modified oligonucleotides, the only masses observed were those of the unmodified sequence. This, in addition to the phosphoramidite ^{31}P NMR results, suggested that the phosphoramidite method was not viable for thioctic acid
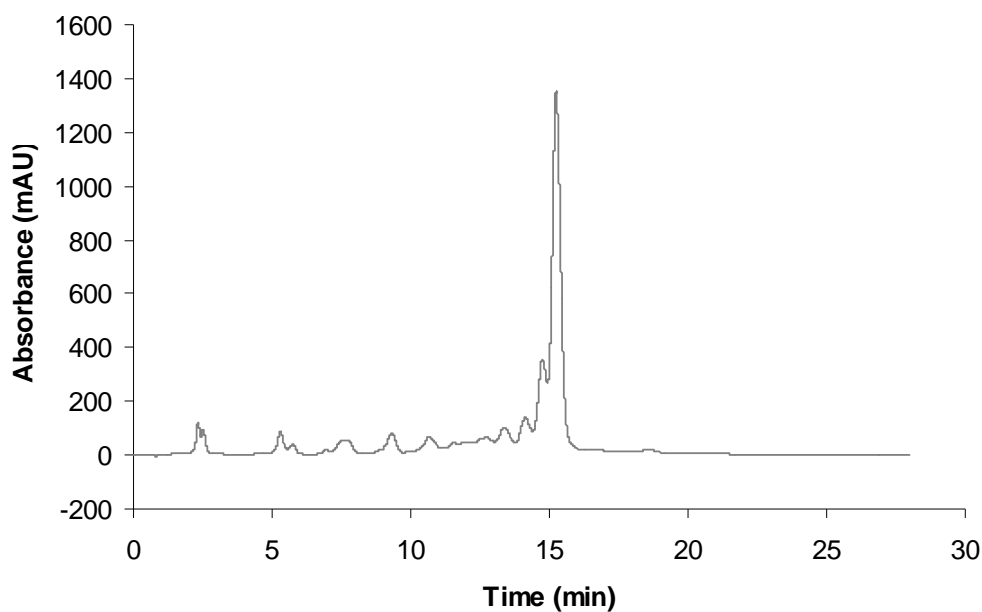
Figure 3.2: Typical IE HPLC of attempted thioctic acid modification by phosphoramidite approach.

modification. It was suspected that the highly reactive nature of the P^{III} intermediate had resulted in reaction with the cyclic disulfide of thioctic acid as well as the alcohol, rendering the product unsuitable for addition to the oligonucleotide chain.
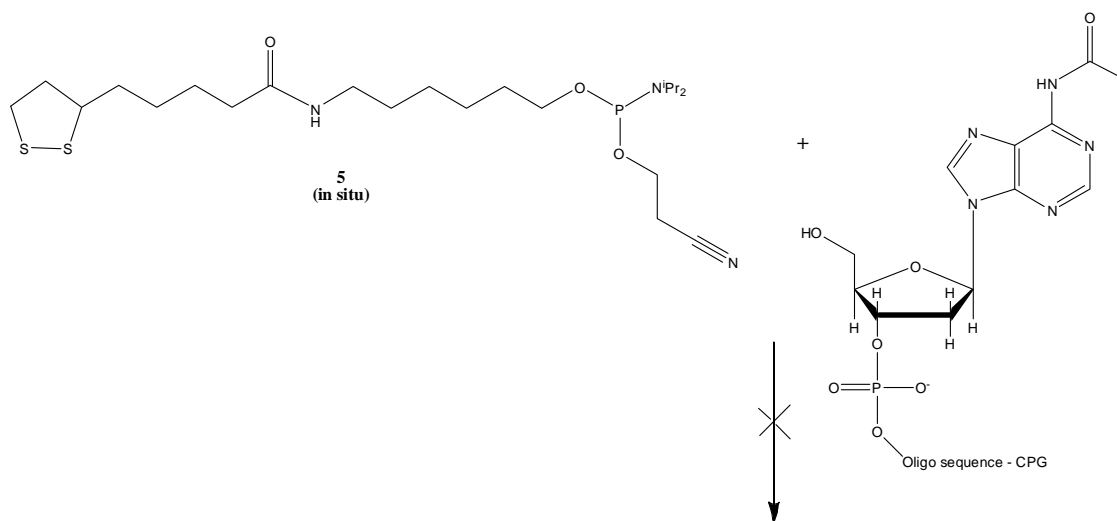
Scheme 3.3, Experimental 7.3.2: The proposed on-column reaction between a synthesised chain of oligonucleotide and the phosphoramidite of thioctic acid which did not yield a modified oligonucleotide.

It was imperative for the ultimate aim of this body of work to obtain thioctic acid modified oligonucleotides. It was decided to attempt an alternative avenue for oligonucleotide modification; H-phosphonate synthesis.

3.2   The H-phosphonate Approach

In order to circumvent the problem of a self-reactive P^{III} species it was decided to attempt H-phosphonate chemistry as an alternative route. H-phosphonate chemistry originated in the 1950's in the laboratory of Lord Todd and co-workers. [23] The H-phosphonate method was found to be suited to solid phase synthesis, [24] [25] [26] particularly when using pivaloyl chloride as an activator. [24] [25] Nevertheless, it was largely superseded by the phosphoramidite approach. However, the H-phosphonate method is used today in situations where the oxidation step of DNA synthesis is best avoided. The H-phosphonate method is attractive in such circumstances since the intermediates formed are tetra-coordinated P^{III} species and, as such, are not susceptible to unwanted oxidation or further reaction. This allows for oxidation of the full sequence to be carried out at the end of the synthesis, thereby exposing the sequence and any modifications to the oxidation cycle only once. Whilst, in the case of TA-modification, oxidation was not a problem, using a tetra-coordinated P^{III} species was an attractive option as it was hoped that it may prevent the side-reactions suspected of hindering the phosphoramidite approach. As such, the viability of H-phosphonate chemistry as an alternative avenue to generating 5'- thioctic acid modified oligonucleotides was investigated.

3.2.1 Thioctic Acid - Pentanol Derivative, N-(5-hydroxypentyl)-5-(1,2-dithiolan-3-yl)pentamide, 7

The H-phosphonate method, once again, required a suitable alcohol for derivatisation. Thioctic acid was coupled with aminopentanol to introduce the required alcohol moiety, **7** (Experimental 7.2.3). The amide formation between thioctic acid and aminopentanol, **6**, was carried out using HATU as the activator with hydroxybenzotriazole as a co-coupler. Following work-up the product was precipitated from hexane but the ^{1}H NMR showed the presence of tetramethyl urea.
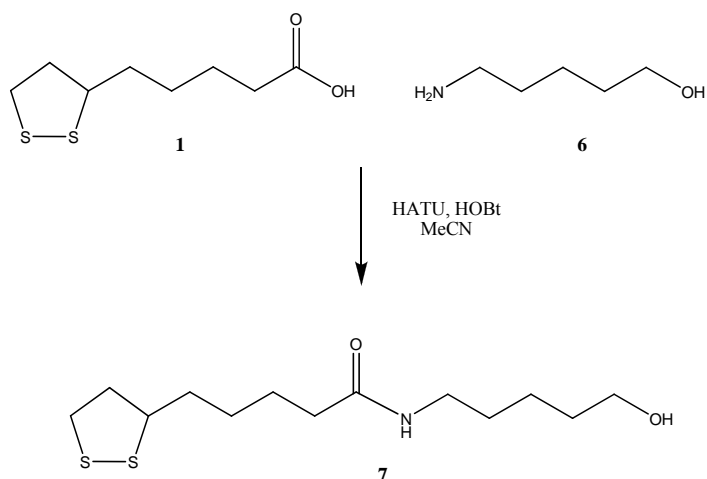
Scheme 3.4, Experiment 7.2.3: HATU-Mediated amide formation between thioctic acid and aminopentanol. Hydroxybenzotriazole was used as a co-coupler.

As such flash column chromatography was carried out and the purified product was obtained in 75 % isolated yield. With the desired alcohol in hand, investigation of the H-phosphonate method could proceed.

3.2.2 The H-Phosphonate Modifier

The H-phosphonate, **10**, was prepared by dissolving *N*-(5-hydroxypentyl)-5-(1,2-dithiolan-3-yl)pentamide, **7**, in 1 M phosphorous acid in anhydrous pyridine.
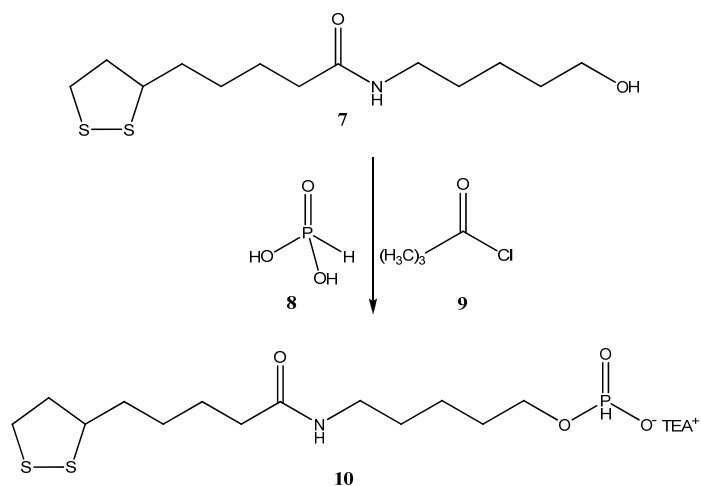
Scheme 3.5, Experimental 7.2.4: Preparation of the H-phosphonate of thioctic acid using phosphorous acid and pivaloyl chloride.

Pivaloyl chloride, **9**, was used as a condensing agent as it promotes the formation of a symmetrical pyrophosphate species in anhydrous pyridine with which the chosen alcohol will react to form the H-phosphonate. The reaction was quenched by TEAB buffer and the H-phosphonate was purified after work-up by flash column chromatography and used directly to modify DNA.

3.2.3 5'-TA-Oligonucleotides via the H-Phosphonate Method

Oligonucleotide sequences were prepared on the synthesiser under standard phosphoramidite conditions. As proof of concept, two sequences were prepared – a cytidine 6-mer and a thymidine 6-mer - both with trityl deprotection as the last step
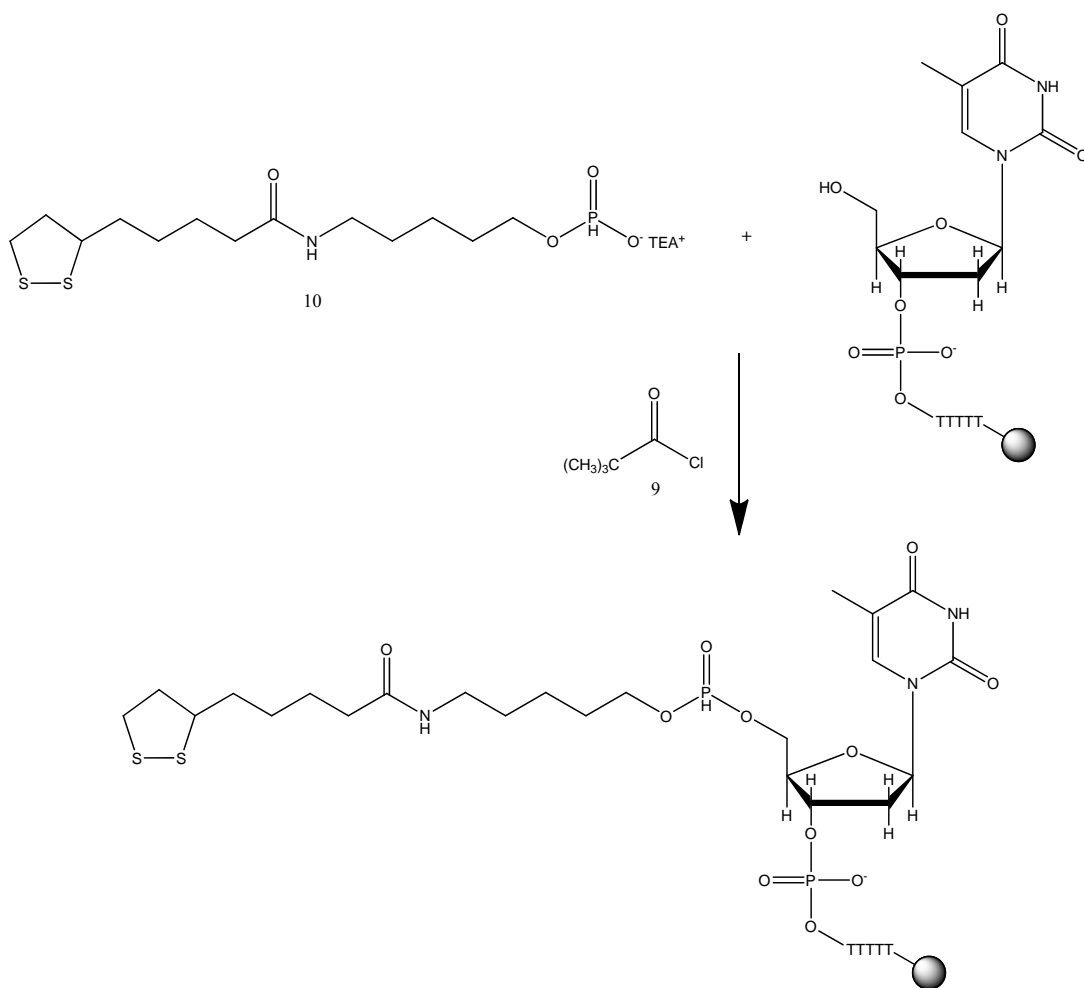
Scheme 3.6, Experimental 7.3.3: Coupling of the H-phosphonate derivative of thioctic acid with a solid supported 6-mer, yielding a modified sequence ready for purification and analysis.

to ensure a 5'-hydroxyl was available for reaction with the H-phosphonate, **10**, Scheme 3.6. The H-phosphonate coupling was carried out with the H-phosphonate, **9**, dissolved in 1:1 MeCN: pyridine and added to both a cytidine-6mer (6C) and a thymidine-6mer (6T) on a solid support again using pivaloyl chloride, **9**, as activator (Experimental 7.3.3). It was necessary to carry out the reaction in a silanised glass vial as reactions in unsilanised vials or eppendorf® tubes were unsuccessful. The vial was sealed and agitated for 5 minutes with a mechanical shaker before the reaction mixture was removed and the CPG washed (3 × MeCN) and then oxidised with standard DNA synthesis oxidizing solution (I_2, THF, H_2O, pyridine). The CPG was treated with conc. ammonium hydroxide to cleave and deprotect the sequences, TA-6T and TA-6C. It should be noted that this reaction could equally be carried out using the automated synthesiser. However, care would be required for the timing of reagent delivery to avoid pre-mixing the H-phosphonate with pivaloyl chloride which could lead to self-reaction and the generation of an unreactive pyrophosphate. Nevertheless, automated modification is advantageous and investigations in this direction should be encouraged.

Reversed-phase HPLC was carried out on the reaction mixtures Experimental 7.4.3). The sequences, being on a solid support at the time

MALDI MS Req: 2025.4

MALDI MS Found: 2023.4
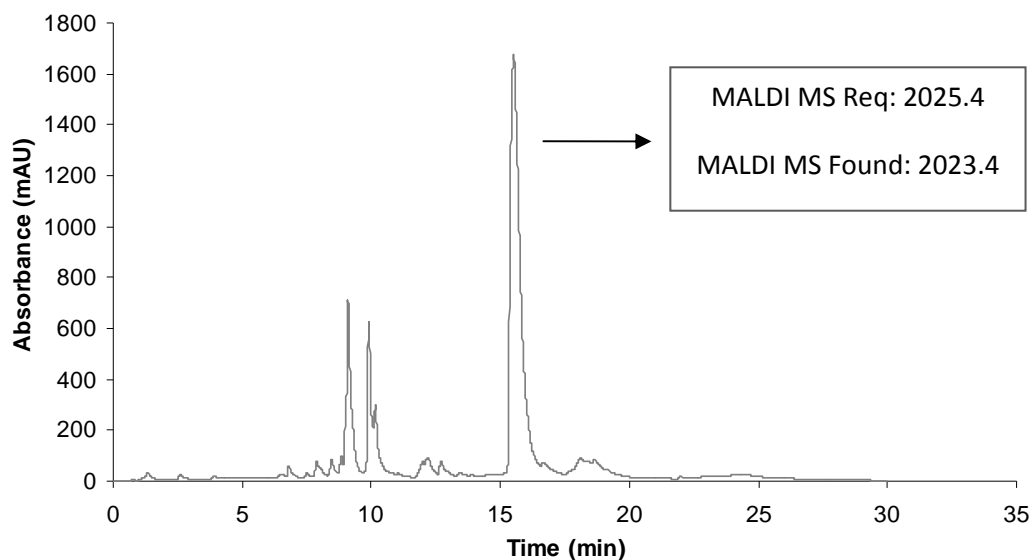
*gure 3.3: RP-HPLC trace of the reaction between 6C and TA H-phosphonate, **10**. The peak at retention time = 15.5 corresponds to TA-6C.*

of H-phosphonate coupling, were not purified prior to reaction and as such the presence of failure sequences are clearly evident (Figure 3.3). Nevertheless, the peak at $T_R = 15.5$ min corresponds to the TA-6C sequence which was confirmed by MALDI-TOF mass spectrometry. The reaction with the poly-pyrimidine (6T) gave equivalent results.

3.3 The Active Ester Approach

During the course of the investigations into 5'-modification, it became clear that obtaining an intermediate to amide formation would be desirable. This would allow a variety of modification strategies (solid phase, solution phase, 5'-, 3'- and mid-sequence) to be exploited whilst the direct 5'-modification techniques were investigated.

3.3.1 N-Hydroxysuccinimidyl Ester: a Versatile Modifier for DNA

N-(3-Dimethylaminopropyl)-*N*'-ethylcarbodiimide, EDC.HCl was chosen as a coupling reagent as it is commercially available, inexpensive and the urea by-product formed is water soluble and thus easily removed from the reaction mixture during work-up. Additionally, EDC.HCl is commonly used in the presence of a "co-
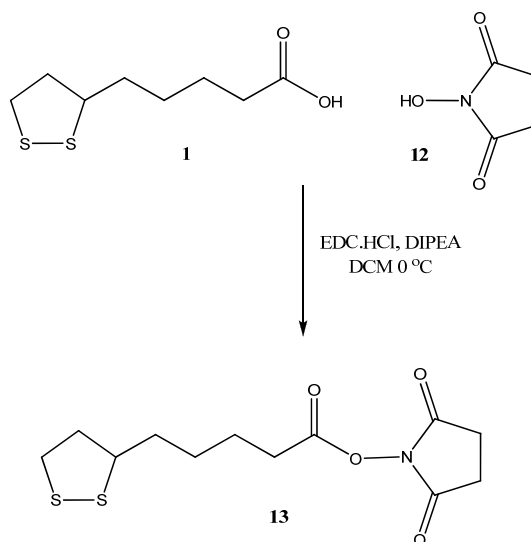
Scheme 3.7, Experimental 7.2.5: Preparation of the N-hydroxysuccinimidyl ester of thioctic acid which was isolated for further use.

coupler" like *N*-hydroxysuccinimide. The amide formation proceeds *via* formation of an active ester. It is not always necessary to isolate this intermediate as amide formation is often carried out *in situ*. However, for bioconjugations it was considered advantageous to have a stable active ester to hand that could be used without any requirement for organic synthesis, and for which the stoichiometry could easily be controlled.

Preparation of the *N*-hydroxysuccinimidyl ester of thioctic acid (TA-NHS), **13**, was carried out at 0 °C with thioctic acid, **1**, added dropwise as a solution in DCM to the coupling mixture. After purification, a yellow solid, **13**, was obtained in 83 % yield (Experimental 7.2.5). The *N*-hydroxysuccinimidyl ester, **13**, can be readily dissolved in an organic solvent, such as DCM, DMF, MeCN, from this point on. However, it should be noted that even when stored in dark conditions (laboratory cupboard in foil coated vial) at room temperature the ester loses some solubility over time (> 6 months). Around that time some flecks of insoluble material can be observed in any attempted dissolution. At this point a fresh batch of active ester should be prepared so that solutions of known molarity can be achieved.

3.3.2 3'-Modification with Thioctic Acid

A 3'-amino modification column was obtained from Link Technologies (Figure 3.4). It was proposed that treatment with piperidine would quantitatively cleave the Fmoc protecting group, yielding the free amine and subsequent reaction with TA-NHS, **13**, would afford a thioctic acid modified column. To prepare 3'-disulfide-modified oligonucleotides (Experimental 7.3.4) the column was first treated with 20 % piperidine/MeCN. This resulted in cleavage of the Fmoc yielding a free primary amine. The column was then washed, manually, with MeCN. Excess TA-NHS, **13**, was then dissolved in MeCN and applied to the column overnight in order to allow for maximum reaction. The column was washed with MeCN before
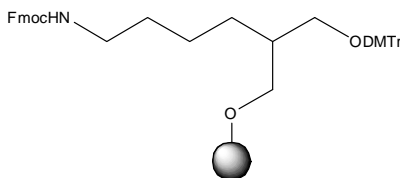
Figure 3.4: An amino-modified CPG support for 3'-modification.
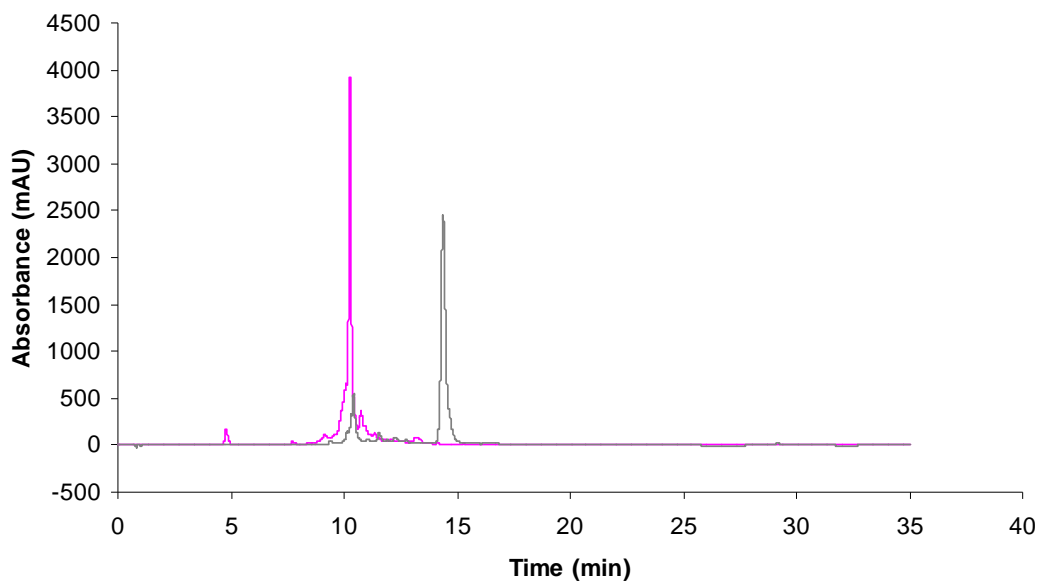
Figure 3.5: RP-HPLC Chromatogram after oligonucleotide synthesis of 3'-TA-modification (TA-Pr1) where a pre-synthetic capping step was employed (grey) c.f. no capping step (pink).

being placed on the DNA synthesizer and a capping step was introduced prior to the standard DNA synthesis cycle. The capping step was necessary to acetylate any unreacted, free amine on the solid support thereby minimizing the complexity of purification due to side reactions. Indeed, DNA synthesis undertaken in the absence of the capping step did not yield the desired oligonucleotide which can clearly be seen from the resulting HPLC traces (see Figure 3.5). After capping, the oligonucleotide sequence was prepared following the standard oligonucleotide synthesis cycle (described in Section 1.1.4). Post-synthesis, cleavage and deprotection was carried out with conc. ammonium hydroxide at room temperature (rather than heating) to minimize the risk of the disulfide ring opening. This resulted in a longer deprotection time of 36 hours rather than overnight.

In the case of 3'-modified oligonucleotides, reversed phase HPLC was chosen for purification as any unmodified oligonucleotides would have the same number of phosphates and would therefore not be separable by ion exchange chromatography. With 3'-modification there are the standard failure sequences from oligonucleotide
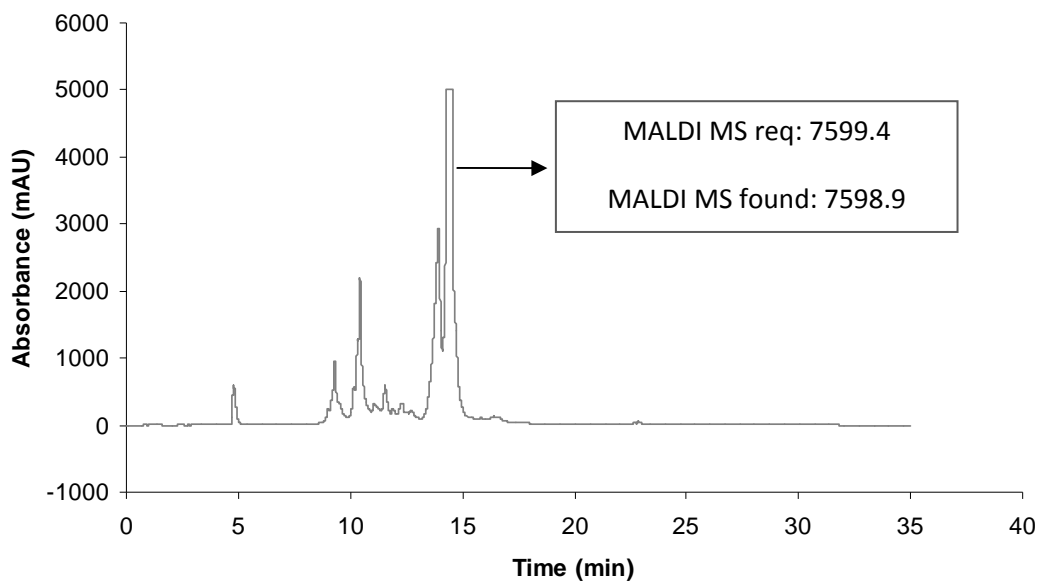
Figure 3.6: HPLC trace, absorbance recorded at 260 nm, of the crude D2 sample. Note the marked separation between the modified peak at t_R = 14.4 min and the failure sequences.

synthesis, each of which may or may not be disulfide-modified as well as both modified and unmodified full length species. Using a Phenomenex Clarity® RP-HPLC column and triethylammonium acetate (TEAA)/MeCN as the mobile phases gave good separation and allowed the desired oligonucleotide to be isolated in a solution with volatile counter-ions. The HPLC trace of the sequence D2, as a typical example, can be seen in Figure 3.6. It is worthy to note, however, that sequence D2 is also FAM modified at the 5'-end which results in two peaks close together with retentions of 13.9 min and 14.5 min, respectively. Consulting a 3D-HPLC array as shown in Figure 3.7 helped to rationalise this. The peaks resulting from absorption in the region 260 to 280 nm are due to oligonucleotide absorption. In addition, however, are peaks with a λ_{max} = 495 nm due to absorption by FAM. There are two peaks with absorption due to FAM, one with a retention time at 10.5 min and one at 14.5 min. Ordinarily, 5'-modification only results in one peak with the corresponding label: a FAM label. However, in this case the sample has full length 3'-disulfide modified as well as 3'-unmodified oligonucleotides each of which could be modified with FAM (Figure 3.8).
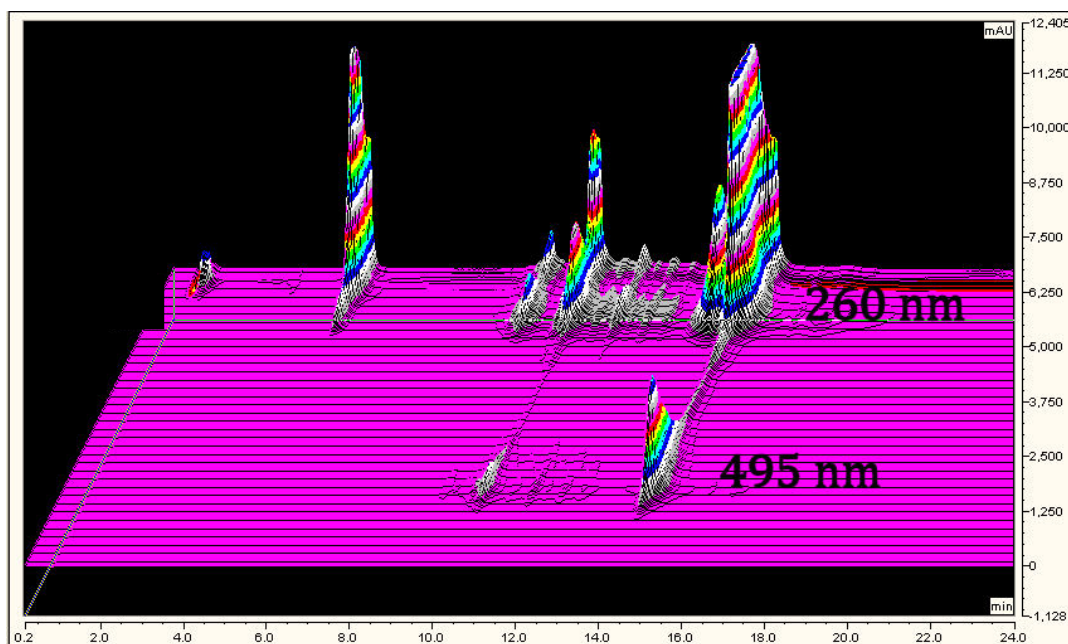
Figure 3.7: 3D Spectra of probe D2. X = Time (min), Y = Absorbance (mAU), Z = Wavelength (200-600 nm).
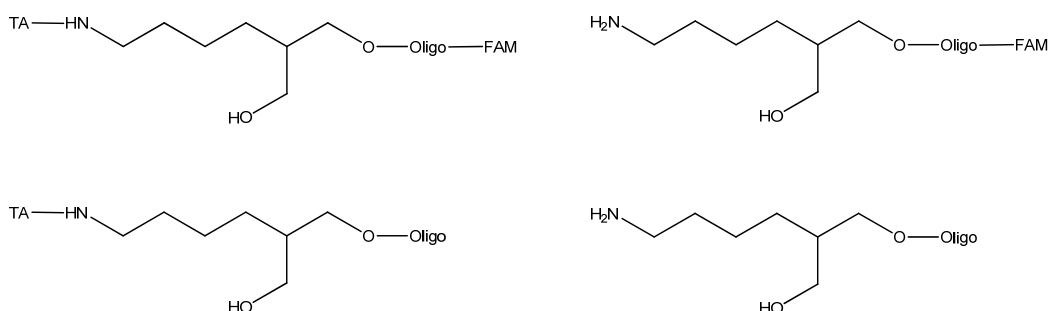
Figure 3.8: The products of 3'-thioctic acid (TA) modification (excluding shorter failure sequences.) 3'- Termini shown explicitly.

As such, it is rationalized that the peak at 10.5 min is the 3'- unmodified, 5'-FAM modified full length sequence and the one at 14.5 min is the desired 3'-thioctic acid modified, 5'-FAM modified full length sequence. The peak with a retention time of 13.9 min can be considered to be due to the 3'-TA mod, 5'-unmod full length sequence. The doubly modified target oligonucleotide was confirmed by MALDI-TOF mass spectrometry.

Once the sequences were isolated they were simply freeze-dried and analysed by MALDI-TOF mass spectrometry after ZipTip™ purification (Experimental 7.4.5). ZipTip™ purification was found to be an essential step to the efficient detection of

oligonucleotide analytes by MALDI-TOF mass spectrometry. ZipTips™ are commercially available 10 µL pipette tips with C_{18} chromatography media fixed at the bottom. A small sample ($\leq$ 10 µL) of oligonucleotide was introduced to the media, to which the oligonucleotide adheres. The sample was then washed with TEAA and Milli-Q water before being eluted from the tip. This was either done in 1 – 4 µL of 50 % MeCN/H_2O or, as was preferable, in MALDI matrix directly onto the MALDI plate. The preferred MALDI matrix is 9 parts of 50 mg mL^{-1} HPA in 50 % MeCN/H_2O to 1 part of 50 mg mL^{-1} ammonium citrate (aq.). That is, there is sufficient MeCN in the MALDI matrix to liberate the oligonucleotide from the C_{18} media of the ZipTip™. For the oligonucleotides prepared in this thesis a negative linear mode for MALDI analysis was found to work most effectively. It is extremely important that the MALDI is calibrated with fresh standards, which bracket the mass expected, immediately prior to sample analysis. This was done with oligonucleotide MALDI standards purchased from Bruker Daltonics. These processes resulted in an easy and reliable method for MALDI-TOF mass spectrometry of the oligonucleotide samples reported herein.

Sequences prepared by the 3'-modification method were used in stability studies, surface coverage studies and hybridization studies (Chapter 4). They are listed in Table 3.1. FAM labels were added *via* a commercially available fluorescein phosphoramidite.

Study	*Name*	*Sequence* (5'-3')
Hybridisation	**TA-Pr1**	CGC ATT CAG GAT AAA AAA AAA A**X**
Stability	**D1**	**FAM** CAT TGA AGC TTC **X**
and	**D2**	**FAM** CAT TGA AGC TTC TTT TTT TTT T **X**
Surface Coverage	**D3**	**FAM** CAT TGA AGC TTC AAA AAA AAA A **X**

Table 3.1: TA-Oligonucleotide sequences prepared by 3'-modification; where X = thioctic acid and FAM is a fluorescein modification.
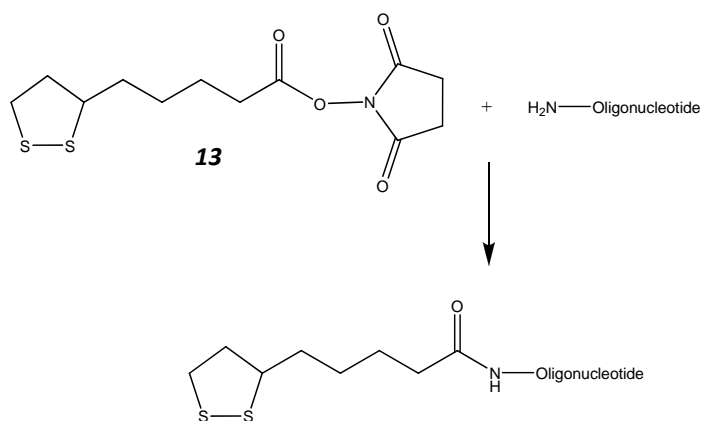
Scheme 3.8, Experimental 7.3.5: Amide formation for modification of an amino-modified oligonucleotide with TA-NHS, 13.

3.3.3 Post-Synthetic 5'-TA-Modification of Oligonucleotides

Thioctic acid oligonucleotides can also be prepared by reaction of the *N*-hydroxysuccinimidyl ester of thioctic acid with a 5'-amino-modified oligonucleotide. This can be achieved *via* two different reaction systems. The first is solution phase amide formation and the second is solid-phase amide formation.

3.3.3 (a) Post-Synthetic Solution Phase Modification

In the solution-phase system, the *N*-hydroxysuccinimidyl ester, **13**, was dissolved to a known concentration in DMF and added to an amino-modified oligonucleotide (Scheme 3.8). A number of criteria for successful biomolecular conjugations using *N*-hydroxysuccinimidyl esters were followed. The buffer used was selected to be between pH 7.5 and 9.5, in order that the primary amine for reaction was not protonated. However, at alkaline pH the half life of the NHS-ester is greatly reduced, as such the reactions were carried out at reduced temperature with a large excess of TA-NHS added. In addition, the concentration of the oligonucleotide was kept relatively high. Buffers with free amines were avoided as they could react with the TA-NHS. In short, the following criteria were adhered to:

- 50 – 200 mM buffer concentration
- 2 – 50 times excess of NHS-ester
- 0.1 – 10 mM NHS-ester
- 10 – 50 µM oligonucleotide concentration
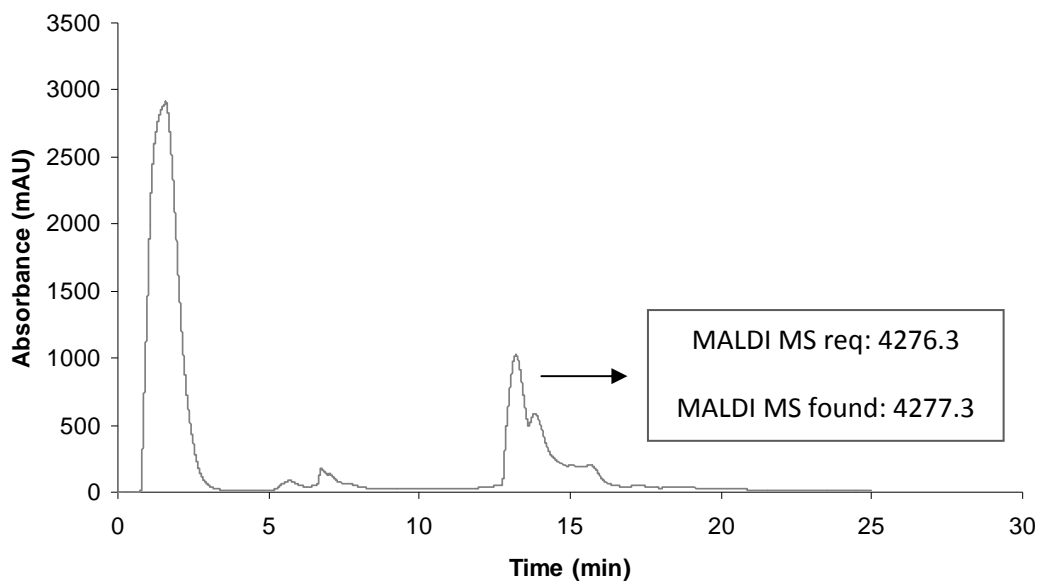
Figure 3.9: HPLC trace of solution phase amide formation with thioctic acid and amino-modified oligonucleotide with the product showing a retention of 13-15 min.

The solution phase amide formation was carried out between the TA-NHS and a commercially obtained amino-modified oligonucleotide of sequence, 5'- Amino-C_6-AAACTCCTGTTCG. Bicarbonate buffer at pH 9.2 was used. However, of all the parameters it was found to be most important to carry out the reaction at low temperature to minimize the competitive hydrolysis reaction. The reaction was most successful when carried out in an ice bath in the fridge overnight. From the HPLC trace of the reaction (Figure 3.9), it can be seen that this amide formation proceeds to ~ 89 % efficiency (as calculated from the area under the peaks) (Experimental 7.3.5). Typically, efficiencies of ~ 70 % were observed. The success of the modification was confirmed by MALDI-TOF mass spectroscopy in which the peaks in the region 13 – 15 min were confirmed as corresponding to the same species.

3.3.3 (b) Post-Synthetic Solid Phase Oligonucleotide Modification

An alternative route to 5'-modification of oligonucleotides with thioctic acid using the *N*-hydroxysuccinimidyl ester was achieved by solid phase synthesis (Experimental 7.3.6). The oligonucleotide synthesis was carried out on the solid support as standard. The final monomer yielded a monomethoxytrityl protected amino group. At the end of the synthesis the monomethoxytrityl was easily cleaved

by treatment with the standard deblocking reagent (3 % trichloroacetic acid in DCM) for 1 h. A longer deblock step *c.f.* standard DNA synthesis with DMTr protected 5'-alcohols, was required as MMTr is a more stable protecting group than DMTr. Nevertheless deprotection was readily achieved by applying the deblock reagent in syringes across the column for the required time (1 h). Treatment of the column with the *N*-hydroxysuccinimidyl ester of thioctic acid in the presence of a hindered base
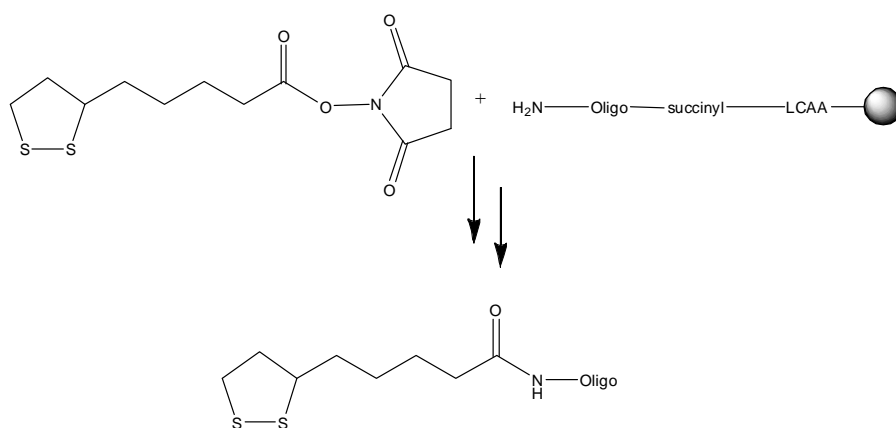
*Scheme 3.9, Experiment 7.3.6: Solid phase amide formation between TA-NHS, **13**, and an immobilised amino-modified oligonucleotide.*
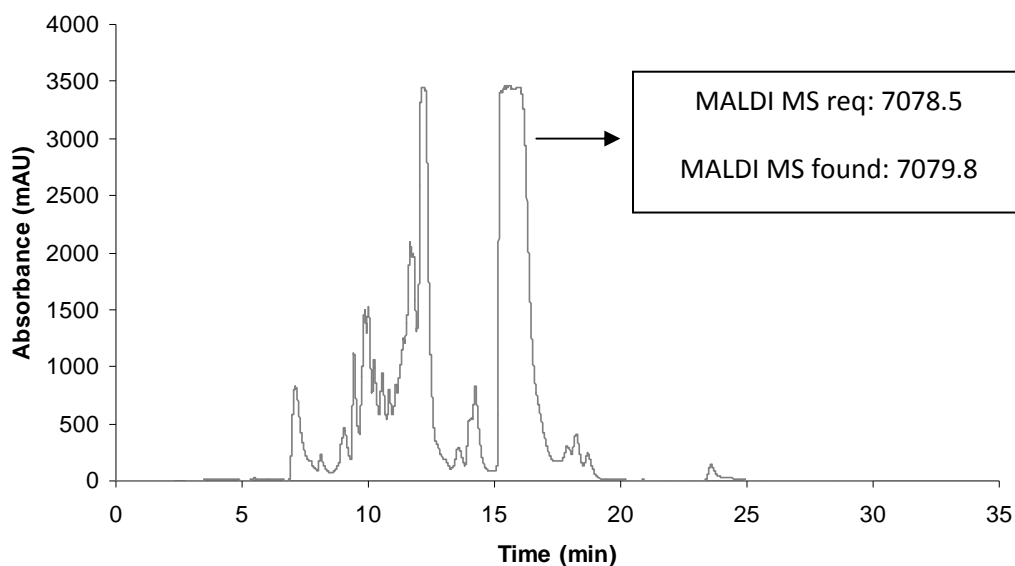
Figure 3.10: RP-HPLC after post-synthetic solid phase amide formation, giving a thioctic acid modified oligonucleotide.

allowed reaction between the deprotected primary amine of the column and the introduced *N*-hydroxysuccinimidyl ester rendering a thioctic acid modified sequence. The solid phase reaction was left to proceed overnight. Subsequent cleavage and deprotection in concentrated ammonium hydroxide and transferring to water rendered the sequence ready for reversed phase HPLC purification (Figure 3.10). Collection of the peak with retention 15-17 min and analysis by MALDI-TOF mass spectrometry confirmed the desired modification.

Hybridisation	*TA-Pr2*	*XA AAA AAA AAA TCT CAA CTC GTA*

Sequence details for 5'-thioctic acid modified oligonucleotides via post-synthetic solid supported amide formation, where X = thioctic acid.

The sequence modified by post-synthetic solid supported amide formation with thioctic acid was used in the nanoparticle hybridization studies discussed in Chapter 4. Sequence details given above.

With the routes to convenient modification of DNA by thioctic acid confirmed, and the desired thioctic acid-modified oligonucleotides now in hand their ability to functionalise nanoparticles in a stable and robust manner was investigated (Chapter 3). The use of thioctic acid-modified oligonucleotides as materials for surface modification and SERRS detection was also investigated (Chapter 4).

3.4   Chapter 3: Conclusions

The results reported herein show that thioctic acid can be modified to provide the alcohols required for the investigation of 5'-DNA modification. A few critical parameters must be observed when engaged in small molecule synthesis with thioctic acid – namely that the temperature must be kept at 30 °C or below and that UV exposure should be minimized.

For 5'-modification, two direct methods were investigated – the phosphoramidite approach and the H-phosphonate method. The phosphoramidite approach was found to be unsuitable for thioctic acid modification. The H-phosphonate method proved successful and provides potential for automated 5'-thioctic acid modification of oligonucleotides. Further investigation to isolate the H-phosphonate and automate the 5'-modification is required. As the H-phosphonate of thioctic acid, allowing automated thioctic acid modification would be an attractive commercial product.

In addition, an active-ester intermediate of thioctic acid, **13**, was isolated which provided a successful route to pre- and post-synthetic modification of DNA either *via* solid or solution phase reactions. 3'-Modification of DNA by thioctic acid is readily achieved when applying the TA-NHS, **13**, to commercially available amino-modified columns providing a capping step is introduced between the modification and oligonucleotide synthesis. 5'-Modification was achieved by the TA-NHS, **13**, in solution phase. This is convenient for situations when an amino-modified oligonucleotide is "in hand" and modification by thioctic acid is required. Alternatively, solid phase modification was possible by reaction between the TA-NHS, **13**, and a suitable amino-modification at the 5'-end of the synthetic chain.

As a result of its utility, described herein, the active ester of thioctic acid is now commercially available for DNA modification *via* Link Technologies. In addition, as a result of their utility described herein (Chapters 4, 5 and Appendix) thioctic acid

modified oligonucleotide probes are now commercially available for purchase through ATDbio.

3.5 Chapter 3: References

1.   Letsinger, R. L., Elghanian, R., Viswanadham, G., Mirkin, C. A., **2000**, *Bioconjug. Chem.*, 11, 289-291.

2.   Li, Z., Jin, R., Mirkin, C. A., Letsinger, R. L., **2002**, *Nucleic Acids Res.*, 30, 1558-1562.

3.   Schmidt, U., Grafen, P., Goedde, H. W., **1965**, *Angew. Chem. Int. Ed. Engl.*, 4, 846-856.

4.   Berchmans, S., Thomas, P. J., Rao, C. N. R., **2002**, *J. Phys. Chem. B*, 106, 4647-4651.

5.   Chechik, V., Wellsted, H. J., Korte, A., Gilbert, B. C., Caldararu, H., Ionita, P., Caragheorgheopol, A., **2004**, *Faraday Discuss.*, 125, 279-291.

6.   Ionita, P., Caragheorgheopol, A., Gilbert, B. C., Chechik, V., **2004**, *Langmuir*, 20, 11536-11544.

7.   Karamanska, R., Mukhopadhyay, B., Russell, D. A., Field, R. A., **2005**, *Chem. Commun.*, 3334-3336.

8.   Abad, J. M., Mertens, S. F. L., Pita, M., Fernandez, V. M., Schiffrin, D. J., **2005**, *J. Am. Chem. Soc.*, 127, 5689-5694.

9.   Chang, J.-Y., Wu, H., Chen, H., Ling, Y.-C., Tan, W., **2005**, *Chem. Commun.*, 1092-1094.

10. Liu, H., Liu, S., Echegoyen, L., **1999**, *Chem. Commun.*, 1493-1494.

11. Mattoussi, H., Mauro, J. M., Goldman, E. R., Anderson, G. P., Sundar, V. C., Mikulec, F. V., Bawendi, M. G., **2000**, *J. Am. Chem. Soc.*, 122, 12142-12150.

12. Uyeda, H. T., Medintz, I. L., Jaiswal, J. K., Simon, S. M., Mattoussi, H., **2005**, *J. Am. Chem. Soc.*, 127, 3870-3878.

13. Harrison, J. G., Balasubramanian, S., **1997**, *Bioorg. Med. Chem. Lett.*, 7, 1041-1046.

14. Thuong, N. T., Asseline, U., *Curr. Protoc. Nucleic Acid Chem.,* **2000**, 4.2.1-4.2.33; 4.3.1-4.3.16.

15. Beaucage, S. L., Caruthers, M. H., **1981**, *Tetrahedron Lett.*, 22, 1859-1862.

16. Matteucci, M. D., Caruthers, M. H., **1981**, *J. Am. Chem. Soc.*, 24, 3185-3191.

17. McBride, L. J., Caruthers, M. H., **1983**, *Tetrahedron Lett.*, 24, 245-248.

18. [ed.] A. L. Katrinzky. *Comprehensive Organic Functional Group Transformations II.* New York : Pergamon, **1995**, Vol. 5.

19. Reed, L. J., Niu, C.-I., **1955**, *J. Am. Chem. Soc.*, 77, 416-419.

20. Thomas, R. C., Reed, L. J., **1956**, *J. Am. Chem. Soc.*, 78, 6148-6149.

21. Wagner, A. F., Walton, E., Boxer, G. E., Pruss, M. P., Holly, F. W., Folkers, K., **1956**, *J. Am. Chem. Soc.*, 78, 5079-5081.

22. Calvin, M., Barltrop, J. A., **1952**, *J. Am. Chem. Soc.*, 74, 6153-6154.

23. Hall, R. H., Todd, A., Webb, R. F., **1957**, *J. Chem. Soc.*, 3291-3296.

24. Froehler, Ng, P. G., Matteucci, M. D., **1986**, *Nucleic Acids Res.*, 14, 5399-5407.

25. Froehler, B. C., Matteucci, M. D., **1986**, *Tetrahedron Lett.*, 27, 469-472.

26. Garegg, P. J., Lindl, I., Regberg, T., Stawinski, J., Stromberg, R., **1986**, *Tetrahedron Lett.*, 27, 4051-4054.

4 Thioctic Acid Modified Oligonucleotide-Nanoparticle Conjugates

I n 1951 Turkevitch reported a method of gold nanoparticle synthesis involving the aqueous reduction of $HAuCl_4$ by sodium citrate (Figure 4.1). [1] In 1973 Frens reported an alteration of the original Turkevitch method whereby altering the trisodium citrate to gold ratio led to monodisperse nanoparticles of predictable size in the range 16 – 147 nm. [2] Other methods to prepare nanoparticles exist, nevertheless, the Frens citrate method is still used to prepare gold nanoparticles of predictable size with a loose ligand shell. [3] [4]

Silver nanoparticle preparation was reported by Lee and Meisel in 1982. [5] The nanoparticles in that paper (gold and silver) were specifically prepared as substrates for Surface Enhanced Resonance Raman Scattering (SERRS) spectroscopic investigations. The particles were produced by the reduction of $AgNO_3$ by either sodium borohydride or sodium citrate (Scheme 4.1). Silver colloids prepared by citrate reduction have been found to have more monodisperse particle size distribution, greater stability and produce greater SERRS enhancement *c.f.* $NaBH_4$ reduction. [6] However, silver nanoparticles by this method are not as reproducibly prepared as gold analogues and suffer from poorer stability. Nevertheless, the greater enhancing ability of the silver particles resulted in their continued usage as substrates for SERRS investigations. [7]

Nanoparticles of predictable size, suitable monodispersity and relative stability can thus be prepared in the size range of 1-100 nm. This size range falls between the realms of individual atoms and aggregates that are large enough to be considered
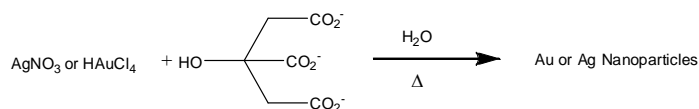
Scheme 4.1: Gold or silver nanoparticle synthesis by citrate reduction.

"bulk" material. The physical properties of these nanomaterials are not like those displayed by the bulk or of molecular compounds. Their properties are influenced by their composition, particle size, shape, inter-particle distance, the nature of surface adsorbate and the dielectric medium in which they are dispersed. [8] [9] [10] [11]

4.1 Thioctic Acid Linked Oligonucleotide Nanoparticle Conjugates: Preparation

4.1.1 Gold Nanoparticle Synthesis by Citrate Reduction

For the studies reported herein, gold nanoparticles were prepared by the citrate reduction method. That is, a solution of sodium tetrachloroaurate ($NaAuCl_4$) was brought to boiling at which point a solution of trisodium citrate was added and boiling was maintained for 15 minutes (Experimental 7.6.1). The syntheses were found to be simple, reproducible and produced stable gold colloids of predictable size. Nanoparticle solutions are commonly assessed using UV-vis as the λ_{max} position is indicative of the monodispersity and size of the particle produced. SEM is an excellent technique for nanoparticle characterisation that gives a detailed image of the size, monodispersity and morphology of the particles produced. However,

Figure 4.1: UV-vis spectra of citrate-reduced gold nanoparticles. (Inset) Scanning electron microscope (SEM) image courtesy of Dr Robert J. Stokes.

SEM is not routinely used to characterize batches. It has been used to show that particles produced by the citrate-reduction method were approximately 15 nm in diameter and spherical. This is in agreement with their UV-vis profile.

4.1.2 Silver Nanoparticle Synthesis by Citrate Reduction

As with the gold colloids discussed above, the silver nanoparticles reported were prepared by the citrate reduction method. That is, a solution of silver nitrate (AgNO$_3$) was added to water which was heated to 40 °C. The solution was then heated rapidly to 98 °C ± 0.5 °C at which point a solution of trisodium citrate was added and the temperature of the solution was maintained at 98°C ± 0.5 °C for 90 minutes (Experimental 7.6.2). The syntheses were found to be relatively reproducible, giving stable silver colloids of predictable size and shape, providing the temperature was carefully maintained throughout. The nanoparticle solutions were commonly assessed using UV-vis, as again, the λ$_{max}$ is indicative of the monodispersity and size of the particle produced. SEM, although not routinely used to characterize the batches, has been used to show that particles of particular UV-vis profile are monodisperse and of regular size and shape (Figure 4.2). Particles produced by this method were found to be approximately 40 nm in diameter and mostly spherical, although a number non-spherical features were observed. Particle
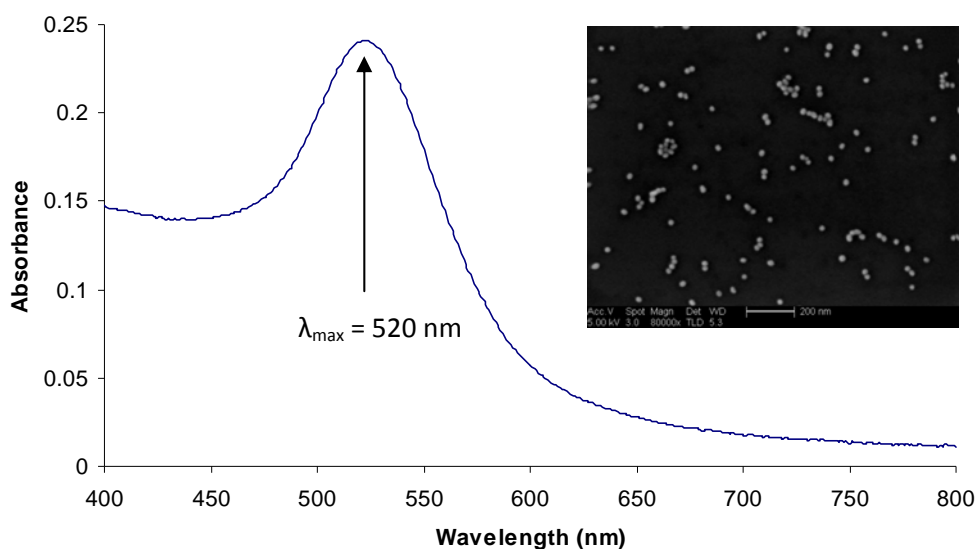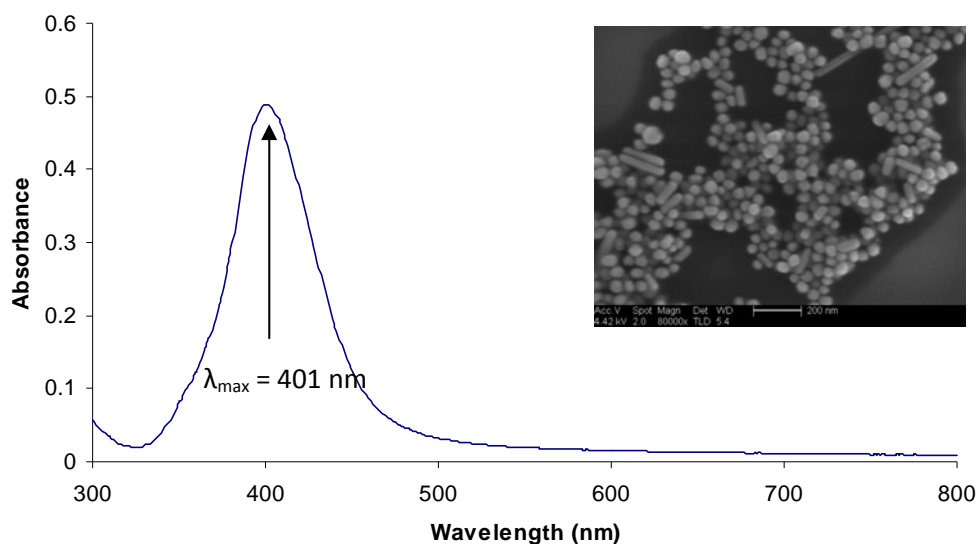

Figure 4.2: UV-vis spectra of citrate-reduced silver nanoparticles. (Inset) Scanning Electron Microscope (SEM) image courtesy of Dr. Robert J. Stokes.

size can also be assessed by dynamic light scattering (DLS) which measures the Brownian motion of the particles and relates this to particle size. The DLS particle size data of the citrate-reduced silver colloid produced was found to be 37.13 nm ± 0.9 nm. This is in agreement with that shown by SEM, reported by other groups and predicted theoretically. [8] [9] The values found here were used to compare with modified particles which were assessed in the same manner (Section 4.1.3).

4.1.3 Oligonucleotide-Nanoparticle Conjugate Preparation

Oligonucleotide-nanoparticle conjugates were prepared using TA-Pr1 and TA-Pr2 oligonucleotide sequences (Table 4.1). Immobilisation of disulfide-modified oligonucleotide sequences on citrate-reduced gold nanoparticles was carried out according to standard protocols as developed for monothiol linked oligonucleotides. This involved addition of the modified oligonucleotide sequences to the nanoparticle suspension. The amount of oligonucleotide to be added to the nanoparticles was calculated by multiplying the total nanoparticle surface area available for reaction by the anticipated surface density of nanoparticle bound oligonucleotide, according to equation 4.1. [12] [Note, an excess is added by a factor of 1.5.]

Equation 4.1: *N^o mol conjugated oligonucleotide = $A_n \times C_n \times D \times V$*

A_n = surface area of nanoparticle

C_n = concentration of nanoparticle solution (in nanoparticles per litre)

D = oligonucleotide density on each particle

V = volume of nanoparticle solution

Name	*Sequence* *(5'-3')*
TA-Pr1	CGC ATT CAG GAT AAA AAA AAA A**Ds**
TA-Pr2	**Ds**A AAA AAA AAA TCT CAA CTC GTA

Table 4.1: Sequences of oligonucleotides that were immobilised on nanoparticles and assessed by gel electrophoresis, where Ds refers to thioctic acid modification.

The starting concentrations of the nanoparticles were 17 nM for Au and 1 nM for Ag. When using monothiol oligonucleotides the standard protocols state that the oligonucleotide should be pre-treated with DTT and desalted, by size exclusion chromatography, directly onto the nanoparticles. However, in the case of thioctic acid modified oligonucleotides the required number of moles of disulfide-modified oligonucleotide was added directly to the nanoparticles (Experimental 7.7.1). This protocol avoids the pre-treatment of the oligonucleotides with DTT, which is usually carried out with monothiol analogues in order to cleave any intermolecular disulfide linkages which may have formed in solution prior to addition. Regardless of the mode of oligonucleotide addition, the samples were then left overnight. Thereafter, 60 mM phosphate (pH 7) was added to a final concentration of 10 mM and again the samples were left overnight. Subsequently, a slow salt-aging process was conducted with thiol oligonucleotide-nanoparticle conjugates. The salt concentration was increased in 0.05 M increments, the thiol systems usually have a salt addition every 12 - 24 h. However, a more rapid salt treatment (3 × 0.05 M increments *per* day to a final concentration of 0.3 M) was carried out with the disulfide systems employed here and the conjugates were found to withstand this process. Salt addition is an important part of the conjugation process as the salt ions associate with the oligonucleotide backbone, minimizing electrostatic repulsion allowing increasing numbers of oligonucleotides to immobilize *per* nanoparticle. In addition, it is ultimately important for salt to be present for an efficient hybridization process. As such, the nanoparticle conjugates are required to be stable in the salt conditions. The final conditions of the oligonucleotide-nanoparticle conjugates were 10 mM phosphate, pH7, 0.3 M NaCl (0.3 M PBS). Once the conjugates were adjusted to 0.3 M PBS, the conjugate systems were centrifuged at 6000 r.p.m. for 15 min (× 1 for Ag, × 2 for Au) which yielded an oily pellet. The supernatant was removed as this would contain excess (unconjugated) oligonucleotide which may interfere with subsequent performance of the conjugates. The conjugates, TA-Pr1-Au, TA-Pr2-Au, TA-Pr1-Ag and TA-Pr2-Ag, where stored at 4 °C in autoclaved eppendorfs and were found to be stable for > 6 months.

Aggregation at any stage of the conjugation process is generally indicative of a failure to conjugate, as oligonucleotide-modified nanoparticles are stable in salt conditions whereas "bare" colloids are not. At the end of the conjugation process the UV-vis spectra were recorded for each sample to ensure no aggregation had occurred. This would be noticeable by a sizeable red-shift in absorbance and marked broadening of the original peak. In addition, successful conjugations should result in an UV-vis spectrum close to that of unmodified nanoparticles, albeit exhibiting a red-shift of a few nanometers and, in the case of silver, a slight broadening of the original plasmon absorbance, due to a change in the local dielectric environment. Typical UV-vis spectra of diluted gold and silver nanoparticle-oligonucleotide conjugates (TA-Pr1-Au and TA-Pr1-Ag, respectively) are shown in Figures 4.3 and 4.4. In the case of TA-Pr1-Au nanoparticle conjugates the plasmon red-shifts slightly from 520 to 525 nm. This is consistent with stable oligonucleotide-nanoparticle conjugates – with no, or minimal, absorbance in the longer wavelength (> 650 nm) region which would be indicative of aggregation. The preparation of the oligonucleotide-Ag nanoparticle conjugates, TA-Pr1-Ag, is also accompanied by a red-shift from 401 nm to 410 nm, and slight broadening of the peak. As with the unmodified particles the particle size was assessed by dynamic light scattering (DLS). Dynamic light
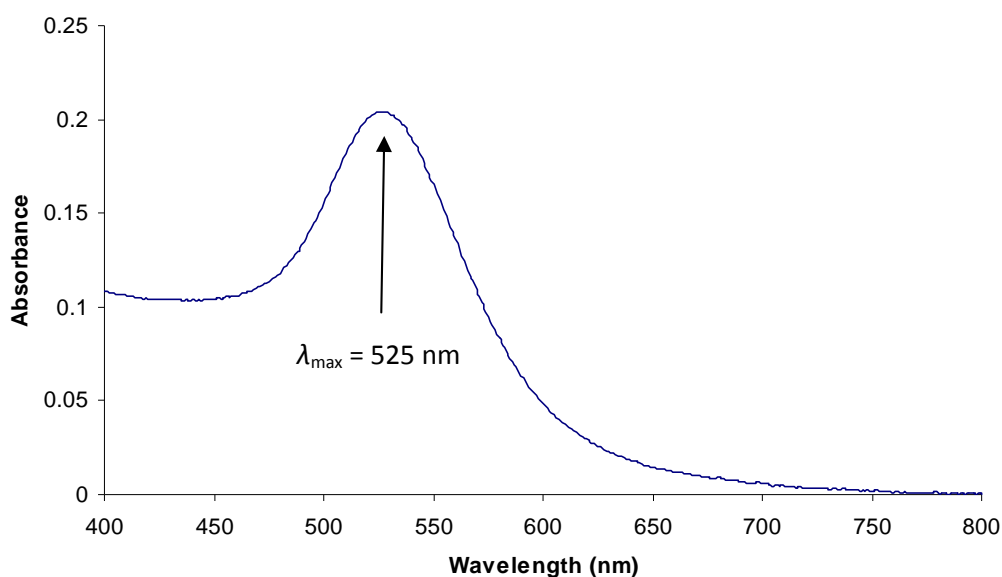
Figure 4.3: UV-vis spectra of TA-Pr1-Au conjugate in 0.3 M PBS.
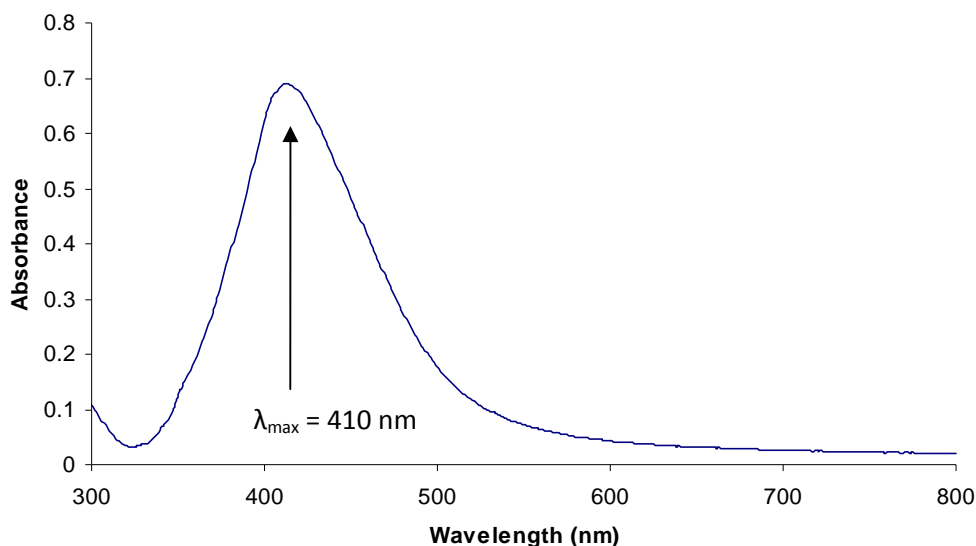
Figure 4.4: UV-vis spectra of TA-Pr1-Ag conjugate in 0.3 M PBS.

scattering provides a measure of the hydrodynamic diameter of the particle. That is to say, not only the particle "core" size but also any surface structure. (Note, it is also influenced by the ionic medium and this must be kept constant for comparative measurements, as such the conjugates were centrifuged and exchanged into water prior to assessment, allowing comparison with the bare Ag NPs). Silver nanoparticles and their conjugates have different diameters as given by DLS. Particle size data suggests that oligonucleotide-silver conjugates have an average size of 42.35 nm ± 1.9 nm *c.f.* 37.13 nm ± 0.9 nm for unmodified particles. This change is indicative of the nanoparticle being surrounded by a different surface layer than that of the citrate of "bare" particles.

4.1.4 Oligonucleotide-Nanoparticle Conjugate Gel Electrophoresis

Gel electrophoresis has been reported as a means of characterizing DNA-Au nanoparticle conjugates. [13] Alivisatos *et al.* have shown that when using a 100 bp sequence on 5 and 10 nm particles, it is possible to separate and purify particles with one to five probes immobilised. An important finding of that study was that nanoparticles with oligonucleotides non-specifically bound did not affect the mobility of the particles *i.e.* without attachment the particles behaved as "bare" when in the presence of non-linked DNA. Smaller 18 bp sequences were also studied and

found that they too could be characterized by gel electrophoresis. It was not possible to separate the singly from the doubly modified particles using the conditions reported but using varying excesses of oligonucleotides to conjugate with the nanoparticles resulted in defined bands that could be collected and stored for later use.

In an experiment conducted to show that the nanoparticles used in this study were modified with oligonucleotides, gel electrophoresis was carried out (Experimental 7.8). The gel electrophoresis conditions were different to those used by Alivisatos *et al.* since in this study 15 nm particles were being used. As such an agarose gel of decreased density (1.5 % *c.f.* 3 %) was used. In this experiment both gold and silver oligonucleotide nanoparticle conjugates were studied. In the literature, to date, only gold nanoparticle conjugates have been studied by gel electrophoresis. A photograph of the gel is shown in Figure 4.5. A DNA ladder has been run in the lanes marked "L", to give an indication of the progress of the gel. In each of the nanoparticle lanes (1 − 6) the nanoparticles were added with loading buffer that contained a blue marker. The loading buffer is used to "weigh down" the samples to prevent them escaping the well prior to the run. The blue marker, in this case, was added to give a clear indication of the progression of the gel during the run. Lane one was loaded with unconjugated, citrate-reduced gold nanoparticles. Upon addition to the well, the "bare" particles aggregate (as indicated by their black colour) and do not progress through the gel at all. Lanes 2 and 3 had TA-Pr1-Au and TA-Pr2-Au loaded, respectively. It was immediately clear that oligonucleotide-modified gold nanoparticles ran distinctly from the unconjugated control. It is usually necessary to add dyes in order to visualise the movement of DNA during gel electrophoresis, however, with oligonucleotide-nanoparticle conjugates the intense colour of the nanoparticles is sufficient for visualization as can be seen from the characteristic red bands. Unconjugated citrate-reduced silver nanoparticles were run in lane 4. As with the gold analogues, they have precipitated with an indicative colour change to green/grey. Lanes 5 and 6 had TA-Pr1-Ag and TA-Pr2-Ag loaded, respectively. Again, the movement of the nanoparticle conjugates could be seen by
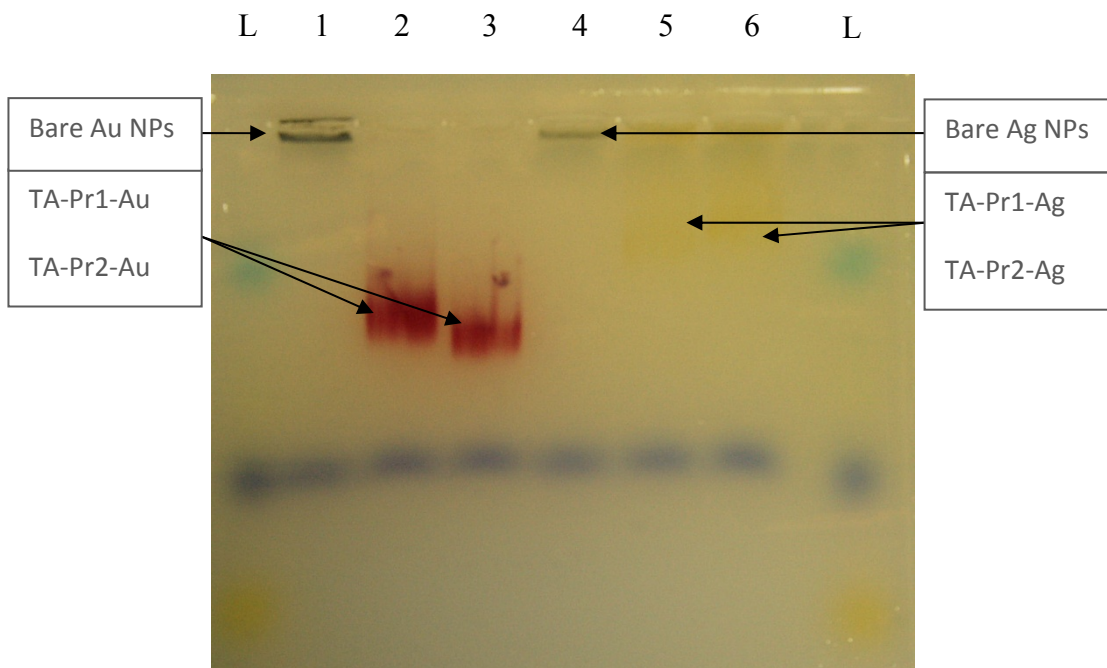
Figure 4.5; Experimental 7.8: Gel electrophoresis of bare nanoparticles and nanoparticle-DNA conjugates in a 1.5 % agarose gel, where L = ladder; 1 = "bare" gold colloid; 2 = TA-Pr1-Au; 3 = TA-Pr2-Au; 4 = "bare" silver colloid; 5 = TA-Pr1-Ag; 6 = TA-Pr2-Ag. [Note, background colour of gel distorted during printing.]

the distinctive yellow colouration of the silver nanoparticle conjugates. One difference that was immediately obvious between the gold and silver conjugate systems is their mobility. The gold-oligonucleotide nanoparticle conjugates moved faster than their silver analogues, which was not surprising given their smaller size (15 nm *c.f.* 40 nm).

In this study it was sufficient to show modification of the nanoparticles by the thioctic-acid modified oligonucleotides. However, an interesting project would be to explore the use of gel electrophoresis as a purification technique during the preparation of oligonucleotide-nanoparticle conjugate, thereby optimizing their surface coverage. This would increase the homogeneity of the nanoparticle conjugates and allow a comprehensive study of the effect of probe density on a variety of subsequent experiments.

4.2 Thioctic Acid Linked Oligonucleotide Nanoparticle Conjugates: Hybridisations

In order for the thioctic-acid modified oligonucleotide nanoparticle conjugates to be analytically significant it was important that they retain the melting characteristics of their thiol analogues. Oligonucleotide-Nanoparticle-Conjugate hybridizations (depicted in Figure 4.6), as studied by Mirkin *et al.*, [14] are governed by a number of factors, including:

- Oligonucleotide density on nanoparticle surface,
- Nanoparticle size,
- Salt concentration, and
- Interparticle distance.

For the oligonucleotide-nanoparticle conjugate melts shown herein the salt conditions were kept constant throughout at 0.3 M PBS. The particle size for each class was constant *i.e.* 15 nm for Au and 40 nm for Ag. Each batch of
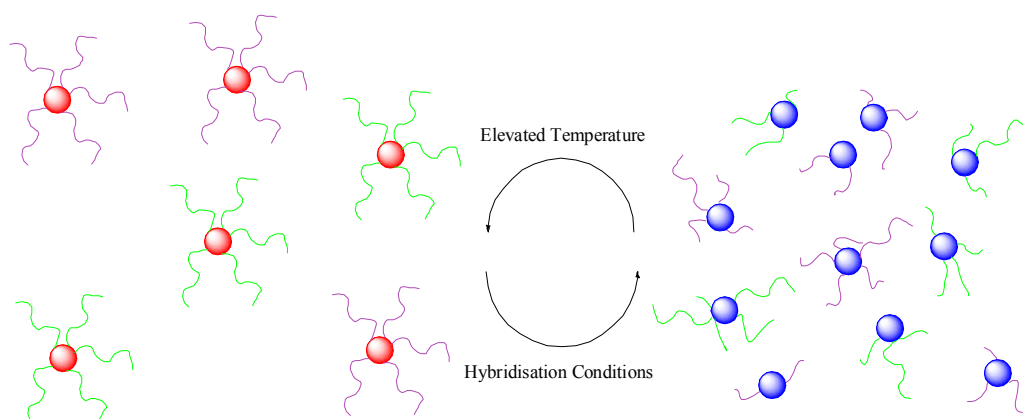
Figure 4.6: Representation of hybridization-induced nanoparticle aggregation. Aggregation occurs only when a target complementary to both probes is introduced under hybridisation conditions. The colour of the particles indicates the colour (to the eye) of the nanoparticle solution when in the disperse state (red) and aggregated state (blue). This colour change is reversible as heating above the melting temperature of the duplex DNA results in the aggregate being re-dispersed.

oligonucleotide-nanoparticle conjugate was prepared in the same way (one method for gold and another for silver) with no attempt to control the oligonucleotide density (values for average oligonucleotide surface densities are discussed in sections 4.3.2 and 4.3.4).

It should be noted that it is widely reported that potentially "any" sequence of oligonucleotide can be targeted by this method. It has been found during the course of these investigations (and in discussion with co-workers) that the oligonucleotide-nanoparticle conjugate stability can be unpredictably sequence specific. Further investigation is required to establish an understanding of this.

4.2.1 Oligonucleotide Gold Nanoparticle Hybridisations

Two arrangements of nanoparticle probes were attempted, with differing interparticle distance. That is, a "head-to-head" and "tail-to-tail" arrangement were compared (see Figure 4.7 for pictorial representation). The probe sequences used in the hybridization experiments are shown in Table 4.2. The probes were used at a nanoparticle concentration of 1 nM. The "target" sequence was added to a final concentration of 0.1 μM in 0.3 M PBS and the sample was cycled between 15 °C and 75 °C with the absorbance monitored at the gold nanoparticle plasmon band, 520 nm (Experimental 7.9.1).   Aggregated gold nanoparticles have reduced absorbance at 520 nm and a red-shift in absorbance maxima to ~ 675 nm. When hybridization occurs there should be a transition observed from aggregated nanoparticles to dispersed colloid accompanied by an increase in absorbance at 520 nm.   Three
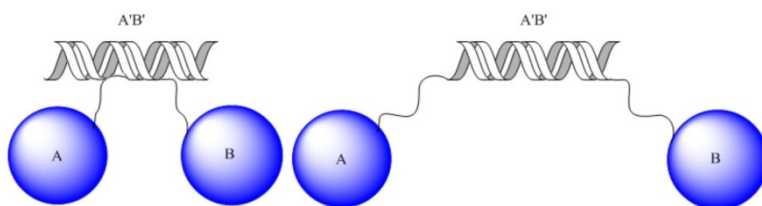
Figure 4.7: "Head-to-head" and "tail-to-tail" arrangement of nanoparticles during hybridization-induced nanoparticle aggregation.

Probe Name	Probe Sequence
TA-Pr1	CGC ATT CAG GAT AAA AAA AAA A-Ds
TA-Pr2	Ds-A AAA AAA AAA TCT CAA CTC GTA
Target (HH)	TAC GAG TTG AGA ATC CTG AAT GCG
SNP (HH)	TAC GAG TTG AGA **C**TC CTG AAT GCG
Nonsense (HH)	TAC GAG TTG AGA CGC ATT CAG GAT
Target (TT)	ATC CTG AAT GCG TAC GAG TTG AGA
SNP (TT)	ATC CTG AAT GCG TAC GAG TTG AG**G**
Nonsense (TT)	TCT CAA CTC GTA CGC ATT CAG GAT

Table 4.2: Sequences for hybridizations. Where Ds = thioctic acid modification, HH refers to "head-to-head" arrangement of nanoparticles and TT refers to "tail-to-tail" arrangement of nanoparticles. All sequences are written 5'-3' by convention.

different "target" systems were tested. A fully complementary target sequence, a single base mismatch sequence (SNP) and a nonsense sequence. Plotting the absorbance at 520 nm against temperature gives a clear indication of the hybridization-induced nanoparticle aggregation.

4.2.1 (a) "Head-to-Head" Au Conjugate Hybridisation

The TA-Pr1 and TA-Pr2 probes were hybridised with a target that was chosen to produce the head-to-head arrangement of nanoparticles (Figure 4.8). As can be seen in Figure 4.9 the complementary sequence and single base mismatched sequence gave a melting transition, whereas the nonsense sequence did not. This is because single base mismatches are tolerated to some degree *i.e.* hybridisation can still occur.

```
T—A—C—G—A—G—T—T—G—A—G—A—A—T—C—C—T—G—A—A—T—G—C—G
A—T—G—C—T—C—A—A—C—T—C—T**T—A—G—G—A—C—T—T—A—C—G—C
```
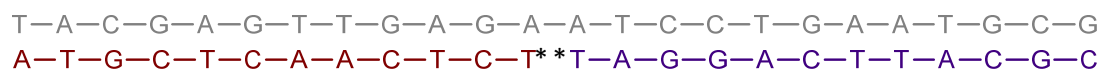
*Figure 4.8: Duplex sequences for "head-to-head" conjugate hybridization. Where, * denotes a 10A spacer group, thioctic acid modification and nanoparticle (Au, 15 nm). TA-Pr1-Au is shown in indigo, TA-Pr2-Au in red. Target (grey) 5'-3'.*

87
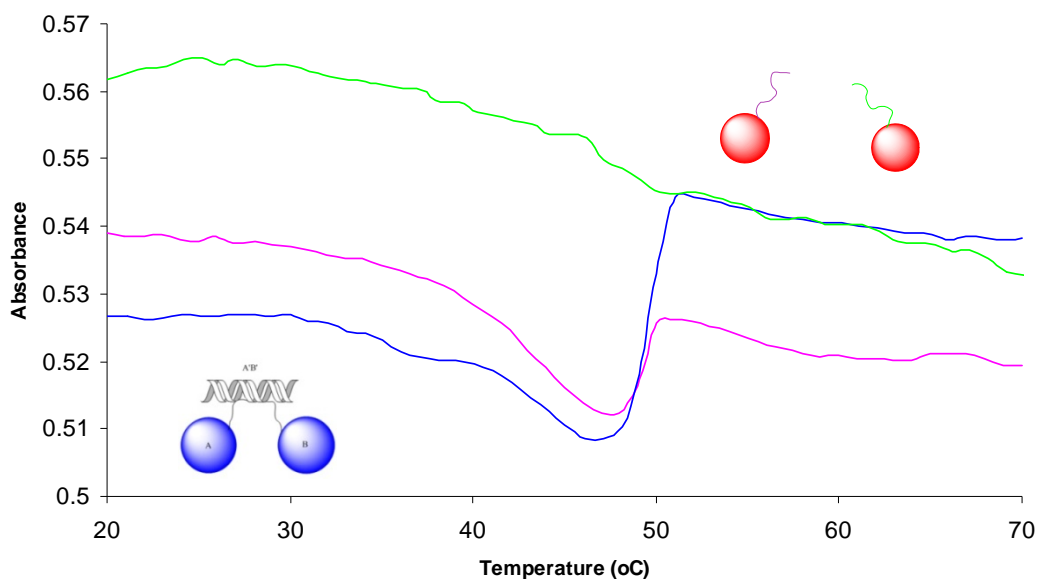
Figure 4.9: "Head-to-head" arrangement of oligonucleotide-gold nanoparticle conjugate melting profile. Blue – Target (HH), Pink – SNP (HH), Green – Nonsense (HH). Absorbance measured at 520 nm. Nanoparticle cartoon added to highlight aggregate condition of nanoparticles with respect to temperature.

A lower melting temperature was observed for the single base mismatch than for the full complement (48.5 °C *c.f.* 50.5 °C). That is, less energy is required to disrupt the duplex and redisperse the nanoparticles. It is worthwhile to note that the absorbance range over which this transition occurred was very low. It can be reasoned that there is a significant stereoelectronic barrier to hybridisation when the nanoparticles are arranged in such a manner at the centre of the duplex.

4.2.1 (b) "Tail-to-Tail" Au Conjugate Hybridisation

```
A—T—C—C—T—G—A—A—T—G—C—G—T—A—C—G—A—G—T—T—G—A—G—A
*T—A—G—G—A—C—T—T—A—C—G—C  A—T—G—C—T—C—A—A—C—T—C—T*
```
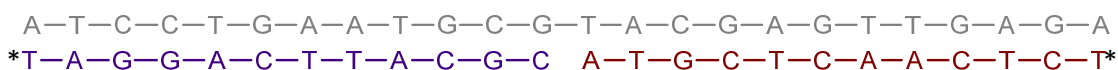
*Figure 4.10: Duplex arrangement for "tail-to-tail" conjugate hybridization. Where * denotes a 10A spacer group, thioctic acid modification and nanoparticle (Au, 15 nm). TA-Pr1-Au is depicted in indigo; TA-Pr2-Au in red. (Target written 5'-3').*

The same probes, TA-Pr1-Au and TA-Pr2-Au, were used to investigate the tail-to-tail arrangement of nanoparticles with the Target (TT) used to alter the arrangement (Figure 4.10). As can be seen in Figure 4.11 only the complementary sequence gave a transition profile, whereas the single base mismatch and nonsense sequence did not. This could be because single base mismatches for the "tail-to-tail" arrangement were in a different position than for the "head-to-head" and were not tolerated. In both cases the mismatch was chosen at a site closest to the nanoparticle of one of the probes. In the case of the "tail-to-tail" arrangement the mismatch was at the terminus of the oligonucleotide target sequence and as such could have a greater inhibitory effect to DNA hybridization than at the centre of the duplex (as with "head-to-head"). The melting transition temperature for the "tail-to-tail" configuration of the DNA nanoparticle conjugate hybrid was 53.1 °C. The hybridization induced aggregation occurred to a greater extent in the "tail-to-tail"
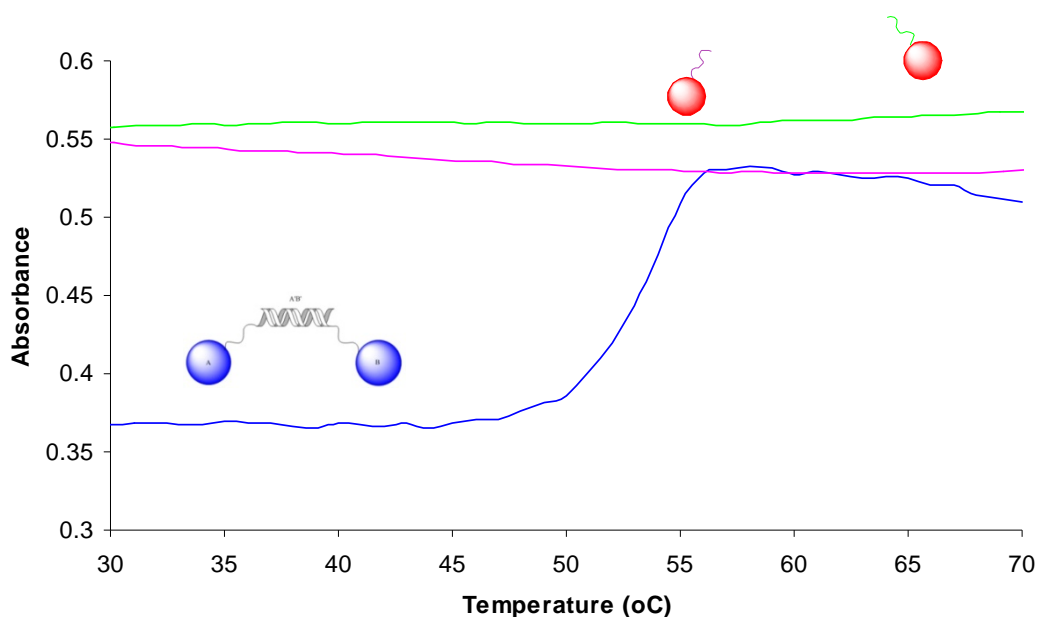
Figure 4.11: "Tail-to-tail" arrangement of oligonucleotide-gold nanoparticle hybridisations. Blue – Target (TT), Pink – SNP (TT), Green – Nonsense (TT). Absorbance measured at 520 nm. Nanoparticle cartoon added to highlight aggregate condition of nanoparticles with respect to temperature and absorption.
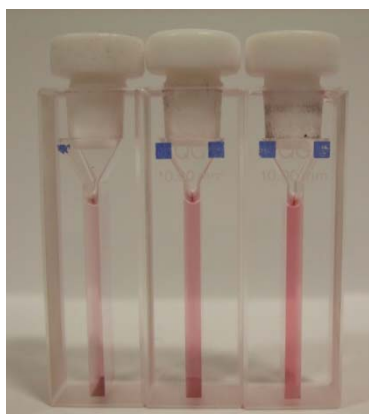
Figure 4.12: Image of gold nanoparticle hybridizations with full complement (left), single base mismatch (middle) and nonsense (right).

configuration than in the "head-to-head" configuration (absorbance change of ~ 0.18 *c.f.* 0.04) which is in agreement with the idea that the nanoparticle arrangement in the "tail-to-tail" system is more favourable for hybridisation, when compared with "head-to-head". This was also evidenced by the fact that in the "tail-to-tail" configuration the hybridization-induced aggregation was visible to the naked eye as can be seen in Figure 4.12. Only the cuvette containing the full complement (far left) showed evidence of hybridization, with the aggregates settling to the bottom. This resulted in an obvious reduction in the ruby hue of the colloidal solution. The gold hybridisation mixtures for the SNP and nonsense sequences retain the characteristic red hue of unaggregated particles.

It was pleasing, at this stage, to have confirmed that the gold nanoparticle-oligonucleotide conjugates tethered *via* thioctic acid modification could perform as hybridization sensors. Silver nanoparticles are considered attractive substrates for detection systems and as such, the thioctic acid-modified oligonucleotides were applied to silver nanoparticles and were used to detect hybridization events.

4.2.2 *Oligonucleotide Silver Nanoparticle Hybridisations*

Oligonucleotide silver nanoparticle conjugates have received considerably less attention in the literature. However, they remain attractive targets for oligonucleotide detection systems as they benefit from a significantly larger extinction coefficient than gold (2.8×10^{10} *c.f.* 2.7×10^{8}). They also offer greater

enhancement when used in SERRS experiments due to the increase in polarisability of their surface electrons. [15] However, the thiol-silver interaction does not benefit from the stability of that of thiol-gold. Thioctic acid modified oligonucleotide-nanoparticle conjugates were thus assessed for applicability in a detection scenario as well as being investigated for stability.

As with the gold nanoparticle investigations, two arrangements of nanoparticle probes were attempted, with differing interparticle distance. That is, a "head-to-head" and "tail-to-tail" arrangement were compared (see Figure 4.7 for pictorial representation). Sequences used for hybridization experiments are shown in Table 4.2.

With both the "head-to-head" and "tail-to-tail" arrangements, the probes were used at nanoparticle concentrations of 10 pM. The target was added to a final concentration of 2 nM in 0.3 M PBS and the sample was cycled between 15 °C at 75 °C with the absorbance at 407 nm monitored (Experimental 7.9.2). Where hybridization occurs there should be a transition observed from aggregated nanoparticles to dispersed colloid indicated by an increase in absorbance at 407 nm. Three different "target" systems were tested: a fully complementary target sequence, a single base sequence and a "nonsense" sequence.

4.2.2 (a) "Head-to-Head" Ag Conjugate Hybridisation

As with the gold nanoparticle conjugates, a target sequence was chosen such that the hybridisation of the probes would result in a "head to head" arrangement of nano--particles (Figure 4.13). The absorbance at 407 nm was plotted against temperature

```
T—A—C—G—A—G—T—T—G—A—G—A—A—T—C—C—T—G—A—A—T—G—C—G
A—T—G—C—T—C—A—A—C—T—C—T**T—A—G—G—A—C—T—T—A—C—G—C
```
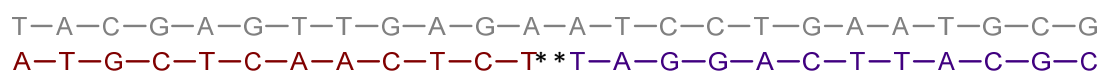
Figure 4.13: Duplex arrangement for "head-to-head" conjugate hybridization. Where, * denotes a 10A spacer group, thioctic acid modification and nanoparticle (Ag, 40 nm). TA-Pr1-Ag is depicted in indigo and TA-Pr2-Ag is depicted in red.
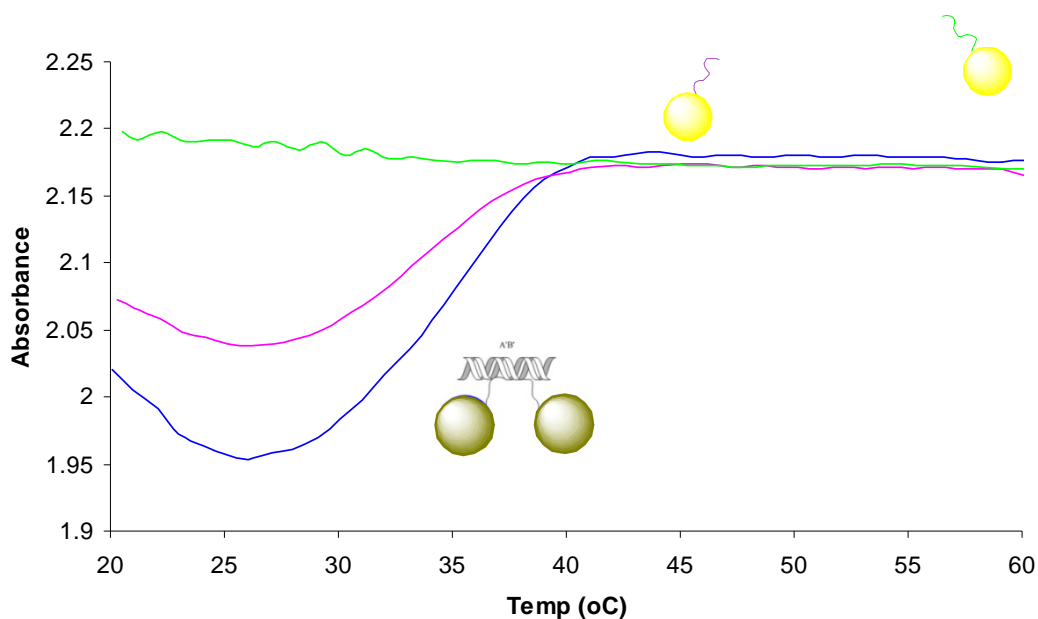
Figure 4.14: "Head-to-head" melting profiles of DNA-Ag conjugates, with absorbance at 407 nm, acquired as a function of temperature. Blue – Target (HH), Pink – SNP (HH), Green – Nonsense (HH).

to give a clear indication of the hybridization-induced nanoparticle aggregation (Figure 4.14). The complementary sequence and single base mismatched sequence gave a melting transition, whereas the nonsense sequence did not. A lower melting temperature was observed for the single base mismatch than for the complement (33.5 °C *c.f.* 34.7 °C) indicating that the SNP hybrid system is, as would be expected, less stable than the full complement.

```
A—T—C—C—T—G—A—A—T—G—C—G—T—A—C—G—A—G—T—T—G—A—G—A
*T—A—G—G—A—C—T—T—A—C—G—C   A—T—G—C—T—C—A—A—C—T—C—T*
```
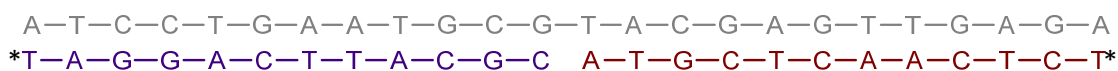
*Figure 4.15: Duplex arrangement for "tail-to-tail" conjugate hybridization. Where, * denotes a 10A spacer group, thioctic acid modification and nanoparticle (Ag, 40 nm). (Target (grey) written 5'-3'). TA-Pr1-Ag is shown in indigo and TA-Pr2-Ag in red.*
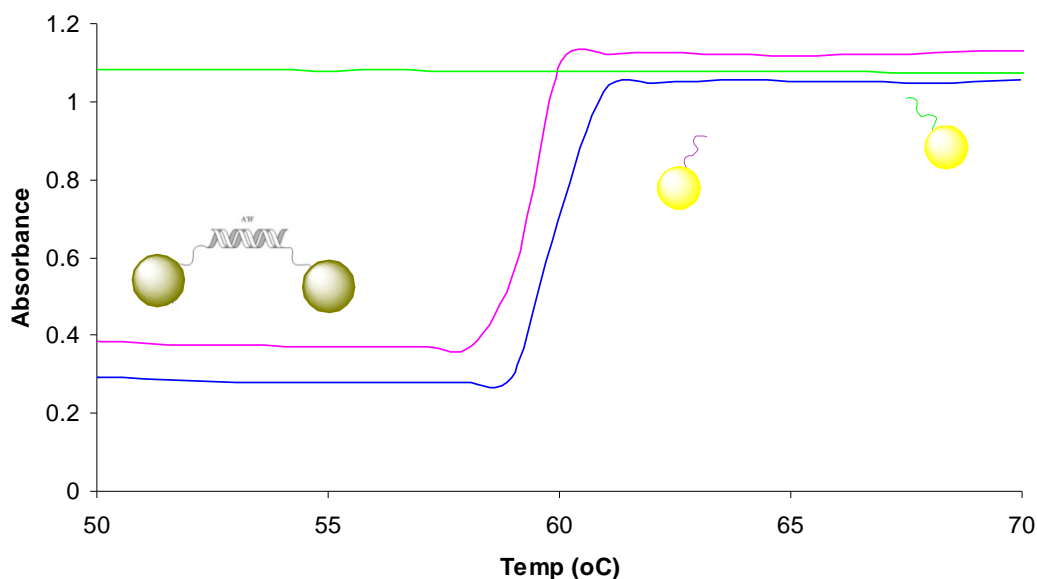
Figure 4.16:   TA-modified oligonucleotide silver nanoparticle conjugates (20 pM) were hybridised in a tail-to-tail arrangement with 2 nM target DNA. Blue – Target (TT), Pink – SNP (TT), Green – Nonsense (TT).

4.2.2 (b) "Tail-to-Tail" Ag Conjugate Hybridisation

A target sequence was chosen to induce a "tail-to-tail" orientation of nanoparticles, upon hybridisation with the immobilised probes (Figure 4.15). Subsequently plotting the absorbance at 407 nm as a function of temperature gave a clear indication of the hybridization-induced nanoparticle aggregation (Figure 4.16). Both the complementary sequence and the single base mismatch gave a transition profile, whereas the nonsense sequence did not. As expected a lower melting temperature is observed for the single base mismatch than for the complement (59.0 °C *c.f.* 59.9 °C). The hybridization induced aggregation also occurred to a greater extent in the "tail-to-tail" configuration than in the "head-to-head" configuration (absorbance change of 0.95 *c.f.* 0.25). Moreover, the "tail-to-tail" arrangement of oligonucleotide-silver nanoparticle conjugate hybrids produced particularly sharp transition profiles *c.f.* gold. This can be rationalized due to the known co-operative nature of the oligonucleotide-nanoparticle melting process. [14] It has been shown by others that the melting transition of oligonucleotide-nanoparticle conjugates is not simply a glimpse at the final oligonucleotide melting events
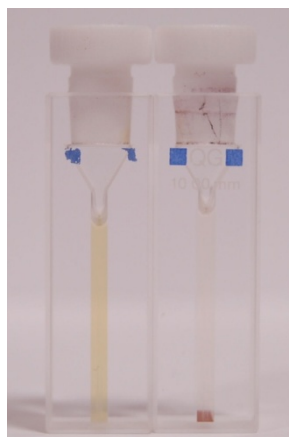
Figure 4.17: TA-modified oligonucleotide silver nanoparticle conjugates in the presence of nonsense (left) and complementary (right) target DNA.

required to separate the particles. Rather, that once a duplex within a conjugate aggregate begins to melt, it causes other duplexes around it to melt in a co-operative manner. It has been argued that this neighbouring influence is responsible for the relatively sharp transitions observed. It follows therefore, that as silver nanoparticles are larger than gold (40 nm *c.f.* 15 nm) and have greater surface coverage of oligonucleotides (Section 4.3.4), that more hybridization events could be occurring and the resulting cooperative duplex melting effect would be greater. The hybridisation-induced aggregation of silver-oligonucleotide nanoparticle conjugates was visible to the naked eye as can be seen in Figure 4.17. The cuvette containing the fully complementary sequence, Target (HH), (right) showed clear evidence of aggregation with the aggregates settling to the bottom and an obvious reduction in the yellow hue of colloidal solution.

The silver nanoparticle-oligonucleotide conjugates tethered *via* thioctic acid modification were successfully implemented as hybridization sensors. The unoptimised detection limits were greater than for the gold analogues and the silver nanoparticle conjugates, although reportedly less stable than their gold analogues, were found to behave more predictably than their gold counterparts in a detection scenario. As a key objective of this project, the stabilities of both the TA-oligonucleotide Au and Ag nanoparticle conjugates were assessed.

4.3 Thioctic Acid Linked Oligonucleotide-Nanoparticle Conjugates: Stability

It is known that oligonucleotide-gold nanoparticle conjugates, linked *via* thiol, are relatively unstable under certain conditions, such as in the presence of certain biological buffer additives *e.g.* DTT or mercaptoethanol, especially at elevated temperatures. [16] Additionally, larger nanoparticles (> 30 nm) are unstable at high salt concentrations (0.3 – 1.0 M NaCl) and elevated temperatures (> 40 °C). Generating conjugates of enhanced stability would allow them to be employed as sensors in environments of greater complexity.

Having isolated thioctic acid modified sequences and prepared both gold and silver nanoparticle conjugates and confirmed their biologically relevant integrity (as described in Section 4.2), it was imperative that their stability be assessed. Monothiol is considered the "standard" linking methodology, and as such, was used as a benchmark for the stability assessment. Following a protocol laid out by Mirkin *et al* [16] dithiothreitol, **14**, DTT (Figure 4.18) was used to displace the modified oligonucleotides from the nanoparticle surface.

Coverage of nanoparticles with oligonucleotides provides stability to the colloid since the electrostatic repulsion and steric protection between oligonucleotides on neighbouring particles is sufficiently high to inhibit their aggregation. The displacement of this polyanionic, oligonucleotide species with a neutrally charged molecule, results in irreversible aggregation in the presence of salts. The aggregation event is coupled with a significant and irreversible red shift in the UV-vis

14
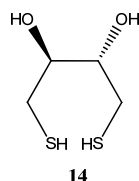
*Figure 4.18: Dithiothreitol, **14**, is a suitable neutral molecule to use in a displacement stability study.*

spectra of the system. This means that the displacement of oligonucleotide sequences and resulting aggregation can be easily monitored by UV-vis spectroscopy. The relative stability of two different linkers can be assessed by comparing the rate of aggregation of the nanoparticle substrates upon treatment with DTT (or other suitable species such as mercaptoethanol).

Three sequences were used with a thioctic acid modification at the 3'-terminus and a 5'-FAM label, thiol analogues of these sequences were also investigated for comparison (Table 4.3). The sequences were chosen to assess whether the presence of spacer bases between the linker moiety and probe sequence would have an affect on the stability and/or surface coverage of the Au and Ag conjugates. Thiol conjugates are usually prepared by treating thiol-modified oligonucleotides with DTT (in order to reduce any disulfide bonds formed in solution during storage) ensuring a mono-thiol form. Before being added to the nanoparticles it was essential to remove the DTT, by size exclusion chromatography; collecting the oligonucleotide directly onto the nanoparticle solutions. It was decided to assess whether this step was necessary. Thiol conjugates were thus prepared in the standard
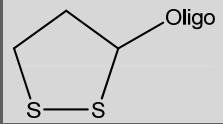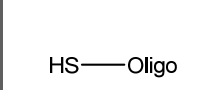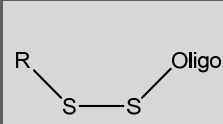
Linker	Probe	Sequence (5'-3')
	D1	FAM CAT TGA AGC TTC **Ds**
	D2	FAM CAT TGA AGC TTC TTT TTT TTT T **Ds**
	D3	FAM CAT TGA AGC TTC AAA AAA AAA A **Ds**
	T1	FAM CAT TGA AGC TTC **SH**
	T2	FAM CAT TGA AGC TTC TTT TTT TTT T **SH**
	T3	FAM CAT TGA AGC TTC AAA AAA AAA A **SH**
	TT1	FAM CAT TGA AGC TTC **SR**
	TT2	FAM CAT TGA AGC TTC TTT TTT TTT T **SR**
	TT3	FAM CAT TGA AGC TTC AAA AAA AAA A **SR**

Table 4.3: Stability study sequences; where Ds, SH and SR represents Thioctic acid, pre-treated thiol (DTT) and untreated thiol respectively, FAM represents a fluorescein modification. R is -CH₂CH₂CH₂OH.

(pre-treated with DTT) fashion (TX) and with omission of the DTT pre-treatment step (TTX) (Experimental 7.7.2 and 7.7.3, respectively). Thioctic acid-modified oligonucleotides were added directly to the nanoparticle suspensions (DX) (Experimental 7.7.1). All sequences were immobilised on both gold and silver citrate reduced nanoparticles yielding the required conjugates. Following literature precedent the stabilities of the oligonucleotide nanoparticle conjugates (gold and silver) were assessed by treatment with DTT (10 mM final concentration) at 40 °C (Experimental 7.10.1). The disappearance of the plasmon peak at 520 nm (Au) or 410 nm (Ag) and the appearance of one between 600 – 700 nm (Au) is indicative of the progressive aggregation event. Absorption spectra were taken at periodic intervals. In the case of the disulfide modified oligonucleotide nanoparticle conjugates, spectra were recorded at 5 or 10 min intervals. However, the rapidity of the aggregation event with the thiol-terminated oligonucleotide nanoparticle conjugates required spectra to be taken at 1 min intervals. Figure 4.19 shows typical UV-vis spectra from DTT stability experiments with spectra recorded at 10 min intervals for disulfide-modified oligonucleotide-gold conjugates. Figure 4.20 shows
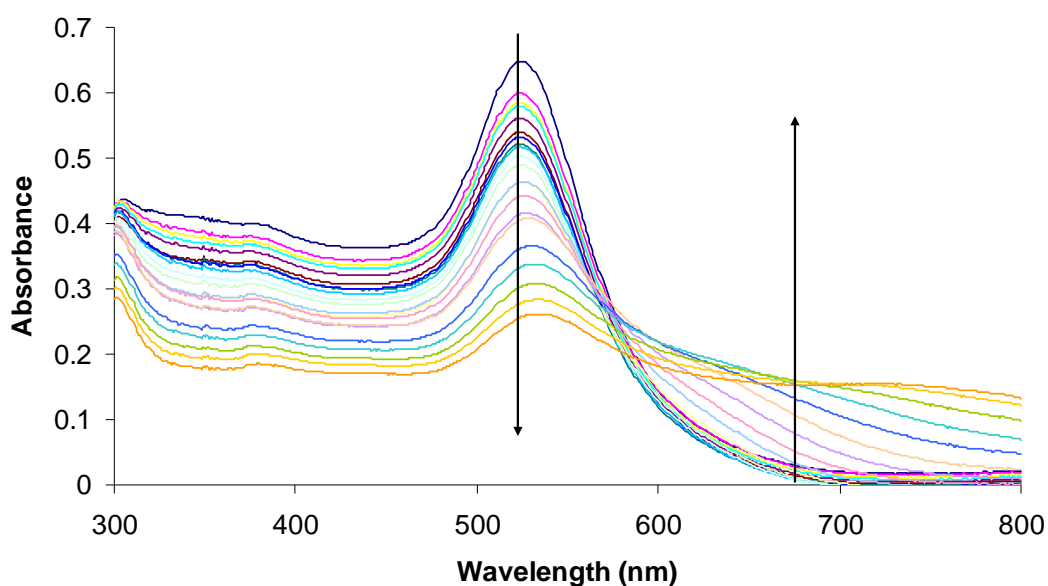
Figure 4.19: Absorbance of thioctic acid-modified oligonucleotide gold nanoparticle conjugates vs. Wavelength (nm) at 10 min intervals. Arrows added to highlight the change in spectra with time.
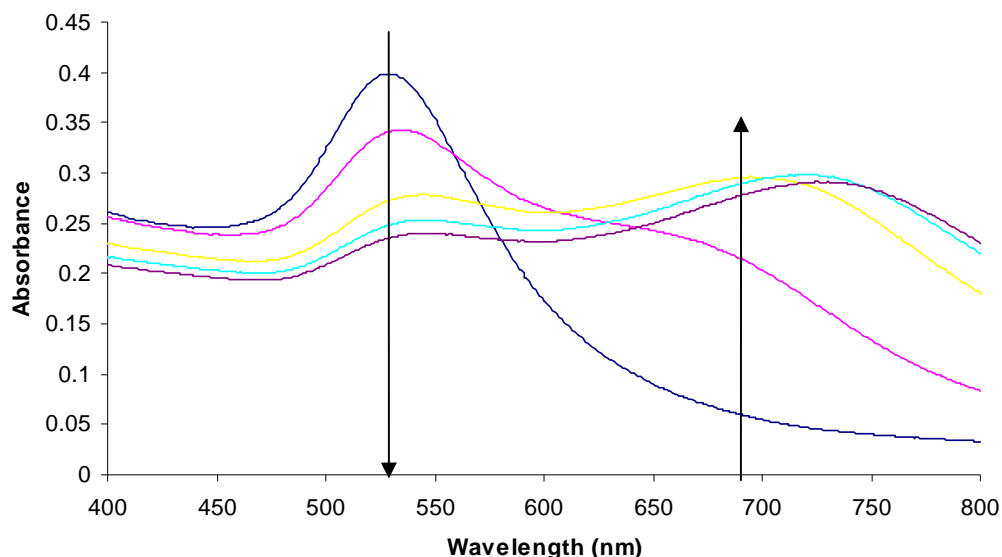
Figure 4.20: Absorbance of monothiol-modified oligonucleotide conjugates vs. Wavelength (nm) at 1 min intervals. Arrows added to indicate change of spectra with the progression of time.

the UV-vis spectra from the thiol analogue under the same experimental conditions but with spectra recorded at 1 min intervals. Even from these "busy" plots, the enhancement in stability of the conjugates can be seen when employing the disulfide modification, where each coloured line signifies another 10 min interval *c.f.* 1 min for the thiol plot. However, viewing the data in this form doesn't allow for an easy comparison of stabilities. Plotting absorbance at a particular wavelength *versus* time for each experiment allows for a more telling comparison.

4.3.1 Gold Nanoparticle-Oligonucleotide Stability

The stability of the D1-Au, D2-Au, D3-Au, T1-Au, T2-Au, T3-Au, TT1-Au, TT2-Au and TT3-Au conjugates can be seen in Figures 4.21 and 4.22. These plots show the absorbance versus time at 675 nm for each of these samples. This wavelength was selected as increasing values at 675 nm indicates the aggregation event is occurring, accompanied by the generation of a plasmon band in that region. The DX results (Figure 4.21) are plotted together to highlight the effect of spacer bases as are the TX (Figure 4.22). The plots for TTX are the same as for TX and are omitted for brevity. The half-life (time taken for absorbance at 675 nm to reach half

maximum for complete aggregation) was calculated for each conjugate for ease of comparison (Table 4.4). The disparate stabilities of the thiol and disulfide systems are striking when comparing the half-lives of the conjugate systems. All of
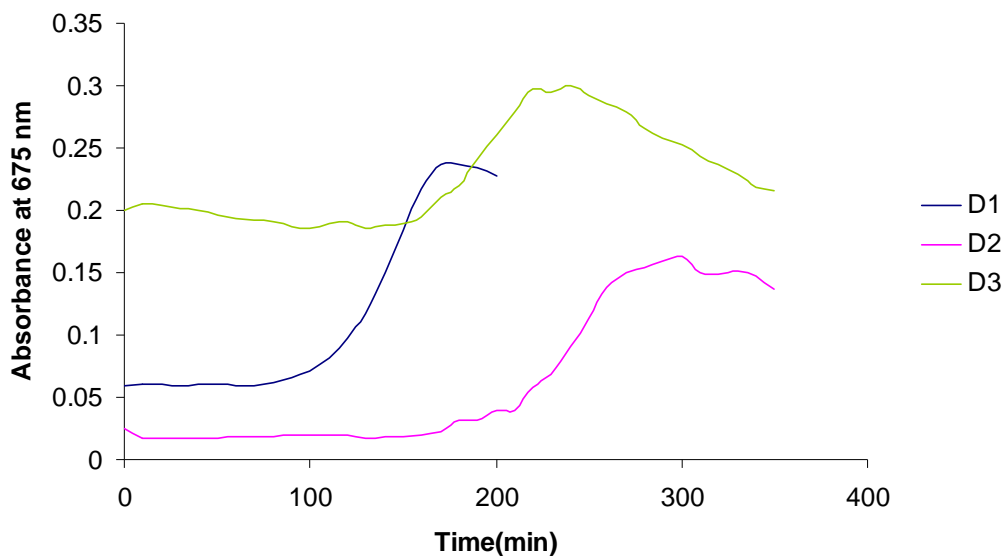
Figure 4.21: DX-Au conjugates, when treated with 10 mM DTT, monitored at 675 nm.
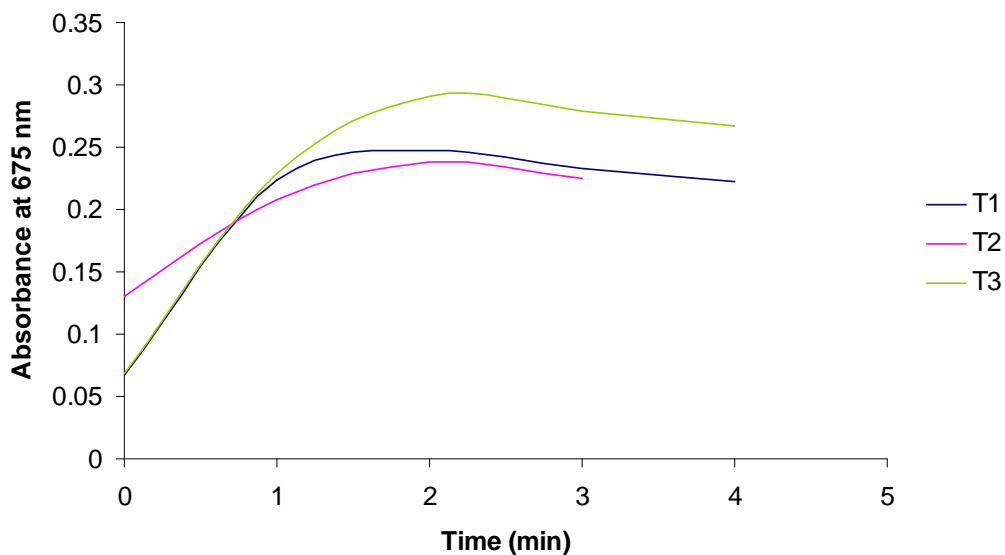
Figure 4.22: TX-Au conjugates, when treated with 10 mM DTT, monitored at 675 nm.
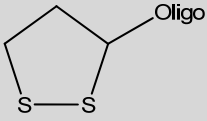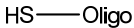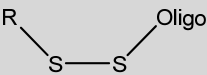
Linker	Probe	$t_{1/2}$ (min)
	D1-Au	140.0
	D2-Au	245.0
	D3-Au	195.0
	T1-Au	0.5
	T2-Au	1.0
	T3-Au	0.5
	TT1-Au	0.75
	TT2-Au	1.0
	TT3-Au	1.0

Table 4.4: Half lives for Au-oligonucleotide conjugates.

the Au-monothiol systems have reached the half-way point of complete aggregation in 1 min or less. Compare this with the thioctic acid disulfide system and the enhanced stability is apparent with half-lives of 140, 195 and 245 min.

It should be noted (as shown in Figure 4.21) that the DTT-induced aggregation event, when applied to thioctic acid linked conjugates, is not linear; a long period of sustained stability is followed by a steady increase in absorbance. It is believed that at the early stages of oligonucleotide displacement by DTT there would remain sufficient oligonucleotide on the surface to inhibit aggregation. However, a critical surface coverage is reached at which point aggregation is no longer prevented and will then continue to completion. With the thioctic acid modified conjugates (Figures 4.21), aggregation begins at 90 min incubation for D1 (no spacers), 2 h for D2 and D3 (polyT and polyA spacers, respectively) and is considerable by 3 h. This shows an excellent enhancement of stability when compared with the monothiol results (Figure 4.22) which show complete aggregation in less than 5 min. The emergence of the 675 nm peak is indicative of nanoparticle aggregation, however, by 300 min in the disulfide system there is a loss of signal altogether; this feature can be attributed to the aggregate species growing in size and eventually settling out of the colloidal solution leaving a colourless supernatant. In similar studies where a steroidal disulfide was used, Mirkin and co-workers state that the structurally complex

steroidal disulfide system begins aggregation after 2 h. This, he argues, is due to a hydrophobic 'screening' effect of the gold surface as well as the formation of a chelate structure. Indeed the dihydrothioctic acid, the reduced dithiol, form of thioctic acid is known to bind through both sulfur atoms, [17] and form stable monolayers on gold surfaces, and this now appears to be the driving factor in stability enhancement as similar results have been obtained in this non-steroidal system

4.3.2 Gold Nanoparticle-Oligonucleotide Surface Coverage

Whilst there is no doubt that the result of employing disulfide attachment of oligonucleotides to nanoparticles is enhanced stability of the conjugate species *c.f.* monothiol, one cannot immediately make the argument that this is due to the disulfide–gold interaction being greater than the thiol–gold one. There are many factors which influence the stability of oligonucleotide conjugates and surface coverage plays an important role. For this reason the surface coverage of each of the conjugate systems was assessed (Table 4.5).

Surface coverage estimation was carried out by a method devised by Mirkin *et al.* [18] (Experimental 7.10.2). Triplicates of the FAM-modified oligonucleotide conjugates were treated with DTT (10 mM) and left overnight to ensure complete aggregation. After which they were centrifuged to ensure that all nanoparticulate sediment was separated from the supernatant. This is an important step as gold nanoparticles can quench or enhance fluorescence – depending upon the proximity of the dye to the surface. Accordingly, the centrifugation and wash cycle was undertaken three times. Aliquots of the supernatant were taken, again in triplicate, and the fluorescence measured. These fluorescence values, when correlated with a standard calibration curve, gave a concentration for FAM-labelled oligonucleotide in solution. This FAM-oligonucleotide concentration divided by the starting molar concentration of nanoparticle gave a value for the number of oligonucleotides *per* nanoparticle and dividing by the surface area of the sphere gave normalized surface coverage values which were easily converted to pmol cm^{-2}.

Interestingly, it was found that D1-Au actually had a reduced oligonucleotide

Probe	Number of Probes per Nanoparticle	Surface Coverage (pmol cm^{-2})	Standard Deviation (pmol cm^{-2})
D1-Au	32	7.4	0.3
D2-Au	255	59.9	6.7
D3-Au	54	12.6	0.8
T1-Au	75	17.5	0.5
T2-Au	51	12.0	0.3
T3-Au	90	21.1	1.2
TT1-Au	54	12.6	0.6
TT2-Au	88	21.1	1.2
TT3-Au	53	12.2	0.7

Table 4.5: Surface coverage of gold nanoparticle-oligonucleotide conjugates.

surface coverage, 7.4 ± 0.3 pmol cm^{-2}, compared with both TT1-Au and T1-Au, 17.5 ± 0.5 pmol cm^{-2} and 12.6 ± 0.6 pmol cm^{-2}, respectively. This shows that with no spacer bases the surface coverage by thioctic acid modified oligonucleotide–Au nanoparticle conjugates was less than that of the standard thiol conjugates. In turn, the surface coverage of standard thiol conjugates was found to be less than, albeit close to, those that were not treated with DTT prior to conjugation (when the oligonucleotides were added directly to the nanoparticles without treating with DTT and purifying with size exclusion chromatography). This indicates that the conjugation process can be improved when using alkyl-thiolated oligonucleotides as there is no trade-off in conjugate stability or surface coverage as a result of omitting reduction by DTT. With the polyT spacer, D2, there was greater surface coverage of the Au nanoparticle by the TA-oligonucleotide, 59.9 ± 6.7 pmol cm^{-2} compared with 12.0 ± 0.3 pmol cm^{-2} and 21.1 ± 1.2 pmol cm^{-2} for the TT2 and T2 samples. It is, therefore, difficult to argue that the enhanced stability is due to an increased surface coverage since in the previous case, without spacers, there was decreased surface coverage and the enhanced conjugate stability was still observed. Indeed, moving to the polyA spacer, D3, the surface coverage is in line with the thiol systems at 12.6 ±

0.8 pmol cm^{-2} *c.f.* 21.1 ± 1.2 pmol cm^{-2} and 12.2 ± 0.7 pmol cm^{-2} for TT3 and T3. Again, as this disulfide conjugate had the same surface coverage as the standard monothiol the enhanced stability cannot be attributed to surface coverage effects.

Whilst these surface coverage results are variable depending upon the linker used and whether spacer bases are present and indeed which spacers are utilized, it can clearly be seen that the enhanced stability of the conjugate systems cannot be determined by surface coverage. If that was the influencing factor we would expect to see the stability of the samples varying in line with the surface coverage. That is, D1 would be the least stable, D3 would be of intermediate stability and D2 would be the most stable. This was not observed as D3 and D2 show very similar stability profiles, despite a reasonably large difference in surface coverage.

4.3.3 Silver Nanoparticle-Oligonucleotide Stability

To demonstrate the versatility of the thioctic acid modified oligonucleotides, silver nanoparticles were used in an analogous study. Silver nanoparticles are less stable than gold and as a consequence have been subject to less scrutiny in the field of DNA sensing, primarily due to the lack of robust surface chemistry. A limited number of studies have been reported but use homo-oligonucleotides or direct hybridization approaches. [19], [20], [21] Figures 4.23 and 4.24, respectively, show the effect of displacement of thioctic acid- and thiol-terminated oligonucleotide sequences immobilized on 37 nm citrate-reduced silver nanoparticles. There is a clear and progressive dampening, broadening and red-shifting of the plasmon absorbance as a result of aggregation. The thioctic acid system showing spectra taken at 10 min intervals is clearly more stable than the thiol which was monitored at only 1 min intervals. It should be noted that with oligonucleotide–Ag conjugates, rather than a new peak appearing at longer wavelengths, the plasmon band broadens and there is a loss of absorbance at 407 nm. For that reason it is less informative to plot an 'emergence' profile for the silver conjugates and their stability was assessed by reference to the 407nm peak.
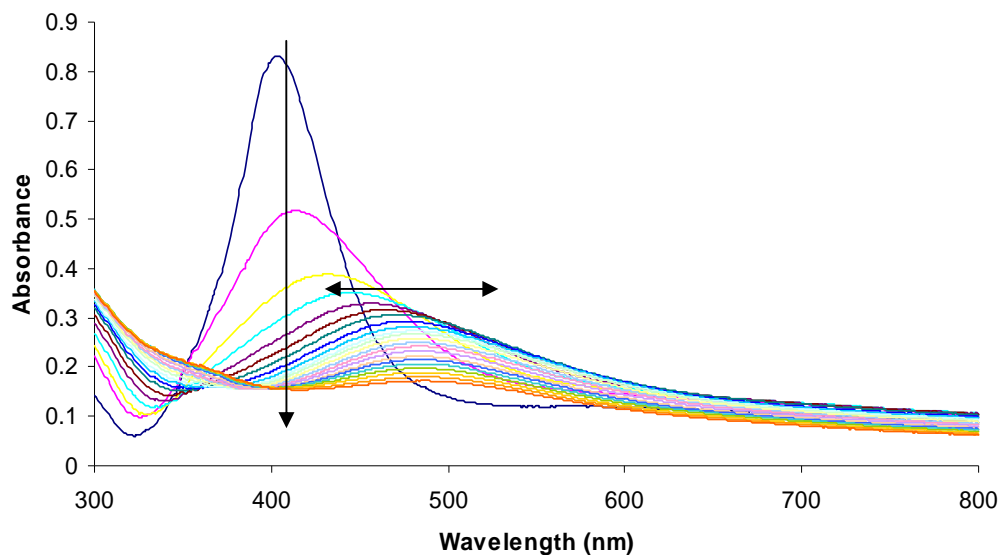
Figure 4.23: Absorbance of thioctic acid-modified oligonucleotide silver nanoparticle conjugates vs. wavelength (nm) at 10 min intervals. Arrows added to indicate change of spectra with time.
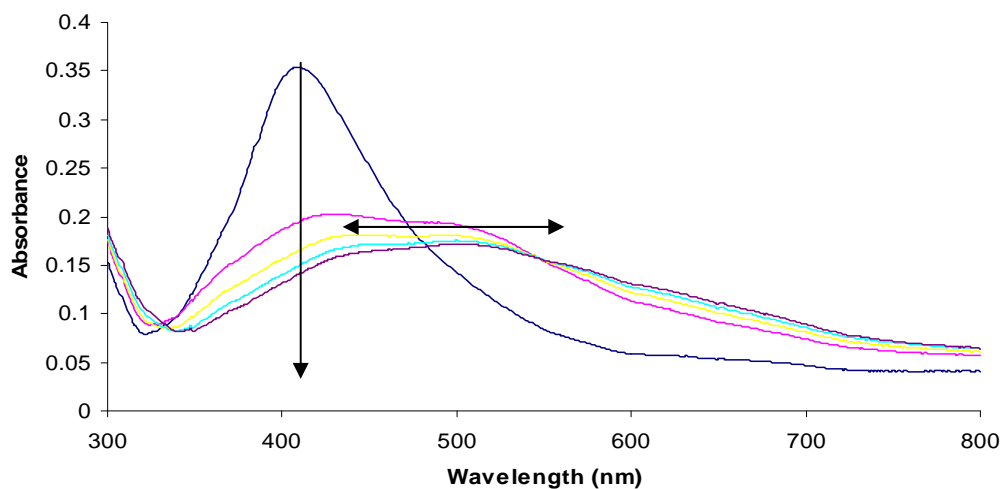
Figure 4.24: Absorbance of monothiol-modified oligonucleotide silver nanoparticle conjugates vs. Wavelength (nm) at 1 min intervals. Arrows added to indicate change in spectra with time.

The absorbance at 407 nm was plotted against time for each of the linking systems – D1-Ag, D2-Ag, D3-Ag, T1-Ag, T2-Ag, T3-Ag, TT1-Ag, TT2-Ag and TT3-Ag. In the case of TA-oligonucleotide-Ag conjugates (Figure 4.25), aggregation begins immediately but is much slower than for the thiol-oligonucleotide analogues (Figure 4.26).
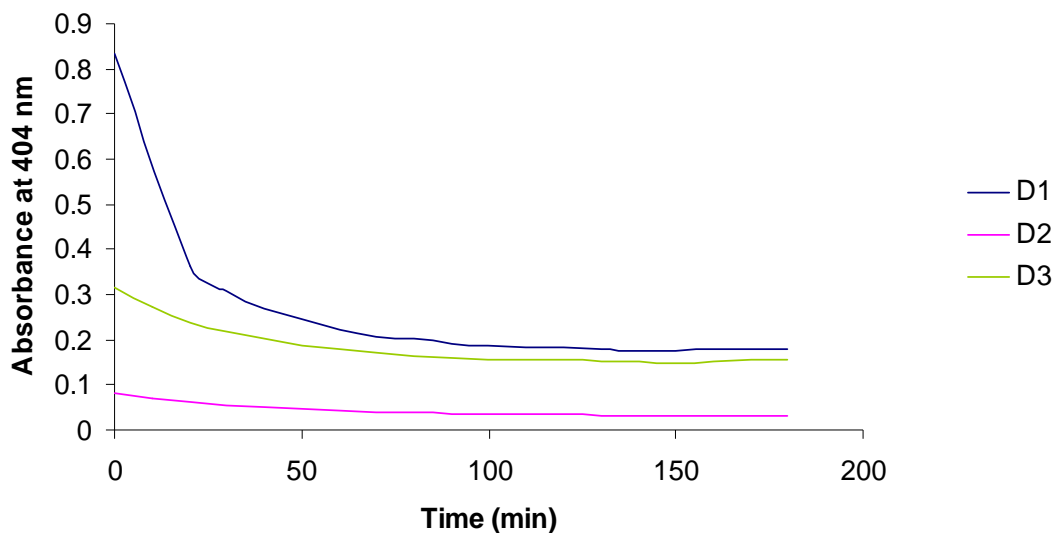
Figure 4.25: Absorbance at 407 nm vs Time plotted for thioctic acid modified oligonucleotide-silver nanoparticle conjugates, for D1, D2 and D3.
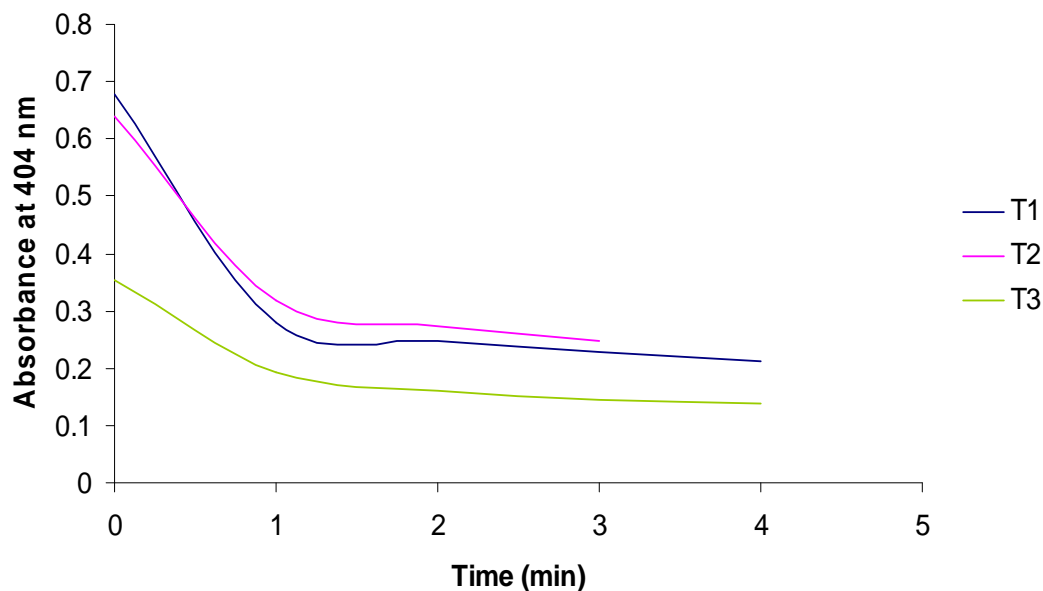
Figure 4.26: Absorbance at 407 nm vs Time plotted for thioctic acid modified oligonucleotide-silver nanoparticle conjugates, for T1, T2 and T3.
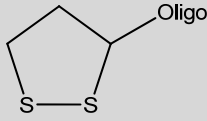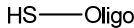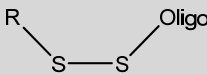
Linker	Probe	$t_{1/2}$ (min)
	D1	15
	D2	25
	D3	30
	T1	0.5
	T2	0.5
	T3	0.75
	TT1	0.5
	TT2	0.5
	TT3	0.5

Table 4.6: Half lives for Ag-oligonucleotide conjugates.

For ease of comparison the 'half-lives' of the conjugate systems were calculated, taken as the time required for half the total absorbance change to occur at 407 nm, the results are shown in Table 4.6. There is a marked difference in the rate of aggregation with all of the thiol systems having a half-life of less than a minute, compared with the disulfide samples which have 15–30 min half-lives. Whilst it is difficult to compare gold and silver conjugate systems in absolute terms, it can be said that the overall conjugate stability displayed by the silver–disulfide systems is more stable (with respect to DTT-induced aggregation) than the 'standard' thiol–gold system (comparing Table 4.5 with Table 4.6).

4.3.4 Silver Nanoparticle-Oligonucleotide Surface Coverage

As with the gold conjugates the surface coverage was assessed (Experimental 7.10.2) and the data found to be variable depending upon whether there are spacer bases and what those spacer bases are (Table 4.7). For example, the surface coverage of oligonucleotide on Ag nanoparticles for D1–Ag conjugates was found to be 21.1 ± 1.3 pmol cm^2, compared with TT1–Ag which had a greater surface coverage, 144.7 ± 14 pmol cm^2. Even T1–Ag had a greater surface coverage than the disulfide species at 31.2 ± 1.5 pmol cm^2, albeit less than the standard thiol sample. Once again, the disparity in surface coverage does not impact the conjugate

Probe	Number of Probes per Nanoparticle	Surface Coverage (pmol cm^{-2})	Standard Deviation (pmol cm^{-2})
D1	640	21.1	1.3
D2	10028	331	8.3
D3	3183	105.7	0.9
T1	4383	144.7	14.0
T2	1153	38.1	6.5
T3	2307	76.1	2.2
TT1	947	31.2	1.5
TT2	1951	64.4	3.0
TT3	3730	123.1	15.1

Table 4.7: Surface coverage of silver nanoparticle-oligonucleotide conjugates.

stability since we have seen that the disulfide systems are by far more stable than both of the thiol conjugates and yet has lower surface coverage. This surface coverage-independent stability is also observed with the polyT and polyA sequence conjugates. By comparing the results for stability of the gold and silver conjugates it can be seen that as anticipated, the disulfide did not stabilize the silver nanoparticles to the same extent as gold, probably due to weaker thiol–silver interactions. Surface coverage effects can again be dismissed as the stabilizing factor when comparing samples D2–Au (with a surface coverage of 59.9 ± 6.7 pmol cm^2) and T2–Ag (with a surface coverage of 64.4 ± 3.0 pmol cm^2) and yet there are vastly differing stabilities. Similarly, D1–Ag (surface coverage of 21.1 ± 1.3 pmol cm^2) is considerably less stable than D3–Au (surface coverage of 12.6 ± 0.8 pmol cm^2) despite their surface coverages being quite similar. It is worthy to note, however, that the disulfide on silver remained more stable than the 'standard' monothiol linker systems on gold and this is in spite of similar surface coverages in some cases *e.g.* D1–Ag (surface coverage of 21.1 ± 1.3 pmol cm^2) and TT3–Au (surface coverage 21.1 ± 1.2 pmol cm^2). This is highly significant as it allows potential for oligonucleotide–silver nanoparticle conjugates to be exploited in a similar manner to gold nanoparticles.

4.3.5 Thermal Stability

A further stability experiment was carried out on disulfide gold and silver nanoparticles.   Thiol systems suffer from temperature-induced irreversible aggregation. This can be observed by a "tailing off" at the high temperature end of T_m melting experiments, when the probe is typically raised in temperature by 1 °C per minute. Often cycling these experiments shows a loss of stability, with latter cycles not reaching the same absorbance maxima as the early cycles. Typical T_m melting experiments are carried out on a temperature range 10 – 80 °C. Figure 4.27 shows the effect of sustained heating at 90 °C on disulfide capped Au-Pr1 conjugates, compared with thiol-linked probes (Experimental 7.10.3). Displaying a marked enhancement in performance, the disulfide capped nanoparticles are stable for 3 hours at this temperature. Considerable aggregation is observed at 4 h and is complete by 5 h. This provides a further benefit over the thiol system which shows stability for 2 h and complete aggregation by 3 h. This allows greater experimental control and reproducibility at elevated temperature and is an attractive feature of the disulfide adsorption strategy.   In comparison the Ag substrate shows immediate aggregation at 90 °C whether the disulfide or thiol linker is exploited, Figure 4.28. It is shown that, despite this fact, the disulfide system appears approximately twice as stable as the thiol.
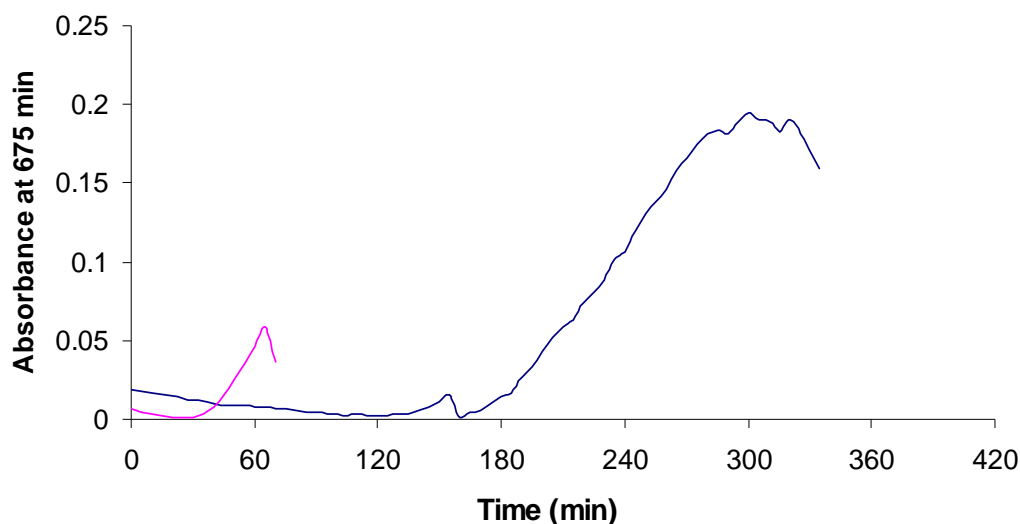
Figure 4.27: The absorbance at 675 nm for disulfide (blue) and thiol (pink) modified oligonucleotide-Au nanoparticle conjugates as a function of time when held at 90 °C.
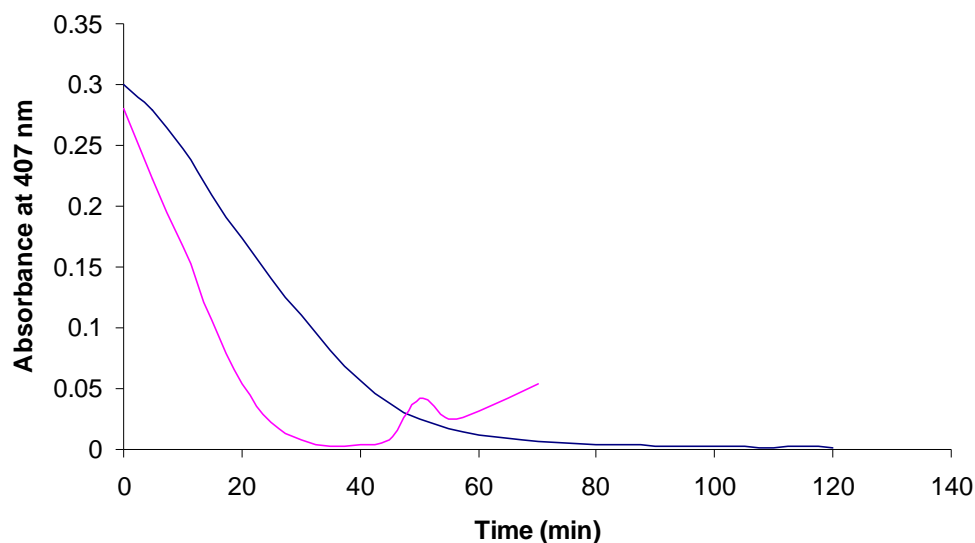
Figure 4.28: A comparison of thiol and disulfide modified oligonucleotide Ag nanoparticle conjugates. The absorbance at 407 nm is plotted against time.

4.4 Chapter 4: Conclusions

Thioctic acid modified oligonucleotides have been used to make conjugates with both gold and silver nanoparticles. The preparation of these conjugates was found to be reproducible. The UV-vis profiles of the conjugates are different from those of the starting "bare" nanoparticles. Further evidence for conjugation can be gained from particle size analysis, although this was found to be more suitable for the silver conjugates than for gold. For either gold or silver conjugates gel electrophoresis also indicated that the nanoparticles had oligonucleotides attached.

Hybridisation of the conjugates prepared herein was carried out to show that the thioctic acid modified oligonucleotides retained their biological utility when conjugated to the nanoparticles. This was shown to be the case for both gold and silver conjugates. In addition the ability to detect the hybridisation events by analysis of the change in surface plasmon band of the nanoparticles was also confirmed. The oligonucleotide silver nanoparticle conjugates were found to be easy

to handle, with sharp melting characteristics and a better (unoptimised) sensitivity of 2.0 nM *c.f.* 0.1 µM for gold. Silver nanoparticle conjugates have received considerably less attention in the literature compared with the gold analogues and using thioctic acid modified oligonucleotides to prepare conjugates allows their further investigation.

The stability of the nanoparticle conjugates was assessed by a displacement study with DTT. The thioctic acid modified oligonucleotide nanoparticle conjugates were assessed in comparison with monothiol analogues. Monothiol analogues were prepared by two methods – one including a pre-treatment with DTT prior to conjugation (as is standard), and the other omitting it. Both methods produced thiol oligonucleotide nanoparticle conjugates of equal characteristics, including stability. This allowed for simpler preparation of thiol oligonucleotide nanoparticle conjugates. Thioctic acid modified oligonucleotide nanoparticle conjugates were found to have greatly enhanced stability when compared with monothiol analogues. TA-Au conjugates showed half lives of up to 245 min compared with 1 min for the thiol analogue. TA-Ag conjugates were not as stable as the gold analogues, with half lives of up to 30 min. Nevertheless, this was still a considerable improvement on the monothiol-linked analogue ($\leq$ 1 min).

The surface coverage of the oligonucleotide nanoparticle conjugates was investigated in order to establish whether the enhanced stability of TA-oligo-NP conjugates was simply due to greater surface coverage. Having carried out the surface coverage experiment there was found to be variability depending upon which spacer groups (polyA or polyT) were used (if any). The linking chemistry *i.e.* whether thioctic acid or either method of thiol preparation was found to have a significant effect on surface coverage. However, there was no systematic pattern to the surface coverages, nor was there any correlation between the surface coverage and stability.

In short, thioctic acid modified oligonucleotides have been conjugated to gold and silver nanoparticle analogues retaining their biological integrity and producing enhanced stability when compared with monothiol analogues.

4.5   Chapter 4: References

1.   Turkevitch, J., Stevenson, P. C., Hillier, J., **1951**, *Discuss. Faraday Soc.* , 11, 55-75.

2.   Frens, G., **1973**, *Nature Phys. Sci.*, 241, 20-22.

3.   Grabar, K. C., Freeman, R. G., Hommer, M. B., Natan, M. J., **1995**, *Anal. Chem.*, 67, 735-743.

4.   Grabar, K. C., Brown, K. R., Keating, C. D., Stranick, S. J., Tang, S.-J., Natan, M. J., **1997**, *Anal. Chem.*, 69, 471-477.

5.   Lee, P. C., Meisel, D., **1982**, *J. Phys. Chem.*, 86, 3391-3395.

6.   Sheng, R.S., Zhu, L., Morris, M. D., **1986**, *Anal. Chem.*, 58, 1116-1119.

7.   Munro, C. H., Smith, W. E., Garner, M., Clarkson, J., White, P. C., **1995**, *Langmuir*, 11, 3712-3720.

8.   Yguerabide, J., Yguerabide, E. E., **1998**, *Anal. Biochem.*, 262, 137-156.

9.   Yguerabide, J., Yguerabide, E. E., **1998**, *Anal. Biochem.*, 262, 157-176.

10.   Daniel, M.-C., Astruc, D., **2004**, *Chem. Rev.*, 104, 293-346.

11.   Ghosh, S. K., Pal, T., **2007**, *Chem. Rev.*, 107, 4797-4862.

12.   Taton, T. A. DNA Nanotechnology, Supplement 9, *Curr. Protoc. Nucleic Acid Chem.*, 12.2.7.

13.   Zanchet, D., Micheel, C. M., Parak, W. J., Gerion, D., Alivisatos, A. P., **2001**, *Nano Lett.*, 1, 32-35.

14.   Jin, R., Wu, G., Li, Z., Mirkin, C. A., Schatz, G. C., **2003**, *J. Am. Chem. Soc.*, 125, 1643-1654.

15.   Stokes, R. J., MacAskill, A., Lundahl, J. P., Smith, W. E., Faulds, K., Graham, D., **2007**, *Small*, 3, 1593 - 1601.

16.   Li, Z., Jin, R., Mirkin, C. A., Letsinger, R. L., **2002**, *Nucleic Acids Res.*, 30, 1558-1562.

17. Garcia, B., Salome, M., Lemelle, L., Bridot, J.-L., Gillet, P., Perriat, P., Roux, S., Tillement, O., **2005**, *Chem. Commun.*, 369-371.

18. Demers, L. M., Mirkin, C. A., Mucic, R. C., Reynolds III, R. A., Letsinger, R. L., Elghanian, R., Viswanadham, G., **2000**, *Anal. Chem.*, 72, 5535-5541.

19. Cai, H., Xu, Y., Zhu, N., He, P., Fang, Y., **2002**, *Analyst*, 127, 803-808.

20. Tokareva, I., Hutter, E., **2004**, *J. Am. Chem. Soc.*, 126, 15784-15789.

21. Vidal, B. C. Jr., Deivaraj, T. C., Yang, J., Too, H.-P, Chow, G.-M., Gan, L. M., Lee, J. Y., **2005**, *New J. Chem.*, 29, 812-816.

5 Thioctic Acid Modified Oligonucleotides for SERRS

Surface Enhanced Resonance Raman Scattering (SERRS) spectroscopy has been shown to be effective in the sensitive detection of dye-labelled oligonucleotides. [1] [2]   SERRS is an optical spectroscopy technique utilising enhancement (by use of a suitable chromophore, roughened metal surface and careful selection of excitation source) of the Raman effect *i.e.* the inelastic scattering of light (Figure 5.1). The sensitivity of the technique has been shown to allow detection of a 0.75 pM solution of Cy3.5™ labelled DNA using silver nanoparticles as the enhancing surface coupled with 632.8 nm excitation. [2]

Arguably the greatest advantage that SERRS offers as an analytical tool is that the SERRS spectra provides distinct vibrational information about the molecule being interrogated making the technique highly suitable for multiplexed analysis. [3]
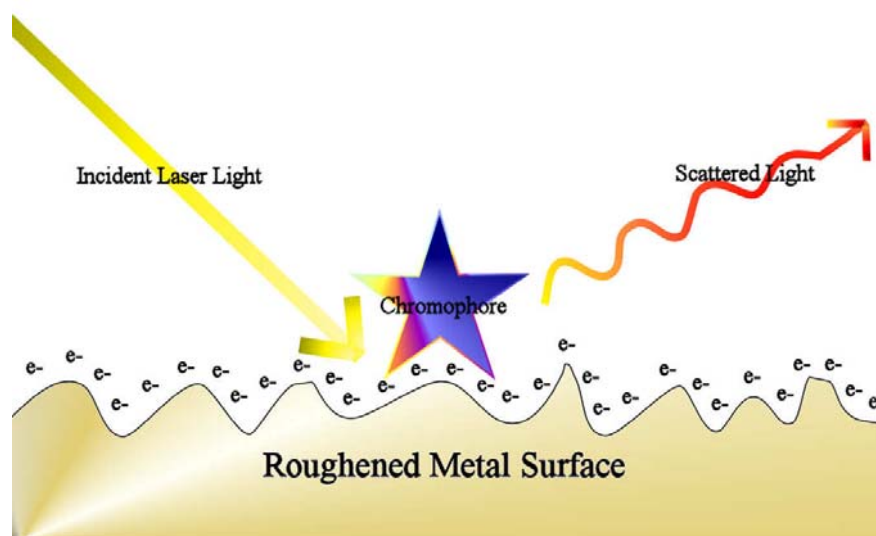
Figure 5.1: Representation of the SERRS process. Incoming laser light interacts with surface plasmon of suitably roughened metal surface and proximal chromophore inducing a scattering effect which gives vibrational information of the molecule interrogated.
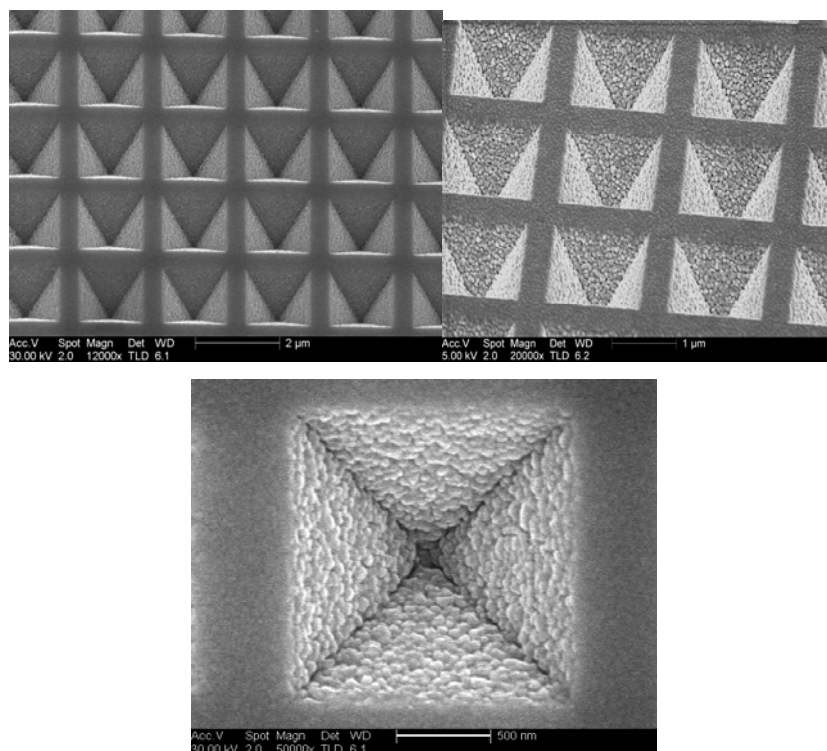
Figure 5.2: Scanning electron micrographs of 302 Klarite™ surfaces at 12000, 20000 and 50000 times magnification, respectively. SEM; RJS.

Nanoparticles are often employed as a substrate for SERRS providing a suitable roughened metal surface. In addition, they are cheap and relatively easy to prepare reproducibly. Au and Ag nanoparticles are most often employed and very high sensitivity has been observed with single biomolecule detection reported. [4] [5] This remarkable sensitivity is attributed to enhancement produced by "hot spots" – areas of high electric field between aggregated nanoparticles or at points of suitable curvature on the particle surface. [6] [7] However, the use of colloidal nanoparticles, as the enhancing surface, requires control of a dynamic aggregation event to producing these "hot spots". This process is essential to yielding sensitive, reproducible and linearly concentration dependent results.

Nanostructured gold surfaces (Klarite™) have been developed such that the plasmon bands are tuned to wavelengths coincident with typical Raman spectrometers *i.e.* 632.8 or 785 nm. [8] The Klarite™ surface consists of a lattice of inverted square pyramidal pits (Figure 5.2). The plasmon bands created are tunable due to the generation of standing waves in the concave geometry of the pits, the variation of pit depth alters the tuning of the plasmon.

114
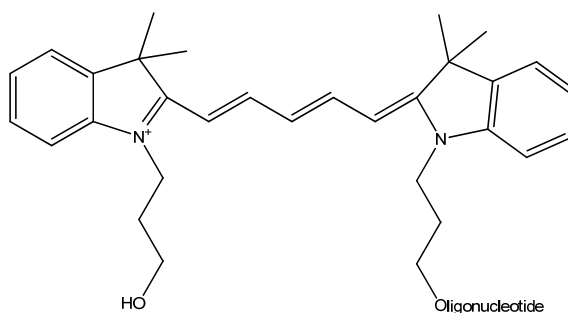
Figure 5.3: Cy5™ labelled oligonucleotide.

It was hoped that the Klarite™ surface would provide a means of sensitive and reproducible DNA detection without the need to control the dynamic aggregation event. However, in order to achieve meaningful and reproducible results from the Klarite™ surface, control of surface adsorption is necessary. [9] Stokes *et al.* showed that although sensitivity was several orders of magnitude greater using dye labels than non resonant targets, there was huge variability in signal, with relatively high RSDs in the range 26.7 – 34.9 % observed, from dye labelled oligonucleotides when "drop-coat" dried onto the Klarite™ surface. It was important, therefore, to ascertain whether surface adsorption is influenced by the use of modified oligonucleotides and optimisation of surface deposition conditions.

For SERRS detection a chromophoric label was required. Cy5™ was chosen as a suitable dye and with which to investigate the applicability of the Klarite™ surface to SERRS detection of labelled oligonucleotides (Figure 5.3). It had been shown previously that Cy5™ labelled oligonucleotides provided allowed excellent senstivities to be achieved when employed with nanoparticles for analysis. [2]

5.1   *SERRS of Dye-Labelled Oligonucleotides on Klarite™*

The investigation into the detection of oligonucleotides by SERRS using Klarite™ as the enhancing surface required confirmation, firstly, that the spectroscopic technique was compatible with the labelled oligonucleotide and the surface and then whether it could be optimised to detect hybridisation events. The SERRS response of the probes was first investigated to ascertain the influence of

chemical factors such as linker type, deposition time and concentration dependence on the SERRS response and to optimise the spectroscopic conditions, in particular the wavelength of excitation. It is important to note that should the sample dry, a much higher response would be observed as material is physically adsorbed onto the surface. In addition, the drying process can give a "coffee ring" effect in which there is a high degree of variability of signal between an outer ring and the inner section of the sample. [9] In order to avoid this problem, the experiments were performed using a small Camlab micro-array hybridisation chamber with water in a reservoir at each end of the chamber to maintain a moist environment.

5.1.1 Wavelength of Excitation Dependence of SERRS Response

It was important, at the outset, to establish the best spectroscopic conditions for SERRS assessment of the samples. A 1 µL spot of TA-oligo-Cy5 at 7.5 µM concentration was applied to the Klarite™ surface and left for 2.5 h in a hybridisation chamber. After which the plate was washed with water, PBS, IPA and water again before being allowed to air dry and the spectra recorded at 632.8, 785 and 830 nm (Experimental 7.11.1). The spectra were obtained using a Streamline™ mapping stage, charge coupled device (CCD) and an *InVia* Raman microscope system. The line mapping operates by line focusing the laser and rastering vertically across the sample, simultaneously collecting multiple spectra across the CCD area. Streamline™ does not often require attenuation of the laser (as is common for point mapping) as the effective power density is lower at the surface. The same instrument was used for all three excitation wavelengths with a different laser and filter set in place for each. Spectra recorded with the 632.8 nm laser produced a very high response compared with the other wavelengths of excitation. In fact, plotted on the same scale, the spectra recorded at 785 nm and 830 nm are dwarfed by that obtained at 632.8 nm (Figure 5.4). However, there is a significant fluorescent background of over 35000 counts when using the 632.8 nm excitation source. This can be rationalised as the λ_{max} of absorbance of Cy5™ is 643 nm. As such, the 632.8 nm wavelength of excitation is closest to the λ_{max} of absorbance which results in significant fluorescent emission. Nevertheless, there are clear SERRS peaks
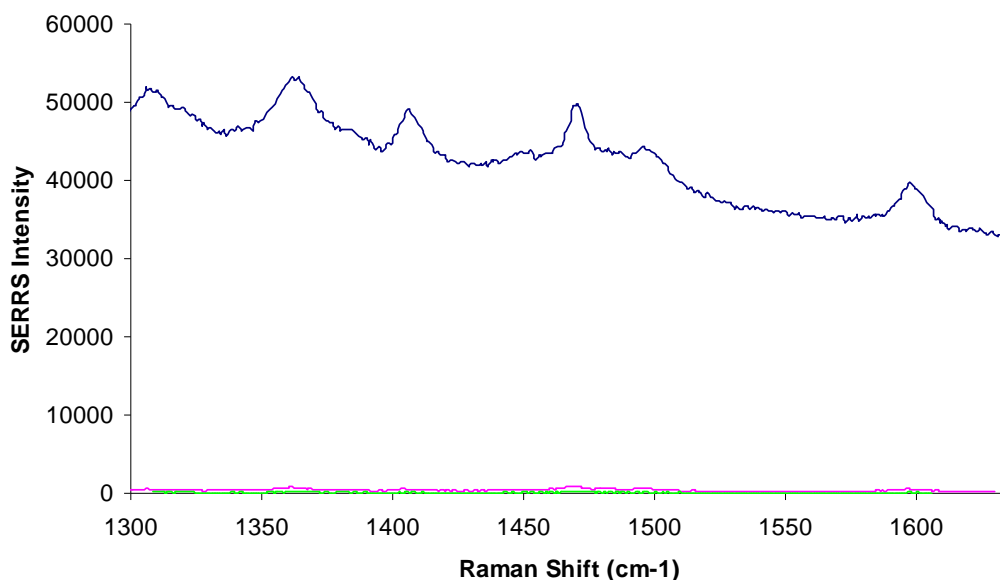
Figure 5.4: TA-oligo-Cy5 (1 µL, 7.5 µM), immobilised on Klarite™ for 2.5 h, excitation wavelength; 632.8 nm (blue), 785 nm (pink) and 830 nm (green).

observed, due to the surface enhanced resonance Raman scattered light. The 785 nm laser produced a spectra dominated by SERRS with no fluorescence observed (Figure 5.5). This was due to moving the excitation source away from the
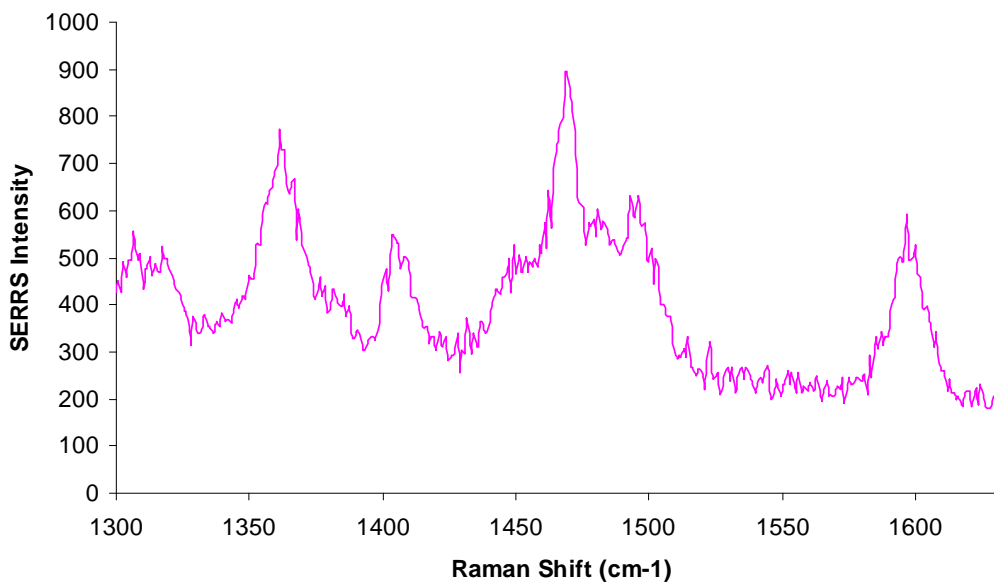
Figure 5.5: TA-oligo-Cy5 (1 µL, 7.5 µM), immobilised on Klarite™ for 2.5 h, interrogated by 785 nm laser.
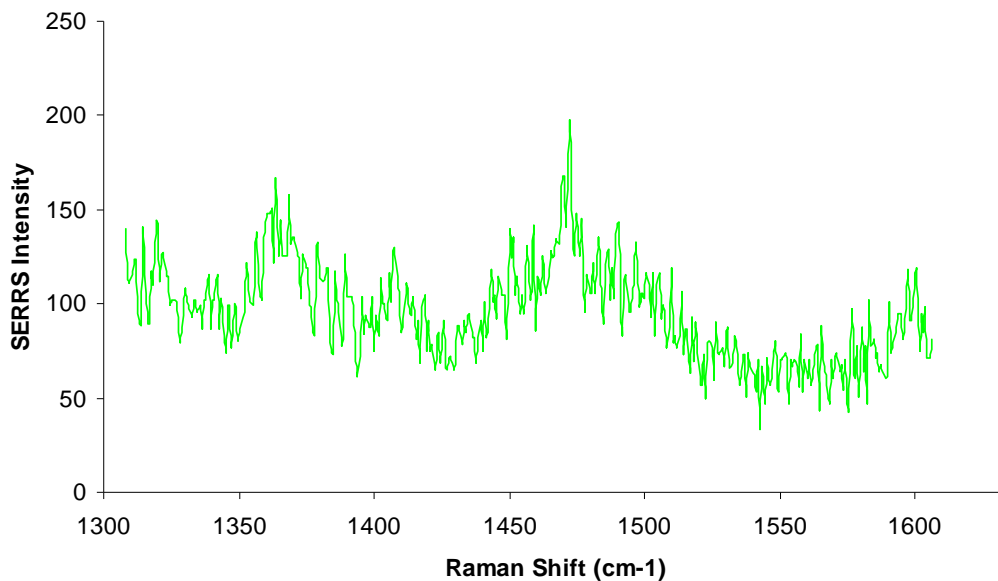
Figure 5.6: TA-oligo-Cy5 (1 µL, 7.5 µM), immobilised on Klarite™ for 2.5 h, interrogated by 830 nm laser.

absorption maxima of the chromophore, to 785 nm, giving a profile that was dominated by the scattered Raman light with minimal fluorescent contribution.

At 830 nm there remained a little of the distinctive SERRS spectra, particularly the strong peak centered at 1470 cm^{-1}. However, the overall effect was very weak as moving the excitation source even further off-resonance, with respect to the dye absorbance maxima, to 830 nm gave a profile that was very weak with no fluorescence and very little SERRS (Figure 5.6). The lack of SERRS is due to the fact that not only, at 830 nm, is the wavelength of excitation off-resonant with respect to the dye it is also off-resonance with respect to the surface Plasmon bands of the Klarite™.

Within this project the surface modification behavior of the thioctic acid modified oligonucleotides was investigated *c.f.* other linkers. From the results of this wavelength-dependence experiment it was decided to use 785 nm as the primary

source of excitation. It is known that the SERRS effect is much stronger the closer the chromphore is to the surface and rapidly drops off as you move away from the enhancing surface. [10] Accordingly SERRS is a spectroscopic technique which gives information about the surface layer. Whereas, over short distances fluorescence can be quenched at a roughened metal surface [11] or enhanced by metal surfaces at slightly longer distances. [12] As such, it would be complex to use fluorescence as a tool to understand the surface modification behaviour of the probes. Furthermore, fluorescence is evident from multilayers and the effect is not dominated by the first monolayer as is the case with SERRS. It was therefore not considered to be as suitable a tool for investigating surface deposition as SERRS is. Background fluorescence is often observed "beneath" the SERRS spectra of a given sample and whilst background correction techniques can be applied to SERRS spectra to correct for this effect, it was felt that, in this case, any alteration of the signal would obscure the understanding of the surface modification studies. Since understanding the effect of surface modification, rather than any effects from multilayer coverage, was desired it was determined that 785 nm was the best excitation option.

5.1.2 Time Dependence of SERRS Response

It is known when generating self assembled monolayers (SAMs) of alkyl thiols that the monolayers are 95 % complete in only a few minutes. However a much slower "re-arrangement" phase to generate a fully ordered SAM can take up to 24 h. [13] It was considered necessary, therefore, to investigate the time required to reach the highest SERRS response. 1 μL of TA-oligo-Cy5 at 7.5 μM was applied to the Klarite™ substrate. At periodic intervals (1 min, 15 min, 1 h and 24 h) the sample was washed from the Klarite™ surface. The surface was washed with water, PBS, IPA and water again to minimise non-specific adsorption before being left to air dry and the SERRS spectra recorded at 785 nm (Experimental 7.11.2).

Once the SERRS spectra were recorded the average peak intensity at 1470 cm^{-1} was plotted as a function of time (Figure 5.7). It can clearly be seen that even with only 1 min of treatment there is significant oligonucleotide surface coverage as evidenced by the SERRS response. Waiting only 15 minutes gave the maximum response. It was thought that perhaps SERRS would provide a tool to monitor the

SAM development of dye labelled oligonucleotides. Indeed significant SERRS
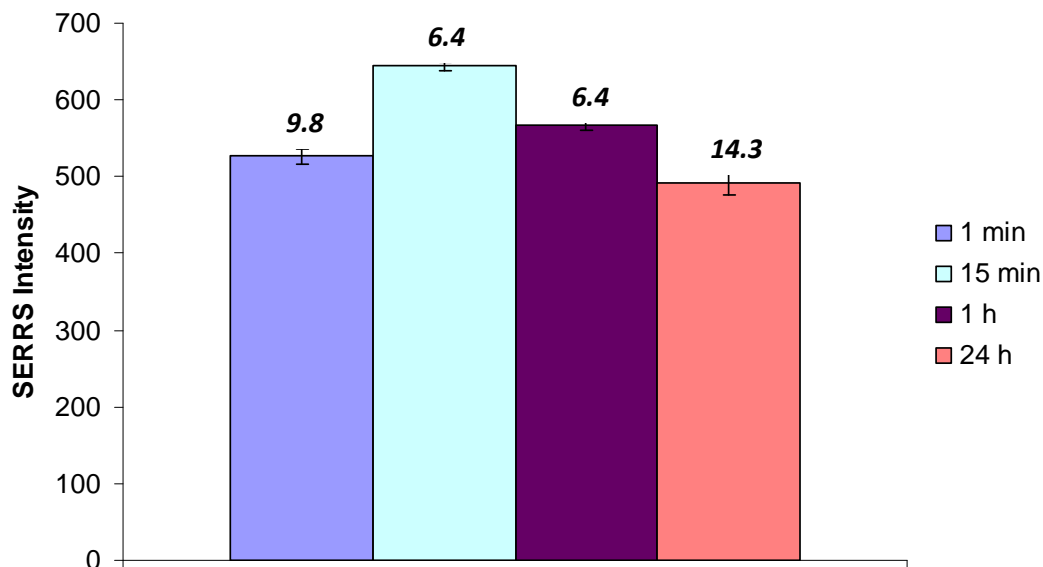
Figure 5.7: A bar chart of the intensity of the dominant SERRS peak at 1470 cm^{-1} for differing surface modification times. In all cases the sample used was 7.5 µm of TA-oligo-Cy5 and interrogated by 785 nm laser excitation. RSD quoted above, n>500.

signals were evident with only 1 minute of incubation. However, it was somewhat surprising to see a reduction in SERRS response in the time period of 15 min to 24 h. Indeed, the sample showed a similar response after 24 h as after 1 min - it was in fact slightly lower. It could be suggested that the samples were photobleached during the course of the timed experiment. However, steps were taken to minimise the likelihood of photobleaching; the laboratory lights were turned off when the chips were handled, while spectra were being acquired and during the SAM development time they were stored in a sealed light-free environment. Another suggestion is that leading up to 15 min there is an increasing amount of oligonucleotide on the surface but that the amount is less than after 24 h, but that the orientation of the oligonucleotides on the surface favours the SERRS process. As time proceeds, and more oligonucleotide deposits on the surface, the SAM becomes more "packed" but the resulting orientation is not as optimal for SERRS response per molecule after 24 hours.

Analogous studies of the self-assembly of alkane thiols on gold typically exhibit a fast initial adsorption process followed by a slower re-ordering process into a
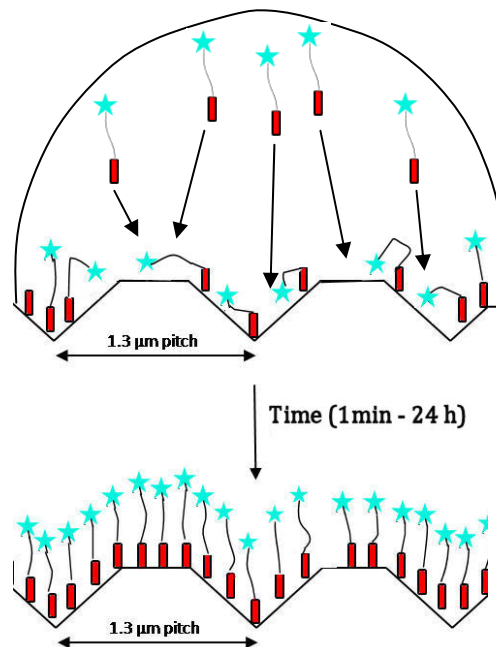
Figure 5.8: Representation of time-dependent surface orientation of TA-oligo-Cy5 on Klarite surface.

packed monolayer. [14] Using the SERRS response as an investigative tool, clearly shows that the initial adsorption is rapid as can be seen from the high SERRS response at only 1 min. Indeed, if, when washing the Klarite™ surface the orientation is such that the washings run over the active area of the surface it will deposit enough sample to generate a signal. That is, with an exposure of only seconds evidence of deposition is apparent from the SERRS response.

In addition, the initial high level of SERRS response could be partially generated by oligonucleotides orienting in such a way as to allow access of the dyes to the active sites of the surface. As more oligonucleotides adsorb onto the surface the access could be restricted. One example would be if the linker group with a higher affinity for the surface displaces the dyes from the active surface sites. This proposed process is demonstrated in Figure 5.8.

5.1.3 Concentration Dependence of SERRS Response

The thioctic acid-modified oligonucleotide, TA-oligo-Cy5 was diluted to different concentrations: 7.5 μM, 0.75 M, 75 nM and 7.5 nM. 1 μL of each concentration was deposited on the Klarite™ surface and the SERRS response assessed (Experimental 7.11.5). There was an unexpectedly sudden drop-off in SERRS intensity with concentration that occurred in the micromolar range (Figure 5.9). This could be due to the adsorption process discussed above (Section 5.1.2). It is important to note that in each case the collection spot is around 1 μm in diameter which is roughly equivalent to a single Klarite microwell per spectra. The data above in section 5.1.2 suggests that there may be a large difference in rates between the initial (fast) partial monolayer coverage and the slower reordering process to complete coverage. Therefore, if only partial monolayer coverage is achieved even after 24 hours, the limit of detection may be a symptom of the fact that there are simply very few molecules within the single microwell interrogated. Collection over a large number of microwells would require a lower magnification objective and with a smaller numerical aperture as a consequence. The wider collection area of lower powered objectives did not offset the loss of collection efficiency in this case. The most sensitive results were always obtained using 50 × (NA = 0.75 or 0.5 LWD) and 100 × (NA = 0.95 or 0.75 LWD) objectives.
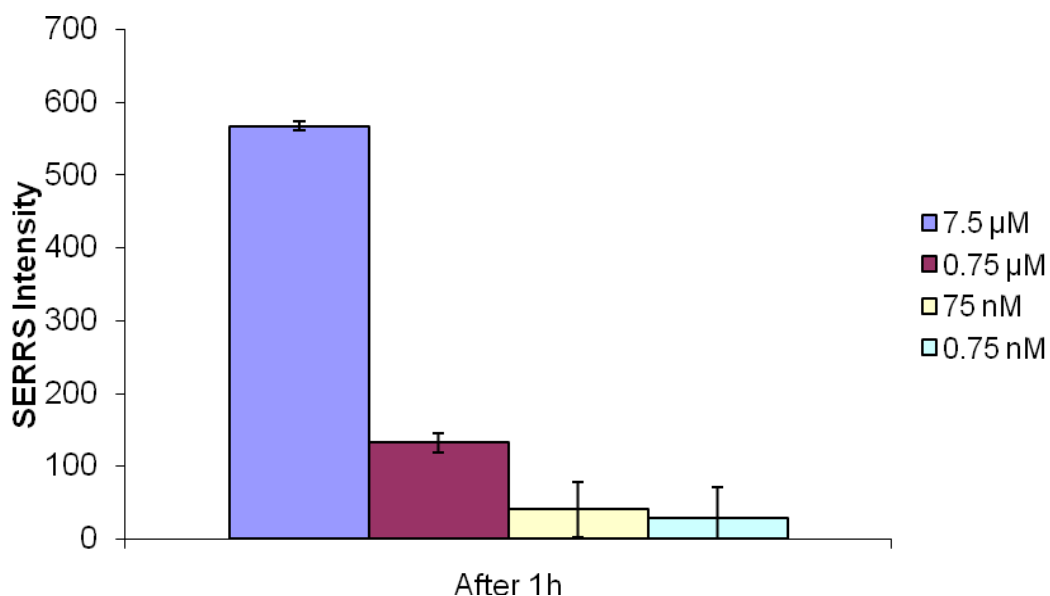
Figure 5.9: *The intensity of the major peak at 1470 cm^{-1}is shown for each concentration of TA-oligo-Cy5 after 1 h incubation.*

Name	Sequence	Surface Linker: X
TA-oligo-Cy5	Cy5 CGC ATT CAG GAT X	Thioctic acid
Th-oligo-Cy5	Cy5 CGC ATT CAG GAT X	Thiol
Am-oligo-Cy5	Cy5 CGC ATT CAG GAT X	Amino
oligo-Cy5	Cy5 CGC ATT CAG GAT	-

Table 5.1: Sequences used in Klarite™ surface immobilisation investigations.

5.1.4 Linker Dependence of SERRS Response

It had been seen that thioctic acid and thiol modified sequences behave differently on nanoparticles, [15] it was therefore suspected that their behavior on Klarite™ may also be different. Four different oligonucleotides, each with a different surface attachment group at the 3'- end: thioctic acid (TA-oligo-Cy5), thiol (Th-oligo-Cy5), amino (Am-oligo-Cy5) and no modification (oligo-Cy5), and all were labelled with Cy5™ at the 5'-end. These sequences, used in the study, are detailed in Table 5.1 (Experimental 7.11.4). Thioctic acid modified oligonucleotide, TA-oligo-Cy5, was compared with other surface linker groups to assess whether the development of a surface layer on the Klarite™ was dependent on linker group or whether it would be dominated by the deposition time and concentration of the oligonucleotide. A 1 µL aliquot of each of the modified oligonucleotides, at 7.5 µM, was spotted onto the surface and left for 15 min. It can clearly be seen, from plotting the spectra of each probe, that there is a marked difference in the SERRS response depending upon which linker group is used (Figure 5.10). The linkers were also assessed over a 24 hour time period. Looking at the development of the SERRS signal with time (plotting the intensity of the major peak (1470 cm^{-1}) against time) as a function of the linker used shows a clear difference between the different groups (Figure 5.12). Thioctic acid modified oligonucleotides for the full time range, 24 h, gave better SERRS signal than the thiol analogue. Indeed, there is a significant and immediate difference after only 1 min; the thioctic acid-modified oligonucleotide

gave more than twice as much SERRS response within the initial time frame. The thiol and amino oligonucleotides gave very similar responses. Over a 24 hour period
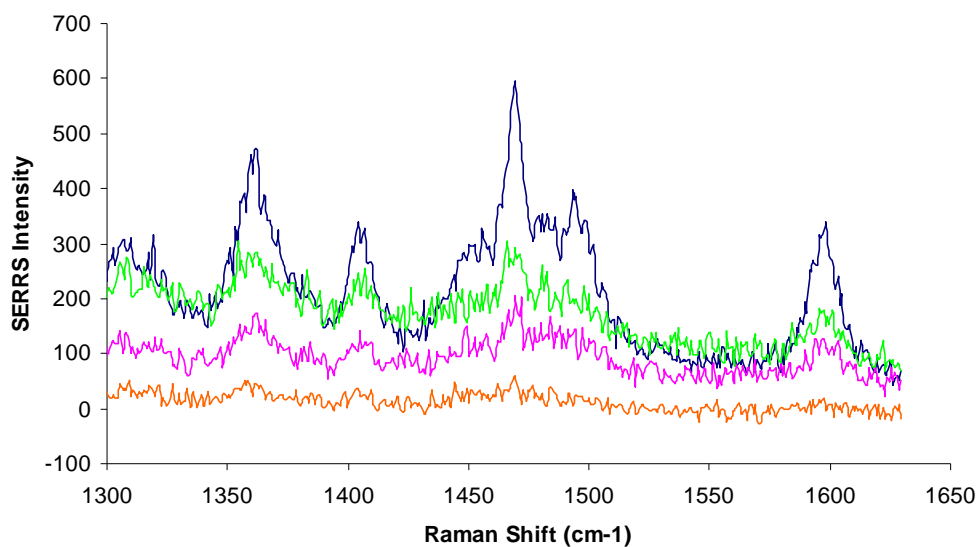
Figure 5.10: SERRS response of Cy5 labelled oligonucleotides immobilised via different linkers. TA-oligo-Cy5 – blue, Th-oligo-Cy5 – pink, Am-oligo-Cy5 – green, oligo-Cy5 – orange. [N.B. Spectra shown are from crosshair position of the respective maps in Figure 5.11]
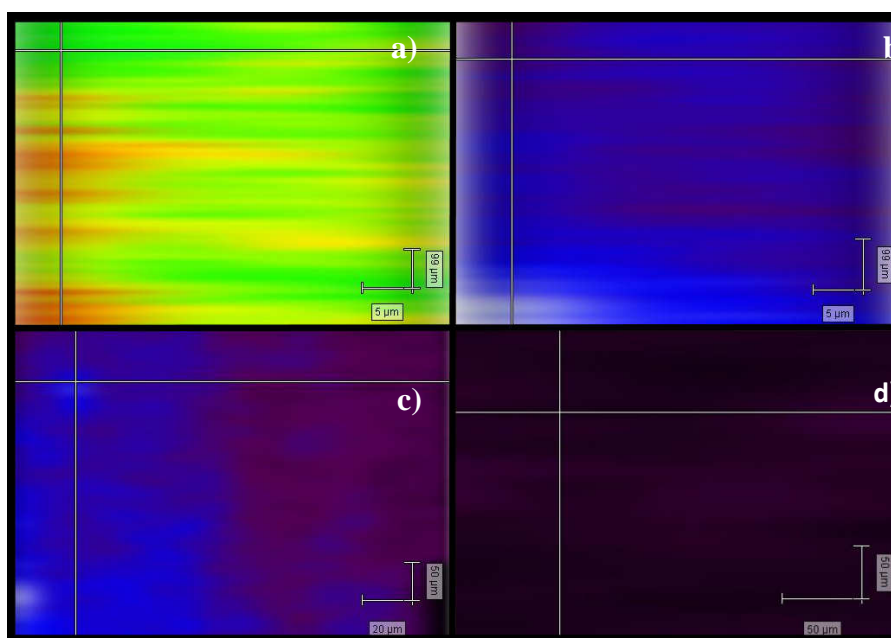
Figure 5.11: False colour images depicting intensity of SERRS response at 1470 cm^{-1} as a function of linker. Maps generated from spectra taken after 15 min incubation. a) TA-oligo-Cy5, b) Th-oligo-Cy5, c) Am-oligo-Cy5 and d) oligo-Cy5. Colours applied as follows: Min (0) ▉▉▉ Diablo9V ▉▉▉ *Max (850).*
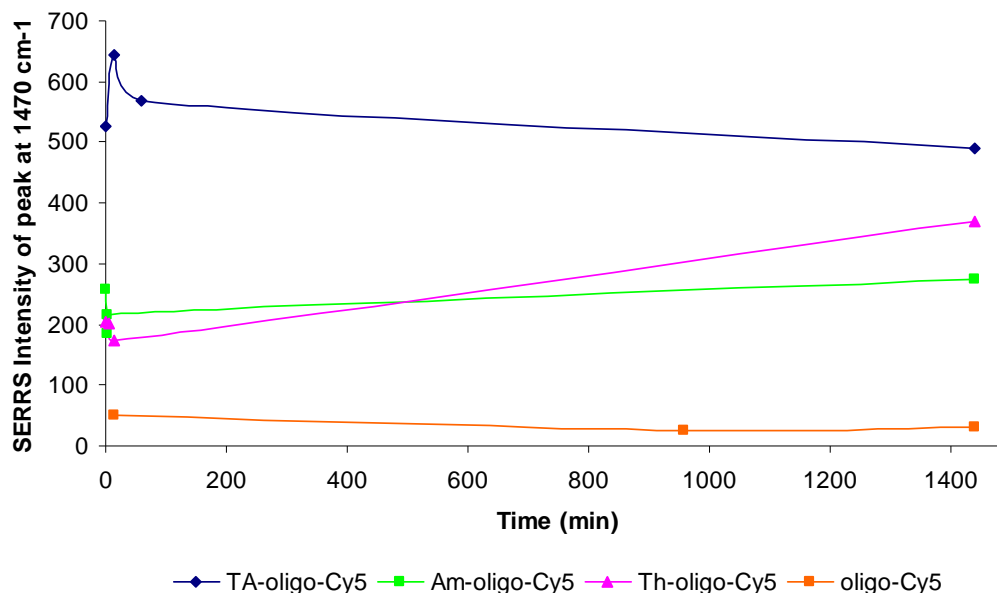
Figure 5.12: Plot of the SERRS intensity at 1470 cm^{-1} versus time for different surface attachment groups.

the Th-oligo-Cy5 signal increased to a maximum which was greater than the comparable amino-linked system. Over the same time scale, whilst TA-oligo-Cy5 maintained a higher SERRS response than any other linking system, it was lower than its initial response. This could be due to a different orientation of TA-oligo-Cy5 on the surface. Pleasingly, where there was no surface attachment group *i.e.* oligo-Cy5, there was a negligible response.

Taking a look at a "snap shot" of the responses, after 15 min and 24 h, clearly shows the difference in each of the systems (Figure 5.13). Not only does TA-oligo-Cy5 give superior SERRS response it also has a much more even surface coverage distribution than the other linkers – as evident by a low relative standard deviation, RSD, only 6.4 % c.f. 15.0 % and 24.9 % for Am-oligo-Cy5 and Th-oligo-Cy5, respectively. After 24 h the RSD of the TA-oligo-Cy5 is larger, indicating less order on the surface. An important finding is that the thioctic acid modified

oligonucleotide outperforms both the thiol and amino linker groups for modifying the Klarite™ surface using SERRS as a detection technique. Either by delivering more dye to the surface or by doing so in an orientation that is more amenable to SERRS.
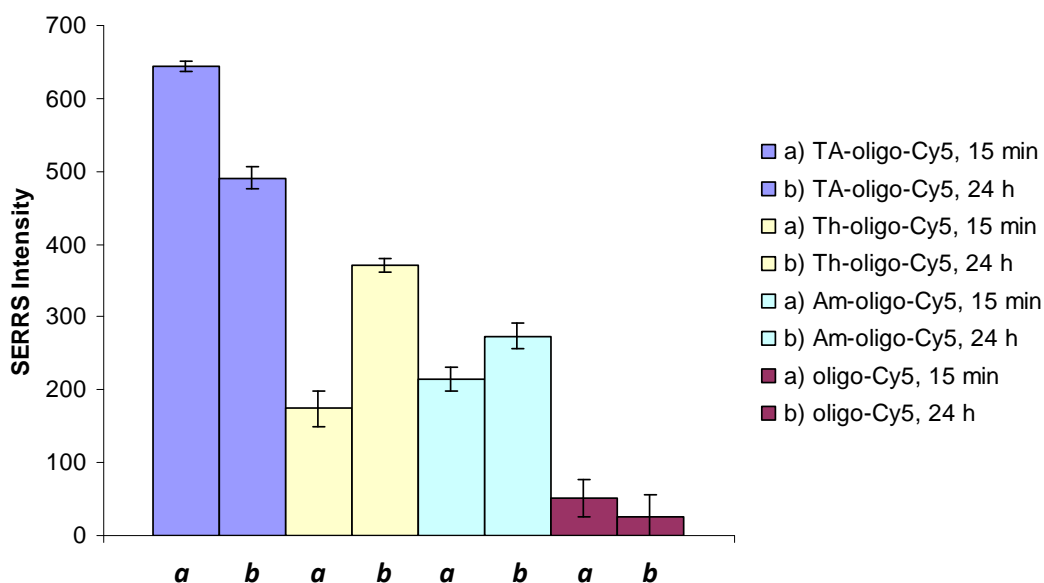
Figure 5.13: The intensity of the major peak at 1470 cm^{-1} is shown for each linker after both a) 15 min and b) 24 h incubation.

5.2 Hybridisation of Oligonucleotides Tethered to Klarite™

Direct hybridisations were attempted with oligonucleotides immobilised on the Klarite™ surface. Relatively short sequences were chosen (12-mer) in order that the dye would be close to the enhancing surface upon hybridisation (sequences detailed in Table 5.2). It was disappointing to find that hybridisation could not be confirmed by SERRS analysis of the substrates despite a number of attempts to

Name	Sequence (5'-3')	Surface Linker: X
TA-oligo-Pr1	CGC ATT CAG GAT X	Thioctic acid
Th-oligo-Pr1	CGC ATT CAG GAT X	Thiol

| Pr1-Target-Cy5 | ATC CTG AAT GCG Cy5 | - |

Table 5.2: Sequence details of probes and dye labelled target for direct hybridisation experiments.
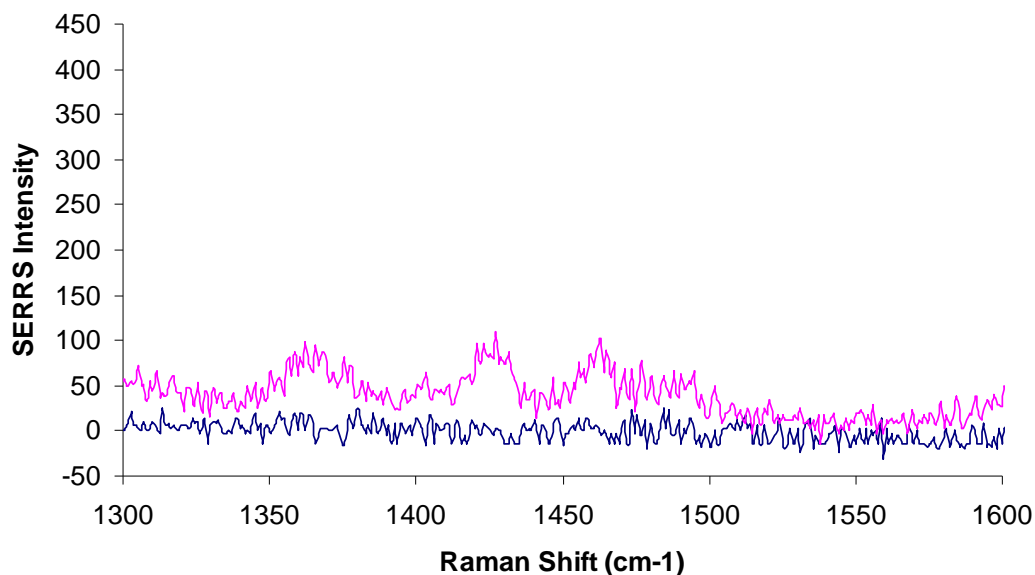
Figure 5.14: Typical SERRS spectra recorded from direct hybridisation experiments between TA-oligo-Pr1 and Pr1-Target-Cy5 on Klarite™. Spectra recorded from positive area – blue and from blank control – pink.

change variables including surface immobilisation time, immobilisation probe concentration, % surface coverage by the immobilised probe, target concentration and hybridisation time (Experimental 7.12.1). The hybridisations were carried out in Camlab hybridisation chambers to ensure a moist environment in which the
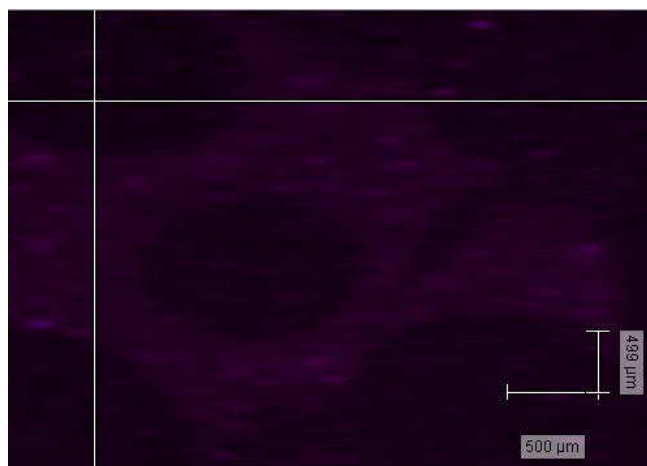
Figure 5.15: Typical false colour map generated from whole Klarite™ surface at 785 nm. Min (0) *Max (850).*

samples would not dry onto the chips. It should also be noted that attempts to obtain SERRS spectra by modifying the spectroscopic technique were applied to these substrates.   Instead of line-mapping, individual spectra were recorded, acquisition time was increased and the wavelength moved to the more sensitive 632.8 nm all without improvement. The lack of spectra is highlighted in Figure 5.14 along with a SERRS map (Figure 5.15) showing a lack of signal intensity. Similar results were obtained for all of the conditions attempted.

Failure to generate signal from the direct hybridisation of the immobilised probes with the dye labelled target was disappointing. There could be a number of reasons for this. Perhaps the packing of the probe oligonucleotide on the surface prevented entry into the concave active areas of the Klarite™ by the dye labelled target due to steric and electronic factors. Or perhaps, the orientation of the dye at the 3'-terminus of the target sequence inhibited hybridisation.

A less direct method was thus attempted in order to improve the ability to detect hybridisation by proceeding via use of the N-HS ester of thioctic acid.

5.3 SERRS Detection of a Dye-Labelled Oligonucleotide Hybridised to Klarite™

It was disappointing that results were poor for direct hybridisations with thioctic acid- or thiol- modified sequences on the Klarite™ surfaces. It was decided to first derivatise the surface with TA-NHS and subsequently react with amino-modified DNA and then hybridise with a BODIP(650) labelled oligonucleotide (Table 5.3) (Experimental 7.12.2). A solution of TA-NHS, **13**, was left on the Klarite™ surface

Probe	Sequence	Modification

	(5'-3')	(X)
Am-Oligo	XGCT AAA ACC ACA GTC AAG GC	Amino
Am-Oligo-MM	XGCT ACA ACC ACA GTC AAG GC	Amino
BODIPY(650)-Oligo	XGCC TTG ACT GTG GTT TTA GC	BODIPY(65)

Table 5.3: Sequence details for indirect hybridisation experiments on Klarite™.
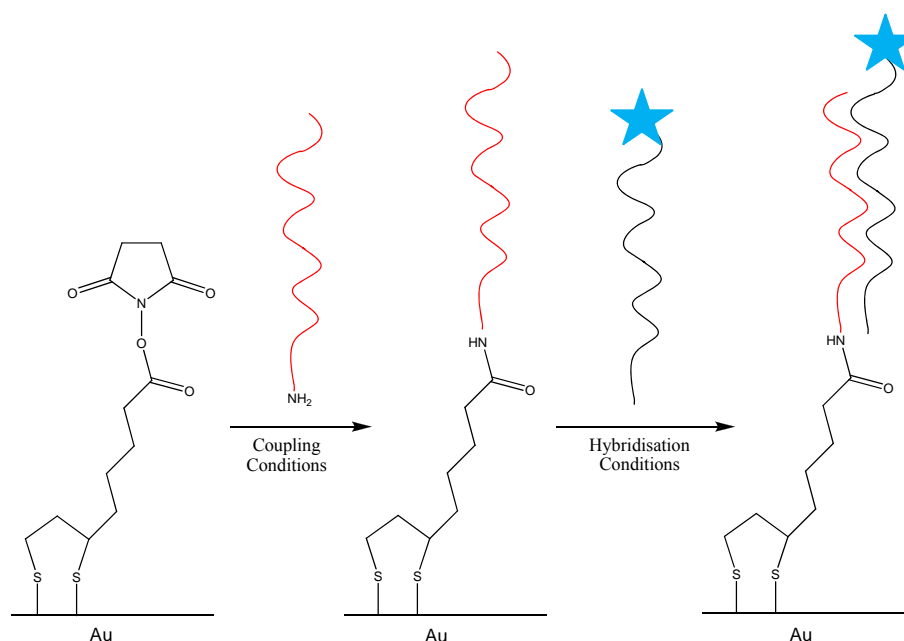
Scheme 5.1: Amide formation to immobilise an amino-modified oligonucleotide probe to the Klarite™ surface by use of the NHS-ester of thioctic acid was followed by hybridisation with a BODIPY (650) labelled target.

before being thoroughly washed off with DMF and EtOH. A 1 µM solution of 3'-amino-modified oligonucleotide, buffered at pH9, was added to the Klarite surface and left for an hour and a half. It was anticipated that, not only, would amide formation occur (as desired) but that competing hydrolysis of the NHS-ester would also occur. This was considered, rather than a hindrance, to be somewhat

129
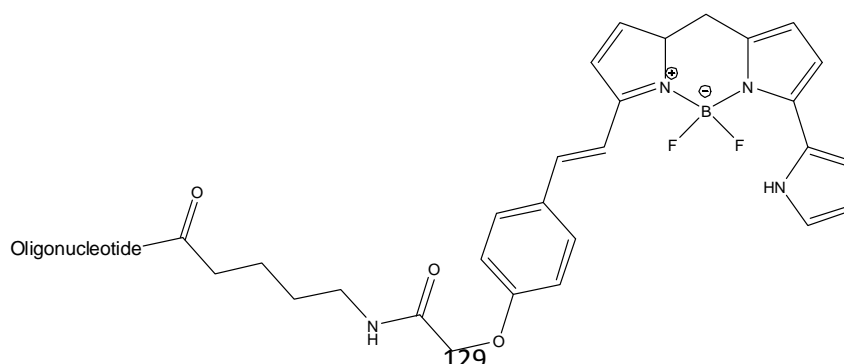
Figure 5.16: BODIPY(650)-labelled oligonucleotide.
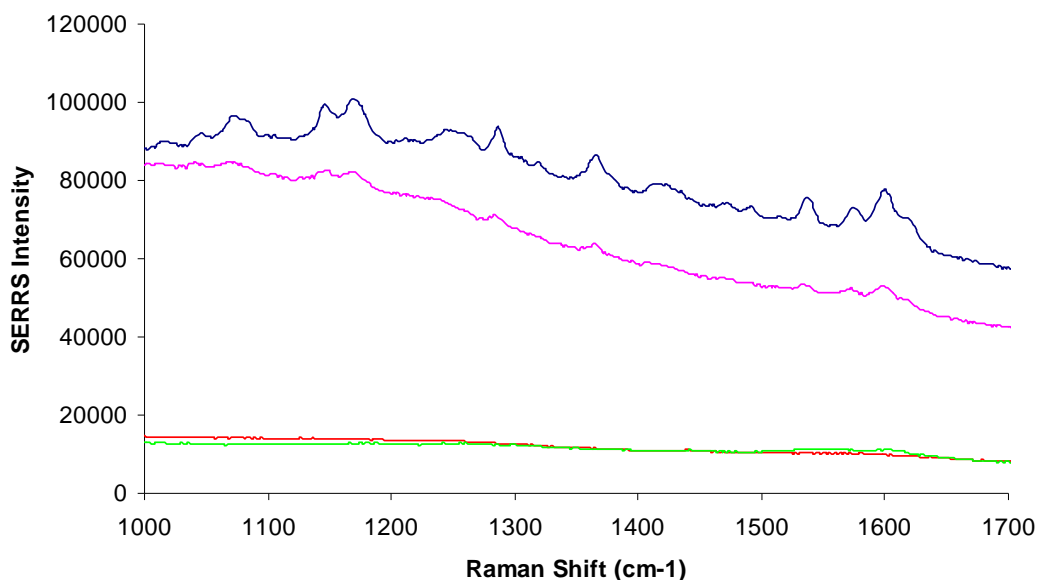
Figure 5.17: SERRS spectra of BODIPY(650) labelled oligonucleotide upon hybridisation with the full complement (blue) along with controls: single base mismatch (pink), linker + target (no capture) (red), linker + capture only (green).

fortuitous as the hydrolysed component would act as a means of "spacing out" the oligonucleotide capture strand on the surface, perhaps being favourable for hybridisation of an approaching target. The surface was rinsed with PBS. It was observed that the surface was much more "wettable" after oligonucleotide attachment than with linker alone. After the capture strand was introduced to the TA-*N*-hydroxysuccinimide (NHS) layer the surface was interrogated by 632.8 nm laser and showed, some background signal but no discernible SERRS (Figure 5.17). The TA-NHS layer was also subject to treatment with the complement (with no pre-capture strand amide formation) and thoroughly washed, again interrogation by the 632.8 nm laser showed the same level of background signal with none of the characteristic SERRS peaks. This was an important result as it showed that there

was no appreciable non-specific adsorption of the dye-labelled target with the TA-NHS surface. Once the TA-NHS had reacted with the capture strand and been hybridised with the full complement a very clear and strong SERRS signal, specific to BODIPY-650 was produced (Figure 5.17). When a mismatched sequence, that is a single base mismatch was introduced there was still a strong SERRS signal observed. This is due to the fact that hybridisation still occurs; the single base mismatch will be tolerated to some degree. Nevertheless, there is a marked reduction in signal from single base mismatch hybridisation experiments could be minimised by the careful selection of experimental temperature to be above the melt temperature (T_m) of the mismatch but below the T_m of the complement. The increased thermal stability of the thioctic acid based linker (with respect to equivalent monothiols) could facilitate this approach. This approach is still to be investigated.

At this time a Dip-Pen Nanolithography (DPN) instrument, the N-Scriptor, was purchased by the Centre for Molecular Nanometrology. It was decided to investigate the synergy between the techniques of DPN deposition on non-flat plasmon resonant surfaces allowing SERRS detection of oligonucleotide hybridisation events by fast Streamline mapping.

5.4 Dip Pen Nanolithography and SERRS for DNA Detection

In his inspiring speech, delivered in 1959, Richard P. Feynman proposed that there was "plenty of room at the bottom". [16] To illustrate his point he challenged *"Why cannot we write the entire 24 volumes of the Encyclopedia Brittanica on the head of a pin?"* Feynman speculated about generating wires only 10-100 atoms wide with circuitry for computers measuring only a few hundred angstroms across. Of course, *how* this writing and manipulation on the nanoscale was to be achieved took more time, research and innovation. In recent years, however, a number of nano-fabrication techniques for biological manipulation have been reported, [17] [18] efforts towards fulfilling Feynman's vision are underway. Indeed the applications of nanotechnology and nanofabrication are far-reaching, from nano-circuitry – transistors and logic gates – to bioanalytical devices. [19]

The first example of the "direct writing" of molecules by scanning probe lithography was reported in 1995 by Jaschke and Butt. [20] They observed the deposition of 1-octadecanethiol (ODT) aggregates onto mica surfaces during scanning probe microscopy. They studied the growth of these depositions over time
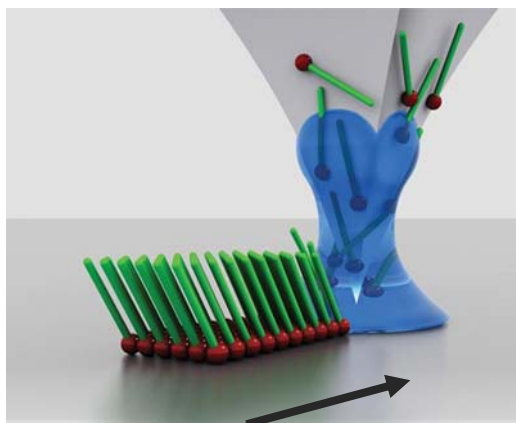
Figure 5.18: Schematic diagram depicting the "writing" process of dip-pen nanolithography. In which the molecular "ink" is represented by the green and red matchsticks, the water meniscus is shown in blue and the writing direction indicated by the arrow. **© Institute of Physics (the "Institute") and IOP Publishing 2009** [21]

and drew the first defined shape, a modest geometric star in the order of 7.5 μm. However, this early work was somewhat limited by the fact that deposition was not observed on glass or gold. Two years later, Mirkin and Piner investigated the effect of atmospheric water on lateral force microscopy (LFM) experiments and, indeed, they were able to "write" with water droplets, again on a mica substrate. [22] However, it was in their 1999 *Science* paper that Mirkin *et al.* coined the phrase "dip-pen" nanolithography (DPN) and the realisation of controlled lithography on the nanoscale was shown. [23] DPN involves the coating of an atomic force microscope (AFM) tip with a molecular "ink". The ink will transport through a water meniscus and onto a substrate with which it has an affinity. Early work involved writing on Au substrates with thiol-functionalised molecules *e.g.* ODT or mercaptohexadecanoic acid (MHA). [23] [24] A 30 nm wide line was achieved with the ODT on Au(111) and a 15 nm wide line was achieved with MHA on Au(111) which

is close to the resolution limit for a conventional "A-type" cantilever. Since the advent of the DPN technology in the late 1990s a variety of ink/substrate combinations have been investigated. [25] [26] [27] [28] [29] [30] Small molecules such as silazanes, alkoxysilanes and alkoxychlorosilanes have been written on Si/SiO_x, biological molecules (DNA, proteins, antibodies) have been written on Au and Si/SiO_x, sols on Si/SiO_x.
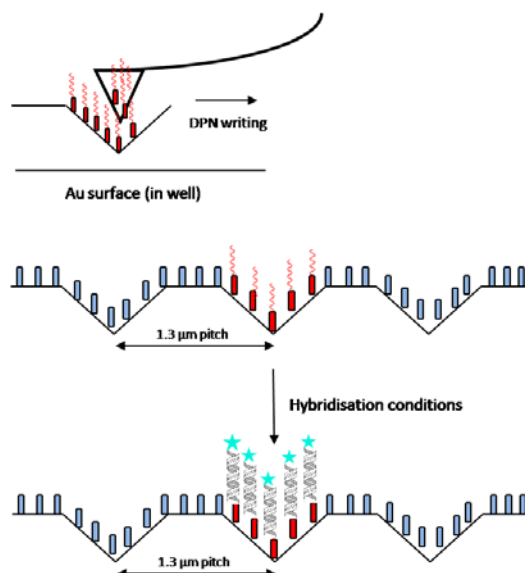
Figure 5.19: Representation of DPN immobilisation and hybridisation processes for detection of the Chlamydia target sequence, Tar-Ch.

5.4.1 DPN and SERRS

To demonstrate the practicality of the combined DPN-SERRS method a DNA detection experiment using an 18 base region of a sequence coding for a *Chlamydia trachomatis* target probe was performed (Figure 5.19, Experimental 7.12.3). Two independently modified complements to the *Chlamydia* target were obtained, each with 9 bases complementary to one half of the target sequence with an additional 3A "spacer" bases at the modified end (Table 5.4). One probe sequence is modified with thioctic acid for surface immobilisation via DPN (TA-Ch). The other is modified at the 5'-end with a Cy5™ label (Cy5-Ch) which will provide a signal by SERRS analysis upon hybridisation with the target sequence (Tar-Ch). The thioctic acid modified probe was mixed with "Just Add DNA" (JAD) carrier fluid [31]. This

Probe	Sequence (5'-3')	Modification
TA-Ch	GGG AGT AAG AAA X	TA
Cy5-Ch	Cy5 AAA GCT GCG ACA	Cy5™
Tar-Ch	CTT ACT CCC TGT CGC AGC	-

Table 5.4: Sequence information for DPN-SERRS assay experiments.
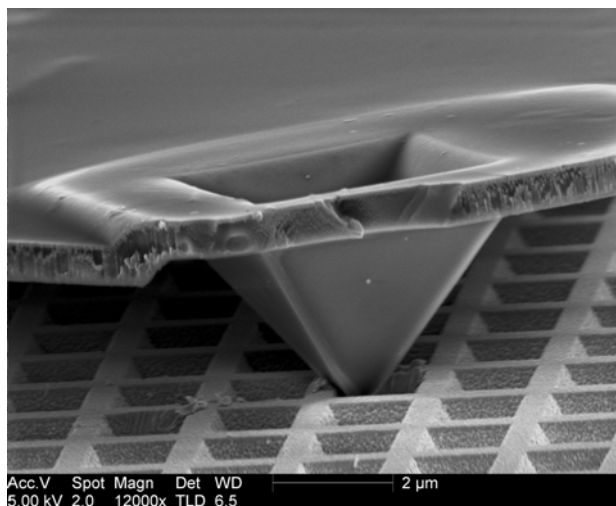
Figure 5.20: SEM of DPN tip in Klarite™ well. SEM; RJS.

mixture was deposited by pipette into a microfluidic inkwell system. A diving board style pen was applied to the microfluidic wells allowing it to take up the JAD/TA-Ch solution. Writing of the sequence into the microwells of the Klarite™ surface was achieved by rastering across the desired area (4 × 4 pixels). The DPN writing experiments were conducted in an environmental chamber of controlled temperature and humidity. An example of the DPN tip when applied to the Klarite™ substrate can be seen in Figure 5.20 (although it should be noted that this SEM is for illustrative purposes and is not taken from the actual experiment described).

The target sequence, Tar-Ch, and dye labelled complement, Cy5-Ch, were pre-mixed under hybridisation conditions. After lithography of the capture strand and removal of the "Just Add DNA" carrier fluid, [31] the surface was passivated with triethylene glycol mono-11-mercaptoundecyl ether to prevent nonspecific binding of the target sequence or the dye-labelled complement.

Only in the presence of the *Chlamydia* target, immobilised by the capture sequence, would the dye labelled complement hybridise and thus provide a reporter for SERRS detection. The pre-mixed target and dye-labelled sequences were added to the surface under hybridisation conditions and left in a moist hybridisation chamber for 1 h. Thereafter the surface was thoroughly washed before being interrogated by the 632.8 nm laser. The 632.8 nm laser was chosen in this case as
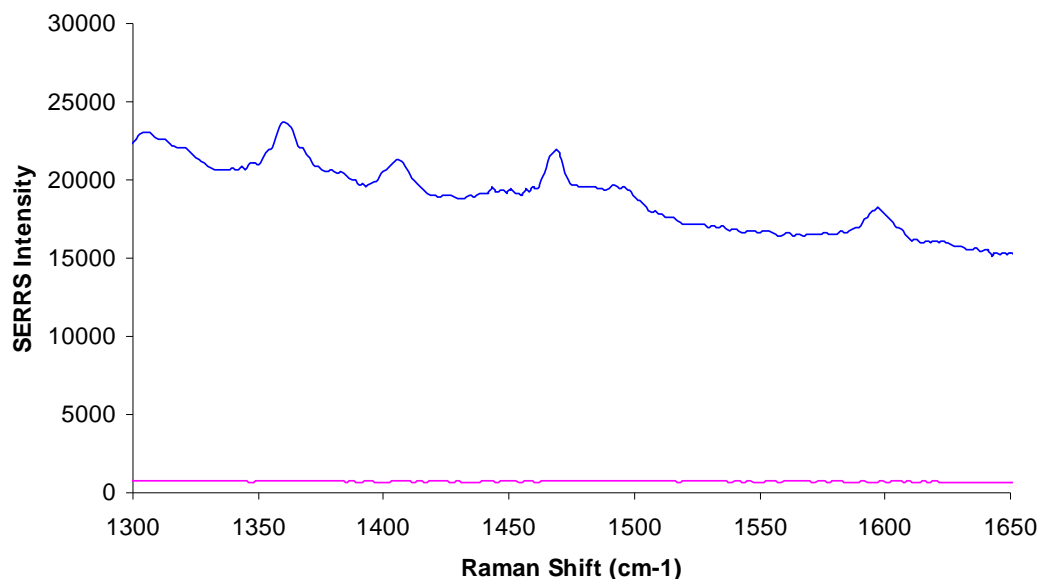
Figure 5.21: SERRS spectra recorded at 632.8 nm from positive area (blue) and from the blank control region (pink) show the presence of the Chlamydia target sequence via sandwich hybridisation with a dye labelled complement and a Klarite™ immobilised probe.

achieving the best response was the priority, rather than minimising any fluorescent background. The signal levels, acquired at 632.8 nm, were >3000:1 and showed good reproducibility from pixel to pixel (RSD <5 %). Significantly, the spectral contrast is very high with no trace of the reporter dye detectable in the "blank" regions that had also been exposed to identical hybridisation materials and conditions with the absence of target sequence as a control measure.

5.5   Chapter 5: Conclusions

Surface enhanced resonance Raman scattering has been used to directly detect dye labelled sequences of oligonucleotides modified by different surface attachment groups.   Thioctic acid modified oligonucleotides were found to allow for better surface modification characteristics with respect to thiol and amino- analogues.   Not only were signals uniformly stronger they also exhibited much lower RSDs. However, it was disappointing to observe an unexpected drop off in sensitivity in the micromolar range of the oligonucleotides immobilised.   In addition, the immobilised oligonucleotides failed to hybridise directly with a dye labelled target.   This was found not to be as a consequence of linking methodology, however, since the monothiol linker showed the same response.

In order to facilitate hybridisation a monolayer of TA-NHS ester was prepared and an amino-modified oligonucleotide was bound to it *via* amide formation.   Since this amide formation would occur alongside the competitive hydrolysis reaction this would cause the resulting oligonucleotide coverage to be spaced by thioctic acid groups.   The resulting hybridisations were found to be successful and were confirmed by SERRS analysis of the BODIPY(650) label.   It should be noted, however, that the orientation of the label with respect to the surface was different than in the unsuccessful direct hybridisations and could be an additional factor.

The immobilisation of thioctic acid modified oligonucleotides on the sensing surface was also controlled by Dip–Pen Nanolithography.   This allowed the detection of an unlabelled target by sandwich hybridisation with a dye-labelled probe.   This was a significant advancement of current methodology since DPN has now been shown to selectively create SERRS active DNA array pixels in a relatively simple manner. Multiplexing potential has been shown by other colleagues given that very high information density and depth can be obtained by embedding multiple reporter dyes within the same sub-diffraction limit area. The generation of high efficiency

SERRS from the surface and fast spectral acquisition times demonstrated in this work ultimately make sensitive, reproducible nanoarrays a practical reality.

5.6 Chapter 5: References

1.   Faulds, K., Barbagallo, R. P., Keer, J. T., Smith, W. E., Graham, D., **2004**, *Chem. Commun.*, 129, 567-568.

2.   Stokes, R. J., MacAskill, A., Lundahl, P. J., Smith, W. E., Faulds, K., Graham, D., **2007**, *Small*, 3, 1593-1601.

3.   Faulds, K., McKenzie, F., Smith, W. E., Graham, D., **2007**, *Angew. Chem., Int. Ed. Engl.*, 46, 1829-1831.

4.   Nie, S., Emory, S. R., **1997**, *Science*, 275, 1102-1106.

5.   Kneipp, K., Wang, Y., Kneipp, H., Perelman, L. T., Itzkan, I., Dasari, R. R., Feld, M. S., **1997**, *Phys. Rev. Lett.*, 78, 1667-1670.

6.   Khan, I., Cunningham, D., Graham, D., McComb, D. W., Smith, W. E., **2005**, *J. Phys. Chem. B*, 109, 3454-3459.

7.   Khan, I., Cunningham, D., Littleford, R. E., Graham, D., Smith, W. E, McComb, D. W., **2006**, *Anal. Chem.*, 78, 224-230.

8.   Perney, N. M. B., Baumberg, J. J., Zoorob, M. E., Charlton, M. D. B., Mahnkopf, S., Netti, C. M., **2006**, *Opt. Express*, 14, 847-857.

9.   Stokes, R. J., MacAskill, A., Dougan, J. A., Hargreaves, P. G., Stanford, H. M., Smith, W. E., Faulds, K., Graham, D., **2007**, *Chem. Commun.*, 2811-2813.

10.   Moskovits, M., **1985**, *Rev. Mod. Phys.*, 57, 783-826.

11.   Pineda, A. C., Ronis, D., **1985**, *J. Chem. Phys.*, 83, 5330-5337.

12.   Aslan, K., Gryczynski, I., Malicka, J., Matveeva, E., Lakowicz, J. R., Geddes, C. D., **2005**, *Curr. Opin. Biotechnol.*, 16, 55-62.

13. Bain, C. D., Troughton, E. B., Tao, Y.-T., Evall, J., **1989**, *J. Am. Chem. Soc.*, 111, 321-335.

14. Ullman, A., **1996**, *Chem. Rev.*, 96, 1533-1554.

15. Dougan, J. A., Karlsson, C., Smith, W. E., Graham, D., **2007**, *Nucleic Acids Res.*, 35, 3668-3675.

16. Feynman, Richard P. Nanotechnology at Zyvex. [Online] [Cited: 11 09 2009.] http://www.zyvex.com/nanotech/feynman.html.

17. Truskett, V. N., Watts, M. P. C., **2006**, *Trends Biotechnol.*, 24, 312-317.

18. Schmidt, R. C., Healy, K. E., **2009**, J. *Biomed. Mater. Res. A*, 1252-1261.

19. Edwards, S. A., *The Nanotech Pioneers: Where Are They Taking Us?* Weinheim : Wiley-VCH, **2006**.

20. Jaschke, M., Butt, H.-J., **1995**, *Langmuir*, 11, 1061-1064.

21. Institute of Physics. [Online] [Cited: 11 09 2009.] http://images.iop.org/dl/nano/DPN.jpg.

22. Piner, R. D., Mirkin, C. A., **1997**, *Langmuir*, 13, 6864-6868.

23. Piner, R. D., Zhu, J., Xu, F., Hong, S., Mirkin, C. A., **1999**, *Science*, 283, 661-663.

24. Hong, S., Zhu, J., Mirkin, C. A., **1999**, *Science*, 286, 523-525.

25. Ivanisevic, A., Mirkin, C. A., **2001**, *J. Am. Chem. Soc.*, 123, 7887-7889.

26. Jung, H., Kulkarni, R., Collier, C. P., **2003**, *J. Am. Chem. Soc.*, 125, 12096-12097.

27. Kooi, S. E., Baker, L. A., Sheehan, P. E., Whitman, L. J., **2004**, *Adv. Mater.*, 16, 1013-1016.

28. Maynor, B. W., Li, Y., Liu, J., **2001**, *Langmuir*, 17, 2575-2578.

29. Fu, L., Liu, X., Zhang, Y., Dravid, V. P., Mirkin, C. A., **2003**, *Nano Lett.*, 3, 757-760.

30. Gundiah, G., John, N. S., Thomas, P. J., Kulkarni, G. U., Rao, C. N. R., Heun, S., **2004**, *Appl. Phys. Lett.*, 84, 5341-5343.

31.   "Just Add DNA" is a proprietry solution available from NanoInk.

6 Conclusions

Thioctic acid has been used to modify oligonucleotides as a means to investigate their suitability as analytical detection probes. The synthesis of thioctic acid modified oligonucleotides has been achieved directly by use of H-phosphonate methodology, but also indirectly by the use of a key intermediate which was isolated during these investigations, namely the *N*-hydroxysuccinimidyl ester of thioctic acid. The isolation of this intermediate allowed both pre- and post-synthetic 5'- and 3'- modifications in the solution or solid phase. A variety of avenues to thioctic acid modified oligonucleotides are now available depending upon the synthetic requirements. As a direct result of this work the *N*-hydroxysuccinimidyl ester of thioctic acid is now a commercially available product from an UK-based DNA synthesis reagents company (Link Technologies). In addition, thioctic acid modified oligonucleotides are available for purchase directly from a UK-based oligonucleotide supplier (ATDbio).

Although H-phosphonate chemistry has been shown to modify oligonucleotides with thioctic acid, this was achieved by manual post-synthetic application of the reagents. It would be useful to optimise the H-phosphonate chemistry for automated synthesis. In addition, terminally modified species (3'- or 5'-) were synthesised and used throughout this report. It would be interesting to modify oligonucleotides internally (*i.e.* at a mid-sequence site) with thioctic acid and to investigate the applications of such species. This could be achieved *via* the *N*-hydroxysuccinimidyl ester of thioctic acid prepared herein and commercially available mid-sequence modifier phosphoramidites.

The successful modification of oligonucleotides by thioctic acid allowed their employment in the surface functionalisation of both gold and silver nanoparticles. The oligonucleotide-nanoparticle conjugates were found to be prepared easily and were stable under long term storage conditions. The conjugation of the thioctic acid oligonucleotides to the nanoparticles was indicated both, by gel electrophoresis and UV-vis spectroscopy. In addition, the biological integrity of the immobilised DNA was confirmed by hybridisation experiments. These experiments showed that the

hybridisation-induced aggregation of nanoparticles could be assessed by UV-vis spectroscopy. Gold nanoparticles have received considerably more attention in the literature than their silver analogues. This report is one of the earliest of oligonucleotide-silver nanoparticle hybridisation sensors and confirms that, due to the increased molar absorptivity of the silver nanoparticles, improved sensitivity is achieved (2 nM *c.f.* 0.1 µM). The stabilities of the conjugates systems were assessed and thioctic acid modified oligonucleotides were shown to confer greatly enhanced stability with respect to standard "monothiol" analogues on both gold and silver conjugates in the presence of additives and at elevated temperature. This result allows for, potentially, increasingly strenuous environments to be investigated that would be inaccessible for monothiol linked conjugates. It would be advantageous, for instance, to develop oligonucleotide-nanoparticle conjugates that would be stable under PCR conditions. Thioctic acid modified oligonucleotides should be investigated to this end. If this were achieved then closed-tube, multiplex detection by SERRS would be a real possibility and would represent a step forward for clinical diagnosis.

Thioctic acid modified oligonucleotides were also investigated as surface modifiers when applied to a commercially available nanoscale roughened metal surface. The roughened surface was prepared in order to generate a plasmon band that could be used for surface enhanced resonance Raman scattering studies. As such SERRS was used to investigate the surface adsorption behaviour of dye-labelled thioctic acid modified oligonucleotides when compared with thiol and amino analogues. The thioctic acid linking chemistry was shown to give greatly enhanced SERRS responses, with smaller RSDs. Disappointingly, attempts at direct hybridisations were unsuccessful, although this was not simply due to the thioctic acid modification as monothiol analogues were also found to be unsuccessful. Nevertheless, this hurdle was overcome by use of the key *N*-hydroxysuccinimidyl ester as a surface modifier and subsequent amide formation with an amino-modified oligonucleotide. Hybridisation was then achieved to a dye-labelled complementary sequence, as confirmed by the characteristic SERRS response of the dye. This was the first confirmation of hybridisation occurring on the Klarite™ surface. However, more useful is the ability to detect unlabeled target oligonucleotide sequences. It

was decided, therefore, to extend this methodology further to the detection of an unlabelled target and, in addition, to combine SERRS analysis of a hybridisation event with the emerging technology of Dip-pen nanolithography. DPN was therefore used to immobilise thioctic acid oligonucleotides on the Klarite™ surface within specific wells. Sandwich hybridisation between an unlabeled target and a dye labelled complement allowed detection of an unmodified target sequence by SERRS.

The concentrations of the oligonucleotide targets for SERRS detection on Klarite™ were in the µM range and to be analytically useful would need to be lowered considerably. This should be investigated as the combination of precision DPN patterning with fast Streamline™ mapping could provide for a wealth of information and the simultaneous detection of multiple targets.

Overall the modification of oligonucleotides by thioctic acid has proven useful for generating analytical materials of enhanced stability or performance. The continuation of this work should be investigated to yield species which are employed in increasingly strenuous sensing environments, capable of achieving multiplex analysis.

7 Experimental

7.1 General

- Solvents were of laboratory grade (unless otherwise stated).

- Anhydrous DMF, DMSO and DIPEA were supplied in SureSeal™ bottles from Aldrich.

- Anhydrous MeCN was supplied in sealed bottles from Link Technologies.

- Anhydrous THF was distilled over sodium/benzophenone and used immediately.

- Anhydrous DCM and pyridine were distilled over CaH_2 and used immediately.

- Chemicals were obtained from a commercial source – Aldrich. Exceptions are stated in the text.

- DNA synthesis reagents were obtained from a commercial source – Link Technologies.

- Thin layer chromatography was carried out on aluminium sheets, silica gel 60 0.2 mm layer (Merck).

- TLC visualization was carried out by:

  o UV absorption at 254 nm

  o Treatment with ninhydrin/ethanol (0.2 % w/v)

  o Treatment with *p*-anisaldehyde/ethanol (2 % v/v) (acidified)

  o Treatment with $KMnO_4$ (1.5 % w/v).

- Purification by flash column chromatography was carried out with silica gel 60 (Merck). [1]

- ^{1}H, ^{13}C and ^{31}P NMR were recorded on a Brüker DPX 400 spectrometer.

- J values are quoted in Hz.

- Elemental analyses were performed by the University of Strathclyde as a service with a Perkin-Elmer 240 elemental analyser.

- Mass spectrometry was conducted by EPSRC National Mass Spectrometry Service Centre. The ionization mode used was positive electrospray. Exceptions are stated.

- Oligonucleotide synthesis was carried out on a Mermade 6 Oligonucleotide Synthesiser.

- Custom oligonucleotides were purchased (where specified) from ATDbio.

- Ion-exchange HPLC purification was carried out using a 1 ml Resource Q ion-exchange column on a Dionex HPLC system, fitted with an UVD170U detector and a P680 pump with method details specified in the text.

- Reverse-phase HPLC purification was carried out using a Phenomenex Clarity column on a Dionex HPLC system, fitted with an UVD170U detector and a P680 pump with method details specified in the text.

- Size-exclusion HPLC purification was carried out using Hi-Trap Desalt columns on a Dionex HPLC system, fitted with an UVD170U detector and a P680 pump, with method details specified in the text.

- UV-vis spectroscopy was carried out on a Cary 300 Bio UV-vis spectrophotometer fitted with a 6 × 6 cell changer and Peltier temperature controller.

- Fluorescence measurements were recorded on a Varian Cary Eclipse.

- SERRS maps were obtained using a Renishaw *InVia* spectrometer and Streamline™ mapping system. Other spectroscopic conditions are stated in the text.

- DPN was carried out on a NanoInk NScriptor.

- SEM was carried out by Dr. Robert J. Stokes at the Department of Physics, University of Strathclyde on a FEI Sirion 200 ultra high resolution shottky field emission scanning electron microscope.

- Klarite™ chips were obtained from a commercial source – D3 Technologies.

7.2 Chemical Synthesis

7.2.1 Preparation of N-(6-hydroxyhexyl)-5(1,2-diothiolan-3-yl)pentamide, 3
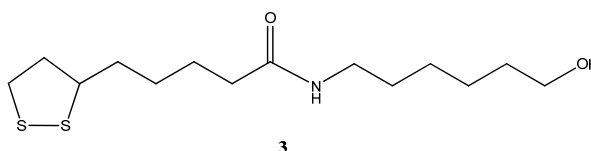
Thioctic acid (1.857 g, 9.0 mmol, 1.05 eq) was dissolved in DCM (anhydrous, 50 mL) under N_2. To this, CDI (1.704 g, 10.5 mmol, 1.2 eq) was added and evolution of gas was observed. The system was stirred for 1 h at room temperature (~ 20 °C) under N_2. 6-Aminohexan-1-ol (1.009 g, 8.6 mmol, 1 eq) was added to the activated acid. The resulting reaction mixture was stirred for 18 h at room temperature (~ 20 °C). The reaction mixture was washed with NaOH (50 mL × 2, 10 % (w/v)), citric acid (50 mL × 2, 10 % (w/v)) and finally NaCl (sat., 50 mL × 2). The combined organic layer was then dried over Na_2SO_4. The sodium sulfate was removed and the solution concentrated *in vacuo* to yield a pale yellow powder, 2.62 g. The sample was purified by dissolving in the minimum amount of DCM and precipitating from an excess of vigorously stirring hexane to give 1.788 g of purified product, **3**, in a 69 % yield. [Found: C, 55.0; H, 8.9; N, 4.4; S, 20.7 %; M^+, 306.1556. $C_{14}H_{27}NO_2S_2$ requires C, 55.0; H, 8.9; N, 4.6; S, 21.0 %; M^+, 306.1556]; δ_H(400 MHz; DMSO) 1.1-1.7 (14 H, m), 1.85 (1H, m, CH), 2.03 (2H, t, J 7.4, CH_2), 2.40 (1 H, m, CH), 3.00 (2 H, m, CH_2), 3.14 (2 H, m, CH_2), 3.38 (2 H, t, J 6.5, CH_2), 3.61 (1 H, quintet, J 3.1, CH), 4.35 (1 H, s, br, OH), 7.75 (1H, t, J 10.8, NH); δ_C(100 MHz, DMSO) 25.51, 25.68, 26.77, 28.73, 29.66, 32.92, 34.54, 35.64, 38.51, 38.77, 56.56, 61.08, 172.09.

7.2.2 Attempts Towards Cyanoethyl-6-{[5-1,2-dithiolan-3-yl) pentanoyl]amino}hexyldi--iso-propylamidophosphite, 5

5
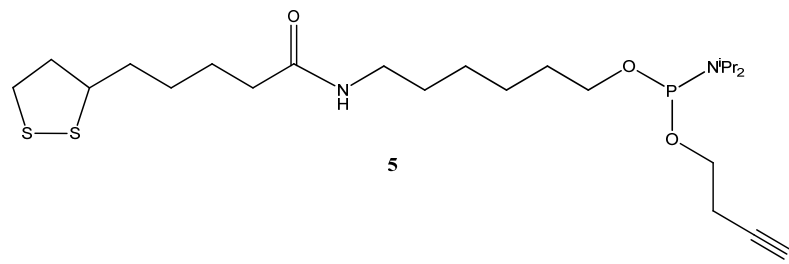
N-(6-Hydroxyhexyl)-5(1,2-diothiolan-3-yl)pentamide, **3**, (0.256 g, 0.84 mmol, 1 eq) was added to dichloromethane (10 mL, anhydrous) which was then removed under vacuum. This was repeated a further two times. Each time the flask was returned to normal pressure under N_2. *N*-(6-Hydroxyhexyl)-5(1,2-diothiolan-3-yl)pentamide, **3**, was re-dissolved in dichloromethane (10 mL, anhydrous). 2-Cyanoethyl-*N,N,N',N'*-tetraisopropylphosphoramidite, (0.4 mL, 1.26 mmol, 1.5 eq) was added under N_2. 5-Benzylthio-1*H*-tetrazole (4.2 mL, 1.26 mmol, 1.5 eq) was added dropwise over 30 min *via* syringe pump. The solution was allowed to stir for 1 h. The reaction mixture was concentrated *in vacuo* and purified by flash column chromatography (silica (pre-treated with Et_3N); eluent: EtOAc) under N_2 (collected into sealed vials). The solvent was removed *in vacuo* to leave a glassy solid. This was kept under N_2 and co-evaporated with acetonitrile (anhydrous, 3×2 mL). ^{31}P NMR (160 MHz; THF): 3.11; 30.52; 69.76; 145.45; 160.17. Variables towards this preparation are listed in Table 7.1.

Reaction	Phosphitylating Reagent	Solvent	Column (pre-Et$_3$N; EtOAc)	Et$_3$N Removal
A	diisopropylamino-	DCM	Y	Co-evap. × 3 (MeCN)
B	diisopropylamino-	DCM	Y	Co-evap. × 3 (50:50 MeCN/THF)
C	diisopropylamino-	DCM	Y	Co-evap. × 3 (THF)
D	diisopropylamino-	DCM	Y	Co-evap. × 2 (THF) Drying pistol (P$_2$O$_5$) overnight
E	diisopropylamino-	THF	Y	Co-evap. × 2 (THF) Drying pistol (P$_2$O$_5$) overnight
H	diisopropylamino	THF	Y	Co-evap. × 3 (THF) P$_2$O$_5$ overnight
I*	diisopropylamino	THF	N	Co-evap. × 3 (THF) P$_2$O$_5$ overnight
F	Chloro-	THF	Y	Co-evap. × 2 (THF) Drying pistol (P$_2$O$_5$) overnight
G	Chloro-	THF	N	Co-evap. × 2 (THF) Drying pistol (P$_2$O$_5$) overnight

* Experiment I was dried over P$_2$O$_5$ before synthesis. All other attempts had alcohol co-evaporated × 3 in reaction solvent under N$_2$ prior to synthesis.

Table 7.1: Variable conditions for the attempted preparations of cyanoethyl-6-{[5-1,2-dithiolan-3-yl)pentanoyl]amino}hexyldi--iso-propylamidophosphite, **5***.*

The product of these reactions were applied to DNA modification (Experimental 7.3.2).

7.2.3 Preparation of N-(6-hydroxypentyl)-5(1,2-diothiolan-3-yl)pentamide, 7
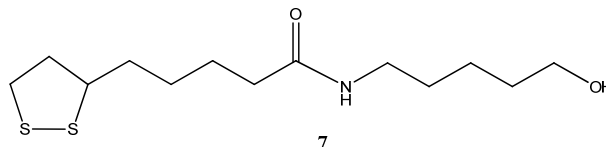
Thioctic acid (1.00 g, 4.9 mmol, 1.05 eq) was dissolved in MeCN (anhydrous, 50 mL) under N_2. To this, HOBT (0.76 g, 5.6 mmol, 1.2 eq) was added, followed by HATU (2.13 g, 5.6 mmol, 1.2 eq), DIPEA (0.72 g, 0.97 mL, 5.6 mmol, 1.2 eq) and, finally, aminopentanol (0.48 g, 4.7 mmol, 1.0 eq). The reaction was stirred for 12 h. The sample was concentrated *in vacuo* to yield a yellow oil, which was taken up in dichloromethane and washed with citric acid (50 mL, 10 % (w/v)), NaOH (50 mL, 10 % (w/v)), and finally saturated NaCl (50 mL). The combined organic layer was then dried over Na_2SO_4. The sodium sulfate was removed and the solution concentrated *in vacuo* to yield a pale yellow powder. The sample was dissolved in the minimum amount of DCM before being added to a vast excess of vigorously stirred hexane (750 mL) producing a precipitate. The precipitate was filtered to give 1.077 g of product, **7**, in 79 % yield. δ_H(500 MHz; DMSO) 1.2-1.7 (12 H, m), 1.85 (1H, *sextet*, *J* 6.6, CH), 2.03 (2H, t, *J* 7.4, CH_2), 2.40 (1 H, *sextet*, *J* 6.3, CH), 3.00-3.21 (4 H, m, 2 × CH_2), 3.35 (2 H, t, *J* 6.5, CH_2), 3.60 (1 H, quintet, *J* 3.1, CH), 4.20 (1 H, s, br, OH), 7.75 (1H, t, *J* 10.8, NH). δ_C (125 MHz; DMSO) 23.44, 25.56, 28.79, 29.57, 31.43, 32.71, 34.60, 35.71, 38.57, 38.72, 56.62, 61.12, 172.14.

7.2.4 Preparation of N-(6-hydroxypentyl)-5(1,2-diothiolan-3-yl)pentamidyl H-phosphonate, 10

10
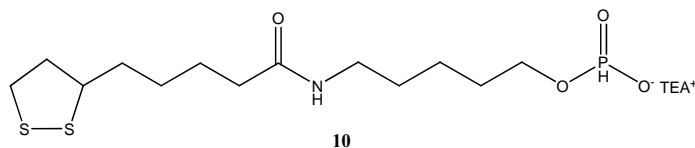
In a flame-dried flask under N_2, *N*-(6-hydroxypentyl)-5(1,2-diothiolan-3-yl)pentamide **7**, (0.26 g, 0.89 mmol, 1 eq) was dissolved in a solution of 1 M phosphorous acid in anhydrous pyridine (10 mL, 8.5 mmol of H_3PO_3). Pivaloyl chloride (0.59 g, 4.9 mmol, 5.5 eq.) was added dropwise from a glass syringe. The solution became briefly opaque, after which a clear mixture was produced upon complete addition, thereafter the reaction was stirred for a further 30 min. Once complete, the reaction mixture was quenched by addition of TEAB buffer (20 mL, 2 M, pH 7.5) and was then extracted twice with DCM. The organic layers were combined, dried over Na_2SO_4 and concentrated *in vacuo* to yield a viscous yellow oil. The reaction was purified by flash column chromatography (through a short pad (~2 × 1 cm) of silica (pre-treated with Et_3N); eluent: DCM). The product eluted in 9:1:0.1 DCM:MeOH:Et_3N. The combined fractions were reduced *in vacuo* to yield a yellow oil. Traces of Et_3N were removed *in vacuo*. The sample was dissolved in the minimum amount of DCM and added to an excess of hexane and the precipitate collected by filtration, 0.19 g, 47 %. ^{31}P NMR (160 MHz, 1:1 acetonitrile:pyridine): -0.4407. This was used directly in the modification of oligonucleotides (Experimental 7.3.3).

7.2.5 Preparation of 1-{[5-(1,2-dithiolan-3-yl)pentanoyl]oxy}-2,5-pyrrolidinedione, 13

13
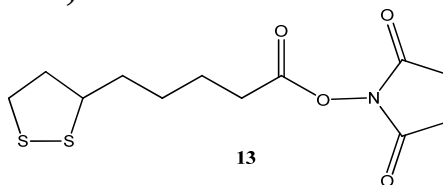
N-(3-Dimethylaminopropyl)-N'-ethylcarbodiimide (1.840 g, 9.6 mmol, 1.2 eq) was dissolved in DCM (anhydrous, 20 ml), to which DIPEA (anhydrous, 1.7 mL, 9.6 mmol, 1.2 eq) was added and stirred for 10 min. To the solution, N-hydroxysuccinimide (1.290 g, 11.2 mmol, 1.4 eq) was added and the reaction mixture was lowered into an ice bath. Thioctic acid (1.643 g, 8.0 mmol, 1.0 eq) was dissolved in DCM (anhydrous, 10 mL) and added to the cooled solution over 5 min dropwise. The reaction mixture was left to stir overnight before being washed with HCl (50 mL × 2, 5 % (v/v)) and water (distilled, 50 mL). The organic layer was dried over Na_2SO_4 and stored overnight in the fridge. The Na_2SO_4 was removed and solvents evaporated *in vacuo* to yield 2.24 g of ester **13**, a yellow solid. The residue was dissolved in the minimum amount of DCM and MeOH and dry-loaded onto Na_2SO_4. The product was purified by flash column chromatography in an 83 % yield (2.09 g, 6.64 mmol). [Found: C, 47.7; H, 5.9; N, 4.5; S, 21.2 %; $M+NH_4^+$, 321.0937. $C_{12}H_{17}NO_4S_2$ requires, C, 47.5; H, 5.7; N, 4.6; S, 21.1 %; $M+NH_4^+$, 321.0927]; δ_H(400 MHz; DMSO) 1.4-1.7 (6H, m, CH_2 × 3), 1.84-1.93 (1H, m, CH), 2.38-2.46 (1H, m, CH), 2.68 (2H, t, J 7.2, CH_2), 2.81 (4H, s, succinimidyl CH_2 × 2), 3.12-3.21 (2H, m, CH_2), 3.56-3.65 (1H, m, CH). δ_C(100 MHz; DMSO) 24.42, 25.83, 28.03, 30.42, 34.22, 38.50, 56.01, 169.29, 170.61.

7.3 Oligonucleotide Synthesis, Modification and Purification

7.3.1 Oligonucleotide Synthesis

The synthesis of oligonucleotide sequences was carried out on 1 μmol, 1000 Å columns. The following cycle was undertaken:

Deblock   × 3   (220 μL, 36 s)

MeCN   × 2   (274 μL, 5 s)

Coupling × 2   (90 μL Amidite, 110 μL Activator, 100 s)

MeCN   × 1   (274 μL, 5 s)

Capping   × 1   (125 μL Mix A, 125 μL Mix B, 50 s)

MeCN   × 1   (274 μL, 5 s)

Oxidise   × 1   (200 μL, 60 s)

MeCN   × 2   (274 μL, 5 s)

Where, the following commercially available solutions were used:

Deblock – 3 % trichloroacetic acid/DCM

Activator – 0.25 M 5-ethylthio-1H-tetrazole/MeCN

Cap Mix A – THF/pyridine/acetic anhydride (8:1:1)

Cap Mix B – 10 % methylimidazole/THF

Oxidiser – 0.02 M Iodine in THF/pyridine/water (7:2:1)

The phosphoramidites were dissolved in anhydrous MeCN to a concentration of 0.1 M prior to synthesis. The following phosphoramidites were used:

Bz-CE-dA phosphoramidite

Ac-CE-dC phosphoramidite

Dmf-CE-dG phosphoramidite

dT-CE-phosphoramidite

7.3.2 5'-TA Modification of an Oligonucleotide – The Phosphoramidite Approach.

The synthesis of cyanoethyl-6-{[5-1,2-dithiolan-3-yl)pentanoyl]amino}hexyldi-isopropylamidophosphite, **5**, was attempted as *per* Experimental 7.2.2. The samples were dissolved in acetonitrile, THF (anhydrous) or a mixture of both – as described in Table 7.1 (same solvent system as used for Et₃N removal) - to a concentration of 0.2 M. In all cases the sample was placed on a port of the Mermade 6 Nucleic Acid Synthesiser and added as the last monomer to a sequence using standard or extended coupling times. Post-synthesis the columns were treated with 1 mL of ammonium hydroxide (conc.) for 36 h at room temperature. The ammonium hydroxide was removed *in vacuo* and the sample dissolved in water (distilled, 1 mL) and stored at 4 °C for analysis by IE-HPLC (Experimental 7.4.1).

7.3.3 5'-TA Modification of an Oligonucleotide – The H-Phosphonate Approach.

Standard CPG (1 µmol) was used to synthesise [CCCCCC], 6C, and [TTTTTT], 6T, by standard automated synthesis (Experiment 7.3.1). The CPG was removed from the column and was added to a previously silanised flask. *N*-(6-Hydroxypentyl)-5(1,2-diothiolan-3-yl)pentamidyl H-phosphonate, **10**, (as prepared in experiment 7.2.4) was dissolved in 1:1 MeCN:pyridine (2 mg, 4 µM) and added to the flask. To this, pivaloyl chloride (1.2 mg, 10 µM) was added and the reaction mixture was agitated for 5 min on a mechanical shaker. The supernatant was removed and the solid support washed with MeCN (1 mL × 3) and treated briefly with standard DNA synthesis oxidizing solution. The CPG was again washed with MeCN, ~ 2 mL. Ammonium hydroxide (conc.) (1 mL) was added to each vial and left for 4 h or 1 h for TA-6C and TA-6T, respectively, before collecting the supernatant and removing the ammonium hydroxide (conc.) *in vacuo*. The residue was taken up in water (distilled, 1 mL) and stored at 4 °C until analysis by RP-HPLC (Experimental 7.4.3).

7.3.4   3'-TA Modification of an Oligonucleotide by use of 1-{[5-(1,2-dithiolan-3-yl)pentanoyl]oxy}-2,5-pyrrolidinedione, 13

DNA synthesis was carried out on a 3'-amino-modifier C7 CPG solid support (1 μmol).   The Fmoc protected column was pre-treated with piperidine/MeCN (1 mL, 20 % (v/v)) for 30 min. 1-{[5-(1,2-Dithiolan-3-yl)pentanoyl]oxy}-2,5-pyrrolidinedione, **13** (20 mg mL^{-1}/MeCN) was applied to the column overnight and then washed with MeCN (3 × 1 mL). The column was then placed in the synthesiser and used as the solid support for oligonucleotide synthesis. The oligonucleotide sequence was prepared on a MerMade 6 Nucleic Acid Synthesiser using an alteration of the standard DNA synthesis cycle (Experimental 7.3.1) to include two capping steps as a pre-treatment. After capping, DNA synthesis was carried out as standard (Experimental 7.3.1).   Where a dye-modification was incorporated at the 5'-terminus, a commercially available phosphoramidite of the desired dye was used as the final monomer.   The solid supports were removed from the synthesiser and treated with conc. NH$_4$OH (1 mL) for 36 h at room temperature.   The ammonium hydroxide was removed *in vacuo* (room temperature).   The clear residue was re-dissolved in H$_2$O (1 mL, distilled) and purified by reversed-phase HPLC (Experimental 7.4.3).

7.3.5   Post-Synthetic 5'-TA Modification of an Oligonucleotide by use of 1-{[5-(1,2-dithiolan-3-yl)pentanoyl]oxy}-2,5-pyrrolidinedione, 13 (solution phase)

An amino-modified oligonucleotide (100 μL, 200 μM) was added to a glass vial and cooled to 0 °C. Sodium bicarbonate buffer (260 μL, 0.18 M, pH 9.2) was added. 1-{[5-(1,2-Dithiolan-3-yl)pentanoyl]oxy}-2,5-pyrrolidinedione, **13** was dissolved in DMF (anhydrous, 40 μL, 25 mM) and added to the aqueous solution.   The reaction was kept at 4 °C overnight before being purified by reversed-phase HPLC (Experimental 7.4.3).

The solution phase method was developed to cover the following guidelines:

- $\leq 10\%$ organic component (DMF)
- 2 - 50 fold excess N-HS ester (1-{[5-(1,2-dithiolan-3-yl)pentanoyl]oxy}-2,5-pyrrolidinedione, **13**)
- pH7.5 – 9.5
- Buffer at 100 mM (final concentration)

7.3.6   Post Synthetic 5'-TA Modification of an Oligonucleotide by use of 1-{[5-(1,2-dithiolan-3-yl)pentanoyl]oxy}-2,5-pyrrolidinedione, 13 (solid phase)

DNA synthesis was carried out on a standard support (1 μmol).   The oligonucleotide sequence was prepared on a MerMade 6 Nucleic Acid Synthesiser using standard DNA synthesis (Experimental 7.3.1).   Once the desired sequence of bases had been added a 5'-monomethoxytrityl protected amino modifier phosphoramidite was added as the final monomer. The final deblock step at the end of the synthesis was omitted. The column was removed from the synthesiser and the standard deblock solution was added across the column for 1 h 30 min. The column was then washed with MeCN before being treated with a solution of 1-{[5-(1,2-dithiolan-3-yl)pentanoyl]oxy}-2,5-pyrrolidinedione, **13**, in MeCN (6 mg mL^{-1}, Et$_3$N 1.0 % v/v) overnight. The column was once again washed with MeCN before being treated with conc. NH$_4$OH (1 mL) for 36 h at room temperature. The ammonium hydroxide was removed *in vacuo* (room temperature). The clear residue was re-dissolved in H$_2$O (1 mL, distilled) and purified by reversed-phase HPLC (Experimental 7.4.3).

7.4 HPLC Purification and Analysis of Oligonucleotides

7.4.1 IE HPLC

Analytical IE HPLC was carried out on a Dionex UVD170U detector fitted with a P680 pump through a Resource Q column. Buffer A: tris(hydroxymethyl) aminomethane (0.25 M, pH 8), Buffer B: sodium perchlorate (0.375 M), Buffer C: water (distilled); T=0, 10 % A: 5 % B: 85 % C; Eluent maintained at 10 % A throughout, with a gradient increase of 6.25 % min^{-1} B over 12 min and held at 80 % B for 3 min at a flow rate of 1 mL/min

7.4.2 SEC HPLC

Size exclusion HPLC was carried out on a Dionex UVD170U detector fitted with a P680 pump through a HiTrap™ Desalting Column. Eluent: 100 % H_2O at 3 mL/min for 10 min.

7.4.3 RP HPLC

Preparative RP HPLC was carried out on a Dionex UVD170U detector fitted with a P680 pump through a Phenomenex Clarity column. Buffer A: TEAA (0.1 M, pH 7), Buffer B: CH_3CN; T=0, 95% A: 5% B, with a gradient increase of 1% min^{-1} B over 15 min and held at 20% B for 5 min at a flow rate of 1 mL/min.

7.4.4 Post-HPLC Sample Isolation

The required peaks were collected at the appropriate retention time (taking into account delay time). The fractions were collated and concentrated *in vacuo* at room temperature and re-suspended in H_2O (1 mL, distilled). They were then freeze-dried and dissolved in H_2O (1 mL, distilled) and stored at 4 °C.

7.4.5 Concentration Evaluation

Once an oligonucleotide has been synthesized and appropriately purified its concentration is calculated. Oligonucleotides absorb strongly in the UV with an absorption maximum, λ_{max}, at 260 – 280 nm. The absorbance is caused by electronic

transitions in the purine and pyrimidines bases. The intensity and exact wavelength is dictated by the base sequence, the presence of base-pairing interactions, the salt concentration and pH of solution. Thus, the concentration of an oligonucleotide can be obtained by measuring the absorbance of the purified, desalted sample in water at 260 nm. According to the Beer-Lambert law:

$$A = \varepsilon Cl$$

Where,

A = Absorbance

ε = Molar extinction coefficient (mol^{-1} cm^{-1})

C = Concentration (mol L^{-1})

l = Path length (cm)

Molar extinction coefficients are additive, and as such, to obtain the molar extinction coefficient of a particular sequence the values for the individual bases are added. The molar extinction coefficients of the bases are as follows:

A $=$ 15,400 mol^{-1} cm^{-1}

C $=$ 7,400 mol^{-1} cm^{-1}

G $=$ 11,500 mol^{-1} cm^{-1}

T $=$ 8,700 mol^{-1} cm^{-1}

The molar extinction coefficient for a given sequence can easily be obtained from the following equation (where 0.9 is a factor for hypochromicity):

$$\varepsilon = \{(n\ \varepsilon dA)+(n\ \varepsilon dC)+(n\ \varepsilon dG)+(n\ \varepsilon dT)\} \times 0.9$$

7.4.6 MALDI-TOF Mass Spectrometry

Oligonucleotides were purified and concentrated by use of ZipTip™ C_{18} pipette tips. Oligonucleotides for MALDI-TOF were eluted from the ZipTip™ directly in the MALDI matrix (2 μL). The MALDI matrix was prepared by dissolving 3-hydroxypiccolinic acid in 50:50 MeCN/H_2O (MQ) (50 mg mL^{-1}) and mixing in a 9:1 ratio with ammonium citrate in H_2O(MQ) 50 mg mL^{-1}. MALDI-TOF experiments were performed using a Shimadzu Axima-CFR in linear negative mode. Calibration was achieved by use of oligonucleotide standards (Brüker Daltonics).

7.6 Nanoparticle Preparation

All glassware was soaked in *aqua regia* for ~ 4 h before being rinsed thoroughly with distilled water.

7.6.1 Gold Nanoparticle Synthesis [2]

Sodium tetrachloroaurate (III) (50 mg, 0.14 mmol) was dissolved in distilled water (500 mL). The solution was heated to boiling with continuous stirring, at which point, sodium citrate (1.5 mL, 1 % (w/v)) was added and boiling maintained for 15 min before allowed to cool at room temperature.

λ_{max} = 520 nm; Particle size ~ 15 nm (by SEM)

7.6.2 Silver Nanoparticle Preparation [3]

500 mL of distilled water was heated to 45 °C at which point silver nitrate (90 mg, 0.5 mmol) pre-dissolved in 10 mL of water was added. The solution was rapidly heated to 98 °C and trisodium citrate (10 mL, 1 % (w/v)) was added. The solution was carefully maintained at 98 °C (± 0.5 °C) for 1 h 30 min before being allowed to cool to room temperature. Vigorous stirring was continued throughout.

λ_{max}= 401 nm; Particle size ~ 40 nm (by SEM)

7.7 Preparation of Oligonucleotide-Nanoparticle Conjugates

7.7.1 Disulfide-Modified Oligonucleotide Nanoparticle Conjugates

TA-oligonucleotide (8.6 nmol) was added to Au (3 mL, 17 nM) or Ag (3 mL, 1.0 nM) colloid in an autoclaved glass vial. After 18 h, phosphate buffer (NaH$_2$PO$_4$ /Na$_2$HPO$_4$, 60 mM) was added to 10 mM final concentration. NaCl (2 M, aq.) was then added at intervals, increasing the salt concentration in 0.05 M increments to a final concentration of 0.3 M. The oligonucleotide-nanoparticle conjugates were added to 1.5 mL eppendorf™ tubes and centrifuged at 6000 r.p.m. for 15 min (×1 for

Ag, ×2 for Au) yielding highly coloured oily pellets. The supernatants were discarded to waste and the oily pellets combined and stored at 4 °C.

Au λ_{max} = 525 nm. Ag λ_{max} = 410 nm.

7.7.2 Pre-Treated Thiol-Modified Oligonucleotide Nanoparticle Conjugates

An aliquot of 1 mL of desalted oligonucleotide (10 mM) in Na_2HPO_4 (pH 8.5) was shaken with DTT (0.1 M) for 30 min. DTT was removed by size exclusion chromatography though a Hi-Trap desalt column and 1 mL of the desalted oligonucleotide collected directly onto 3 mL of Au (17 nM) or Ag (1.0 nM) colloid. After 18 h, phosphate (NaH_2PO_4 /Na_2HPO_4) buffer (60 mM) was added to 10mM final concentration. NaCl (2 M, Aq.) was then added at intervals, increasing the salt concentration by 0.05 M (final concentration) increments to a final concentration of 0.3 M. The oligonucleotide-nanoparticle conjugates were added to 1.5 mL eppendorf™ tubes and centrifuged at 6000 r.p.m. for 15 min (×1 for Ag, ×2 for Au) yielding highly coloured oily pellets. The supernatants were discarded to waste and the oily pellets combined and stored at 4 °C.

Au λ_{max} = 527 nm. Ag λ_{max} = 410 nm.

7.7.3 Thiol-Modified Oligonucleotide Nanoparticle Conjugates

Thiol-oligonucleotide (5.70 nmol) was added to Au (3 ml, 17 nM) or Ag (3 mL, 1.0 nM) colloid in an autoclaved glass vial. After 18 h, phosphate (NaH_2PO_4 /Na_2HPO_4) buffer (60 mM) was added to 10 mM final concentration. NaCl (2 M, Aq.) was then added at intervals, increasing the salt concentration by 0.05 M (final concentration) increments to a final concentration of 0.3 M. The oligonucleotide-nanoparticle conjugates were added to 1.5 mL eppendorf™ tubes and centrifuged at 6000 r.p.m. for 15 min (×1 for Ag, ×2 for Au) yielding highly coloured oily pellets. The supernatants were discarded to waste and the oily pellets combined and stored at 4 °C.

Au λ_{max} = 526 nm. Ag λ_{max} = 411 nm.

7.8 Oligonucleotide-Nanoparticle Gel Electrophoresis

An agarose gel (1.5% w/v) in 0.5 × Tris Borate EDTA (TBE) buffer (Sigma) and stained with GelStar Gel Stain (Lonza, Switzerland) 10,000 × dilution was prepared. Gel Pilot 50 bp ladder 7.5 μL (Qiagen, UK) was run. Each sample* (50 μL) was combined with 1/10 volume DNA loading buffer, blue (5 μL) (Qiagen, UK). The electrophoresis was run at 120 V for 1 hour. The gels were photographed using a digital camera and a gel transilluminator imager, BioDoc-It™ Imaging System (UVP, UK).

* Au-NP and AU-DNA @ 1.9×10^{-8} M

  Ag-NP and Ag-DNA @ 1.9×10^{-10} M.

7.9 Oligonucleotide-Nanoparticle Hybridisation

The same protocol was followed whether the target introduced was the full complement, single base mismatch or nonsense sequence.

7.9.1 Oligonucleotide-Au NP Hybridization

Oligonucleotide-Au hybridisation probes 1 and 2 were combined to a final concentration of 1 nM with target oligonucleotide at a final concentration of 0.1 μM in 0.3 M PBS. The temperature was cycled between 15 °C and 75 °C four times, with the absorbance monitored at 520 nm.‡

‡In the case of the head-to-tail hybridization arrangement the temperature was maintained at 15 °C for 1 h at the bottom of each temperature cycle.

7.9.2 Oligonucleotide-Ag Nanoparticle Hybridization

Oligonucleotide-Ag hybridisation probes 1 and 2 were combined to a final concentration of 10 pM with target oligonucleotide at a final concentration of 2 nM

in 0.3 M PBS. The temperature was cycled between 15 °C and 75 °C four times, with the absorbance monitored at 410 nm.

7.10 Oligonucleotide-Nanoparticle Conjugate Stability

7.10.1 DTT Stability Assessment

Oligonucleotide nanoparticle conjugates were diluted to an appropriate concentration to which an addition of DTT (1 M) to a final concentration of 10 mM was made with UV-vis spectra recorded at appropriate intervals *i.e.* one full spectra (200 – 800 nm) *per* minute for thiol-oligonucleotide nanoparticle conjugates and one full spectra *per* 10 min for TA-oligonucleotide nanoparticle conjugates.

7.10.2 Surface Coverage Estimation

Triplicates of FAM-modified oligonucleotide conjugates were treated with DTT (10 mM) and left to completely aggregate (18 h). After which they were centrifuged (6000 r.p.m., 30 min) to ensure that all nanoparticulate sediment was separated from the supernatant. Aliquots of the supernatant were taken, again in triplicate, and the fluorescence measured at 495 nm in a microtitre place. The concentration of the oligonucleotide in the supernatant was taken from a standard calibration curve.

7.10.3 Temperature Stability Assessment

Oligonucleotide nanoparticle conjugates were diluted to an appropriate concentration and heated to 90 °C. The temperature was maintained and spectra recorded at regular intervals from 200 – 800 nm.

7.11 SERRS Analysis of Labelled Oligonucleotides on Klarite™

7.11.1 Wavelength of Excitation Dependence of SERRS Response

TA-Oligo-Cy5 (1 µL, 7.5 µM) was applied to the active area of the Klarite™ surface and was left to incubate in a Camlab micro-array hybridization chamber for 2.5 h. Thereafter, the plate was washed with H_2O (distilled), PBS, IPA and H_2O (distilled) before being allowed to air dry. Spectra were recorded at 633, 785 and 830 nm using a Streamline™ mapping stage, charge coupled device (CCD) and an *InVia* Raman spectrometer through a 20 × LWD objective.

7.11.2 Time Dependence of SERRS Response

TA-Oligo-Cy5 (1 µL, 7.5 µM) was applied to the active area of the Klarite™ surface and was left to incubate in a Camlab micro-array hybridization chamber for varying times – 1 min, 15 min, 1 h and 24 h. Thereafter, the plate was washed with H_2O (distilled), PBS, IPA and H_2O (distilled) before being allowed to air dry. Spectra were recorded at 785 nm using a Streamline™ mapping stage, charge coupled device (CCD) and an *InVia* Raman spectrometer through a 20 × LWD objective.

7.11.3 Concentration Dependence of SERRS Response

TA-Oligo-Cy5 (1 µL) of varying concentrations - 7.5 µM, 0.75 µM, 75 nM and 7.5 nM – was applied to the active area of the Klarite™ surface and was left to incubate in a Camlab micro-array hybridization chamber for 1 h. Thereafter, the plate was washed with H_2O (distilled), PBS, IPA and H_2O (distilled) before being allowed to air dry. Spectra were recorded at 785 nm using a Streamline™ mapping stage, charge coupled device (CCD) and an *InVia* Raman spectrometer through a 20 × LWD objective.

7.11.4 Linker Dependence of SERRS Response

TA-oligo-Cy5, Th-oligo-Cy5, Am-oligo-Cy5 and oligo-Cy5 (1 µL, 7.5 µM) was applied to the active area of the Klarite™ surface and was left to incubate in a Camlab micro-array hybridization chamber for various times – 1 min, 15 min, 1h, 24 h. Thereafter, the plate was washed with H_2O (distilled), PBS, IPA and H_2O (distilled) before being allowed to air dry. Spectra were recorded at 785 nm using a Streamline™ mapping stage, charge coupled device (CCD) and an *InVia* Raman spectrometer through a 20 × LWD objective.

7.12 SERRS Analysis of Hybridisations on Klarite™

7.12.1 Hybridisation on Klarite™ via TA-Oligonucleotide Directly Immobilised

A spot of probe sequence, TA-oligo-Pr1 or Th-oligo-Pr1 (1 µL) was added to the Klarite™ surface and left for the immobilization time. The target sequence, Pr1-Target-Cy5, was added to the surface in hybridization buffer (1 M NaCl, 10 mM Tris-HCl, 1 mM EDTA and 0.01 % SDS) and left before the surface was washed with PBS, IPA and water. The variables for the immobilizations and hybridization are stated in Table 7.2. The chip was left to air dry before the spectra were recorded at 785 nm using a Streamline™ mapping stage, charge coupled device (CCD) and an *InVia* Raman spectrometer through a 20 × LWD objective.

Probe Conc.	% Probe	Diluent	Immobilisation Time	Target Conc.	Hybridisation Time
7.5 μM	100	-	24 h	7.5 μM	1 h
	75	PEG-SH			
	50				
	25				
7.5 μM	100	-	24 h	7.5 μM	22 h
	75	PEG-SH			
	50				
	25				
7.5 μM	100	-	24 h	7.5 μM	22 h
	75	TA			
	50				
	25				
7.5 μM	100	-	1 h	7.5 μM	4 h
0.75 μM	100	-	1 h	7.5 μM	4 h
7.5 μM	100	-	15 min	7.5 μM	1 h
	75	TA			
	50				
	25				
1 μM	100	-	15 min	1 μM	1 h
7.5 μM	100	-	15 min	7.5 μM	1 h
1 mM	100	-	15 min	7.5 μM	22 h
	75	TA-oligo 1 mM			
	50				
	25				

Table 7.2: Experimental conditions for direct hybridizations on Klarite™ substrate. Directly comparable monothiol- linked analogues were also assessed with the same result.

7.12.2 Hybridisation on Klarite™ via 1-{[5-(1,2-dithiolan-3-yl)pentanoyl]oxy}-2,5-pyrrolidinedione, 13

A Klarite™ surface was immersed in a solution of 1-{[5-(1,2-dithiolan-3-yl)pentanoyl]oxy}-2,5-pyrrolidinedione, **13**, (0.1 mg mL^{-1}/ DMF) for 30 min. After this the surface was washed with DMF (5 × 10 mL) and EtOH (5 × 10 mL). A solution of amino-modified oligonucleotide[*] (1 μM) in bicarbonate buffer (100 mM, pH 9.0) was added to the Klarite™ surface and left in a Camlab micro-array

hybridization chamber for 1.5 h. The surface was rinsed with PBS (5 × 10 mL, 0.3 M, pH 7.0).

A hybridization solution was prepared with the target oligonucleotide. BODIPY(650)-Oligo, 1 μM (1 M NaCl, 10 mM Tris-HCl, 1 mM EDTA and 0.01 % SDS). Hybridisation was allowed to proceed at room termperature for 1 h in a Camlab micro-array hybridization chamber. The surface was washed with PBS (5 × 10 mL, 0.3 M, pH7).

* Am-oligo was added for fully complementary experiments and Am-oligo-MM was used for the single based mismatch experiments.

Point SERRS spectra were recorded using a Renishaw *System 2000* Raman spectrometer at 632.8 nm excitation; 2.5 mW laser power (at sample), 1 s acquisition, defocused (76 %) through a 50 ×/0.75 Leica objective.

7.12.3 Hybridisation on Klarite™ of DPN Immobilised TA-Modified Oligonucleotides

A thioctic acid modified oligonucleotide (TA-Ch, 97 μM) in JAD solution (NanoInk) was delivered to a diving board probe (NanoInk) *via* a microfluidic inkwell (NanoInk). The probe was added to a pen support and used with an NScriptor DPN device to write on Klarite™, rastering across the desired area at 0.5 Hz (4 × 4 pixel array) under ambient conditions (temp = 20 °C, % humidity). Once removed from the DPN environmental chamber, the chip was washed thoroughly with water (distilled), IPA and water (distilled) before being briefly treated with a solution of triethylene glycol mono-11-mercaptoundecyl ether (~ 2 min, 10 mg mL^{-1}, DMF). The surface was then washed with DMF and water (distilled).

The target sequence, Tar-Ch, (20 μL, 47.0 μM) and labeled sequence, Cy5-Ch, (10 μL, 96 μM) were mixed together in buffer (70 μL, 670 mM Tris-HCl, 160 mM (NH$_4$)$_2$SO$_4$ and 0.1 % TWEEN-20) for 30 min before being applied to the surface

removed from the DPN (20 µL). The sample was placed in a moistened hybridization chamber for 1 h at room temperature. The plate was then removed from the chamber and washed with water (distilled).

7.13 Chapter 7: References

1.   Still, W. C., Kahn M., Mitra, A., *J. Org. Chem.,* **1978**, 43, 2923-2925.

2.   Frens, G., **1973**, *Nature Phys. Sci.,* 241, 20-22.

3.   Munro, C. H., Smith, W. E., Garner, M., Clarkson, J., White, P. C., **1995**, *Langmuir*, 11, 3712-3720.

Dougan, J. A., Karlsson, C. K., Smith, W. E., Graham, D., *Nucleic Acids Res.*, **2007**¸ 35, 3668-3675.

Enhanced oligonucleotide–nanoparticle conjugate stability using thioctic acid modified oligonucleotides

Jennifer A. Dougan, Camilla Karlsson, W. Ewen Smith and Duncan Graham*

Centre for Molecular Nanometrology, WestCHEM, Department of Pure and Applied Chemistry, University of Strathclyde, 295 Cathedral St., Glasgow, Scotland, G1 1XL, UK

ABSTRACT

Metallic nanoparticles of gold functionalized with oligonucleotides conventionally use a terminal thiol modification and have been used in a wide range of applications. Although readily available, the oligonucleotide–nanoparticle conjugates prepared in this way suffer from a lack of stability when exposed to a variety of small molecules or elevated temperatures. If silver is used in place of gold then this lack of stability is even more pronounced. In this study we report the synthesis of highly stabilized oligonucleotide–nanoparticle conjugates using a simple oligonucleotide modification. A modified solid support was used to generate 3′-thioctic acid modified oligonucleotides by treatment with an *N*-hydroxysuccimidyl ester of thioctic acid. Unusually, both gold and silver nanoparticles have been investigated in this study and show that these disulphide-modified oligonucleotide probes offer significant improvements in nanoparticle stability when treated with dithiothreitol (DTT) compared with monothiol analogues. This is a significant advance in oligonucleotide–nanoparticle conjugate stability and for the first time allows silver nanoparticles to be prepared that are more stable than standard gold-thiol functionalized nanoparticles. This opens up the possibility of using silver nanoparticles functionalized with oligonucleotides as an alternative to gold.

INTRODUCTION

The area of molecular diagnostics is at the forefront of modern bioanalytical research and a sector of growing importance is the interface with materials science on the nanoscale and the conjugation of metallic nanoparticles with biomolecules (1–5). The ability to detect DNA sequences in an highly selective manner for the rapid detection of genetic mutations and disease states is of ever growing interest and central to a number of new approaches to disease management. Specific DNA sequences can be detected by hybridization to complementary oligonucleotide probes conjugated with nanoparticle substrates in a number of different ways (1). Gold nanoparticles have been most widely used in this manner with oligonucleotide adsorption typically achieved through thiol modification, following Brust's observation that alkylthiols stabilize gold colloidal solutions (6–8). Bioanalytical probes based on those observations have been shown to be capable of discriminating between fully complementary and single base mismatched sequences (9). This approach relies on the hybridization-induced reversible aggregation of the nanoparticles resulting in a distinctive red-shifting of the plasmon of the nanoparticles. The nanoparticles have unusually high extinction coefficients in the visible region of the spectrum which makes them easy to visualize colourimetrically, by eye or instrumentation, when a change in the plasmon relating to hybridization takes place. A particular disadvantage of the thiol adsorption strategy to immobilize the oligonucleotide probe on the gold is its lability under certain conditions such as prolonged or cycled elevated temperatures, high NaCl concentrations and treatment with biological buffer additives e.g. dithiothreitol (DTT) or mercaptoethanol (10). Upon thiol desorption, irreversible aggregation occurs and the probe system is rendered inactive. To minimize these undesirable aggregation events, structurally complex multiple thiol linker systems have been investigated but were only ever reported as being used with gold nanoparticles (10,11).

Thioctic acid is an inexpensive, commercially available and structurally simple disulphide species. Herein we report its preliminary employment as a linker molecule for oligonucleotide nanoparticle functionalization of greater stability than standard thiol analogues. Thioctic acid has received great attention in recent years in the area of gold and silver nanoparticle functionalization for a variety of applications (12–18), ranging from the immobilization of tetrathiofulvalenes as cation sensors on gold electrodes (12) and the investigation of metal ion chelation (13), to the probing of nanoparticle surface adsorption by

*To whom correspondence should be addressed. Tel: 0141 548 4701; Fax: 00 44 141 552 0876; Email: duncan.graham@strath.ac.uk

nitroxide-modified thioctic ester spin labelled probes (14). Indeed, it has also been used to immobilize molecules for bioanalytical applications; carbohydrates for non-specific protein interactions (15), antibodies (16) and transition metal complexes for protein capture (17). From an oligonucleotide perspective thioctic acid oligonucleotide templates have been generated by attachment to gold nanoparticles via mid-sequence amino-modified sites (18) and via multiple-step post-synthetic modification (19), however, there was no data presented on the subsequent improved properties of the oligonucleotide–nanoparticle conjugates (18). Until now, the stability of thioctic acid functionalized oligonucleotide–nanoparticle conjugates has not been reported and their ultimate application to oligonucleotide sequence analysis has not been realized.

INSTRUMENTATION

^{1}H NMR and ^{13}C NMR were recorded on a Brüker DPX 400 MHz spectrometer with the appropriate solvent peak as reference. *J* values are quoted in Hertz. Mass spectrometry was carried out as a service by Swansea EPSRC mass spectrometry centre. Preparative reversed phase HPLC was carried out on a Dionex UVD170U detector fitted with a P680 pump through a Phenomenex Clarity column. Desalting HPLC was carried out on a Biocad Sprint HPLC using a HiTrap (5 ml) size exclusion column. Oligonucleotides were synthesized on an MerMade 6 Nucleic Acid Synthesiser, unless otherwise stated. ZipTip$_{C18}$ purification pipette tips were purchased from Millipore Corp. Oligonucleotide synthesis reagents were purchased from Link Technologies.

MATERIALS AND METHODS

1-{[5-(1,2-dithiolan-3-yl)pantanoyl]oxy}-2,5-pyrrolidinedione, 1

N-(3-Dimethylaminopropyl)-*N*′-ethylcarbodiimide hydrochloride (EDC.HCl) (1.840 g, 9.6 mmol, 1.2 eq) was dissolved in DCM (anhydrous, 20 ml), which, 1.7 ml diisopropylethylamine (DIPEA) (anhydrous, 9.6 mmol, 1.2 eq) was added and stirred for 10 min. To the solution *N*-hydroxysuccinimide (1.290 g, 11.2 mmol, 1.4 eq) was added and the reaction mixture stirred in an ice bath. Thioctic acid (1.643 g, 8.0 mmol, 1.0 eq) was dissolved in anhydrous DCM (10 ml) and added to the reaction over 5 min and stirred overnight. The reaction mixture was washed with HCl (5% (v/v), 50 ml × 2) and water (distilled, 50 ml). The organic layer was dried over Na$_2$SO$_4$. Solvents were concentrated *in vacuo* to yield 2.236 g of ester **1**, as a yellow, solid. The residue was dry-loaded on Na$_2$SO$_4$ and the product purified by flash column chromatography giving the product in 83% yield. δ$_H$(400 MHz; DMSO) 1.4–1.7 (6H, *m*, CH$_2$ × 3), 1.84–1.93 (1H, *m*, CH), 2.38–2.46 (1H, m, CH), 2.68 (2H, t, *J* 7.2, CH$_2$), 2.81 (4H, s, succinimidyl CH$_2$ × 2), 3.12–3.21 (2H, m, CH$_2$), 3.56–3.65 (1H, m, CH). δ$_C$(400 MHz; DMSO) 24.415, 25.830, 28.026, 30.425, 34.217, 38.485, 56.011, 169.287, 170.612. *M/Z* 321.0937 ([M+NH$_4$+] C$_{12}$H$_{17}$NO$_4$S$_2$ requires, 321.0937).

Synthesis of 3′-disulphide-modified oligonucleotides

The NHS ester, **1**, was added to the 3′-end of oligonucleotides (5′- FAM CAT TGA AGC TTC (Pr1), 5′- FAM CAT TGA AGC TTC TTT TTT TTT T (Pr2), 5′-FAM CAT TGA AGC TTC AAA AAA AAA A (Pr3) and 5′- ATC CTG AAT GCG AAA AAA AAA A (Pr4)) using 3′-amino-modifier C7 CPG solid supports (1 μmol). The Fmoc protecting group was removed from the 3′-amino group by treatment with 20% (v/v) piperidine/MeCN for 30 min. The NHS ester, **1** (20 mg in 1 ml of MeCN) was applied to the column overnight then washed with MeCN (3 × 1 ml) before being used as the solid support for oligonucleotide synthesis. The oligonucleotide sequence was prepared on a MerMade 6 Nucleic Acid Synthesiser with the FAM introduced as a commercially available terminal phosphoramidite. The oligonucleotides were cleaved from the CPG supports by incubation in 1 ml of conc. NH$_4$OH for 3 days at room temperature. The ammonium hydroxide was removed *in vacuo* (room temperature) and re-dissolved in H$_2$O (1 ml, distilled) and purified by reversed-phase HPLC on a Dionex UVD170U detector fitted with a P680 pump through a Phenomenex Clarity column. Buffer A: TEAA (0.1 M, pH 7), Buffer B: CH$_3$CN; *T* = 0, 95% TEAA: 5% MeCN, with a gradient of 1% min^{-1} B over 15 min and held at 20% B for 5 min at a flow rate of 1 ml/min. After HPLC purification the fractions were collated and concentrated *in vacuo* (room temperature) and redissolved in H$_2$O (1 ml, distilled), they were then freeze-dried and redissolved in H$_2$O (1 ml, distilled) and stored at 4°C. HPLC analysis of 3′-thioctic acid, 5′-FAM-modified oligonucleotides indicated modification had occurred. Confirmation of this was achieved by reference to MALDI mass spectrometry of a known thioctic acid modified sequence, *M/Z* 3977.6 ([MALDI] C$_{15}$H$_{28}$NO$_3$S$_2$-ATGCTCAACTCT requires, 3977.4).

Synthesis of 3′-thiol-modified oligonucleotide probes

Sequences were prepared on a MerMade 6 Nucleic Acid Synthesiser with commercially available 3′-thiol-modified universal support (propyl) and FAM introduced at the 5′-end by a commercially available phosphoramidite. The oligonucleotides were cleaved from the CPG supports by incubation in 1 ml of conc. NH$_4$OH for 3 days at room temperature. The ammonium hydroxide was removed *in vacuo* (room temperature) and re-dissolved in H$_2$O (1 ml, distilled) and purified by reversed-phase HPLC on a Dionex UVD170U detector fitted with a P680 pump through a Phenomenex Clarity column. Buffer A: TEAA (0.1 M, pH 7), Buffer B: CH$_3$CN; *T* = 0, 95% TEAA: 5% MeCN, with a gradient of 1% min^{-1} B over 15 min and held at 20% B for 5 min at a flow rate of 1 ml/min. After HPLC purification, the fractions were collated and concentrated *in vacuo* (room temperature) and redissolved in H$_2$O (1 ml, distilled), they were then freeze-dried and then redissolved in H$_2$O (1 ml, distilled) and stored at 4°C.

Functionalization of nanoparticles with oligonucleotides

Thirteen nanometre gold nanoparticles were prepared *via* citrate reduction of HAuCl₄. Thirty seven nanometre silver nanoparticles were prepared *via* citrate reduction of AgNO₃.

Disulphide-modified oligonucleotides. Desalted oligonucleotide (5.71 nmol) was added to Au (3 ml, 17 nM) or Ag (3 ml, 1.0 nM) colloid in an autoclaved glass vial. After 18 h, phosphate (NaH₂PO₄/Na₂HPO₄) buffer (60 mM) was added to 10 mM final concentration. 2 M NaCl was then added at intervals, increasing the salt concentration by 0.05 M ncrements to a final concentration of 0.3 M. The oligonucleotide–gold conjugates were stored at 4°C.

Thiol-modified oligonucleotides. Desalted oligonucleotide (5.71 nmol) was added to Au (3 ml 17 nM) or Ag (3 ml, 1.0 nM) colloid in an autoclaved glass vial. After 18 h, phosphate (NaH₂PO₄/Na₂HPO₄) buffer (60 mM) was added to 10 mM final concentration. 2 M NaCl was then added at intervals, increasing the salt concentration by 0.05 M (final concentration) increments to a final concentration of 0.3 M. The oligonucleotide–gold conjugates were stored at 4°C.

Pre-treated thiol-modified oligonucleotides. An aliquot of 1 ml of desalted oligonucleotide (10 μM) in Na₂HPO₄ (pH 8.5) was shaken with DTT (0.1 M) for 30 min. DTT was removed by size exclusion chromatography though a Hi-Trap desalt column and 1 ml of the oligonucleotide collected directly onto 3 ml of Au or Ag colloid.

RESULTS

Synthesis of thioctic-modified oligonucleotides

A number of options were considered for the attachment of thioctic acid to oligonucleotides. Ultimately, the synthesis of an active ester of the thioctic acid was determined as being the most versatile approach to functionalizing the termini of oligonucleotides. Primary amine groups are readily added to the 3′- or 5′-termini of oligonucleotides and will react with the active ester of thioctic acid either on a solid support or in solution to provide the disulphide functionalized oligonucleotide. In addition the thioctic acid was shown to be stable to the conditions used for oligonucleotide synthesis and deprotection indicating its compatibility with routine oligonucleotide synthesis. The *N*-hydroxysuccinimidyl ester, **1**, of thioctic acid was prepared in good yield by the esterification of the carboxylic acid with hydroxysuccinimide using EDC (Scheme 1). This active ester was then used in two different approaches.

Modification at the 3′-terminus was achieved by using an amino-modified solid support. Initially, the Fmoc protecting group was removed using standard piperidine deprotection to give the free amine on the CPG. The active ester was added to the CPG in acetonitrile and left overnight (Scheme 2). Following washing with acetonitrile, the thioctic acid solid support was used with standard phosphoramidite chemistry.

Three sequences were generated with the thioctic acid modification at the 3′-terminus and a FAM label at the 5′-terminus: 5′- FAM CAT TGA AGC TTC (Probe 1), 5′- FAM CAT TGA AGC TTC TTT TTT TTT T (Probe 2) and 5′-FAM CAT TGA AGC TTC AAA AAA AAA A (Probe 3), respectively. The sequences chosen were designed to assess whether the presence of spacer bases (adenine or thymine) would affect stability and/or surface coverage of the Au or Ag conjugates. Preparing both disulphide (DX) and thiol (TX) analogues allows for comparison of surface coverage and assessment of stability of the nanoparticle–oligonucleotide conjugates (where X denotes the Probe sequence as indicated above). In addition, thiol conjugates were prepared that omitted the treatment of DTT prior to conjugation (TTX).
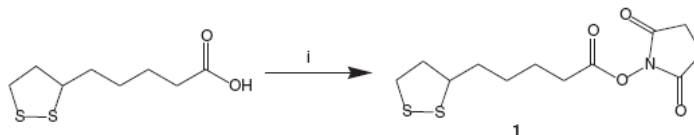
Scheme 1. (i) EDC, NHS, 0°C, DCM, 83%.
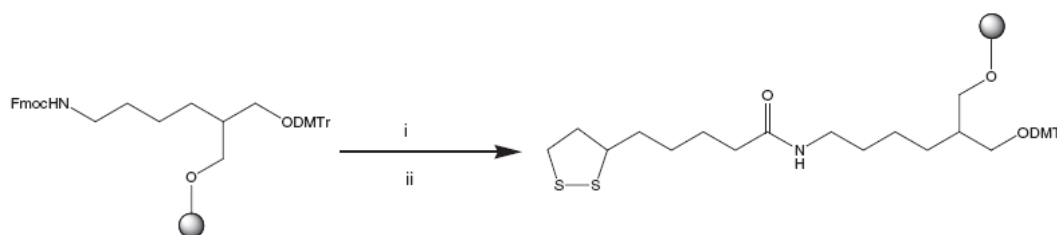
Scheme 2. (i) 20% Piperidine/MeCN (v/v), 30 min and (ii) **1**, MeCN, overnight.
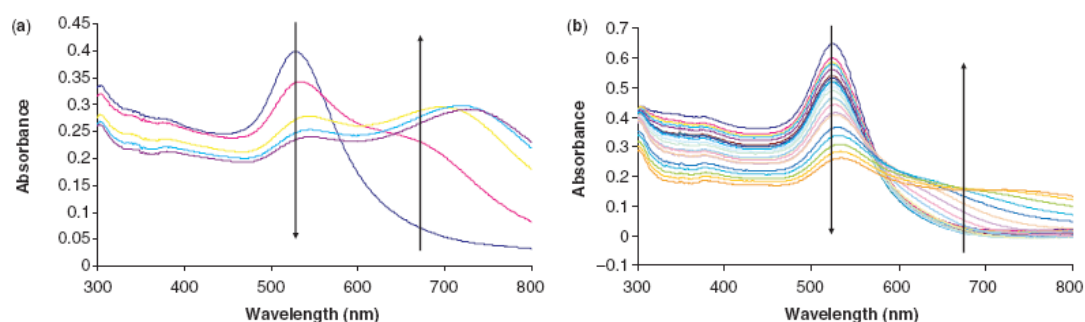
Figure 1. UV–Vis spectra showing degradation upon treatment with 10 mM DTT of (a) T3–Au conjugates at 1 min intervals and (b) D1–Au conjugates at 10 min intervals. Arrows added to highlight the 'movement' of the spectra with time.

This is usually carried out to ensure that the thiol-modified oligonucleotide is in a mono-thiol form, rather than disulphide, when applied to the nanoparticles.

Nanoparticle functionalization and stability studies

Gold nanoparticle stability. Immobilization of the disulphide-modified oligonucleotide sequences, D1, D2 and D3 on citrate-reduced gold nanoparticles (20) was carried out using standard protocols with incremental elevation of NaCl concentration. In earlier investigations, thioctic acid oligonucleotides were added to gold nano-particles in water and after 18 h phosphate buffer added followed by aliquots of NaCl over 5 days to give a final salt concentration of 0.3 M. If the salt concentration is raised too rapidly then the nanoparticles can precipitate if a thiolated oligonucleotide is used. The NaCl concen-tration of the disulphide-modified sequences, while still raised incrementally, was condensed to a considerably shorter timescale of 2 days, whilst maintaining nanopar-ticle stability on citrate-reduced gold and silver nano-particles. The final conditions of the conjugate materials were 10 mM phosphate, pH 7, 0.3 M NaCl (0.3 M PBS). Thiol-modified oligonucleotides (1 ml, 10 µM) were subjected, as standard, to treatment with DTT, 0.1 M, phosphate at pH 8.5 for 30 min before desalting directly onto the nanoparticles, generating probes T1, T2 and T3. A set of oligonucleotide–nanoparticle conjugates were also prepared without this DTT treatment prior to addition of oligonucleotide, probes TT1, TT2 and TT3. Both sets of thiol-modified oligonucleotides were treated to a 'softer' salt-ageing process and were complete in 5 days.

Following literature precedent, the effect of the thioctic acid linker moiety on the stability of oligonucleotide–nanoparticle conjugates, was assessed by treating the conjugates with DTT (10 mM final concentration) at 40°C (10,22). Typical UV–Vis spectra taken periodically for both thiolated (T3 at 1 min intervals) and disulphide-modified oligonucleotide (D1 at 10 min intervals) gold conjugates are shown in Figure 1. Figure 1a shows the rapid degradation of the conjugates typical of thiolated oligonucleotides. Even from these 'busy' plots, the

enhancement in stability of the conjugates can be seen when employing the disulphide modification, as each entry signifies another 10 min interval cf. 1 min for the thiol plot.

Monitoring the disappearance of the plasmon band at 520 nm and the appearance of one between 600 and 700 nm indicates the progressive aggregation event when gold nanoparticles are used. Absorption spectra were taken at periodic intervals. Plotting absorbance at a particular wavelength versus time for each experiment clearly shows the stability of the system. This was carried out for the D1–Au, D2–Au, D3–Au, TT1–Au, TT2–Au, TT3–Au, T1–Au, T2–Au and T3–Au conjugates. Figure 2 shows the absorbance versus time at the 'significant' 675 nm plasmon wavelength for each of these samples. The DX results (Figure 2a) are plotted together to highlight the effect of spacer bases as are TX (Figure 2b). Note that TTX–Au conjugates show the same profile as those in Figure 2b.

The half-life (time taken for absorbance at 675 nm to reach half the value for complete aggregation) was calculated for each conjugate (Table 1) for ease of comparison.

The disparate stabilities of the thiol and disulphide systems are striking when comparing the half-lives of the conjugate systems. All of the Au-monothiol systems have reached the half-way point of complete aggregation in 1 min or less. Compare this with the thioctic acid disulphide system and the enhanced stability is clear with half-lives of 140, 195 and 245 min. It should be noted (as shown in Figure 2a) that DTT-induced aggregation event is not linear, a long period of sustained stability is followed by a sharp increase in absorbance. With the disulphide conjugates (Figures 2a), aggregation begins at 90 min for D1 (no spacers) or 2 h incubation for D2 and D3 (polyT and polyA spacers, respectively) and is considerable by 3 h. This is an excellent enhancement when compared with the monothiol results (Figure 2b) which show complete aggregation in <5 min. The emer-gence of the 675 nm peak is indicative of nanoparticle aggregation, however, by 300 min in the disulphide system there is a loss of signal altogether; this feature can be attributed to the aggregate species growing in size and
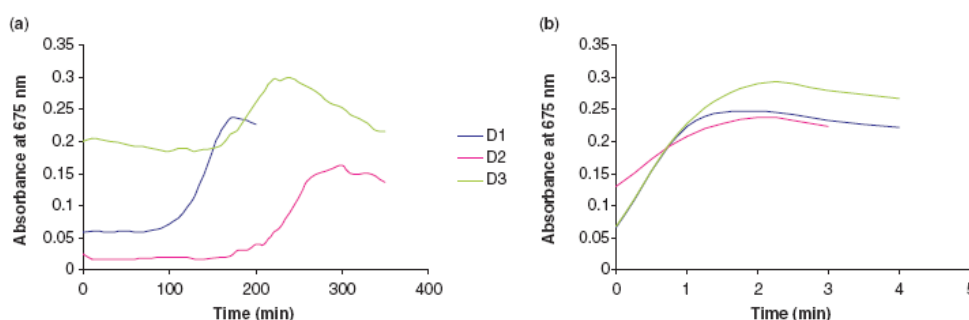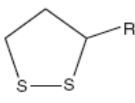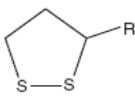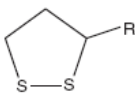
Figure 2. Monitoring the emergence of the plasmon at 675 nm against time gives an indication of the durability of the oligonucleotide conjugates when subject to the same conditions. Figures (a) and (b) show the plots of the DX–Au and TX–Au conjugates at 675 nm, respectively. These results are pronounced when the timescale over which they were acquired are considered.

Table 1. Half-lives for Au–oligonucleotide conjugates

Probe	$t_{1/2}$ (min)
D1–Au	140.0
D2–Au	245.0
D3–Au	195.0
TT1–Au	0.5
TT2–Au	1.0
TT3–Au	0.5
T1–Au	0.75
T2–Au	1.0
T3–Au	1.0

Table 2. Surface coverage data for oligonucleotide–nanoparticle conjugates

| Probe name	Surface coverage ($pmol \cdot cm^{-2}$)	Standard deviation	Probe name	Surface coverage ($pmol \cdot cm^{-2}$)	Standard deviation
D1–Au	7.4	0.3	D1–Ag	21.1	1.3
D2–Au	59.9	6.7	D2–Ag	331	8.3
D3–Au	12.6	0.8	D3–Ag	105.7	0.9
TT1–Au	17.5	0.5	TT1–Ag	144.7	14.0
TT2–Au	12.0	0.3	TT2–Ag	38.1	6.5
TT3–Au	21.1	1.2	TT3–Ag	76.1	2.2
T1–Au	12.6	0.6	T1–Ag	31.2	1.5
T2–Au	21.1	1.2	T2–Ag	64.4	3.0
T3–Au	12.2	0.7	T3–Ag	123.1	15.1

eventually settling out of the colloidal solution leaving a colourless mother liquor.

In similar studies where a steroidal disulphide was used Mirkin and co-workers state that the structurally complex steroidal disulphide system begins aggregation after 2 h (10). This, he argues, is due to a hydrophobic 'screening' effect of the gold surface as well as the formation of a chelate structure. Indeed the dihydrothioctic acid, the reduced dithiol, form of thioctic acid is known to bind through both sulphur atoms (22), and form stable monolayers on gold surfaces, and this now appears to be the driving factor in stability enhancement as similar results have been obtained in this non-steroidal system. It is worthy to note that Mirkin achieved further enhancement of stability when employing a complex trithiol head group (which maintained optical stability for 10 h) (10).

Comparison of thiol and disulphide surface coverage

Whilst there is no doubt that the result of employing disulphide attachment of oligonucleotides to nanoparticles is enhanced stability of the 'conjugate' species cf. mono-thiol, one cannot immediately make the argument that this is due to the disulphide–gold interaction being greater than the thiol–gold one. There are many factors which influence the stability of oligonucleotide conjugates and surface coverage plays an important role.

For this reason the surface coverage of each of the conjugate systems was assessed (Table 2). This was carried out by a method devised by Mirkin *et al.* (23) Triplicates of the FAM-modified oligonucleotide conjugates were treated with DTT (10 mM) and left to completely aggregate. After which they were centrifuged to ensure that all nanoparticulate sediment was separated from the supernatant. Aliquots of the supernatant were taken, again in triplicate, and fluorescence measured. These fluorescence values when correlated with a standard calibration curve gave a concentration for FAM-labelled oligonucleotide in solution. This FAM-oligonucleotide concentration divided by the starting molar concentration of nanoparticle gives a value of oligonucleotides per nanoparticle and dividing by the surface area of the sphere gives normalized surface coverage values which are easily converted to $pmol \cdot cm^{-2}$.
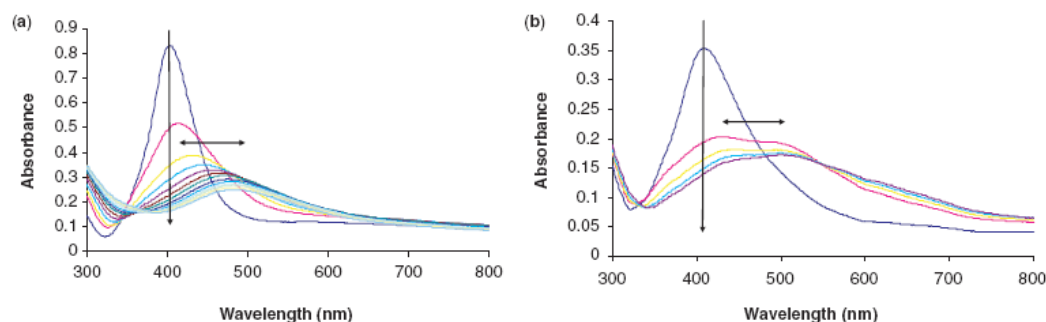
Figure 3. UV–Vis spectra taken for (a) D1–Ag conjugates at 10 min intervals and (b) T3–Ag conjugates at 1 min intervals again clearly shows enhanced stability on the conjugates when thioctic acid tethering to the nanoparticles is employed.

Interestingly, it was found that D1 actually has less oligonucleotide surface coverage than both TT1 and T1 7.4 ± 0.3 pmol·cm^{-2} cf. 17.5 ± 0.5 pmol·cm^{-2} and 12.6 ± 0.6 pmol·cm^{-2}, respectively. This shows that with no spacer bases the surface coverage by thioctic acid modified oligonucleotide–Au nanoparticle conjugates is less than that of the standard thiol conjugates. In turn, the surface coverage of standard thiol conjugates is found to be less than those that are not treated with DTT prior to conjugation (when the oligonucleotides are added directly to the nanoparticles without treating with DTT and purifying with size exclusion chromatography). This indicates that the conjugation process can be improved when using alkyl-thiolated oligonucleotides as there is no trade-off in conjugate stability or surface coverage as a result of omitting reduction by DTT.

With the polyT spacer, D2, there is greater surface coverage of the Au nanoparticle by the oligonucleotide, 59.9 ± 6.7 pmol·cm^{-2} compared with 12.0 ± 0.3 pmol·cm^{-2} and 21.1 ± 1.2 pmol·cm^{-2} for the TT2 and T2 samples. Therefore, it is difficult to argue that the enhanced stability was due to an increased surface coverage since in the previous case, without spacers, there is decreased surface coverage and the enhanced conjugate stability is still observed.

Indeed, moving to the polyA spacer, D3, the surface coverage is in line with the thiol systems at 12.6 ± 0.8 pmol·cm^{-2} cf. 21.1 ± 1.2 pmol·cm^{-2} and 12.2 ± 0.7 pmol·cm^{-2} for TT3 and T3. Again, as this disulphide conjugate has the same surface coverage as the standard monothiol the enhanced stability cannot be attributed to surface coverage effects.

Whilst these surface coverage results are variable depending upon whether spacer bases are present and indeed which spacers are utilized, it can clearly be seen that the enhanced stability of the conjugate systems cannot be determined by surface coverage. If that was the influencing factor we would expect to see discrepancies in the stability between the disulphide examples in line with surface coverage. That is, D1 would be the least stable, D3 would be of intermediate stability and D2 would be the most stable. This is not observed as D3 and

D2 show very similar stability profiles, despite a reasonably large difference in surface coverage.

Silver nanoparticle–oligonucleotide conjugate stability

To demonstrate the versatility of the thioctic acid modified oligonucleotides, silver nanoparticles were used in a similar study. Silver nanoparticles are considerably less stable than gold and as a consequence have been subject to less success in DNA sensing primarily due to the lack of robust surface chemistry. A limited number of studies have been reported but use homo-oligonucleotides or direct hybridization approaches (24–26). Figure 3 shows the degradation of thioctic acid- and thiol-terminated oligonucleotide sequences immobilized on 37 nm citrate-reduced silver nanoparticles. Figure 3 again shows the progressive red-shift of absorbance as a result of aggregation. The thiol system taken at 1 min intervals is clearly less stable than the disulphide which was monitored at 10 min intervals.

It should be noted that with oligonucleotide–Ag conjugates rather than a new peak appearing at red-shifted wavelength due to a change in plasmon on the nanoparticle surface, the plasmon broadens and there is a loss of absorbance at 407 nm. For that reason it is less informative to plot an 'emergence' profile for the silver conjugates and their stability was assessed by reference to the 407 nm peak. For ease of comparison the 'half-lives' of the conjugate systems were calculated, taken as the time required for half the total absorbance change to occur at 407 nm, the results are shown in Table 3.

With both the thiol and disulphide–Ag conjugate systems aggregation commences immediately upon treatment with DTT (10 mM). There is a marked difference in the rate of aggregation, however, with all of the thiol systems having a half-life of less than a minute, compared with the disulphide examples which have 15–30 min half-lives. Whilst it is difficult to compare gold and silver conjugate systems, we can say that the overall 'conjugate' stability displayed by the silver–disulphide systems is more stable (with respect to DTT-induced aggregation) than the 'standard' thiol–gold system (see Figure 2).

Table 3. Half-lives for Ag–oligonucleotide conjugates

Probe	$t_{1/2}$ (min)
D1–Ag	15
D2–Ag	25
D3–Ag	30
TT1–Ag	0.5
TT2–Ag	0.5
TT3–Ag	0.75
T1–Ag	0.5
T2–Ag	0.5
T3–Ag	0.5

Figure 4. The melting profiles of functionalized silver nanoparticles hybridized with a fully complementary sequence (413 nm).

Due consideration must be given to the surface coverage of the conjugates as a high surface coverage could explain enhanced stability. As with the gold conjugates the surface coverage data is variable depending upon whether there are spacer bases and what those spacer bases are. For example, the surface coverage of oligonucleotide on Ag nanoparticles for D1–Ag conjugates was found to be 21.1 ± 1.3 pmol·cm^{-2}, compared with TT1–Ag which have a greater surface coverage, 144.7 ± 14 pmol·cm^{-2}. Even T1–Ag has a greater surface coverage than the disulphide species at 31.2 ± 1.5 pmol·cm^{-2}, albeit less than the standard thiol sample.

Once again, the disparity in surface coverage does not impact the conjugate stability since we have seen that the disulphide systems are by far more stable than both of the thiol conjugates and yet has lower surface coverage. This surface-coverage-independent stability is also observed with the polyT and polyA sequence conjugates (refer to Table 2).

Comparing the results for stability of gold and silver 'conjugates' it can be seen that as anticipated, the disulphide does not stabilize the silver nanoparticles to the same extent as gold, due to weaker thiol–silver interactions. Surface coverage effects can again be dismissed as the stabilizing factor when comparing samples D2–Au (with a surface coverage of 59.9 ± 6.7 pmol·cm^{-2}) and T2–Ag (with a surface coverage of 64.4 ± 3.0 pmol·cm^{-2}) and yet there are vastly differing stabilities. Similarly, D1–Ag (surface coverage of 21.1 ± 1.3 pmol·cm^{-2}) is considerably less stable than D3–Au (surface coverage of 12.6 ± 0.8 pmol·cm^{-2}) despite their surface coverages being quite similar. It is worthy to note, however, that the disulphide on silver remains more stable than the 'standard' monothiol linker systems on gold and this is in spite of similar surface coverages in some cases e.g. D1–Ag (surface coverage of 21.1 ± 1.3 pmol·cm^{-2}) and TT3–Au (surface coverage 21.1 ± 1.2 pmol·cm^{-2}). This is highly significant as it now allows oligonucleotide–silver nanoparticle conjugates to be exploited in a similar manner to gold nanoparticles.

Silver–oligonucleotide conjugate hybridization

As shown in Figure 4, hybridization between the disulphide-immobilized oligonucleotide and a fully complementary sequence induces a characteristically sharp T_m melting profile (monitored at 413 nm). This is a particularly excit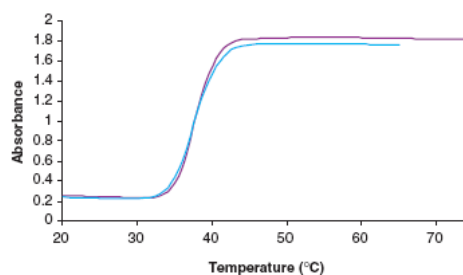ing result since the hybridization was not carried out in the normal 'sandwich' fashion. Instead silver nanoparticles conjugated with a thioctic acid modified sequence, 5′- ATC CTG AAT GCG AAA AAA AAA A MOD 3′ (D4) were hybridized with the 'unconjugated' complement. This has been observed previously with gold nanoparticles, but not silver (27–29). This shows the efficacy of the thioctic acid terminated oligonucleotide–Ag conjugates and their potential for employment in DNA detection. Furthermore, investigations are underway to establish oligonucleotide–Ag nanoparticle conjugates for DNA detection purposes in a manner similar to that of the established gold analogues. This is particularly attractive as silver nanoparticles have a higher molar extinction coefficient than gold.

In conclusion, this data demonstrates the applicability of thioctic acid to simple modification of oligonucleotides, producing enhanced performance with respect to oligonucleotide–nanoparticle 'conjugate' stability. This offers a routine way forward for those requiring more robust surface attachment chemistry for oligonucleotides on gold or silver nanoparticles and in particular provides surface chemistry for silver nanoparticles that allows their use in a wide variety of conditions previously unthinkable.

REFERENCES

1. Rosi,N.L. and Mirkin,C.A. (2005) Nanostructures in biodiagnostics. *Chem.Rev.*, **105**, 1547–1562.
2. Yguerabide,J. and Yguerabide,E.E. (1998) Light-scattering submicroscopic particles as highly fluorescent analogs and their use as tracer labels in clinical and biological applications – I. Theory. *Anal. Biochem.*, **262**, 137–156.
3. Yguerabide,J. and Yguerabide,E.E. (1998) Light-scattering submicroscopicparticles as highly fluorescent analogs and their use as tracer labels in clinical and biological applications – II. Experimental characterization. *Anal. Biochem.*, **262**, 157–176.

4. Niemeyer,C.M. (2001) Nanoparticles, proteins, and nucleic acids: Biotechnology meets materials science. *Angew. Chem. Int. Ed.*, **40**, 4128–4156.

5. Verma,A. and Rotello,V. (2005) Surface recognition of biomacro-molecules using nanoparticle receptors. *Chem. Commun.*, **20**, 303–312.

6. Brust,M. and Kiely,C.J. (2002) Some recent advances in nanostructure preparation from gold and silver particles: a short topical review. *Colloids Surf. A Physicochem. Eng. Asp.*, **202**, 175–186.

7. Brust,M., Walker,M., Bethell,D., Schiffrin,D.J. and Whyman,R. (1994) Synthesis of thiol-derivatized gold nanoparticles in a 2-phase liquid-liquid system. *J. Chem. Soc. Chem. Commun.*, **7**, 801–802.

8. Brust,M., Fink,J., Bethell,D., Schiffrin,D.J. and Kiely,C. (1995) Synthesis and reactions of functionalized gold nanoparticles. *J. Chem. Soc. Chem. Commun.*, **16**, 1655–1656.

9. Storhoff,J.J., Elghanian,R., Mucic,R.C., Mirkin,C.A. and Letsinger,R.L. (1998) One-pot colorimetric differentiation of polynucleotides with singlebase imperfections using gold nanoparticle probes. *J. Am. Chem. Soc.*, **120**, 1959–1964.

10. Li,Z., Jin,R., Mirkin,C.A. and Letsinger,R.L. (2002) Multiple thiol-anchor capped DNA-gold nanoparticle conjugates. *Nucleic Acids Res.*, **30**, 1558–1562.

11. Letsinger,R.L., Elghanian,R., Viswanadham,G. and Mirkin,C.A. (2000) Use of a steroid cyclic disulphide anchor in constructing gold nanoparticle-oligonucleotide conjugates. *Bioconjugate Chem.*, **11**, 289–291.

12. Liu,H., Liu,S. and Echegoyen,L. (1999) Remarkably stable self-assembled monolayers of new crown-ether annelated tetrathia-fulvalene derivatives and their cation recognition properties. *Chem. Commun.*, **16**, 1493–1494.

13. Berchmans,S., Thomas,P.J. and Rao,C.N.R. (2002) Novel effects of metal ion chelation on the properties of lipoic acid-capped Ag and An nanoparticles. *J. Phys. Chem. B*, **106**, 4647–4651.

14. Checkik,V., Wellsted,H.J., Korte,A., Gilbert,B.C., Caldararu,H., Ionita,P. and Caragheorgheopol,A. (2004) Spin-labelled Au nanoparticles. *FaradayDiscuss.*, **125**, 279–291.

15. Karamanska,R., Mukhopadhyay,B., Russell,D.A. and Field,R.A. (2005) Thioctic acid amides: convenient tethers for achieving low nonspecific protein binding to carbohydrates presented on gold surfaces. *Chem. Commun.*, **26**, 3334–3336.

16. Chang,J.-Y., Wu,H., Chen,H., Ling,Y.-C. and Tan,W. (2005) Oriented assembly of Au nanorods using biorecognition system. *Chem. Commun.*, **8**, 1092–1094.

17. Abad,J.M., Mertens,S.F.M., Pita,M., Fernández,V.M. and Schiffrin,D.J. (2004) Functionalization of thioctic acid-capped gold

18. Stevenson,K.A., Muralidharan,G., Maya,L., Wells,J.C., Barhen,J. and Thundat,T. (2002) Covalent attachment of gold nanoparticles to DNA templates. *J. Nanosci. Nanotech.*, **2**, 397–404.

19. Harrison,J.G. and Balasubramanian,S. (1997) A convenient syn-thetic route to oligonucleotide conjugates. 7, 1041–1046.

20. Grabar,K.C., Freeman,R.G., Hommer,M.B. and Natan,M.J. (1995) Preparation and characterization of au colloid monolayers. *Anal. Chem.*, **67**, 735–743.

21. Roux,S., Garcia,B., Bridot,J.-L., Salomé,M., Marquette,C., Lemelle,L., Gillet,P., Blum,L., Perriat,P. *et al.* (2005) Synthesis, characterization of dihydrolipoic acid capped gold nanoparticles, and functionalization by the electroluminescent luminol. *Langmuir*, **21**, 2526–2536.

22. Garcia,B., Salomé,M., Lemelle,L., Bridot,J.-L., Gillet,P., Perriat,P., Roux,S. and Tillement,O. (2005) Sulfur K-edge XANES study of dihydrolipoic acid capped gold nanoparticles: dihydrolipoc acid is bound by both sulphur ends. *Chem. Commun.*, **3**, 369–371.

23. Demers,L.M., Mirkin,C.A., Mucic,R.C., Reynolds III,R.A., Letsinger,R.L., Elghanian,R. and Viswanadham,G. (2000) A fluorescence-based method for determining the surface coverage and hybridization efficiency of thiol-capped oligonucleotides bound to gold thin films and nanoparticles. *Anal. Chem.*, **72**, 5535–5541.

24. Cai,H., Xu,Y., Zhu,N., He,P. and Fang,Y. (2002) An electrochemical DNA hybridization detection assay based on a silver nanoparticle label. *Analyst*, **127**, 803–808.

25. Tokareva,I. and Hutter,E. (2004) Hybridization of oligonucleotide-modified silver and gold nanoparticles in aqueous dispersions and on gold films. *J. Am. Chem. Soc.*, **126**, 15784–15789.

26. Vidal,B.C.Jr., Deivaraj,T.C., Yang,J., Too,H.-P., Chow,G.-M., Gan,L.M. and Lee,J.Y. (2005) Stability and hybridization-driven aggregation of silver nanoparticle-oligonucleotide conjugates. *New J. Chem.*, **29**, 812–816.

27. Sato,K., Hosokawa,K. and Maeda,M. (2003) Rapid aggregation of gold nanoparticles induced by non-cross-linking DNA hybridisation. *J. Am. Chem. Soc.*, **125**, 8102–8103.

28. Sato,K., Hosokawa,K. and Maeda,M. (2005) Non-cross-linking gold nanoparticle aggregation as a detection method for single-base substitutions. *Nucleic Acids Res.*, **33**, e4.

29. Sato,K., Hosokawa,K. and Maeda,M. (2007) Colorimetric biosensors based on DNA-nanoparticle conjugates. *Anal. Sci.*, **23**, 17–20.

Stokes, R. J., MacAskill, A., Dougan, J. A., Hargreaves, P. G., Stanford, H. M., Smith, W. E., Faulds, K., Graham, D., *Chem. Commun.*, **2007**¸ 2811-2813.

Highly sensitive detection of dye-labelled DNA using nanostructured gold surfaces†

Robert J. Stokes,[a] Alexandra Macaskill,[a] Jennifer A. Dougan,[a] Philip G. Hargreaves,[b] Helen M. Stanford,[b] W. Ewen Smith,[a] Karen Faulds[a] and Duncan Graham*[a]

Careful control of surface chemistry results in strong surface enhanced resonance Raman scattering from dye-labelled oligonucleotides assembled on nanostructured gold surfaces, releasing their potential as reliable enhancing surfaces.

Surface enhanced resonance Raman scattering (SERRS) has been demonstrated to be a highly sensitive technique for the detection of dye-labelled oligonucleotides.[1–3] Very high sensitivity has been obtained using metal nanoparticles. This has ultimately resulted in reports of the identification of single dye molecules in "hot spots" of high electric field gradients between nanoparticles.[4] However, in a typical colloidal analysis the process of aggregation is dynamic and it is necessary to control this in order to achieve sensitive, reproducible and linear concentration dependent results.[5] Although nanoparticles of a number of metals have been used for SERRS, in practice, silver and gold are often the most suitable materials.[6] Successful exploitation of the resonance element of the technique is important in obtaining the most sensitive measurements. This relies on good spectral overlap between the resonance excitation profile of the chromophore and the local surface plasmon properties of dynamic aggregates in solution at the excitation wavelength (λ_{ex}).[7]

The use of nanostructured surfaces as SERRS substrates is of great interest as they allow simple direct analysis and could allow SERRS to be applied where careful control of aggregation is not possible. For example, Vo-Dinh and co-workers have utilised a 9 nm thick silver island film to detect the breast cancer gene *BRCA1* by labelling with the dye Rhodamine B using a λ_{ex} of 632.8 nm.[8] This strategy involved the immobilisation of the complementary probe *via* mixed self-assembled monolayers (SAMs) of 1-mercaptoundecanol and 1-mercaptodecanoic acid. Surface attachment was achieved by the formation on the surface of a succinimidyl ester and subsequent reaction with amino modified DNA. The alkyl alcohols were needed in this SAM to act as spacers for the oligonucleotides allowing hybridisation to occur. In this case, silver was used rather than gold due to the higher levels of SERRS enhancement expected using 632.8 nm excitation.

However, surface modification chemistry is more developed for gold and the possibility of surface degradation is reduced.

A potential drawback of randomly dispersed nanoparticle-based arrays of this type is the inconsistency of the enhancement factor across the film, resulting in variability in signal intensity. Recently, nanostructured gold surfaces (Klarite™) have been developed that utilise a standing wave generated in small surface wells (~ 1 μm in diameter) to enhance the effective magnitude of the incident and scattered photons leading to a 10^6-fold increase in signal over the bulk Raman intensity.[9] Studies using SAMs of benzenethiol have shown that the enhancement is very reproducible across the whole area of the substrate.[10] Typically the lowest observable concentrations from non-chromophoric species are around 10^{-6} to 10^{-7} M. To investigate the importance of the resonance aspect of SERRS and the attractiveness of these surfaces for bioanalysis, a series of experiments using dye-labelled oligonucleotides were conducted. These were directly analogous to nanoparticle based approaches to allow comparisons to be made.

Examining oligonucleotides labelled with dyes chosen for their spectral overlap with both the properties of the surface and the λ_{ex} resulted in a dramatic, resonance enhanced, increase in signal sensitivity of at least two orders of magnitude. When the dye-labelled oligonucleotide sequences were deposited directly onto the gold surface, clear unambiguous SERRS spectra from TAMRA, ROX, and BODIPY 650 could be recorded over and above any signal from the bases themselves. Matching the dye label ROX (λ_{max} 585 nm) with 632.8 nm λ_{ex} (Renishaw system 1000) gave the most sensitive results for this sequence. Examples of the spectra
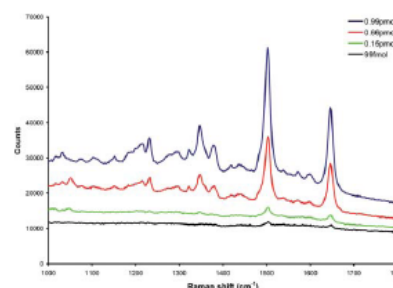

Fig. 1 Spectra of 500 nL oligonucleotide samples labelled with the dye ROX deposited onto Klarite™ substrate. (Renishaw 1000, 632.8 nm λ_{ex}, 2.5 mW, 76% defocus, 1×10 s accumulation). No background correction has been applied.

[a]Centre for Molecular Nanometrology, Thomas Graham Building, 295 Cathedral Street, Glasgow, UK G1 1XL.
E-mail: Duncan.Graham@strath.ac.uk; Fax: +44(0)141 552 0876;
Tel: +44(0)141 548 4701
[b]Mesophotonics Ltd., 2 Venture Road, Chilworth Science Park, Southampton, UK SO16 7NP. Fax: +44(0)23 8076 3757;
Tel: +44(0)23 8076 3752
† Electronic supplementary information (ESI) available: Synthesis, SAM formation and hybridisation. See DOI: 10.1039/b705873j
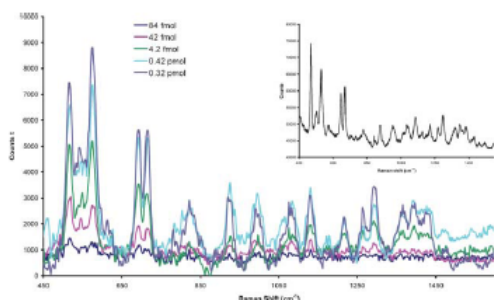
Fig. 2 Spectra of 500 nL oligonucleotide samples labelled with the dye Cy7 deposited onto Klarite™ surface modified with drying wells (Mesophotonics SE1000, 785 nm λ_{ex}, 1 × 10 s accumulation). Background correction has been applied. *Inset*: High resolution spectra of the most concentrated sample (Renishaw 1000, 785 nm λ_{ex}, 1 × 10 s accumulation). Background correction has been applied.

obtained are shown in Fig. 1. The most dilute solution that was detected and identified in this case was ~1 × 10^{-9} M.

The observed signal was spectrally identical to that observed when the same dye-labelled oligonucleotide was analysed using gold nanoparticles. When designing a SERRS analysis careful selection of the chromophore is necessary to achieve the most sensitive results. A large study recently carried out, using citrate reduced gold nanoparticles and a full range of dyes, has indicated that the best resonance enhancement is obtained when the λ_{max} of the dye is within 50 nm of the laser λ_{ex}.[6] Despite this, some benefit would be expected from using a chromophore with an absorbance maximum even further from the laser wavelength as the resonance excitation profile would be expected to decay in a Lorentzian profile. Theoretical and experimental studies of gold nanoparticle-arrays for SERRS have shown that the plasmon resonant frequency should have a maximum in the region between the excitation source and the absolute position of the enhanced Raman line.[11] Spectra could not be obtained when samples of a concentration lower than 10^{-7} M were tested using 514.5 and 406 nm λ_{ex}. Contributions from interband transitions of gold result in higher background and a much lower signal/noise ratio when excitation wavelengths in the green and blue are used (532, 514.5 and 406 nm). Gold surfaces, such as the ones used in this study, have broad plasmon resonances tuned in the red and near infrared wavelength regions (632.8 and 785 nm). The gold substrate plasmon resonance is dependent on the geometry and form factor of the surface texture and can be easily tuned by variation in the shape and depth of the wells.

Matching Cy7 (λ_{max} 748 nm) labelled oligonucleotides to a 785 nm laser (Mesophotonics SE1000 Raman spectrometer)

yielded a further increase in sensitivity, when microwell structures were applied to the surface (Fig. 2). This modification may have the effect of concentrating the samples as it dries, allowing solutions as dilute as 1 × 10^{-11} M to be identified. At the concentrations tested, signals attributed to the DNA bases were not observed.[12]

The sample to sample variation is composed of the variation across the active area of the Klarite (*i.e.* the substrate) and the variability of the sample itself. With a SAM system (*e.g.* benzenethiol), the variability expressed as relative standard deviation (RSD) across the active area is typically 2–3%. Experimentally, the sample to sample RSD could be lowered at a cost of sensitivity by creating a broader laser spot using a beam expander. A trade-off between sensitivity (small spot) and signal consistency (larger spot) has to be established for each sample concentration and in this study it was found that exciting surface plasmons across a number of surface features (1 µm inverted pyramids) achieved the most consistent results.

At higher concentrations, in a drop coat test, the sample appears to dry in a visible 'coffee ring' pattern (when examined under a microscope). This implies that the dye containing component dries unevenly across the surface. This effect explains the higher RSD values shown for drop coat tests shown in Table 1. The majority of the signal probably arises from the first layer of molecules closest to the surface and any subsequent layers would contribute weakly to the SERRS signals and increase background fluorescence. Therefore, the deposition technique is critical in achieving reproducible results when using surfaces of this kind. As the active area has a gold coated surface, thiol based linker chemistries, similar to those used in surface plasmon resonance (SPR) technologies,[13] could be potentially combined with SERRS to improve reproducibility and to add functionality. Successful modification of the surface opens up the possibility of utilising the impressive sensitivity and multiplexing ability previously demonstrated using SERRS.[14]

Modification of the surface using a thioctic acid linker molecule enabled facile immobilisation of DNA capture strands, resulting in dramatically improved signal reproducibility. When dye-labelled oligonucleotides (BODIPY 650) were immobilised by hybridisation onto the surface using a SAM technique, no coloration was observed, yet the SERRS signal was strong and easily identifiable.

Capture experiments were performed by preparing a SAM based on a thioctic acid derived *N*-hydroxysuccinimide-ester linker according to the scheme shown in Fig. 3.

Hybridisation (at room temperature) of a dye-labelled target resulted in a strong SERRS response that allowed identification of the target dye in all tests. Density functional theory (DFT) studies of this linker using the DMol[3] module of Materials Studio (Accelrys, UK) indicate the linker occupies an area on the surface of around 50 nm^2 molecule^{-1}, due to a significant tilt angle. This is

Table 1 Overall sample to sample relative standard deviations observed during this study from samples of low concentration (>1 × 10^{-8} M)^{a,b}

Sample and instrument	Deposition technique	RSD (%)
BODIPY 650 *Renishaw 1000*(50 µm spot size)	Drop coat	28.2
ROX *Renishaw 1000*(50 µm spot size)	Drop coat	34.9
Cy7 *Mesophotonics SE1000*(140 µm spot size)	Drop coat into microwell	26.7
BODIPY 650 *Renishaw 1000*(50 µm spot size)	Hybridisation onto prepared SAM	9.3

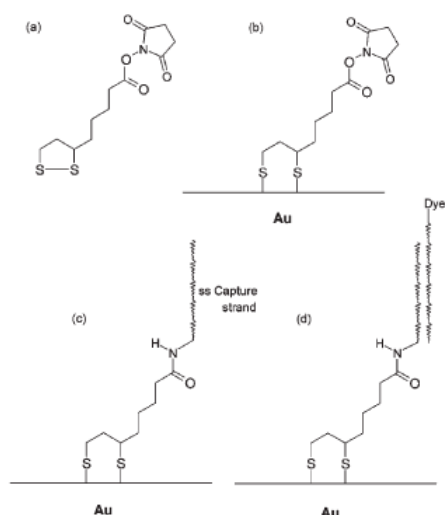^{a} SAMs of benzenethiol report RSDs of 2–3%. ^{b} $n > 10$ in all cases.

Fig. 3 Modification of Klarite surface with a oligonucleotide capture strand *via* a thioctic acid derived *N*-hydroxysuccinimide-ester linker; (a) 1-{[5-(1,2-dithiolan-3-yl)pentanoyl]oxy}-2,5-pyrrolidinedione, (b) linker bonded to the surface, (c) attachment of capture single-stranded DNA (ssDNA) strand, (d) hybridisation of dye-labelled complement.
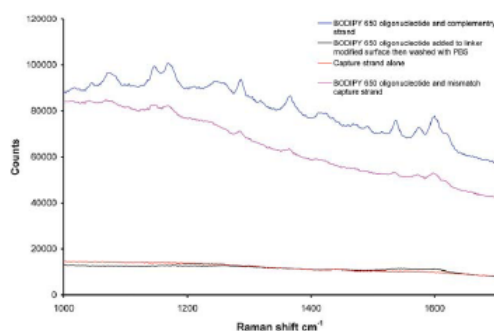

Fig. 4 Spectra obtained from dye-labelled DNA capture experiments (Renishaw 1000, 632.8 nm, 2.5 mW, 76% defocus, 1 × 1 s). No baseline correction applied.

greater than would be expected from a typically ordered alkyl thiol SAM and would explain why the oligonucleotides are not packed closely together to the extent where hybridisation is hindered significantly and a mixed SAM is necessary.[15]

Examples of the spectra obtained from capture experiments are show in Fig. 4. Target signal was not observed when the

dye-labelled strand was added directly to the surface and then washed with phosphate buffered saline. As anticipated, a weaker signal can be observed from a SAM prepared with a mismatch strand as some hybridisation will still occur. This could be minimised by the careful selection of experimental temperature to be above the melt temperature (T_m) of the mismatch but below the T_m of the complement. The increased thermal stability of the thioctic acid based linker (with respect to equivalent monothiols) would facilitate this approach.

This series of experiments demonstrate that careful selection and use of a chromophore in experimental design can result in a significant increase in Raman signal from gold nanostructured surfaces in accordance with the resonance selection rules. When analysing samples of a low concentration the sample to sample reproducibility can be increased to an acceptable level by modification of the surface with a prepared SAM comprising oligonucleotide strands. Subsequent hybridisation of a dye-labelled complementary strand results in easily identifiable signals from the dye labels. The linker reported here potentially allows the easy attachment of other amine containing biomolecules to gold surfaces. Combining the effects described above will allow the design of surface based arrays that incorporate the versatility of gold surface chemistry with the sensitivity and multiplexing potential of SERRS.

Notes and references

1 K. Faulds, W. E. Smith and D. Graham, *Analyst*, 2005, **130**, 1125–1131.
2 T. Vo-Dinh, K. Houck and D. L. Stokes, *Anal. Chem.*, 1994, **66**(20), 3379–3383.
3 Y. C. Cao, R. Jin and C. A. Mirkin, *Science*, 2002, **297**(5586), 1536–1540.
4 (*a*) S. Nie and S. Emory, *Science*, 1997, **275**, 1102–1106; (*b*) K. Kneipp, Y. Wang, H. Kneipp, L. T. Perelman, I. Itzkan, R. R. Dasari and M. S. Feld, *Phys. Rev. Lett.*, 1997, **78**(9), 1667–1670.
5 K. Faulds, R. P. Barbagallo, J. T. Keer, W. E. Smith and D. Graham, *Analyst*, 2004, **129**, 567–568.
6 R. J. Stokes, A. Macaskill, P. J. Lundahl, K. Faulds, W. E. Smith and D. Graham, *Small*, 2007, DOI: 10.1002/smll.200600662.
7 C. Mclaughlin, D. Graham and W. E. Smith, *J. Phys. Chem. B*, 2002, **106**(21), 5408–5412.
8 L. R. Allain and T. Vo-Dinh, *Anal. Chim. Acta*, 2002, **469**, 149–154.
9 N. M. B. Perney, J. J. Baumberg, M. E. Zoorob, M. D. B. Charlton, S. Mahnkopf and C. M. Netti, *Opt. Express*, 2006, **14**(2), 847–857.
10 C. M. Netti and H. M. Stanford, *Spectroscopy (supplement)*, June 2006, 8, Advanstar Communications, http://www.spectroscopymag.com/spectroscopy/content/contentDetail.jsp?id=368979.
11 N. Felidj, J. Aubard, G. Levi, J. R. Krenn, A. Hohenau, G. Schider, A. Leitner and F. R. Aussenegg, *Appl. Phys. Lett.*, 2003, **82**(18), 3095–3097.
12 S. E. J. Bell and N. M. S. Sirimuthu, *J. Am. Chem. Soc.*, 2006, **128**, 15580–15581.
13 K. A. Peterlinz, R. M. Georgiadis, T. M. Herne and M. J. Tarlov, *J. Am. Chem. Soc.*, 1997, **119**, 3401–3402.
14 K. Faulds, F. McKenzie and D. Graham, *Angew. Chem., Int. Ed*, 2007, **46**, 1829–1831.
15 T. M. Herne and M. J. Tarlov, *J. Am. Chem. Soc.*, 1997, **119**, 8916–8920.

176

Stokes, R. J., Dougan, J. A., Graham, D., *Chem. Commun.*, **2008**, 5734-5736.

Dip-pen nanolithography and SERRS as synergic techniques†

Robert J. Stokes, Jennifer A. Dougan and Duncan Graham*

We demonstrate the powerful combination of dip-pen nanolithography (DPN) performed on non-flat plasmonic gold surfaces and subsequent detection by surface enhanced resonance Raman scattering (SERRS).

Dip-pen nanolithography (DPN),[1] is a versatile technique in which a scanning probe microscope tip can be used to deliver a material ("ink") to a surface *via* a water meniscus. DPN allows controlled deposition of a wide range of materials such as (but not limited to) alkyl thiols,[1] silazanes,[2] Au(III) complexes[3] and nanoparticles.[4,5] The size of the feature being written is related to a complex interaction between the tip, ink, meniscus and surface.[6] Development of the technique has allowed Mirkin and co-workers to report direct[7] and indirect[8] writing of biological materials onto suitable surfaces to form highly structured arrays. Because the feature sizes produced by DPN are so small (potentially down to 15 nm), detection of biological interactions is often achieved by atomic force microscopy (AFM) or, as is most common in the case of DPN-directed DNA arrays, fluorescence.[9] However, surface enhanced resonance Raman scattering (SERRS) potentially offers a number of significant advantages over conventional fluorescence detection.

SERRS is a highly sensitive spectroscopic technique that has been used in an increasing number of applications in biodiagnostics including novel gene probes,[10,11] and DNA detection.[12] The technique is flexible and with controlled chemistry can be performed using longer, biologically compatible, wavelengths of excitation (λ_{ex}) either in solution,[13] or on nanostructured plasmonic gold surfaces.[14] When considering the simultaneous detection of multiple targets, it is significant to note that a large proportion of the overall enhancement derives from the additional 'resonance' with the molecular chromophore. This is a major advantage of the technique, when applied in a real assay, as a number of characteristic bands within each dye class are enhanced to a greater extent than other materials in the matrix.[15,16] The characteristic narrow SERRS lines (~ 0.5 nm width) have the potential to form the basis of a highly effective multiplexed analysis from a single excitation source. A further advantage of SERRS is that the excitation wavelength can be selected anywhere in the optical range and wavelength selectivity can be observed using combinations of reporter dyes.[17] A

number of effective SE(R)RS substrates have been reported in recent years, including those fabricated by nanosphere lithography,[18] silver metal island films[19] and nanostructured gold surfaces.[20,21] Herein, we demonstrate for the first time the powerful combination of DPN on non-flat surfaces and SERRS, highlighting the potential to generate high density biosensor arrays.

The method presented is synergic in that the high specificity, sensitivity and speed of the SERRS technique is complemented by the high spatial precision and scalability of DPN onto high density three-dimensional micro- and nanostructured plasmonic gold surfaces. The fact that the SERRS spectrum from each reporter dye is so distinct and retains a quantitative response when overlaid means that active features can potentially be placed in high spatial (sub-diffraction limit) proximity by DPN, thus maximising the array density. Using simple, cheap optics this is an ability of SERRS that is very difficult to replicate using molecular fluorescence or quantum dots.

Oligonucleotides modified with 5′-dye labels, previously reported to be strongly SERRS active,[13,14] were directly patterned onto nanostructured gold surfaces (Fig. 1A) by DPN. 3′-Thiol or thiotic acid and 5′-dye modified oligonucleotides were delivered to the surface using diving board type probes (max $k = 0.041$ N m^{-1}) a carrier fluid and a microfluidic inkwell system.† The carrier fluid method is important as it allows a wide variety of biological materials to be patterned that would otherwise be difficult to deposit using DPN tips. High density writing was achieved by rastering at 0.5 Hz in an area 0.6×0.6 µm centred in single microwell of width 1.3 µm (Fig. 1B). The SERRS spectra and map obtained are shown below in Fig. 1C–D. The spectra of each dye label are identical matches to those reported previously using silver and gold nanoparticles as the enhancing surface.[13] Typically between 600–2000 counts per second were obtained at 632.8 using short accumulation times (1 s) and low laser power (~ 0.6 µW at 0.75 NA) resulting in an "active" to "blank" pixel ratio of about 70 : 1. The intensity of the response depends, to some extent, on the degree of interaction between the molecular chromophore and the surface plasmon modes resonant in the red and near infrared (NIR).[14,21] Similar signal strengths were obtained when arrays were patterned by means of fast piezo drops to the centre of each well with minimum dwell times at the surface. The limits of detection in each case were found to be similar to or better than those reported previously where 1×10^{-11} M solutions of Cy7 labelled target strands could be recorded using 785 nm λ_{ex}.[14] This optimal enhancement in the near infrared is understandable as this type of surface has a broad plasmon resonance in this region.[21] Parallel multi-pen alignment and

Centre for Molecular Nanometrology, WestCHEM,, Department of Pure and Applied Chemistry, University of Strathclyde, 295 Cathedral Street, Glasgow, UK. E-mail: Duncan.Graham@strath.ac.uk; Tel: +44(0)141 548 4701
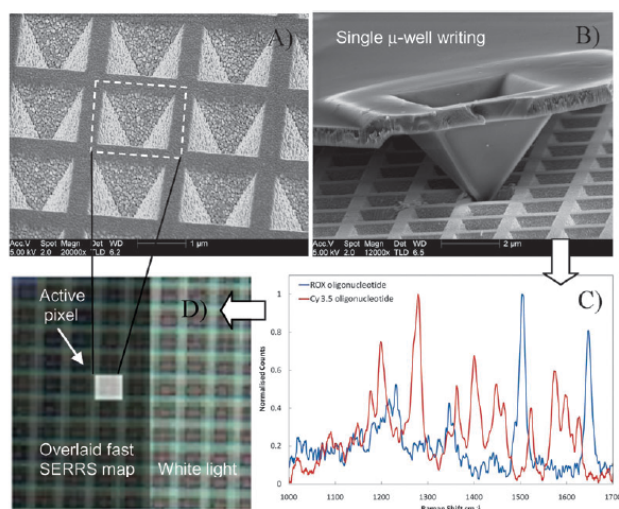
Fig. 1 SEM micrographs of (A) Klarite™ nanostructured gold surface (25 M μwells cm^{-2}), (B) AFM tip interaction with surface. (C) SERRS spectra obtained from ROX and Cy3.5™ dye-labelled oligonucleotide sequences written (1×1 μm area) into single well [1×1 s, λ_{ex} = 632.8 nm, 0.6 μW]. (D) SERRS map of single Cy3.5 oligonucleotide pixel (false colour map over white light image), showing signal (at 1280 cm^{-1}) from only one pixel (1.3 μm per map pixel).

writing was achieved by contact mode AFM imaging at tips at either end of the pen array, thus alignment could be performed by rotation relative to the very regular surface features.

The DPN technique has been shown to be massively scalable with the recent report of 55 000 pens arranged in a 2D-array.[22,23] Therefore, any complementary spectroscopic technique would need to be performed both with sufficient sensitivity and speed in order to read the large number of small array pixels within a reasonable timescale. Spectra in this case were obtained using a Streamline™ mapping stage, charge coupled device (CCD) and an *InVia* Raman microscope system (Renishaw, UK). The line mapping system operates by line focussing the laser and rastering vertically across the sample, simultaneously collecting multiple spectra across the CCD area. Using a 42 CCD line setup it was possible to acquire spectra at ~16 Hz from the surface of the nanostructured gold surface with sufficient sensitivity to identify the target dye. The laser power in SE(R)RS point mapping or confocal scanning is often attenuated to avoid sample damage to the monolayer or photo-degradation of the reporter dye. However, DPN and readout by fast line mapping allows the laser to be deployed more efficiently, illuminating a wider area (30–60 times as many active pixels) with a correspondingly lower surface power density.

The ability of DPN to pattern features that complement the spectroscopic collection geometry allowed the lateral resolution and detection speed to be optimized. DPN patterning of broad lines, 3 μwells wide (Fig. 2A), enabled the rapid identification of adjacent targets by scanning orthogonally in a SERRS "bar-code". In this example scan rates of 16–32 Hz (lines per second) were obtained, although the high signal to background ratio means that significantly faster scanning rates could be achieved, potentially up to 350 Hz. An example

SERRS false-colour image using Cy3.5 and Cy5 labelled oligonucleotides is shown in Fig. 2B. Patterning long, narrow lines also removes the need for complex sample alignment with the reader in a manner broadly analogous to a supermarket checkout scanner, further increasing the throughput of the combined technique.
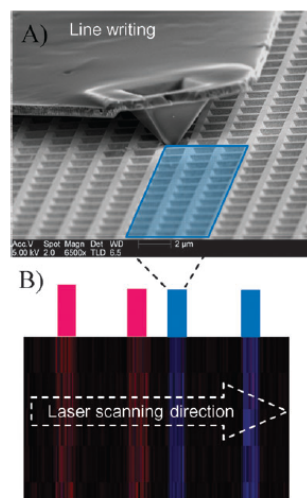
Fig. 2 (A) Representation of DPN line writing. (B) Dual overlaid Streamline™ mapping images recorded orthogonally to broad DPN lines drawn onto Klarite. Image consists of overlaid false colour maps with the intensity based on 1370 cm^{-1} (Cy3.5™, **Purple**) and 1600 cm^{-1} (Cy5™, **Blue**) integrated peak area to base line. Recorded and processed at 16 Hz (spectra per second).

179
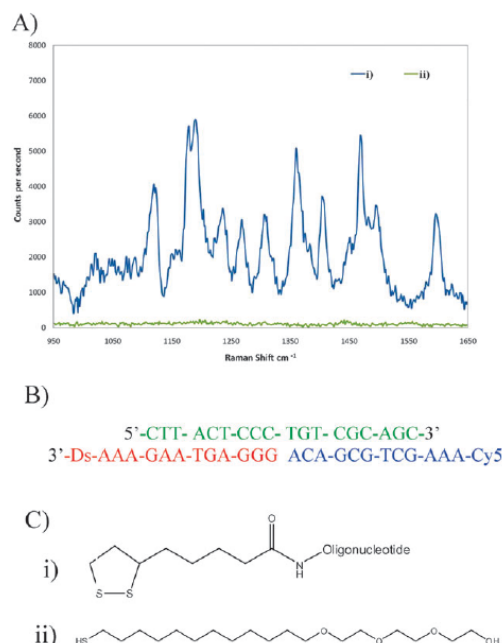
Fig. 3 (A) (i) SERRS spectra (4 × 4 microwells) from active area after hybridisation of disease target probe and dye labelled complement oligonucleotide (Cy5™). (ii) Spectra recorded from adjacent blank region. [1 × 1 s, λ_{ex} = 632.8 nm, 0.6 μW, 0.75 NA, levelled and set to zero]†. (B) Oligonucleotide sequences used. (C) (i) 3′ Disulfide modification to capture oligonucleotide. (ii) PEG-passivator.

To demonstrate the practicality of the combined DPN-SERRS method a DNA detection experiment using an 18 base region of a sequence coding for a *Chlamydia trachomatis* target probe was performed (Fig. 3). Two independently modified complements to the Chlamydia target were obtained, one is a 12mer modified at the 3′-end with a disulfide surface attachment moiety[14] and a triple "A" spacer, suitable for DPN. A triple "A" region was added to the 3′-end of the sequence as a spacer to remove the active probe region from the gold surface. After lithography of the capture strand and removal of the "Just Add DNA" carrier fluid, the surface was passivated with triethylene glycol mono-11-mercaptoundecyl ether to prevent nonspecific binding of the disease target sequence or the dye-labelled complement. Only in the presence of the *Chlamydia* target, immobilised by the capture sequence, would the dye labelled complement hybridise and thus provide a reporter for SERRS detection. The signal levels were >3000 : 1 and show good reproducibility from pixel to pixel (RSD <5%, with 99 of data points falling within ±1.96 σ of the mean).† Significantly, the spectral contrast is very high with no trace of the reporter dye detectable in the "blank"

regions that had also been exposed to identical hybridisation materials and conditions.

In conclusion, we have shown how DPN performed on non-flat plasmonic gold surfaces can be used to selectively create SERRS active DNA array pixels in a relatively simple manner. Very high information density and depth can be obtained by embedding multiple reporter dyes within the same sub-diffraction limit area. Careful tuning of the surface chemistry and spectroscopic conditions enable the most sensitive results to be gained from this combined method. The generation of high efficiency SERRS from the surface translates directly into the fast acquisition times demonstrated in this work that will ultimately make sensitive reproducible nanoarrays a practical reality.

Notes and references

1 R. D. Piner, J. Zhu, F. Xu, S. Hong and C. A. Mirkin, *Science*, 1999, **283**, 661.
2 A. Ivanisevic and C. A. Mirkin, *J. Am. Chem. Soc.*, 2001, **123**, 7887–7889.
3 B. W. Maynor, Y. Li and J. Liu, *Langmuir*, 2001, **17**, 2575–2578.
4 M. B. Ali, T. Ondarçuhu, M. Brust and C. Joachim, *Langmuir*, 2002, **18**, 872–876.
5 D. Prime, S. Paul, C. Pearson, M. Green and M. C. Petty, *Mater. Sci. Eng., C*, 2005, **25**, 33–38.
6 S. Rozhok, R. Piner and C. A. Mirkin, *J. Phys. Chem. B*, 2003, **107**, 751–757.
7 L. M. Demers, D. S. Ginger, S.-J. Park, Z. Li, S.-W. Chung and C. A. Mirkin, *Science*, 2002, **296**, 1836.
8 L. M. Demers, S.-J. Park, T. A. Taton, Z. Li and C. A. Mirkin, *Angew. Chem., Int. Ed.*, 2001, **40**, 3071.
9 D. S. Ginger, H. Zhang and C. A. Mirkin, *Angew. Chem., Int. Ed.*, 2004, **43**, 30 (and references therein.).
10 T. Vo-Dinh, K. Houck and D. L. Stokes, *Anal. Chem.*, 1994, **66**(20), 3379–3383.
11 L. R. Allain and T. Vo-Dinh, *Anal. Chim. Acta*, 2002, **469**, 149–154.
12 Y. C. Cao, R. Jin and C. A. Mirkin, *Science*, 2002, **297**(5586), 1536–1540.
13 R. J. Stokes, A. Macaskill, P. J. Lundahl, K. Faulds, W. E. Smith and D. Graham, *Small*, 2007, **3**(9), 1593–1601.
14 R. J. Stokes, A. Macaskill, J. A. Dougan, P. G. Hargreaves, H. M. Stanford, W. E. Smith, K. Faulds and D. Graham, *Chem. Commun.*, 2007, 2811–2813.
15 (a) D. Graham, C. McLaughlin, G. McAnally, J. C. Jones, P. C. White and W. E. Smith, *Chem. Commun.*, 1998, 1187; (b) G. M. McAnally, C. McLaughlin, R. Brown, D. Robson, K. Faulds, D. R. Tackley, W. E. Smith and D. Graham, *Analyst*, 2002, **127**, 838.
16 R. J. Stokes, A. Ingram, J. Gallagher, D. Armstrong, W. E. Smith and D. Graham, *Chem. Commun.*, 2008, 567.
17 K. Faulds, F. McKenzie and D. Graham, *Angew. Chem., Int. Ed.*, 2007, **46**, 1829–1831.
18 A. J. Haes, C. L. Haynes, A. D. McFarland, S. Zou, G. C. Schatz and R. P. Van Duyne, *MRS Bull.*, 2005, **30**, 368.
19 R. Allain and T. Vo-Dinh, *Anal. Chim. Acta*, 2002, **469**, 149–154.
20 D. M. Kuncicky, B. G. Prevo and O. D. Velev, *J. Mater. Chem.*, 2006, **16**, 1207.
21 N. M. B. Perney, J. J. Baumberg, M. E. Zoorob, M. D. B. Charlton, S. Mahnkopf and C. M. Netti, *Opt. Express*, 2006, **14**(2), 847–857.
22 K. Saliata, S. W. Lee, X. Wang, L. Huang, T. M. Dellinger, Chang Liu and C. A. Mirkin, *Small*, 2005, **1**, 940.
23 K. Salaita, Y. Wang, J. Fragala, R. A. Vega, C. Liu and C. A. Mirkin, *Angew. Chem., Int. Ed.*, 2006, **45**, 1–4.

180